Investigation of BRD proteins and BET-inhibitors in tumor intrinsic killing and regulation of the tumor microenvironment

Dissertation
der Mathematisch-Naturwissenschaftlichen Fakultät
der Eberhard Karls Universität Tübingen
zur Erlangung des Grades eines
Doktors der Naturwissenschaften
(Dr. rer. nat.)

vorgelegt von
Lisa Christina Wellinger
aus Lörrach

Tübingen
2020

Gedruckt mit Genehmigung der Mathematisch-Naturwissenschaftlichen Fakultät der Eberhard Karls Universität Tübingen.

Tag der mündlichen Qualifikation: 03.02.2021
Stellvertretender Dekan: Prof. Dr. József Fortágh
1. Berichterstatter: Prof. Dr. Hans-Georg Rammensee
2. Berichterstatter: Prof. Dr. Ricky Johnstone

Für meine Familie

Acknowledgments

For my PhD studies I got the great opportunity to pursue my experiments in a laboratory filled with interesting science, a lot of laughter and awful music. I was able to present my work at three international conferences and was supported to work and learn at the Peter MacCallum Cancer center in Melbourne for a few months. However, writing a thesis in the middle of a worldwide pandemic, isolated in home office with hardly any contact to my colleagues, friends and family was for sure one of the bigger challenges during this time.

I am unbelievably thankful for all the people who supported me during difficult times and laughed with me during the countless positive moments. I want to first and foremost thank Astrid and Dan for their great support, ideas, discussions and always believing in me. Both of you were great supervisors and I cannot describe how happy I am to have you as role models. I also would like to thank my academic supervisors Prof. Rammensee and Prof. Johnstone for supporting me with new ideas and challenging me with critical questions throughout the years. A big thank you to everyone who contributed to this thesis through experimental support and/or discussions. Just to name a few: Simon, Dane, Thomas, Stefanie, Daniela, Tanja, Laura, Patrick and Marina-you were all of great help! A big thank you to Chiara, Nuria, Matthias, Dan and Phillip for proof-reading my thesis. Of course, I also have to thank Dan's group for all the fun in the lab and my office mates Chiara and Andrea for giving me a free Italian language course and one of the best road trips of a lifetime. I would also like to thank all the members from the MTT research department, which filled my day with discussions, daily lunch-dates and after work fun. I am also grateful for the possibility to work at the Peter MacCallum Cancer center in Ricky's group. I really had an awesome time in Australia and learnt a lot in the lab. A big thank you to my friends who have accompanied me in the past years on this journey. A huge thank you also to my family and Matthias, who always support me with their love, kind words, critical comments and open heart. Without all of you, I would have not been able to be where I am today.

Thank you!

List of research publications

Parts of this thesis have been published, presented at conferences or are in preparation for submission to different journals.

- Astrid Rueflibrasse, Thomas Friess, Stefanie Lechner, **Lisa Wellinger**, Jurriaan Brouwer, William E. Pierceall. Clinical BET Inhibitor RG6146 Demonstrates Potent and on-Target Activity in Pre-Clinical Models of Hematological Malignancy and Combines with Anti-CD20 and BCL-2 Inhibition to Provide Superior Efficacy. *Blood* Poster Presentation 2017

- **Lisa C. Wellinger**, Simon J. Hogg, Dane Newman, Thomas Friess, Daniela Geiss, Marina Bacac, Tanja Fauti, Astrid Ruefli-Brasse, Ricky W. Johnstone and Daniel Rohle. Abstract 1703: Sensitizing cancer cells to TNF induced cell death by the BET-inhibitor RG6146. *Tumor Biology* American Association for Cancer Research, Poster Presentation 2020

Patent:

- Marina, Bacac, Tanja A. Fauti, Simon J. Hogg, Ricky W. Johnstone, Astrid Ruefli-Brasse, Daniel Rohle, **Lisa C. Wellinger**. Sensitization of cancer cells to TNF by BET inhibition *WO 2020/169698*, August 2020

Manuscripts in preparation:

- **Lisa C. Wellinger***, Simon J. Hogg*, Dane M. Newman, Thomas Friess, Daniela Geiss, Jessica Michie, Kelly M. Ramsbottom, Marina Bacac, Tanja Fauti, Daniel Marbach, Laura Jarassier, Phillip Thienger, Axel Paehler, Leonie A. Cluse, Conor J. Kearney, Stephin J. Vervoort, Jane Oliaro, Jake Shortt, Astrid Ruefli-Brasse, Daniel Rohle#, Ricky W. Johnstone#. BET Inhibition Enhances TNF Mediated Anti-Tumor Immunity
  *these authors contributed equally; #these authors contributed equally
  Manuscript under review at Cancer Discovery
  Preprint available on bioRxiv:
  bioRxiv 2021.02.15.429851; doi: https://doi.org/10.1101/2021.02.15.429851

- **Lisa C. Wellinger***, Simon J. Hogg*, Dane M. Newman, Thomas Friess, Daniela Geiss, Stefanie Lechner, Andrea Newbold, Peter Fraser, Jake Shortt, Daniel Rohle, Astrid Ruefli-Brasse, Ricky W. Johnstone. Targeting Hematologic Malignancies With Second-Generation BET Bromodomain Inhibitor RG6146
  *these authors contributed equally

Contents

List of Figures

List of Tables

Abbreviations

Table 1: List of abbreviations used in this thesis

ABCB1	ATP-binding cassette sub-family B member 1
AML	acute myeloid leukemia
APC	antigen presenting cells
APAF-1	Apoptotic protease activating factor 1
BAX	Bcl-2 associated X protein
BAK	Bcl-2 homologous antagonist/killer
Bcl-2	B-cell lymphoma 2
Bcl-xL	B-cell lymphoma-extra large
BET	bromodomains and extra-terminal
BETi/s	BET-inhibitor/s
Bid	BH3 Interacting Domain Death Agonist
BIM	Bcl-2-like protein 11
BiTE	bispecific T cell engagers
BD	bromodomain
BRD2,3,4	bromodomain containing protein 2,3,4
BRDT	Bromodomain testis associated
CA9	carbonic anhydrase 9
CAR	chimeric antigen receptor
CEA	Carcinoembryonic antigen
CEA-TCB	CEA-T cell bispecific antibody
CEACAM5	CEA-related cell adhesion molecule 5
CCR	chemokine receptor
CD25	Cluster of differentiation 25
CD3	Cluster of differentiation 3
CD40L	CD40 Ligand
CDK9	cycline dependent kinase 9
cIAP	cellular inhibitor of apoptosis protein
CIMP	CpG island methylator phenotype
CtIP	C-terminal binding protein 1 (CtBP1) interacting protein
CTM	C-terminal domain
CTLA4	Cytotoxic lymphocyte antigen 4
cPARP	cleaved PARP
CRPC	castration resistant prostate cancer
DC	Dendritic Cell

DLBCL	diffuse large B-cell lymphoma
DMSO	Dimethyl sulfoxid
DMT	DNA-Methyltransferase
ET	extraterminal
FasL	Fas-Ligand
FasR	Fas-Receptor
FBS	Fetal bovine serum
FLIP	FLICE-like inhibitory protein
$FLIP_L$	long isoform of FLIP
GITR	glucocorticoid-induced tumor necrosis factor receptor
HAT	histone acetyltransferases
HDAC	histone deacetylases
HDACi/s	HDAC-inhibitor/s
HIF	Hypoxia Inducible Factor
HR	homologous repair
ICOS	inducible co-stimulatory molecule
IDO1	indoleamine 2,3-dioxygenase-1
IFNγ	Interferon-gamma
IFNGR	IFNγ-Receptor
IL	interleukin
IκBα	Inhibitor of NF-κBα
IKKβ	inhibitor of κB Kinase β
irAE	immune-related adverse events
IO	immune oncology
LAG3	Lymphocyte-activation gene 3
LUBAC	linear Ub chain assembly complex
M6PR	Mannose-6 phosphate receptor
MAPK	Mitogen Activated Protein Kinase
MHC	major histocompatibility complex
MDR1	multidrug resistance protein 1
MDSC	myeloid-derived suppressor cells
MLKL	mixed lineage kinase domain like protein
MLR	mixed lymphocyte reaction
MM	Multiple Myeloma
MOMP	membrane permeabilization
NEMO	NF-kappa-B essential modulator
NF-κB	nuclear factor kappa-light-chain-enhancer of activated B cells
NIK	NF-κB inducing kinase

NUT	nuclear protein in testis
Ova	Ovalbumin
PAMP	pathogen-associated molecular patterns
PARP	Poly(ADP-ribose) polymerase
PARPi/s	PARP-inhibitor/s
PBS	Phosphate-buffered saline
PD-1	programmed cell death protein 1
PD-L1	Programmed death-ligand 1
P-gp	permeability glycoprotein
PHD	plant homeodomains
Pol II	RNA polymerase II
p-TEFb	positive transcription elongation factor
PUMA	p53 upregulated modulator of apoptosis
RIPK1	Receptor-interacting serine/threonine-protein kinase 1
scr	scrambled non targeting control of siRNA
scFv	single chain variable fragments
SODD	silencer of death domain
SNP	single-nucleotide polymorphism
SIRPα	signal regulatory proteinα
TAA	tumor associated antigen
TAB	TAK1-Binding Protein
TACE	TNF-converting enzyme
TAK1	transforming growth factor-β-activated kinase 1
TAM	tumor associated macrophages
TBS	Tris Buffered Saline
TCB	T cell bispecific antibody
TCM	central memory T cells
TCR	T cell receptor
T conv/s	conventional T cell/s
TEM	effector memory T cells
TF	Transcription Factor
TGI	tumor growth inhibition
TGS	Tris-Glycine-SDS
Th	T helper cell
TIGIT	T cell immunoreceptor with Ig and ITIM domains
TIM-3	T cell immunoglobulin and mucin domain-containing protein 3
TME	tumor microenvironment
TNF	tumor-necrosis-factor-α

TNFR	TNF receptor
TNBC	triple negative breast cancer
TRADD	TNFR type 1-associated DEATH domain protein
TRAF	TNF receptor-associated factor
T reg/s	regulatory T cell/s
TSCM	stem cell-like memory T cells
Ub	Ubiquitin
VEGF-A	vascular endothelial growth factor-A

1 Summary

The epigenetic code is modulated through writers, readers and erasers, which add, interpret and remove post-translational modifications on DNA and histones, respectively. However, while this process is essential to regulate gene expression and adapt to environmental influences, it is also exploited by cancer cells to enhance expression of oncogenes or silence transcription of tumor suppressors. BET proteins are epigenetic readers, which bind to acetylated lysine residues on histones and modulate transcription of target genes including the oncogene *MYC*. BET-inhibitors displace BET proteins from the chromatin and thereby suppress transcription of target genes. However, the complete catalogue of BET targets is still unknown and the function of BET-inhibitors especially on immune cells is under high debate showing immune suppressive and activating capabilities. In this thesis, the effect of the small molecule BET-inhibitor RG6146 was elucidated by assessing potential resistance mechanisms of Multiple Myeloma cell lines *in vitro*. Different hypothesis including overexpression of *MYC*, modulation of proteins of the intrinsic apoptosis pathway and presence of the export transporter ABCB1 were assessed in sensitive and resistant cell lines. While the effect of BET-inhibitors on cancer cells has been the main focus of research studies thus far, only little is known on the function of BET-inhibitors on immune cells. Therefore, one part of this research also focused on discovering the effect of RG6146 on $CD4^+$ and $CD8^+$ T cell activation using various *in vitro* assays. While T cell proliferation was strongly suppressed at early time points, longer treatment with RG6146 even enhanced cell division. The main part of this thesis describes the effect of BET-inhibitors in the interface between immune and cancer cells. RG6146 and structurally distinct BET-inhibitors were shown to sensitize cancer cells to TNF induced cell death by modulating pro-survival proteins of the NF-κB pathway thereby enhancing cell death in combination with a T cell bispecific antibody *in vitro* and *in vivo*.
This thesis in collaboration with other research works is the basis for future potential combination strategies of BET-inhibitors with small molecules or immunotherapy.

Zusammenfassung

Epigenetik ist ein dynamischer Prozess zur Regulation der Genexpression, der sich über die Zeit Umwelteinflüssen anpasst. Der epigenetische Code wird durch Schreib- und Löschenzyme verändert, die Post-Translationale Modifikationen an DNA und Histonen anbringen oder entfernen. Lesedomänen erkennen die Modifikationen, binden daran und interpretieren den Code indem sie Gentranskription an- oder ausschalten. Während die Epigenetik ein wichtiger Prozess für die Entwicklung und Funktion von gesunden Zellen darstellt, haben Krebszellen mit Hilfe der Epigenetik einen Weg gefunden um die Expression von Onkogenen zu verstärken oder die Expression von Tumorsuppressoren zu unterdrücken. BET Proteine gehören zur Gruppe der Lesedomänen und erkennen acetylierte Lysinreste an Histonen oder DNA. Durch Bindung an diese posttranslationale Modifikation inhibieren BET Proteine die Transkription von Zielgenen zum Beispiel dem Onkogen *MYC*. BET-inhibitoren sind im Moment in der klinischen Entwicklung und verhindern die Interaktion von BET Proteinen mit den acetylierten Lysin-Resten. Dadurch wird die Transkription von Zielgenen unterdrückt. Allerdings sind noch nicht alle Zielgene von BET Proteinen identifiziert und daher steht zum Beispiel zur Debatte, ob BET-inhibitoren einen positiven oder negativen Effekt auf T Zell Aktivierung haben.
In dieser Dissertation wurden die Effekte des BET-inhibitors RG6146 untersucht indem mögliche Resistenzmechanismen von Multiplen Myelom Zellen *in vitro* getestet wurden. Die unterschiedlichen Hypothesen, welche die Überexpression von *MYC*, Proteine im intrinsischen Apoptose Signalweg und den Export-Transporter ABCB1 beinhalten, wurden untersucht. Die meisten Forschungsprojekte haben sich bisher auf den Effekt von BET-inhibitoren auf Krebszellen fokussiert und nur wenige haben den Effekt in Immunzellen untersucht. Diese Studien zeigen zudem gegensätzliche Resultate in Bezug auf den Effekt von BET-inhibitoren auf die Aktivierung und Funktion von T Zellen. Deshalb wurde in dieser Dissertation der Effekt von RG6146 auf $CD4^+$ und $CD8^+$ T Zellen untersucht. Vor allem nach kurzer Behandlung mit RG6146 wurde die T Zell Proliferation stark verringert, dies hat sich allerdings nach einer längeren Inkubationszeit normalisiert. Der Hauptteil dieser Dissertation fokussiert sich auf den Effekt von RG6146 und strukturell unterschiedlichen BET-inhibitoren im Kontext von Krebs- und Immunzellen. Es wird gezeigt, dass BET-inhibitoren die überlebensfördernden Proteine im NF-κB Signalweg modulieren und dadurch Zellen für TNF induzierten Zelltod sensibilisieren. Diese Hypothese wird von positiven Resultaten einer Kombinationsbehandlung von RG6146 und einem T Zell bispezifischen Antikörper untermauert.
Die Ergebnisse die in dieser Dissertation vorgestellt werden sind zusammen mit anderen Veröffentlichungen die Basis für weitere Forschungsarbeiten um eine potentielle Kombination von BET-inhibitor und Immuntherapie in der Klinik zu ermöglichen.

2 Introduction

2.1 Epigenetics

In eukaryotic organisms, the chromosomal DNA is present in a highly compact structure called chromatin, which is built up by nucleosomes [1]. Nucleosomes contain tightly packed DNA wrapped around eight histones [1, 2]. Post-translational modifications of DNA and histones such as ubiquitination, phosphorylation, sumoylation but most importantly methylation and acetylation are key for defining the so-called epigenome.[2, 3] The orchestra of post-translational modifications and interacting proteins determines the packaging of chromatin leading to a specific transcriptional landscape in a given cell [4]. Epigenetic changes in gene expression rely on the combination of DNA methylation as well as histone marks and their protein binders and do not involve modifications in the underlying DNA sequence [2]. While epigenetics are heritable between cell divisions and occasionally generations, they evolve over time and reprogram cells to adapt and respond to environmental changes [2, 5, 6].

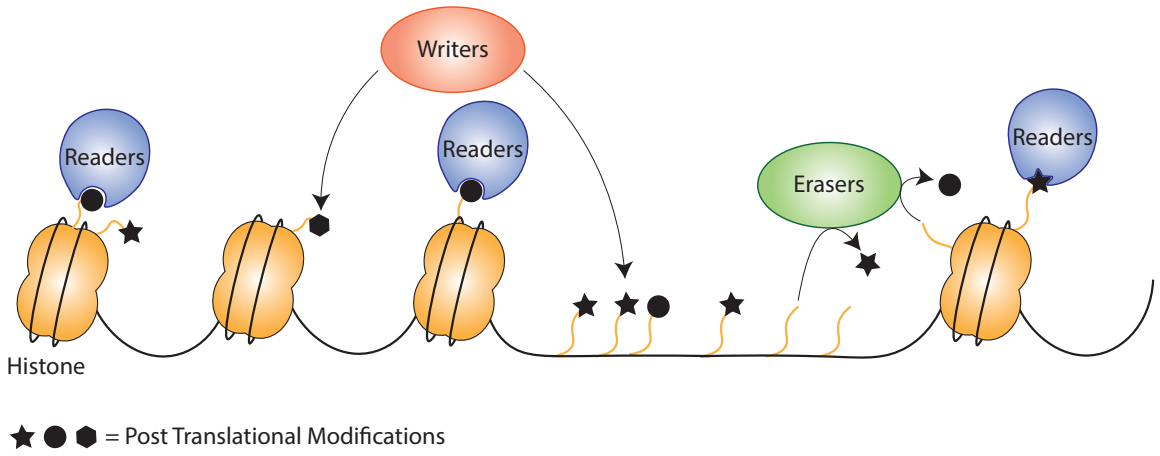

Figure 1: Post translational modifications are added to histone tails or DNA directly through writers, while erasers remove these modifications. Readers bind to modifications and thereby modulate gene transcription of target genes

The epigenetic landscape is mediated through writers, readers, and erasers. Writer proteins add histone marks including methylation or acetylation to lysine or arginine residues on histone tails. They are in equilibrium with eraser proteins removing these post-translational modifications. While having these marks themselves might not have an effect, readers interpret the epigenetic code and translate it to modulate chromatin struc-

ture or gene expression (Figure 1).[2] Histone acetyltransferases (HAT) are an example for epigenetic writers and have been described to use Acetyl-CoA as the acetyl-donor for adding an acetyl group to the ε-amino group of a lysine side chain in a histone [7]. Different mechanisms have been proposed on how acetylated histones modulate chromatin packaging and gene expression. If the acetylated lysine residue is located on the histone tail, it neutralizes its positive charge thereby loosening chromatin packaging and enhancing the accessibility of genes for the transcriptional machinery [2]. Specific histone marks are involved in chromatin folding including H4K16 acetylation. Upon acetylation, H4K16 has been shown to switch from heterochromatin, describing the tightly packed form of DNA, to euchromatin, which is a lightly packed version of DNA [8, 9, 10]. Besides effects on chromatin packaging, lysine acetylation creates binding sites for readers, which contain conserved protein motifs. Specific recognition of post-translational modifications by readers induces recruitment of transcription factors to enhancer and promoter regions of target genes [11, 12]. Among others, specific protein motifs in reader proteins include bromodomains (BD), chromodomains, plant homeodomains (PHD) fingers or tudor domains [13].

2.1.1 Epigenetic Dysregulation in Cancer

Given that the epigenetic code is vital to correctly regulate gene expression, it is not surprising that dysfunction of writers, readers and erasers or their binding partners promotes various diseases including cancer [2]. Cancer cells are known to harbor mutations in the DNA sequence causing dysfunctional proteins or the complete loss of tumor suppressor genes [14]. However, cancer cells also exploit epigenetic mechanisms to modify the proteome to their own advantage. The first epigenetic difference between cancer cells and healthy tissue was discovered in 1983. It was shown that cancer cells exhibit a distinct DNA methylation pattern at CpG dinucleotides when compared to normal tissue [15]. In this respect, the level of histone marks is globally altered in many cancer cells leading to the activation of oncogenes or the transcriptional repression of tumor suppressors [16]. One example is the CpG-island methylator phenotype (CIMP) describing colorectal cancer cells that exhibit specific methylated CpG islands in promoter regions thereby silencing tumor suppressor genes and inducing mismatch repair deficiency [17, 18].

2.1.2 BET proteins

One family of epigenetic readers is the family of bromodomain containing proteins that bind to acetylated lysine marks and are classified into nine different subgroups depending on their main function depicted in Figure 2 and described in detail by Zaware et al. [19].

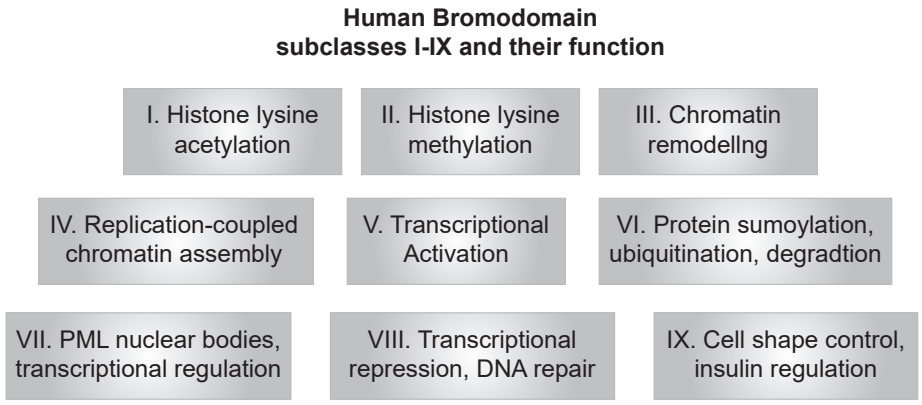

Figure 2: Human Bromodomain containing proteins can be divided into nine subclasses depending on their main function as described in [19].

One subgroup describes Bromodomain and extraterminal (BET) proteins which consist of bromodomain containing protein 2 (BRD2), BRD3, short and long isoform of BRD4 (BRD4S, BRD4L) and testis specific BRDT. They contain two bromodomains (BD) at the N-terminus and one extraterminal (ET) domain at the C-terminal end. The long isoform BRD4L contains a C-terminal motif (CTM), which is also present in BRDT.[20] Even though bromodomains exhibit a large variation in the 110 amino acid sequence [21], they adapt the same conserved fold allowing specific recognition and binding of acetylated lysine residues on histone tails [22]. At the same time, BET proteins form interactions with the transcription coactivator mediator complex and transcription factors allowing them to localize to active enhancer and promoter regions and activate gene transcription [11, 12]. BRD4 has also been shown to interact with the positive transcription elongation factor (P-TEFb), which consists of the catalytic subunit cyclin dependent kinase 9 (CDK9) and one of the activator subunits cyclin T1, T2 and K [23, 24]. Upon BRD4 mediated recruitment of P-TEFb to the chromatin, the kinase function of the complex phosphorylates and activates RNA polymerase II (RNA Pol II) inducing transcriptional elongation of certain genes [23, 24] (Figure 3).
The fact that BET proteins are ubiquitously expressed across cell types [25] raises the question why these proteins were identified as promising drug targets and how to specifically inhibit BET proteins in target cells. Recently, the understanding of how BET proteins function has become more evident, but it is not entirely understood why healthy cells are not adversely affected by BET-inhibition. One potential reason is the differential recruitment and usage of BET proteins at super-enhancers versus typical enhancers [26, 27].

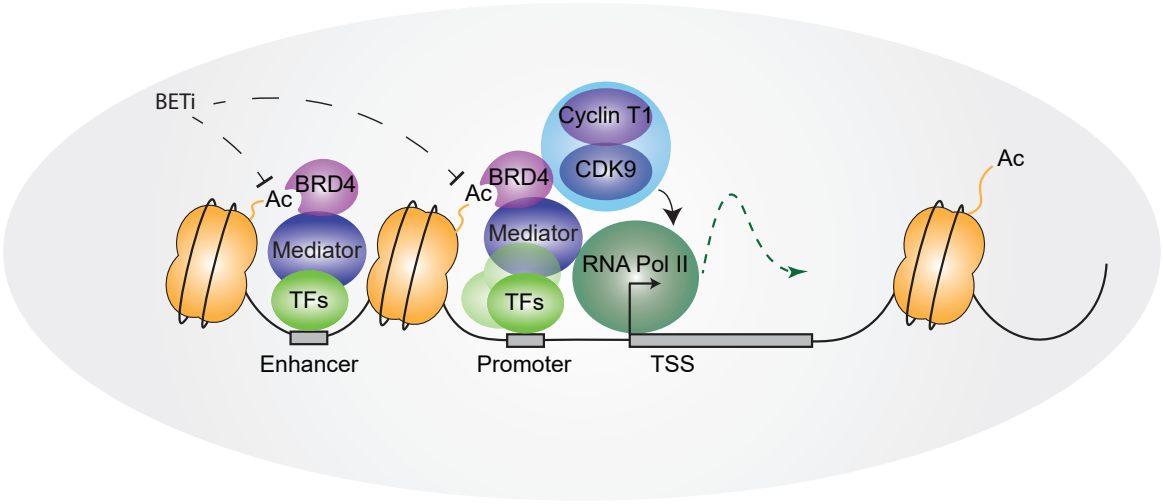

Figure 3: In the nucleus BRD4 binding to chromatin is mediated through acetylated lysine residues on histone tails. BRD4 forms an interaction with mediators and transcription factors (TF) at promoters proximal to the transcriptional start site (TSS) or at enhancers (distal to the TSS) [11, 12]. BRD4 recruits pTEFb containing Cyclin T1 and CDK9, which in turn activates RNA polymerase II (RNA Pol II) to induce gene transcription [23, 24]. BET-inhibitors (BETi) diplace BRD4 from the chromatin and thereby modulate gene transcription.

2.1.3 Super-enhancers

Classical enhancer regions are defined as specific DNA elements in close proximity of genes, which are bound by transcription factors and mediators to regulate gene activation. The function of these enhancers is independent of their orientation on DNA and they are adjacent to histones exhibiting post-translational modifications.[28] It has been shown that enhancers regulate gene transcription from a distance by looping the DNA strand thereby bringing promoter and enhancer regions in close proximity [29, 30, 31]. Studies over the last years have revealed that some enhancers seem to form clusters over a large span of DNA-sequence mediating the enriched binding of several factors as compared to classical enhancers [28]. These so-called super-enhancers show a high degree of transcription factor, mediator coactivator complex and RNA Pol II binding and have been linked to a higher expression of adjacent genes [32, 33]. They also exhibit an enrichment of post-translational modifications of histones like H3K27ac and H3K4me1 as well as DNase I hypersensitivity [32, 33]. In healthy cells, super-enhancers usually regulate the expression of genes involved in cell identity and cell function [32]. However, in a disease state, super-enhancers are placed in close proximity of oncogenic drivers including *MYC* [26] or are enriched for disease associated single-nucleotide polymorphisms (SNPs) [33].

Since super-enhancers show enhanced binding of transcription factors, coactivators like BRD4 and mediators at their site, inhibition of these binding factors has a much stronger impact on correct gene activation as compared to classical enhancers, which do not depend on the binding of a large amount of these interacting factors [26] (Figure 4).

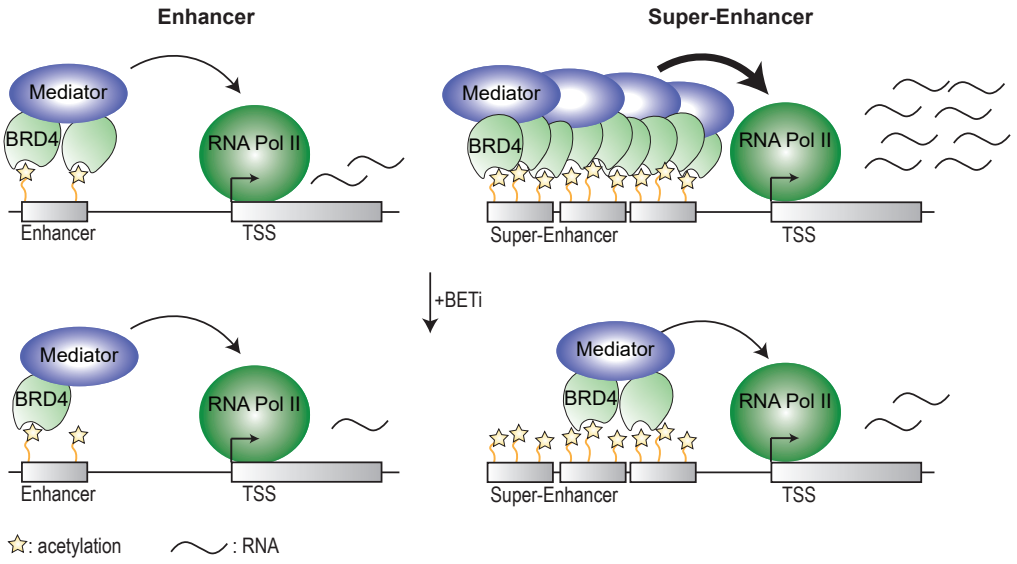

Figure 4: Super-enhancers exhibit a higher degree of post-translational modifications including H3K27ac, as well as mediator and BRD4 binding as compared to classical enhancer [32, 33]. Loss of mediator and BRD4 at super-enhancers has, therefore, a stronger impact on active gene transcription [26]. TSS: Transcriptional Start Site; RNA Pol II: RNA Polymerase II

2.1.4 BET-inhibitors

In recent years, BET proteins have emerged as a potential drug target in oncology and other disease fields including inflammation and viral treatment [19, 34]. BET-inhibitors (BETi) work by displacing BET proteins from the chromatin thereby modulating the transcription of target genes. Most BETis belong to the acetyl lysine mimetic class of bromodomains-inhibitors [27]. These small molecules compete with the acetylated lysine residue to form a hydrogen bond with the conserved asparagine residue located in the hydrophobic pocket of the bromodomain [27]. Various BETis have been developed and are currently investigated in clinical trials for a broad spectrum of disease treatment as described in detail by Cochran et al. and Zaware et al. [19, 34].

2.1.4.1 The BET-inhibitors JQ1 and RG6146 JQ1 was developed by the James Bradner laboratory [35] and belongs to the acetyl-lysine mimetic class of BETis [27] (Figure 5). This small molecule BETi has been extensively used for *in vitro* and *in vivo* studies in the past years.

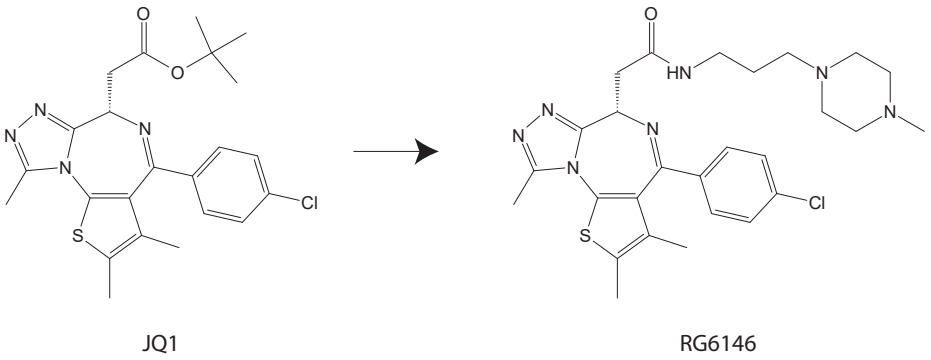

Figure 5: Chemical structure of the small molecule JQ1 and the advanced molecule RG6146

To understand the mechanism of how BETis displace BET proteins from the chromatin, it is important to comprehend how Bromodomains interact with the acetylated lysine residue. Bromodomains are constructed of a left-handed four helix-bundle and together with the inter-helical ZA and BC loop form a hydrophobic pocket at the end of the bundle [36, 37, 38] (Figure 6 A-B). Bromodomains preferably bind more than one acetylated lysine residue [22]. Binding is mediated through a hydrogen bond between the carbonyl oxygen of the acetylated lysine residue and the side-chain NH2 of a conserved asparagine residue within the bromodomain. This interaction is stabilized through hydrogen bonds with five conserved water molecules located in the cavity of the bromodomain. The neutralized charge of the second acetylated lysine residue facilitates the formation of hydrophobic interactions with the bromodomain.[36, 39] The thieno-triazol-1, 4-diazepene scaffold of JQ1 consists of a triazole ring, which mimics the acetylated lysine residue thereby forming a bond with the conserved asparagine residue in the bromodomain [35]. Further interactions are mediated through the chlorophenyl substituent of the diazepine ring and the dimethyl-substituted thieno ring [27]. By displacing BET proteins from chromatin, JQ1 has been shown to potently reduce tumor growth and improve survival *in vivo* [35]. Even though various effects on cancer and immune cells have been described for JQ1, due to its short half life in plasma [35], this small molecule could not be utilized in clinical trials. RG6146 (RO6870810) is a derivative of JQ1 with improved pharmacokinetic properties (Figure 5). RG6146 was used in Phase I clinical trials in various tumor types as single agent (NCT02308761) and in combination (NCT03255096, NCT03068351, NCT03292172).

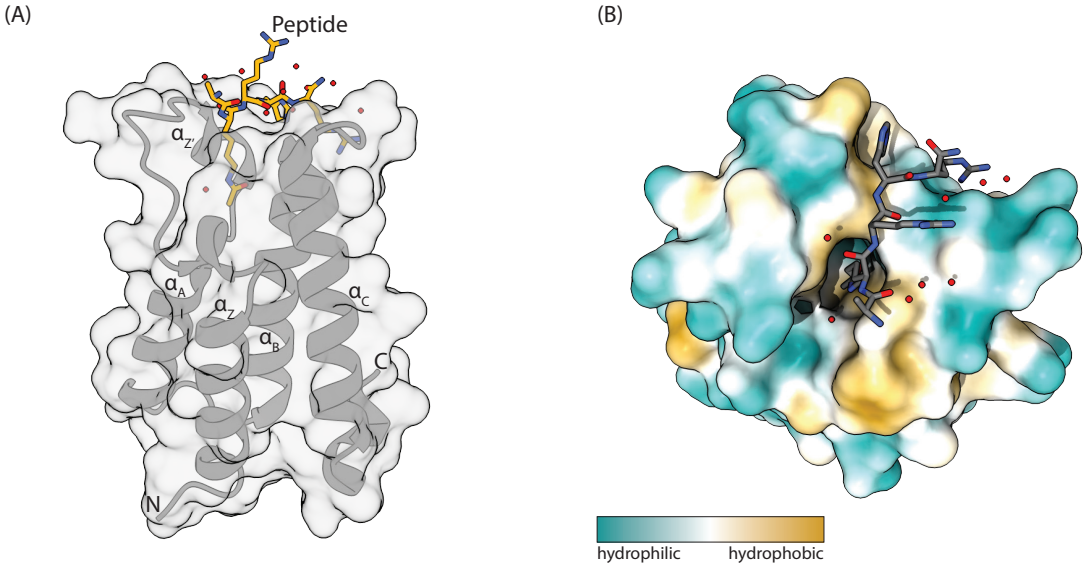

Figure 6: Structure of the bromodomain of Gcn5p binding to a peptide of the acetylated Histone H4. (A) Cartoon and surface representation of the bromodomain, which shows four alpha helices Z, A, B, C and bound peptide (orange). (B) Surface representation of the bromodomain. Coloured by hydrophobic potential (most hydrophilic (blue) and most hydrophobic (orange)). Acetylated peptide is shown in grey. PDB: 1E6I, [36]

2.1.4.2 Effects of BETis on cancer cells Transcription factors like the oncogene Myc are intrinsically unstructured and therefore thought to be undruggable [40]. Interestingly, BET proteins have been shown to enhance the transcriptional activation of *MYC* making them interesting targets for cancer therapy [41]. Indeed, treatment with JQ1 in hematological malignancies showed suppression of *MYC* transcription as well as its downstream targets and induces anti-proliferative effects [26, 41].
Further, BETis have been shown to suppress other cancer-associated phenotypes such as hypoxia and angiogenesis [42]. In particular, BETis block the expression of carbonic anhydrase 9 (*CA9*) and vascular endothelial growth factor-A (*VEGF-A*) in triple negative breast cancer (TNBC) [42]. Binding of Hypoxia Inducible Factor (HIF) to the promoter of *CA9* has been impaired with BETi treatment and since BRD4 binding is increased at promoter regions of *CA9* and *VEGF* under hypoxic conditions, it was suggested that transcription induced by HIF is dependent on BET proteins [42].
Cancer cells have also been shown to produce highly tumorigenic fusion proteins through a translocation between *BRD3* or *BRD4* with nuclear protein in testis (*NUT*). Thereby the oncogenic fusion proteins BRD3-NUT and BRD4-NUT are generated, which lead to NUT midline carcinomas introducing them as promising drug targets for BETis even in rare and highly aggressive malignancies.[43, 44, 45]

Besides single agent activity, various studies have focused on the effect of BETis in combination with other molecules to overcome drug resistance or enhance treatment outcome. One example is the combination of Poly(ADP-ribose) polymerase (PARP) and BET-inhibition. PARP-inhibitors (PARPis) are known to be effective in cells with mutations in *BRCA1* or *BRCA2* causing homologous recombination deficiency [46, 47]. BETis were able to induce synthetic lethality in combination with PARPis by suppressing the level of C-terminal binding protein 1 (CtBP1) interacting protein (CtIP), which is involved in DNA double strand break repair [47]. On the other hand, BETis have been considered as promising molecules to be combined with immunotherapy. Specifically, JQ1 was shown to displace BRD4 at the locus of programmed-death ligand 1 (PD-L1, CD274) thereby reducing *CD274* expression [48, 49]. PD-L1 is a binding partner for the programmed cell death protein 1 (PD-1) expressed on T cells. Interaction of this ligand-receptor pair suppresses T cell function as shown for reduced cytokine secretion and proliferative potential [50]. Therefore, PD-L1 function is utilized by cancer cells to negatively regulate the immune response inducing a resistance mechanism to anti-tumor immunity [51]. Hence, downregulation of PD-L1 protein by BETis enhances tumor-specific T cell effector functions [48] and places BETis as promising combination partners for immunotherapy.

2.1.4.3 Effects of BETis on T cells Historically, the main interest of research was to elucidate the effect of BETis on cancer cells. However, in recent years the transcriptional regulation driven by BET proteins in immune cells has become an emerging field of interest. Studies of BETis on immune cells have led to contradictory results that will be discussed in depth in section 5.2. Briefly, BETis have been shown to suppress T cell differentiation of specific T cell subsets which makes them a promising treatment strategy for autoimmune diseases [52]. Conversely, another group has identified BETis as promising combination partners for chimeric antigen receptor (CAR) T cell therapy by enhancing persistence of adoptively transferred CAR T cells [53]. Yet, the broad effect of BETis on immune cells is still vastly unknown. To evaluate how BETis shape the effect of immune cell subtypes in the context of cancer, it is important to understand general T cell function and the mechanisms that cancer cells exploit in the tumor microenvironment (TME) to modulate immune cell activity.

2.2 T cell subtypes, their function and role in cancer elimination

T cells originate in the bone marrow and mature in the thymus, where they are primed to specifically recognize an antigen bound major histocompatibility complex (MHC) using their T cell receptor (TCR). Naïve T cells leave the thymus, circulate throughout the body searching for their specific antigen, and get in contact with antigen presenting cells (APCs) in the secondary lymphoid organs. APCs circulate through the body, recognize and take up infected cells leading to the presentation of antigens on their MHC molecules.[54] While all nucleated cells of the human body possess MHC I molecules, only professional APCs hold MHC II molecules, which are recognized by the co-receptor CD4 on $CD4^+$ T cells [55]. CD8 on the surface of $CD8^+$ T cells specifically recognizes an antigen presented by the MHC I molecule [55]. CD4 and CD8-molecules bind MHC molecules at a different site than the TCR and enhance sensitivity of T cells to the recognized MHC:antigen complex [55]. However, additional secondary signals are required to initiate proper T cell activation (Figure 7). One of these is the interaction of CD28 receptors located on T cells with B7.1 (CD80) or B7.2 (CD86) molecules on APCs [56]. Lack of secondary signals induces T cell anergy meaning the inability of T cells to produce interleukin (IL)-2 and therefore hinder proliferation and differentiation [56]. Further receptors and ligands are upregulated on the surface of T cells and APCs ensuring the receipt of survival signals. Among these receptors and ligands on T cells are CD40 Ligand (CD40L), 4-1BB and inducible co-stimulatory molecule (ICOS) [56]. A third necessary signal for T cell activation are cytokines, which determine the differentiation into specific subtypes. Upon activation and proliferation in the lymphoid organ, T cells migrate to the site of infection or to tumor targets presenting specific antigens to initiate killing of target cells [56].

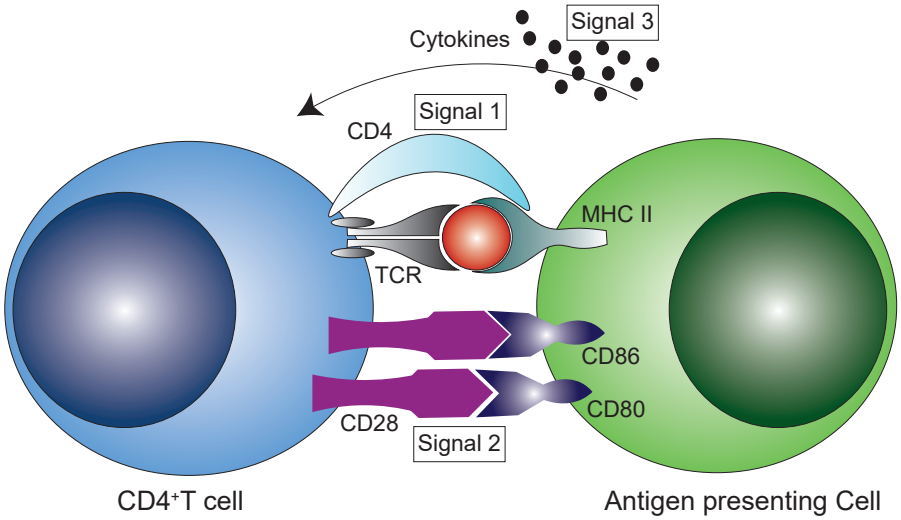

Figure 7: T cell activation as an example for $CD4^+$ T cells. The first recquired signal is the specific recognition of an MHC molecule bound antigen by the TCR and CD4 [55]. The second signal is mediated through co-stimulatory molecules such as CD28 binding to CD80 or CD86 located on antigen presenting cells [56]. Cytokines as a third signal are also recquired to initiate proper T cell activation.

2.2.1 $CD4^+$ T helper cells

Upon antigen encounter, $CD4^+$ T helper cells differentiate into specific subclasses and thereby support the immune system to respond effectively to various kinds of infections [56].

- T helper-1 (Th1) cells are activated by interleukin (IL)-12 and interferon-gamma (IFNγ). The transcription factors STAT4 and TBET also play an important role in Th1 cell differentiation. Th1 cells are mainly involved in the defense against viruses and intracellular bacteria by producing the effector cytokines IFNγ, TNF, IL-2 and by activating macrophages.[57, 58, 59, 60, 61, 62]
- T helper-2 (Th2) cells, are involved in the defense of helminthic parasites and are activated through the cytokines IL-4 and IL-6. The transcription factors STAT6 and GATA3 are important regulators of Th2 cell differentiation. Th2 cells release various cytokines including IL-4, IL-5, IL-10 and IL-13 to activate, eosinophils and B-cells.[60, 61, 62, 63, 64]
- T helper-17 (Th17) cells are characterized by the release of IL-17A, IL-17F and IL-22, the expression of the transcription factors ROR-γt as well as STAT3 and are involved in the defense against intracellular and extracellular bacteria as well as fungi [61].

Furthermore, $CD4^+$ cells have been shown to enhance the activation of $CD8^+$ T cells during priming. In the lymph nodes, $CD4^+$ T helper cells bind to dendritic cells (DCs) presenting antigens on the MHC I molecule. Upon interaction, $CD4^+$ cells induce binding of CD40L with CD40 present on DCs thereby activating them leading to increased levels of MHC I and MHC II as well as the costimulatory molecules CD80 and CD86. Hence, activated DCs are able to induce $CD8^+$ T cell activation, killing and enhance T cell memory.[65, 66, 67]

2.2.2 $CD4^+$ T regulatory cells

Regulatory T cells (T regs) are a subpopulation of $CD4^+$ T cells that are classified by the expression of the transcription factor FoxP3 in the nucleus and constitutive expression of Cluster of differentiation 25 (CD25) and Cytotoxic lymphocyte antigen 4 (CTLA-4) on the cell surface [61, 68, 69, 70, 71, 72]. The main role of T regs is to maintain immunological self-tolerance and protection from autoimmunity [73]. Although the exact mechanism of T reg function remains to be elucidated, some factors such as FoxP3, CD25, CTLA-4 and IL-2 are indispensable in this context [74, 75, 76, 77, 78, 79].
CTLA4 is an inhibitory receptor, which is constitutively expressed on T regs, and induces a lack of co-stimulatory signals for proper activation of conventional T cells (T convs) [80]. This is mediated through various mechanisms. CTLA4 has a high sequence similarity to CD28 and competes on binding to CD80 and CD86, but exhibits a higher affinity to its ligands than CD28 [74, 75]. Moreover, upon binding, CTLA4 decreases CD80 and CD86 levels on the surface of APCs through trans-endocytosis [76, 77].
FoxP3, also, plays a role in T reg mediated suppression of T convs. FoxP3 has been shown to suppress the production of IL-2. By recruiting class I histone deacetylases (HDAC) to the *IL2* promoter site, FoxP3 leads to *IL2* gene silencing, thereby inducing a strong dependence of T regs on exogenous IL-2 [81]. CD25 on T regs is highly specific for IL-2 binding and, presumably, generates an IL-2 sink to deplete this cytokine for the activation of T convs [78, 79]. Albeit, this is not entirely understood, since other groups have shown that IL-2 deprivation is not essential for $CD4^+$ T cell suppression [82, 83] and only needed for the suppression of $CD8^+$ T cells [83].
The described mechanisms and potentially others lead to a lack of co-stimulatory signals and inhibit T convs to exhibit their full potential. Even though T regs are crucial to protect the organisms from autoimmunity, T regs are also important players in suppressing anti-tumor immunity [84].

2.2.3 Cytotoxic CD8$^+$ T cells

Cytotoxic CD8$^+$ T cells have the possibility to directly kill other cells by using various mechanisms summarized in Figure 8.

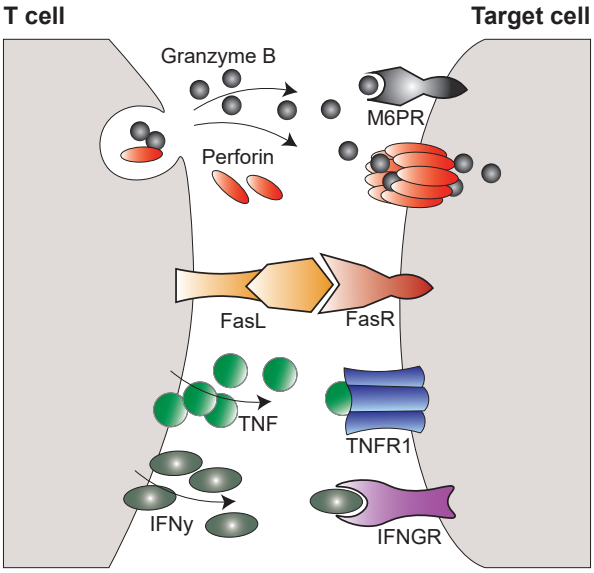

Figure 8: Shematic of CD8$^+$ mediated killing of target cells. Activated CD8$^+$ T cells kill target cells through various mechanisms. One is the release of cytotoxic granules containing perforin and granzyme B into the immunological synapse [85]. Granzyme B can enter the target cell by binding the Mannose-6-Phosphate Receptor (M6PR) and receptor-mediated endocytosis or through pores formed by perforin [85, 86, 87]. Another mechanism is the binding of Fas-Ligand (FasL), tumor necrosis factor (TNF) or interferon-γ (IFNγ) to their respective receptor on the target cell [85]. FasR: Fas-Receptor; TNFR1: TNF-receptor 1; IFNGR: IFNγ-receptor

The most prominent pathway includes the serine esterase granzyme-B [88] and perforin directed killing of target cells [85]. These proteins are stored in lytic granules [85]. Upon cell-cell interaction, the microtubule-organizing center, golgi apparatus and lytic granules are reorganized to direct the release of the granules to the site of T cell:target cell interaction [85, 87]. Ca^{2+}-dependent release of granules containing perforin and granzyme [85], induces several mechanisms on the target cell membrane. Perforin has been shown to form pores in the plasma membrane of the target cells [89, 90, 91], which allows granzyme to enter into the cytoplasm [92]. An alternative perforin-independent entry mechanism has been described with granzyme B being able to enter the target cell through receptor-mediated endocytosis, which is regulated by the mannose-6-phosphate receptor (M6PR) [86, 87]. Still, perforin is indispensable to release granzyme B from endosome-like vesi-

cles and induce its full killing potential [87, 93]. Upon entering the cytoplasm, granzyme cleaves and thereby activates Caspase-3 and Caspase-8 [94, 95, 96]. Granzyme can also activate BH3 Interacting Domain Death Agonist (Bid) and induce the release of cytochrome c from mitochondria [97, 98]. Both pathways eventually lead to the induction of target cell death [99].
Another important mechanism of cytotoxic T cells to kill target cells is mediated through the interaction of Fas-Ligand (FasL) present on the membrane of T cells engaging with the Fas-receptor on target cells . This Ca^{2+} independent process induces extrinsic apoptosis of the target cell.[85]
T cell mediated cytotoxicity is also realized through the release of cytokines like IFNγ and tumor-necrosis-factor-α (TNF) [85] with the latter being described in detail in the following sections.

2.2.4 TNF

TNF is a multifunctional pro-inflammatory cytokine, which plays an important role in various processes, including the initiation of inflammatory gene expression programs, the promotion of proliferation and the activation of cellular suicide programs such as apoptosis and necrosis [100, 101]. TNF is expressed as a trimeric type II transmembrane protein [102], but is also present as a soluble extracellular molecule when it is cleaved by the metalloproteinase TNF-converting enzyme (TACE) [101, 103]. The two forms of TNF can bind to the corresponding TNF receptors (TNFR) 1 and 2 [104].
TNFR1 is expressed on nearly all tissues and responds to both, the soluble and membrane-bound form of TNF, whereas TNFR2 is mostly found in immune cells and is only fully activated by the membrane-bound form of TNF [104]. TNF-mediated signaling through TNFR1 preferably drives a pro-inflammatory program, while modulation of immune cells and tissue regeneration are induced by TNF binding to TNFR2 [104]. Upon contact with the ligand, TNF receptors induce a conformational change leading to the dissociation of the inhibitory protein silencer of death domain (SODD) allowing the binding of the adaptor protein Tumor necrosis factor receptor type 1-associated DEATH domain protein (TRADD) that recognize the death domain of the receptor [105, 106]. Following TRADD binding, three pathways can be initiated such as the Mitogen Activated Protein Kinase pathway (MAPK), the classical nuclear factor kappa light chain enhancer of activated B cells (NF-κB) pathway and death signaling pathways [105]. In this thesis, the last two pathways are explained in further detail.

2.2.4.1 TNF activation of classical NF-κB signaling As previously mentioned, the classical NF-κB-pathway (Figure 9) starts with the binding of TNF to TNFR1 leading to receptor oligomerization [107] in the plasma membrane and translocation to lipid rafts [108]. Subsequently, TRADD binds to the cytoplasmic death domain of TNFR1 [109, 110], which allows the recruitment of the Receptor-interacting serine/threonine-protein kinase 1 (RIPK1) [111]. TRADD simultaneously interacts with TNF receptor-associated factor 2 (TRAF2) through its N-terminal TRAF binding domain [111, 112]. The cellular inhibitor of apoptosis protein-1 (cIAP1) and cIAP2 are brought to the complex through TRAF2 binding [113, 114]. cIAP1 and cIAP2 contain a RING finger domain, which exhibit an ubiquitin E3 ligase activity leading to K-63 and K-11 linked polyubiquitination of RIPK1 as well as autoubiquitylation [115, 116, 117, 118, 119]. Ubiquitination in turn allows recruitment of the kinase complex formed by the transforming growth factor-beta-activated kinase 1, TAK1-Binding Protein 2 and 3 (TAK1/TAB2/TAB3) as well as NF-kappa-B essential modulator (NEMO), and the E3 ligase linear Ub chain assembly complex (LUBAC) [115, 119, 120, 121, 122, 123]. LUBAC-mediated linear ubiquitination of different components of this complex [124, 125, 126] appears to stabilize or reinforce the complex formation and promote TAK1-dependent phosphorylation of inhibitor of κB Kinase β (IKKβ) [127] present in the IKK complex containing IKKα, IKKβ and NEMO [128]. IKKβ phosphorylation results in the dissociation and subsequent degradation of IκBα [129, 130, 131]. Finally, NF-κB (p65/p50) is free to translocate into the nucleus and induce transcription of NF-κB target genes, which are mainly involved in inflammation and cell survival [128].

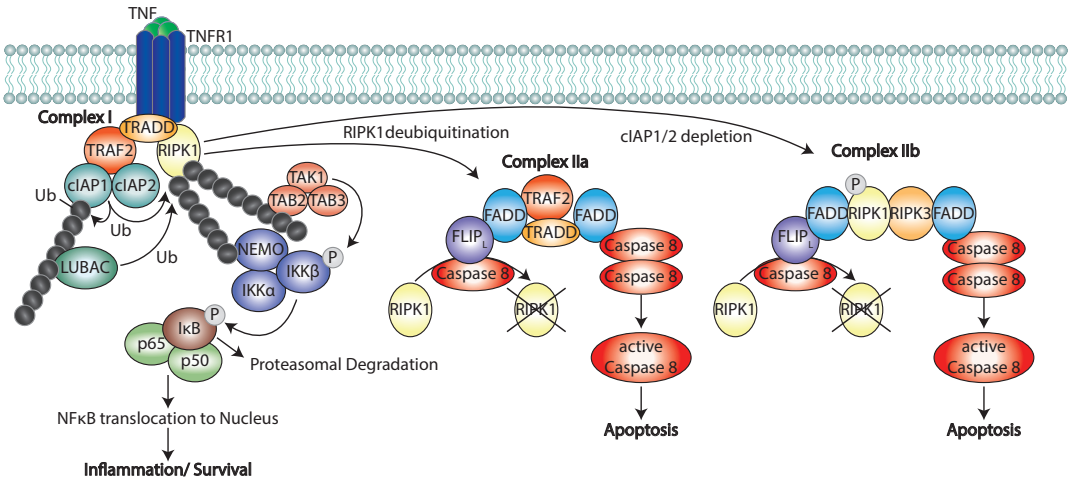

Figure 9: Binding of TNF to the TNFR1 induces formation of complex I containing TRADD, TRAF2, cIAP1 and cIAP2 thereby inducing ubiquitination of RIPK1 and cIAP1 and further binding of proteins through these ubiquitination sites leading eventually to phosphorylation of IKKβ, proteasomal degradation of IkBα and induction of the NF-κB pathway. RIPK1 deubiquitination or cIAP1 and cIAP2 depletion induces the formation of complex IIa and IIb and induction of apoptosis. For a more detailed description refer to section 2.2.4.1 and 2.2.4.2. Ub: Ubiquitination; P: Phosphorylation

2.2.4.2 TNF induces death signaling Binding of TNF to TNFR1 mostly leads to the activation of the classical NF-κB-pathway, however, it can also trigger death-signaling programs including apoptosis or necrosis [101]. Different mechanisms have been described to induce apoptosis by either forming the complex IIa or IIb [101] (Figure 9). The formation of these complexes is initiated proximal to the membrane and continues to form upon translocation into the cytoplasm [101, 112]. Complex IIa formation involves deubiquitylation of K-63 linked polyubiquitin chains of RIPK1 by A20, Cezanne and CYLD [132, 133, 134, 135]. De-ubiquitinated RIPK1 dissociates from the TNFR1 complex to interact with TRAF2, TRADD, FADD, a homodimer of pro-caspase 8, and a procaspase 8 and cleaved long isoform of FLICE-like inhibitory protein ($FLIP_L$) heterodimer [101, 112]. Complex IIa activation results in the activation of downstream caspase cascades leading to apoptosis [112].

The formation of complex IIb is initiated when the level of cIAP1 and cIAP2 are decreased through autodegradation of these proteins [136, 137]. Depletion of cIAP1 and cIAP2 diminishes RIPK1 ubiquitination [138]. Hence, RIPK1 is free to form a complex with FADD, RIPK3 and pro-caspase-8 leading to Caspase-8 activation [101, 139]. Activation of initiator caspase-8 induces cleavage of downstream effector caspase-3/7 and the

induction of the extrinsic apoptosis pathway leading to proteolytic cleavage of proteins like PARP [140, 141, 142, 143]. However, the downstream cleavage of caspase-3 and 7 is not always sufficient to induce cell death and therefore some cells rely on the crosstalk between the intrinsic and extrinsic apoptosis pathway to induce killing [144]. The intrinsic apoptotic pathway is initiated by caspase-8 mediated cleavage of Bid, which subsequently translocates to the mitochondria where it interacts with Bcl-2-associated X protein (BAX) and Bcl-2 homologous antagonist/killer (BAK1) inducing cytochrome c release [145].
In general, apoptosis can be repressed by anti-apoptotic proteins including cIAP1 and cIAP2, which have been shown to directly inhibit the cleavage of caspase-3 and 7 [146]. On the other hand, the heterodimer of $FLIP_L$ and pro-caspase 8 found in both complexes are essential for RIPK1 and RIPK3 proteolytic cleavage thereby inhibiting their kinase function and repressing the induction of cell death through necrosis [147, 148].

2.2.5 The role of T cells in cancer cell elimination

As described, T cells have a variety of ways to eliminate infected or foreign cells. Nevertheless, T cell mediated killing of cells is only mediated upon successful recognition of target cells including cancer cells.
Negative selection in the thymus is necessary to induce tolerance of T cells towards self-antigens thereby suppressing autoimmunity [149]. Tumor cells, however, exhibit mutations, post-translation modifications and modifications in splicing of certain proteins, thereby generating promising new targets for the recognition and attack by immune cells [150, 151, 152, 153, 154, 155]. When presented on the MHC molecules, these antigens are distinct from their healthy cell counterparts and are so called neoantigens [150, 151, 152, 153, 154, 155]. Some cancer cells even harbour tumor-specific proteins, which are not present in other cells of the organism including MAGE-1 expressed in melanoma and breast carcinoma or mucins on pancreatic and breast tumors [156, 157, 158, 159, 160, 161, 162, 163]. As reviewed by Chen and Mellman, not all neoantigens are necessarily immunogenic and induce a T cell response [164]. To the contrary, mutations in a protein can lead to a loss of binding to the MHC I molecule. Also, antigens could not be recognized by T cells, because the mutated sites are facing away from the TCR. On the other hand, immunogenic peptides can be created when mutations face towards the TCR or when completely new peptides are generated through insertions, deletions or frame-shift mutations [152].[164]
Even though immune cells theoretically can recognize tumor-specific antigens, cancer cells have developed mechanisms to circumvent attack by the immune system.

2.3 Immunoediting of cancer cells

The interaction of immune cells and cancer cells is complex, evolves over time and leads not only to protection of the host from developing tumors, but can also induce tumor growth in a process termed immunoediting [165]. Immunoediting is divided in three phases: elimination, equilibrium and escape [165, 166, 167]. The first phase called elimination describes the process of immunosurveillance, in which the interplay between the innate and the adaptive immune system is able to recognize and eradicate tumor cells [165, 167]. During the equilibrium phase, immune cell attack and loss of immune cell recognition, through newly arising cancer cell mutations, balance each other [165, 167]. The process of T cells recognizing neoantigens presented on cancer cells induces immunoselection. Immunoselection describes the removal of highly immunogenic cells leading to outgrowth of cancer cells, which lack strong rejection antigens [151, 168]. The equilibrium phase is the longest and can take up to several years before the tumor develops certain variants that completely lose sensitivity to immune destruction and thereby escape the immune system [165, 167]. Prominent escape processes include (1) loss of tumor antigen expression through silencing upon promoter CpG island methylation [161, 168, 169, 170] or (2) downregulation or modification of the antigen processing and presentation pathway specifically focusing on the modification of MHC proteins [171, 172, 173]. For example, oncogenic BRAF (V600E) has been shown to induce constitutive Serine-335 phosphorylation dependent MHC I internalization, which is rescued by BRAF or MEK inhibition [174].

2.3.1 Immune suppression in cancer

Besides modifying the antigen presenting machinery, cancer cells have evolved various mechanisms to reduce the attack of the immune system. T cells do not only harbor co-stimulatory receptors, but also increase the level of co-inhibitory receptors upon activation. In concert with high antigen load, immunosuppressive cytokines and a lack of $CD4^+$ T cell mediated stimulation, T cells lose their effector function [175, 176, 177]. The inability to induce effector function was originally identified in chronic viral infection, but also holds true for tumor sites exhibiting a high tumor antigen load [177]. Loss of target cell killing by T cells is mediated through the loss of IL-2, TNF and IFNγ production and upregulation of inhibitory receptors including PD-1, T cell immunoglobulin and mucin domain-containing protein 3 (TIM-3), Lymphocyte-activation gene 3 (LAG3), T cell immunoreceptor with Ig and ITIM domains (TIGIT) and CTLA-4 [177, 178, 179, 180]. Also, loss of proliferative capacity and the transcriptional modulation of genes involved in metabolic pathways suppress T cell mediated killing [177, 178, 179]. This process is called T cell exhaustion and is important to prevent overstimulation of the immune sys-

tem, which could induce autoimmunity [177]. Tumor cells further induce the process of T cell exhaustion and immune evasion by inducing the expression of ligands specifically binding to co-inhibitory receptors on T cells [177]. For instance, PD-L1 and PD-L2, which are highly expressed on different tumor types, induce cell cycle arrest as well as a reduction in cytokine production upon PD-1 binding leading to suppression of antitumor immunity [50, 51, 181, 182, 183]. Another example is CD155. CD155 is widely expressed on cancer cells and is a ligand for TIGIT expressed on NK and T cells [184]. Loss of CD155 on cancer cells has been shown to enhance antitumor immunity and reduce tumor growth [185, 186, 187, 188].

T cell activation can also be compromised by terminally differentiated effector T regs, which infiltrate the TME and exert immunosuppressive functions [73, 84, 189, 190]. In this context, a high prevalence of T regs in different tumor types was linked to a poor prognosis in patients [190, 191, 192]. T regs possess elevated levels of CD25, CTLA-4, OX40, 4-1BB, TIGIT, glucocorticoid-induced tumor necrosis factor receptor (GITR), and PD-1 and thereby suppress activation of tumor associated antigen (TAA)-specific T cells [73, 190, 193, 194, 195].

Another immune compartment that can play a role in immune suppression is the myeloid cell lineage. Myeloid cells can differentiate into various cell types including DCs, macrophages and neutrophils and are essential in promoting an efficient innate immune response [196, 197]. However, it has been shown that chronic inflammation as well as the TME diminish the number of peripheral myeloid cells [196]. This induces migration and accumulation of not yet fully differentiated myeloid cells to the TME so-called myeloid-derived suppressor cells (MDSCs) [196]. MDSCs exhibit a strong immunosuppressive function [198], which has been reviewed in detail by Groth et al. [196]. Among other functions, MDSC have been shown to increase the number of other immunosuppressive cells like T regs, have high levels of negative immune checkpoint molecules including PD-L1 and deplete metabolites important for proper T cell function [196].

Macrophages that are present in the TME are referred to as tumor associated macrophages (TAMs) [199]. In healthy tissue, macrophages can be classified according to their specific functions. M1-like macrophages exhibit an effector function with the ability to kill pathogens, infected or cancer cells, whereas cell proliferation and tissue repair is supported by M2-like macrophages [200]. In early stages of the tumor, TAMs exhibit an M1-phenotype, suppressing tumor growth by expressing high levels of IL-12, IL-23, inflammatory cytokines and act as inducer and effector cells in the Th1 response [201, 202]. To avoid attack of macrophages, human cancer cells express the surface receptor CD47 - a “do not eat me” signal, recognized by macrophages through interaction with the signal regulatory protein α (SIRPα) thereby suppressing phagocytosis [203, 204, 205]. Specific blockade of this interaction has been shown to enhance survival, reduce tumor growth and

metastasis [206, 207]. On the other hand, TAMs can also resemble the phenotype and function of M2-macrophages [208]. Cancer cells foster the polarization into M2-like TAMs through the production of lactate thereby generating a hypoxic TME and stabilizing the transcription factor HIF1α, which induces expression of VEGF in TAMs [202, 209]. These alternatively activated TAMs promote tumor growth, angiogenesis and immunosuppressive functions and are distinct from M1-like TAMs in regards of receptor expression, cytokine production and antigen-presentation [202]. To name a few immunosuppressive mechanisms, TAMs have been shown to increase the level of PD-L1 and PD-L2 and, overexpress indoleamine 2,3-dioxygenase-1 (IDO1) leading to suppression of T cells and induction of angiogenesis [202, 208, 210].

2.3.2 Immunotherapy

Immunotherapies have been a great contribution for the treatment of different tumor types and have increased survival in patients [211]. There are three main classes of immunotherapeutic approaches. (1) The immune checkpoint blockade, that aims to release powerful T cell responses, (2) the adoptive cellular therapies, where specific anti-tumor immune cells are infused into the body, and (3) prophylactic or therapeutic cancer vaccines [211]. The immune checkpoint therapy is based on the blockade of negative regulators of the T cell activation. CTLA-4 and PD-1, are known as 'checkpoint molecules' and have been successfully targeted by various groups as treatment for cancer [211]. In particular, blockade of PD-L1 or direct engagement of its receptor PD-1 using antibody based therapies have shown promising anti-tumor effects in various cancer types [212, 213, 214]. While blockade of PD-1 stops interaction with its ligands PD-L1 and PD-L2 simultaneously, blockade of PD-L1 also exerts functions beyond preventing this interaction. In this context, PD-L1 has been shown to directly interact with other surface molecules found in antigen presenting cells such as B7.1 and thereby reduce proper T cell activation [215]. Further, antibodies for other co-inhibitory receptors including CTLA-4, TIGIT, TIM-3 and LAG3 have been developed and are in clinical trials as single agents or in combination with anti-PD-1 or anti-PD-L1 therapy [177, 216, 217, 218].

Adoptive cellular therapies are based on the infusion of autologous or allogeneic tumor specific T cells back into the cancer patient with the goal to specifically recognize, target and destroy tumor cells. One example is the genetic modification of T cells to express CARs. These CAR-T cells are not restricted to recognize an MHC:antigen complex, but can directly recognize a target molecule on the cell surface and initiate target cell killing.[211]

Another focus is the refinement of existing immunotherapies to enhance specific activation in the TME and thereby reduce the effect of immune-related adverse events (irAE) [177]. Examples include the development of pH-sensitive CTLA-4 antibodies that are released

from binding to CTLA-4 upon receptor internalization and thereby enhance recycling of CTLA-4 to the plasma membrane [219]. This process is essential to reduce irAE and to successfully deplete T regs [219]. Another interesting approach is the development of photoreactive Fc deficient CD25 antibodies depleting T regs specifically in the TME by applying light to the tumor location [220]. Interestingly, depletion of T regs induced CD8 and NK cell activation and potent tumor regression not only at the site of light application, but also at distinct sites of the body harboring the same tumor type [220].
It has to be noted that in some cases immunotherapy does not work as expected. One prominent distinction includes the differentiation between hot and cold tumors [221]. On one hand, hot tumors describe highly inflamed tumors with T cells and other immune cells infiltrating the TME. On the other hand, cold tumors are immune cell excluded with only a low number of T cells infiltrating the tumor and unable to provoke a strong immune response. Various treatment strategies involving immunotherapies have been shown to be more efficient in hot tumors rather than cold tumors.[221] Recent studies addressed some strategies to overcome this therapeutic challenge. For example, it has been shown that cold tumors can be converted into hot tumors by oncolytic virus therapy and sustained immune activation is mediated by additional PD-1 treatment [222, 223].

2.3.2.1 T cell bispecific Antibodies Checkpoint inhibitors discussed in the previous section can in some cases potently induce systemic activation of immune cells. One approach to specifically induce targeted attack of tumor cells is the use of bispecific T cell engagers (BiTEs) [224]. BiTEs consist of two single chain variable fragments (scFv) and simultaneously bind a TAA and cluster of differentiation 3 (CD3) on T cells in a 1:1 manner thereby generating a lytic immune synapse [224]. The CrossMab technology enables the generation of versatile bispecific antibodies through the crossover of individual light-chain as well as heavy-chain domains [225, 226]. This allows the interaction of TAA and CD3 in a bivalent (1:1), trivalent (2:1) or tetravalent (2:2) manner [225, 226]. Since these molecules are based on an IgG-like format containing an Fc-domain, they exhibit an extended half-life as compared to Fc-free BiTEs [225, 226].
One type of TAA is the carcinoembryonic antigen (CEA). CEA is a glycoprotein, which is a biomarker and overexpressed in various solid tumors including breast, colorectal, gastric, non-small cell lung and pancreatic cancer [227]. The CEA- T cell bispecific antibody (TCB) specifically binds two CEA molecules expressed on cancer cells as well as CD3 on T cells [228]. The 2:1 format enhances the binding of the molecule to cancer cells expressing high levels of CEA and thus enables target specificity [228]. Monovalent low affinity binding to CD3 prevents T cells from being activated in the periphery [228]. The crosslinking of target cells and T cells induces $CD4^+$ and $CD8^+$ T cell activation and proliferation, cytokine and granzyme release thereby inducing tumor cell lysis *in vitro*

and tumor regression *in vivo* [228, 229]. Hence, the CEA-TCB is a promising treatment option for cancer cells presenting high levels of CEA on the cell surface. *CEA* expression in normal tissue is mainly restricted to the colon where CEA faces the apical site [230] and due to tight junctions is inaccessible for therapeutic antibodies [227]. Currently, the CEA-TCB is being tested in clinical trials as single agent and in combination with the PD-L1 inhibitor Atezolizumab for treatment of solid tumors [227].

2.3.3 Combination of Epigenetic small molecule modifiers and immunotherapy

In line with other treatments including surgery, radiotherapy, chemotherapy and targeted therapy, immunotherapy is currently used as a standard of care treatment for various tumor types [231]. Despite promising treatment prognosis and T cell activation, it is likely that cancer cells also develop resistance to immunotherapy [232]. Epigenetic modifiers that target writers, readers and erasers induce transcriptional reprogramming of cells. The question arises if the combination of immunotherapy with epigenetic modifiers might be a promising treatment strategy to enhance tumor regression or overcome resistance to therapy. One example of a potential combination strategy describes the sensitization of cancer cells to immunotherapy through treatment with DNA methyltransferase inhibitors, which enhance the expression of genes in immunoregulatory pathways [233, 234, 235]. Furthermore, blockade of *de novo* DNA methylation has been shown to retain the effector function of terminally exhausted T cells and combination of a DNA demethylating agent with immunotherapy enhanced T cell expansion in this context [236].
In literature, it has been extensively described how epigenetic modifiers enhance antitumor immunity through either targeting immune cells directly or by enhancing immunogenicity of cancer cells [237]. Another interesting approach- and one aim of this thesis- is the use of epigenetic small molecule modifiers to sensitize cancer cells to T cell mediated cytotoxicity.

3 Aim of this Thesis

Epigenetic modulation of cancer cells give rise to changes in gene expression of tumor suppressors or oncogenes thereby enhancing tumor growth [16]. While various small molecule epigenetic modifiers exist, the effect of BETis was investigated in this thesis by specifically focusing on the small molecule inhibitor RG6146. Several research articles have described how BETis modulate the transcriptional landscape of cells. However, the holistic mechanism of how BETis shape the signaling of cancer cells, immune cells, and the interplay between the two, remains vastly unknown. The aim of this thesis was to assess the effect of RG6146 on (1) cancer cells intrinsically, (2) T cell activation and (3) the interface between both cell types (Figure 10).

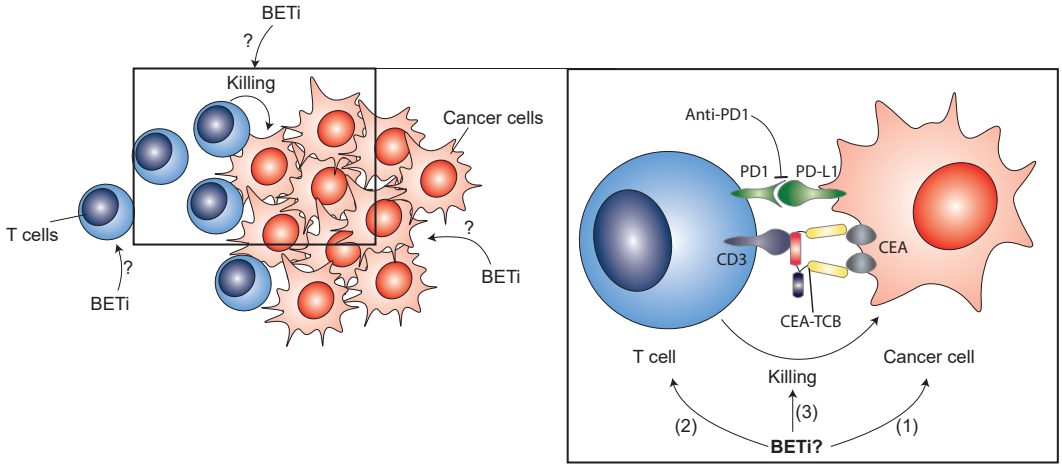

Figure 10: Effects of BETis were elucidated on (1) cancer cells intrinsically, on (2) the activation of T cells and (3) the interface between both cell types. The understanding of how BETis function on both cell types will also give insights into potential combination strategies with immunotherapy like anti-PD-1 or CEA-TCB treatment.

Effect of RG6146 on cancer cells:
The first part of this thesis will focus on why some Multiple Myeloma (MM) tumor models are resistant to RG6146 treatment. The focus was on three potential mechanisms of resistance including expression of the transcription factor c-Myc, pro- and anti-apoptotic proteins as well as presence of a drug export transporter.

Effect of RG6146 on Immune cells:
In literature the effect of BETis on T cells is of debate showing immunosuppressive and activating functions upon treatment [52, 53]. Therefore, the effect of RG6146 on T cell activation, function and proliferation was assessed using methods including a mixed lymphocyte reaction and a T reg suppression assay.

Effect of BETis on the interface between T cells and cancer cells:
The main part of this thesis will evaluate the effect of RG6146 in the interface between cancer and immune cells and a new mechanism on how to reprogram cells to be sensitized to TNF dependent cell death. This is of major interest in order to combine the effect of small molecules and immunotherapy and identify potential intertwined mechanisms that induce tumor regression in a synergistic manner.
Since RG6146 targets ubiquitously expressed BET proteins [25], the effect on non-cancerous cells as well as the comparison of RG6146 to other small molecule BETis was assessed, thereby showing a broader picture of the influence of BETis on cells.

4 Results

4.1 Cell intrinsic effects of BETis on Multiple Myeloma cells

Small molecule BETis were initially developed for the treatment of cancer. In order to understand how MM respond to BETi treatment, the effect of JQ1 and RG6146 on viability was tested *in vitro* on seven MM cell lines. To compare the effect of RG6146 with other pan-BET-inhibitors, OTX015, which is currently tested in Phase I clinical trials (NCT01713582; NCT02259114), was also included in this assay (Figure 11 A). Treatment with RG6146 showed the lowest IC_{50} values as compared to JQ1 or OTX015 treatment for three cell lines tested (Table 2). According to these IC_{50} values, KMS-34 and MM1S cells were the most resistant to BETi treatment (Figure 11 A).
Also, RG6146 enhanced cleaved PARP (cPARP) levels, indicating cell death, even though strength of cPARP induction varied among tested cell lines (Figure 11 B-C).

Table 2: IC_{50} values in µM of MM cell lines treated with different BETis. Calculation was performed with GraphPadPrism 8 of graphs shown in Figure 11 A

	IC_{50} (µM)		
Cell line	JQ1	RG6146	OTX015
OPM-2	0.09	0.002	0.002
MM1S	0.76	>10	0.95
KMS-12-BM	0.15	0.018	0.2
KMS-20	0.07	0.01	0.02
NCI-H929	0.18	0.01	0.04
KMS-11	0.01	0.015	0.01
KMS-34	0.17	0.69	0.08

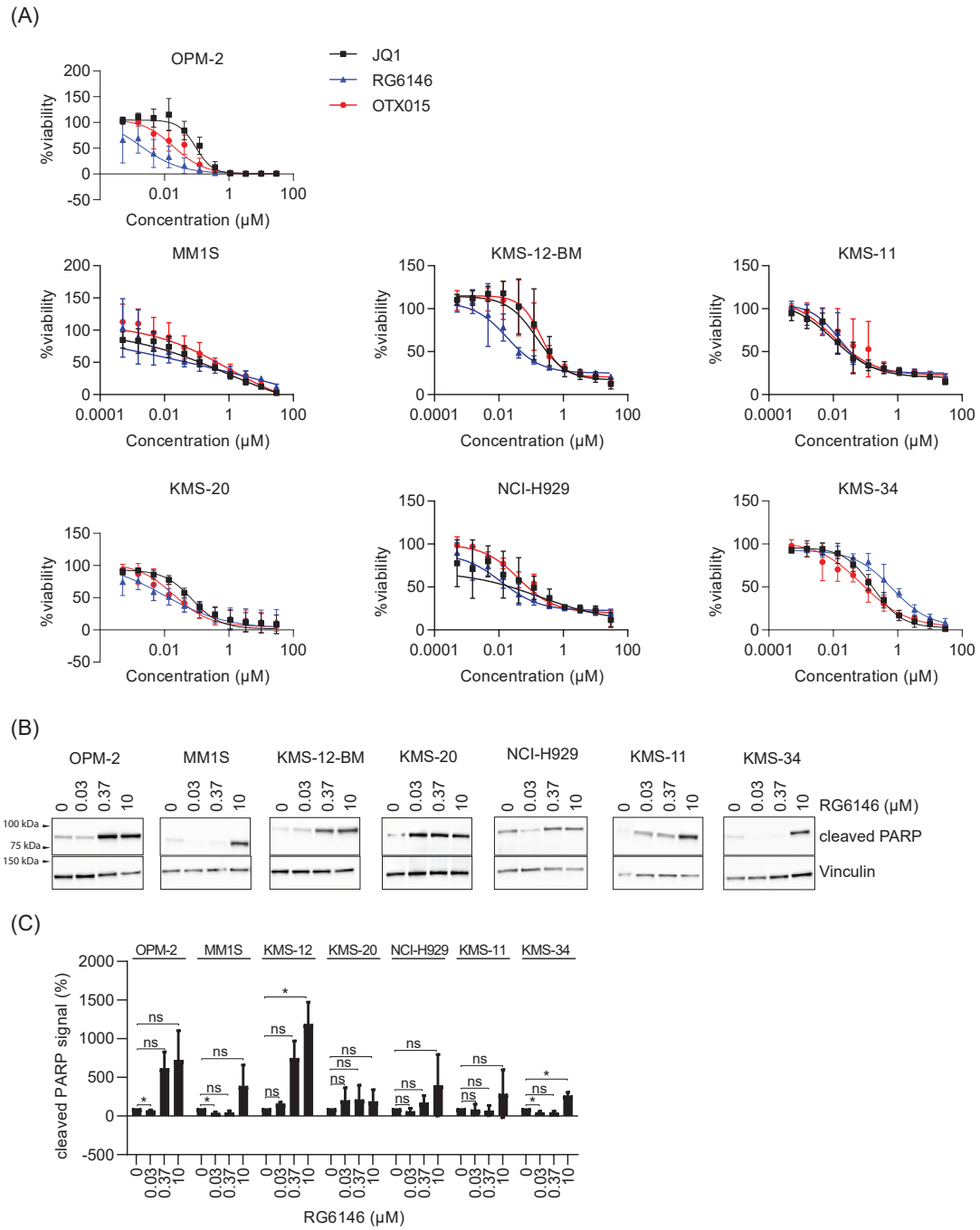

Figure 11: (A) Viability of MM cell lines treated for 72 h with BETis was analyzed by CellTiter-Glo2.0 (CTG2.0). Data was normalized to DMSO and represents mean of three independent biological experiments. (B) MM cell lines were treated with increasing concentration of RG6146 for 48 h and cleaved PARP or Vinculin as control were visualized by western blot. Data of one representative experiment is shown. (C) Cleaved PARP levels of three biological independent exepriments as described in *B* were quantified and normalized to DMSO. Data represents mean and statistical significance indicates difference between RG6146 and DMSO control (2-way ANOVA, *p<0.05, ns: not-significant).

The results of the *in vitro* findings were recapitulated *in vivo*. The group of Thomas Friess' tested different concentrations and routes of administration of RG6146 in the MM cell line OPM-2. Split dosing induced a similar efficacy as administration once daily (QD) (Figure 12 C). Six additional MM tumor models were treated with 30 mg/kg RG6146 QD or vehicle control (Figure 12 A). While RG6146 induced potent tumor growth inhibition (TGI) in five tumor models (responders), RG6146 treatment did not show an effect in the tumor models KMS-11 and KMS-34 (non-responders). While the resistance of KMS-34 to RG646 was comparable *in vitro* and *in vivo*, KMS-11 cells were only resistant to RG6146 treatment *in vivo* showing discrepancy with the previous *in vitro* data (Figure 11 A). MM1S cells showed the opposite phenotype with sensitivity to RG6146 *in vivo*, but not *in vitro* (Figure 11 A and 12 A). Furthermore, it was still unclear why responders showed such a strong sensitivity to BETi treatment *in vivo*, while non-responders were resistant.

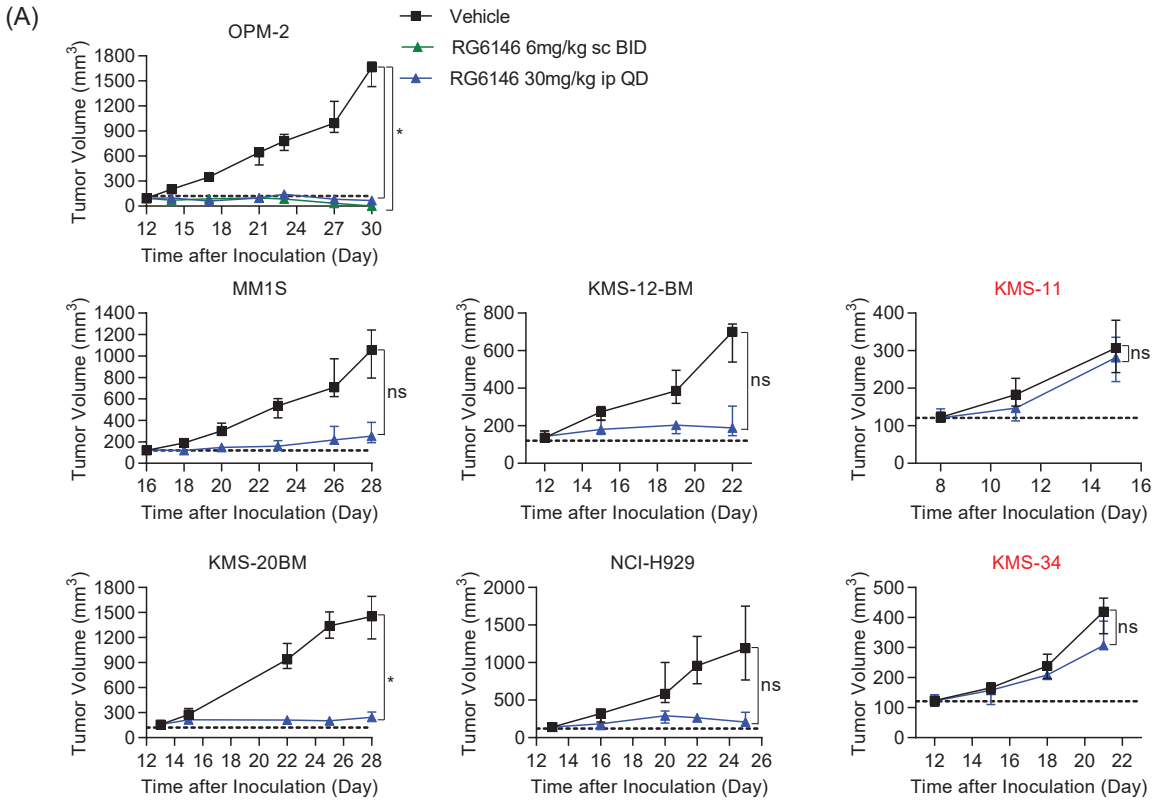

Figure 12: (A) CIA NOG mice bearing solid MM1S, KMS-12-BM, KMS-11 or KMS-34 tumor xenografts as well as SCID beige mice bearing solid OPM-2, KMS-20BM or NCI-H929 tumor xenografts (n=10 mice per treatment group) were treated once daily (QD) with 30 mg/kg RG6146 intraperitoneal (ip) injection or twice daily (BID) with 6 mg/kg RG6146 subcutaneous (sc) injection. Average tumor growth curve describe tumor volume in each treatment condition during the course of treatment. Statistical significance indicates difference between RG6146 and Vehicle control (Unpaired t-test (two-tailed P value), *p<0.05, ns: not-significant).

Three hypothesis were established, which potentially explain the inconsistency in sensitivity to RG6146 treatment between MM cell lines. (1) The first hypothesis describes a dependence on high level of the transcription factor c-Myc in responders, which is decreased upon RG6146 treatment. In this case, non-responders might not depend on c-Myc or do not suppress c-Myc by BETi treatment. (2) In the second hypothesis non-responders show an upregulation of the drug transporter ABCB1 (also known as P-gp, MDR1), which is known to remove RG6146 from the cytoplasm and thereby reduces sensitivity to treatment [238]. (3) In another hypothesis responders exhibit a high level of pro-apoptotic proteins as compared to non-responders. The downregulation of anti-apoptotic proteins by RG6146 would therefore tip the balance towards induction of cell death in responders. In contrast, non-responders might have a low level of pro-apoptotic proteins and reduction of anti-apoptotic proteins is not sufficient to induce programmed cell death.

4.1.1 The effect of RG6146 on c-Myc level

Enhanced expression of the transcription factor *MYC* is prevalent in many cancer types such as MM thereby inducing addiction to this protein [239]. However, transcription factors like c-Myc are known to be intrinsically unstructured, difficult to target and therefore often termed undruggable [40]. Nevertheless, BRD4 has been shown to bind to the super-enhancers of *IgH-MYC* rearrangements and BETis potently decrease c-Myc in MM cell lines harbouring such a rearrangement by displacing BRD4 from the *IgH* enhancer [26, 41]. To study if c-Myc is involved in conferring resistance to RG6146, *MYC* baseline expression, rearrangements of *MYC* with the *IgH* gene and changes of c-Myc level upon BETi treatment were assessed in responders and non-responders. First, the expression levels of *MYC* were assessed using the Roche-internal dataset CELLO containing RNA-seq data of the tested cell lines. No striking difference of *MYC* expression was seen between responders and non-responders (Table 3). Next, it was assessed if MM cell lines harbour a rearrangement of *MYC* with the *IgH* enhancer. For most responders a juxtaposition of *MYC* to the enhancer of *IgH* was prevalent, but this was also true for the non-responder cell line KMS-11 [240, 241]. The non-responder cell line KMS-34 and the responder cell line NCI-H929 do not have a translocation that place c-Myc and IgH next to each other (Table 3) indicating that juxtaposition of *MYC* and *IgH* are not involved in conferring resistance to RG6146.

Table 3: List of RG6146 efficacy in MM cell lines *in vivo* calculated through a tumor growth inhibition (TGI) greater than 80 % from data in Figure 12 A, *MYC* expression according to RNA-seq data in the Roche internal CELLO database as well as potential translocations of *MYC* with the *IgH* enhancer as described in [240, 241]

Cell line	Efficacy *in vivo* TGI > 80%	Myc Expression	juxtaposition of *MYC* gene to *IgH*
OPM-2	yes	178.06	yes
MM1s	yes	144.68	yes
KMS-12-BM	yes	325.67	yes
KMS-20	yes	168.2	-
NCI-H929	yes	131.11	No
KMS-11	no	260.48	yes
KMS-34	no	150.58	No

Since the baseline expression of *MYC* does not correlate with sensitivity to RG6146, it was tested how responders and non-responders modulate c-Myc level upon RG6146 treatment. c-Myc levels of all seven MM cell lines were assessed 48 h post treatment with RG6146 (Figure 13 A-B). RG6146 potently decreased c-Myc in all cell lines tested, with the non-responder cell line KMS-34 being the least sensitive. In conclusion, c-Myc levels and response to RG6146 did not differ between responders and non-responders, expression of this transcription factor might therefore not determine sensitivity to BETi treatment.

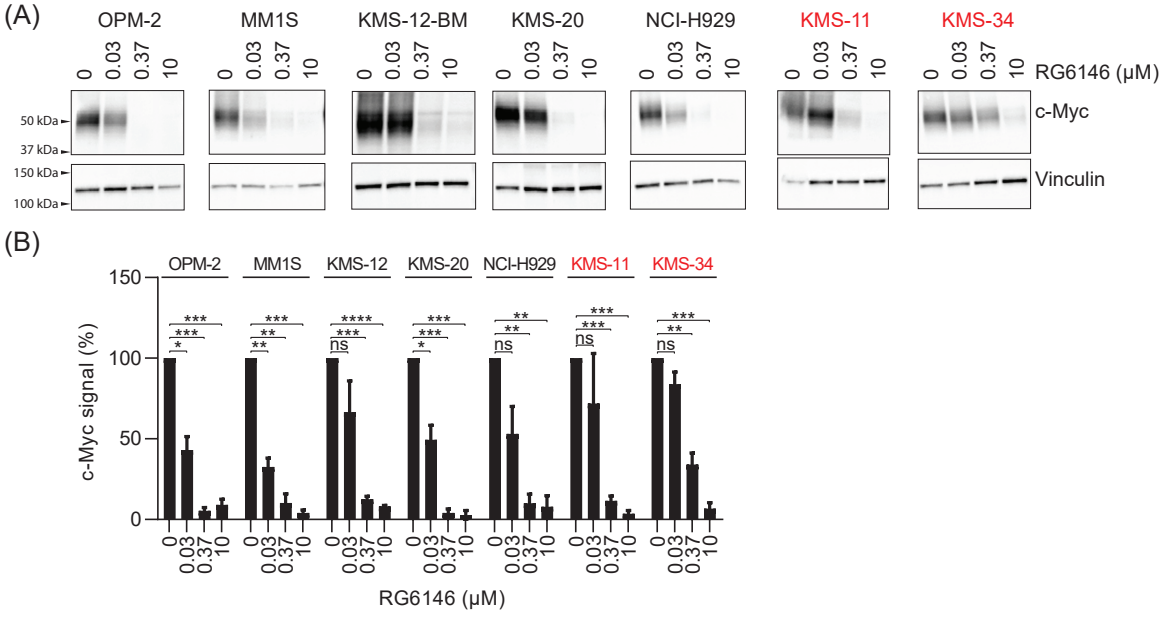

Figure 13: (A) MM cell lines were treated for 48 h with increasing concentration of RG6146 or control and c-Myc or Vinculin level were visualized by western blot. Data of one representative experiment is shown. (B) c-Myc levels of experiment described in *A* were quantified and results normalized to DMSO control. Mean of three biological independent experiments are shown. Statistical significance indicates difference between RG6146 and DMSO control (2-way ANOVA, *p<0.05, **p<0.01, ***p<0.001, ****p<0.0001, ns: not-significant).

4.1.2 ABCB1 confers resistance to RG6146 treatment in KMS-34 cells

ABCB1 is a p-glycoprotein transporter that actively removes small molecules from the cytoplasm and thereby induces drug resistance in a variety of cell lines [242]. RG6146 is a known substrate of this transporter and presence of ABCB1 generates resistance towards RG6146 treatment [238].

Therefore, the effect of RG6146 on ABCB1 level was assessed by western blot and flow cytometry in responders and non-responders (Figure 14 A-C). KMS-34 and MM1S cells exhibited a high baseline level of total ABCB1 protein, which was enhanced upon RG6146 treatment (Figure 14 A). However, cell surface level of ABCB1 was only induced by RG6146 in KMS-34 cells (Figure 14 B-C). To verify that ABCB1 confers resistance to RG6146 in KMS-34 cells, a non-toxic concentration of the P-gp inhibitor Zosuquidar (Figure 14 D) was combined with a dose response of RG6146 and viability assessed 72 h post treatment (Figure 14 E). While KMS-11 and MM1S cells did not modulate sensitivity to RG6146 upon ABCB1 blockade, interference of this efflux transporter in KMS-34 cells potently sensitized cells to RG6146 treatment. The combination of JQ1 and Zosuquidar hardly affected viability when compared to JQ1 single agent treatment (Figure 14 E). In summary, ABCB1 in KMS-34 cells induces resistance to RG6146 to some extent.

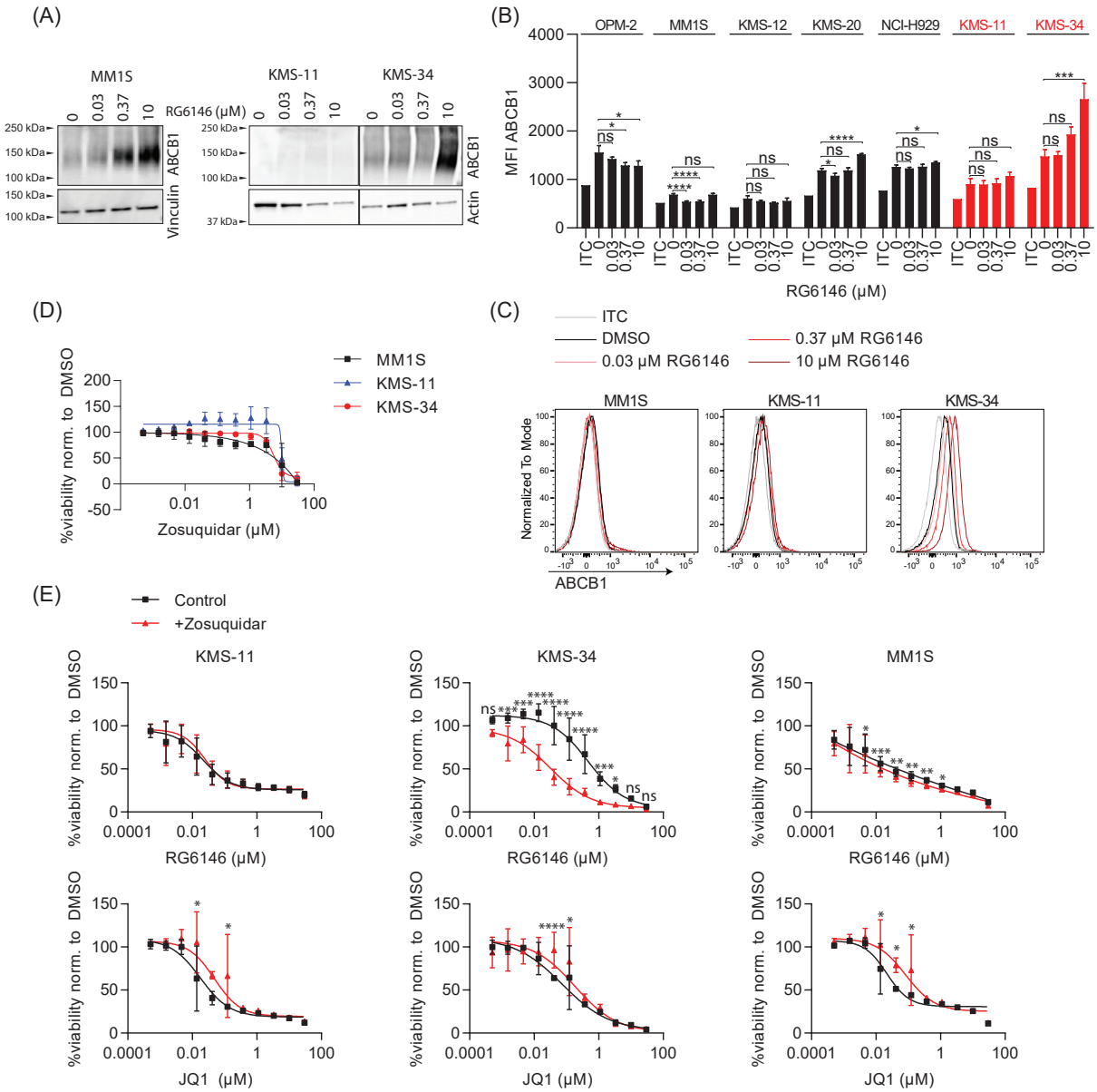

Figure 14: (A) Western blot to identify ABCB1 and Actin levels 48 h post treatment with RG6146 in MM1S, KMS-11 and KMS-34 cell lines (B) Flow cytometry of ABCB1 on MM cell lines treated with RG6146 or control for 48 h. Median Fluorescence Intensity (MFI) of ABCB1 is shown for three independent experiments. ITC: Isotype control. Statistical significance indicates difference between RG6146 and control (1-way ANOVA, *p<0.05, ***p<0.001, ****p<0.0001, ns: not-significant) (C) Representative histogram of data described in *B* (D) Viability of MM1S, KMS-11 and KMS-34 cell lines upon treatment with a dose response of Zosuquidar after 72 h of treatment was detected by CTG2.0. Data was normalized to DMSO and represents mean of three independent experiments. (E) Viability of MM1S, KMS-11 and KMS-34 cell lines upon treatment with a dose response of BETi alone or in combination with 0.5 µM Zosuquidar after 72 h of treatment was detected by CTG2.0. Data was normalized to DMSO and represents mean of three independent experiments. Statistical significance indicates difference between RG6146+Zosuquidar and RG6146 single agent treatment (2-way ANOVA, *p<0.05, **p<0.01, ***p<0.001, ****p<0.0001, if not shown: not-significant (ns))

4.1.3 The effect of RG6146 on pro- and anti-apoptotic proteins

The intrinsic cell death pathway is activated by multiple stimuli including hypoxia, toxins or radiation [99]. These stimuli eventually lead to mitochondrial outer membrane permeabilization (MOMP) through activation of Bid and other BH3-only proteins leading to oligomerization of BAX and BAK1 and pore formation in the outer mitochondrial membrane [243, 244, 245, 246, 247, 248, 249, 250]. This induces a loss in mitochondrial membrane potential and the release of mitochondrial proteins including cytochrome c into the cytosol [246, 251]. Cytochrome c forms a complex with Procaspase-9 and Apoptotic protease activating factor 1 (APAF-1) called the Apoptosome. This leads to activation of caspase-9 and subsequent cleavage of downstream effector caspases-3/7 [252, 253, 254]. The activation or suppression of the intrinsic apoptotic pathway is regulated through the Bcl-2 family of proteins consisting of pro- and anti-apoptotic proteins. Pro-apoptotic proteins are classified into activators (e.g. BIM, Bid and PUMA) and sensitizers (e.g. BAD, NOXA, BIK) [255, 256, 257, 258]. Activators are known to directly activate BAX and BAK1 to undergo conformational changes and oligomerization to induce MOMP [247, 255, 259]. Anti-apoptotic proteins (e.g. Bcl-2, Bcl-xL, and Mcl1) bind to activators and cytochrome c to inhibit induction of cell death [255, 257, 260, 261, 262, 263]. Sensitizers have been shown to neutralize anti-apoptotic proteins and thereby release activators to induce MOMP [255, 258].

Even though pro-apoptotic proteins are essential to induce programmed cell death, upregulation of anti-apoptotic proteins is one mechanism of cancer cells to inhibit apoptosis and promote cell survival [264]. BETis have been shown to modulate the level of pro- and anti-apoptotic proteins in Eμ-Myc lymphoma, MM and other tumors types [265, 266]. Therefore, it was assessed by western blot how RG6146 changes the expression of pro- and anti-apoptotic factors in responders versus non-responders (Figure 15 A-B).

Most cell lines tested showed a decrease of Bcl-2, PUMA and Bcl-xL. The pro-apoptotic factor BIM was strongly increased in most responders and the anti-apoptotic protein Mcl-1 was either unchanged or suppressed upon RG6146 treatment (Figure 15 A-B). In contrast, the non-responder cell line KMS-11 showed a trend in enhancing Mcl-1 level after 48 h of treatment (Figure 15 A-B). Consequently, it was tested if a combination of Mcl-1 and BET inhibition sensitizes non-responders to RG6146 treatment in a viability assay (Figure 16 A). The Mcl-1 inhibitor A-1210477 from the company Abbvie, showing potent binding to Mcl-1 [267], was used for combination studies with RG6146. The combination treatment did not show a synergistic effect. Only the highest concentration of A-1210477 enhanced sensitivity to RG6146 treatment (Figure 16 A).

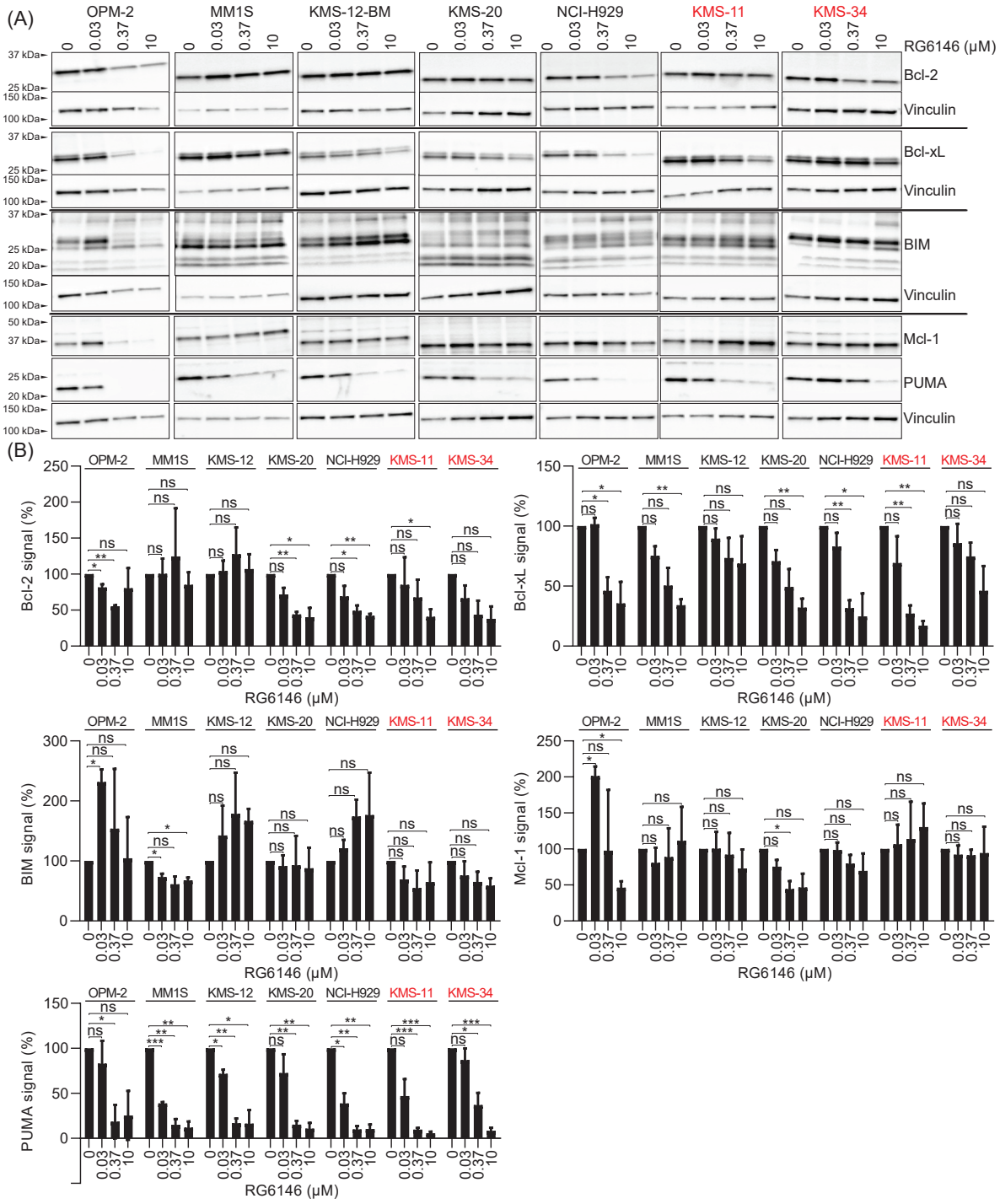

Figure 15: (A) MM cell lines were treated with increasing concentration of RG6146 for 48 h and levels of pro-(BIM, PUMA) or anti-apoptotic (Bcl-2, Bcl-xL, Mcl-1) proteins as well as Vinculin analyzed by western blot. Data of one representative experiment is shown. (B) Results of experiment described in *A* were quantified and normalized to DMSO control. Mean of three biological independent experiments is shown. Statistical significance indicates difference between RG6146 and DMSO control (2-way ANOVA, *p<0.05, **p<0.01, ***p<0.001, ns: not-significant).

While the anti-apoptotic protein Bcl-2 was decreased in most cell lines by RG6146 treatment, this protein was slightly enhanced in the KMS-12-BM cells under the same conditions (Figure 16 B). Using the Bcl-2 inhibitor Venetoclax in combination with RG6146, it was tested if growth inhibition could be further enhanced as compared to RG6146 single agent treatment (Figure 16 B). Indeed, combination treatment sensitized KMS-12-BM cells to RG146 treatment even further and these results could be verified by Thomas Friess's group *in vivo* (Figure 16 C).

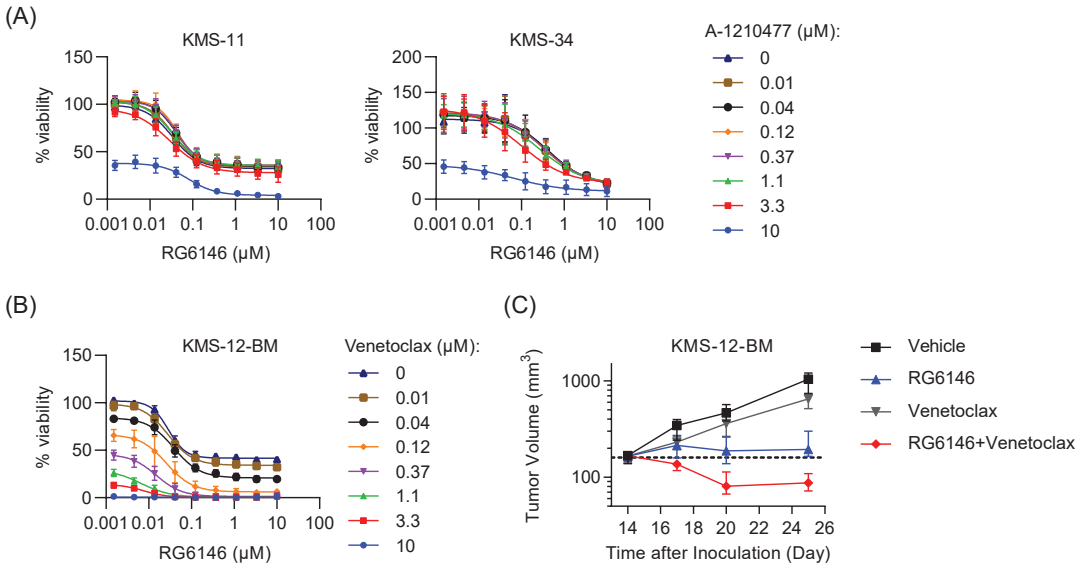

Figure 16: (A) Viability of KMS-11 and KMS-34 cell lines was determined by CTG2.0 after 72 h of treatment with a dose response of RG6146 alone or in combination with the Mcl-1 inhibitor A-1210477. Data was normalized to DMSO and represents mean of three independent experiments. (B) Viability of KMS-11 cells was determined by CTG2.0 after 72 h of treatment with a dose response of RG6146 alone or in combination with the Bcl-2 inhibitor Venetoclax. Data was normalized to DMSO and represents mean of three independent experiments. (D) CIA NOG mice bearing solid KMS-12-BM tumor xenografts (n=10 mice per treatment group) were treated QD with 30 mg/kg RG6146 (ip) or 100 mg/kg Venetoclax per os (po) or the combination. Average tumor growth curves describe tumor volume in each treatment condition during the course of treatment.

In conclusion, expression of pro- and anti-apoptotic proteins and their response to RG6146 treatment is vastly different between cell lines, which potentially explains the discrepancy in response to BETi treatment. However, no clear conclusion could be drawn regarding the role of pro- and anti-apoptotic protein levels mediating resistance of non-responders KMS-11 and KMS-34 to RG6146 *in vivo*. While it is important to assess the effect of BETi on cancer cell intrinsically, the effect on other cell types like immune cells should also be considered and will be presented in the next section.

4.2 The effect of RG6146 on Immune Cells

Since the development of the first BETi, the main research focus was to elucidate their effect on cancer cells. Only recently it has been acknowledged, that BETis modulate other cell types including immune cells [52, 53]. Controversial effects described for BETis in literature range from an immunosuppressive function, indicating promising therapeutics for autoimmune disease [52], to enhancing persistence of adoptively transferred CAR T cells [53]. However, the holistic effect of BETis is still not determined. Therefore, the effect of RG6146 on T cell activation was tested in different *in vitro* studies. These studies in combination with literature will contribute to the understanding of how BETis should be utilized in a clinical setting, and thereby ultimately enhance the therapeutic effect in patients.

4.2.1 RG6146 modulates T cell activation induced by CD3 and CD28 stimulation

To assess the effect of RG6146 on T cell activation *in vitro*, plates were coated with anti-CD3 and anti-CD28 antibodies. Pan-T cells (as described in 7.2.7) were added and treated with RG6146 or control for 4 days. T cell proliferation, viability and cell surface markers were analyzed by flow cytometry (Figure 17 A). A trend that RG6146 decreases T cell viability was visible, but not statistically significant (Figure 17 B). However, proliferation of both $CD4^+$ and $CD8^+$ cells was significantly decreased in a dose dependent manner upon RG6146 treatment (Figure 17 C-D).
Interestingly, a significant increase of CD69 levels on the cell surface of $CD4^+$ and $CD8^+$ cells was observed when treated with RG6146 (Figure 17 E-F), while the level of co-inhibitory receptors TIM3 and LAG3 were decreased (Figure 18 A-D). Further, a trend in RG6146 dependent downregulation of the inhibitory cell surface marker PD-1 was detected (Figure 18 E-F). These results indicate that RG6146 suppresses T cell activation after 4 days of treatment.

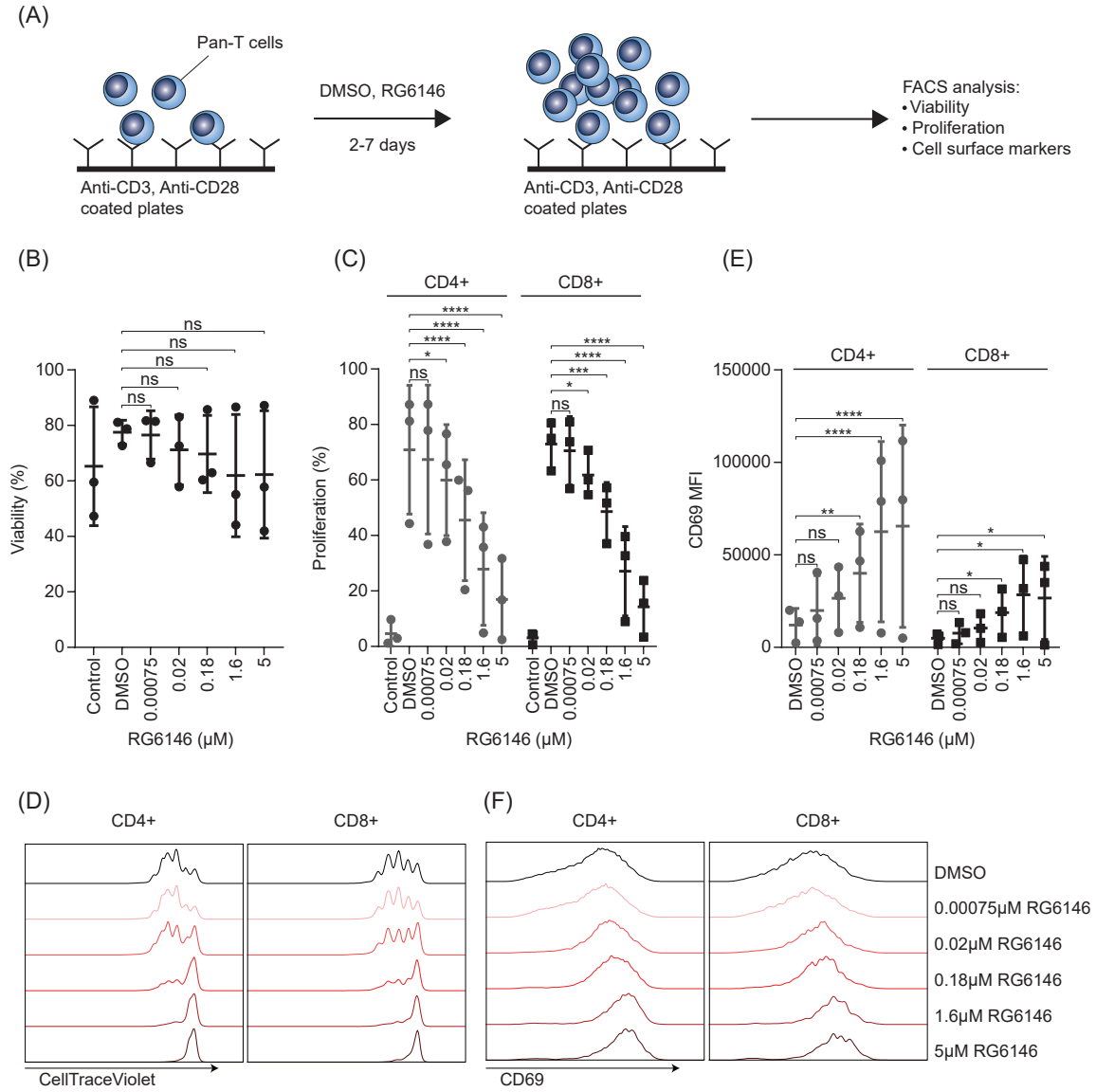

Figure 17: (A) Shematic of T cell proliferation assay. Pan-T cells isolated from PBMCs were activated through binding to anti-CD3 and anti-CD28 coated wells and incubated for 2-7 days with DMSO, RG6146 or untreated control. T cell viability, proliferation and cell surface markers were assessed on live single cells by flow cytometry. (B-F) Results of experiment described in *A* and treatment for 4 days (B) Percentage of viable Pan-T cells. Data represents three biological independent PBMC Donors. Statistical significance indicates difference between DMSO and RG6146 (2-way ANOVA, ns: not-significant). (C) Percentage of proliferating $CD4^+$ and $CD8^+$ T cells. Data represents three biological independent PBMC Donors. Statistical significance indicates difference between DMSO and RG6146 (2-way ANOVA, *p<0.05, ****p<0.0001, ns: not-significant). (D) Representative histograms of experiment described in *C*. (E) Median fluorescence intensity (MFI) of CD69 on $CD4^+$ and $CD8^+$ T cells. Data represents three biological independent PBMC Donors. Statistical significance indicates difference between DMSO and RG6146 (2-way ANOVA, *p<0.05, **p<0.01, ****p<0.0001, ns: not-significant). (F) Representative histograms of experiment described in *E*.

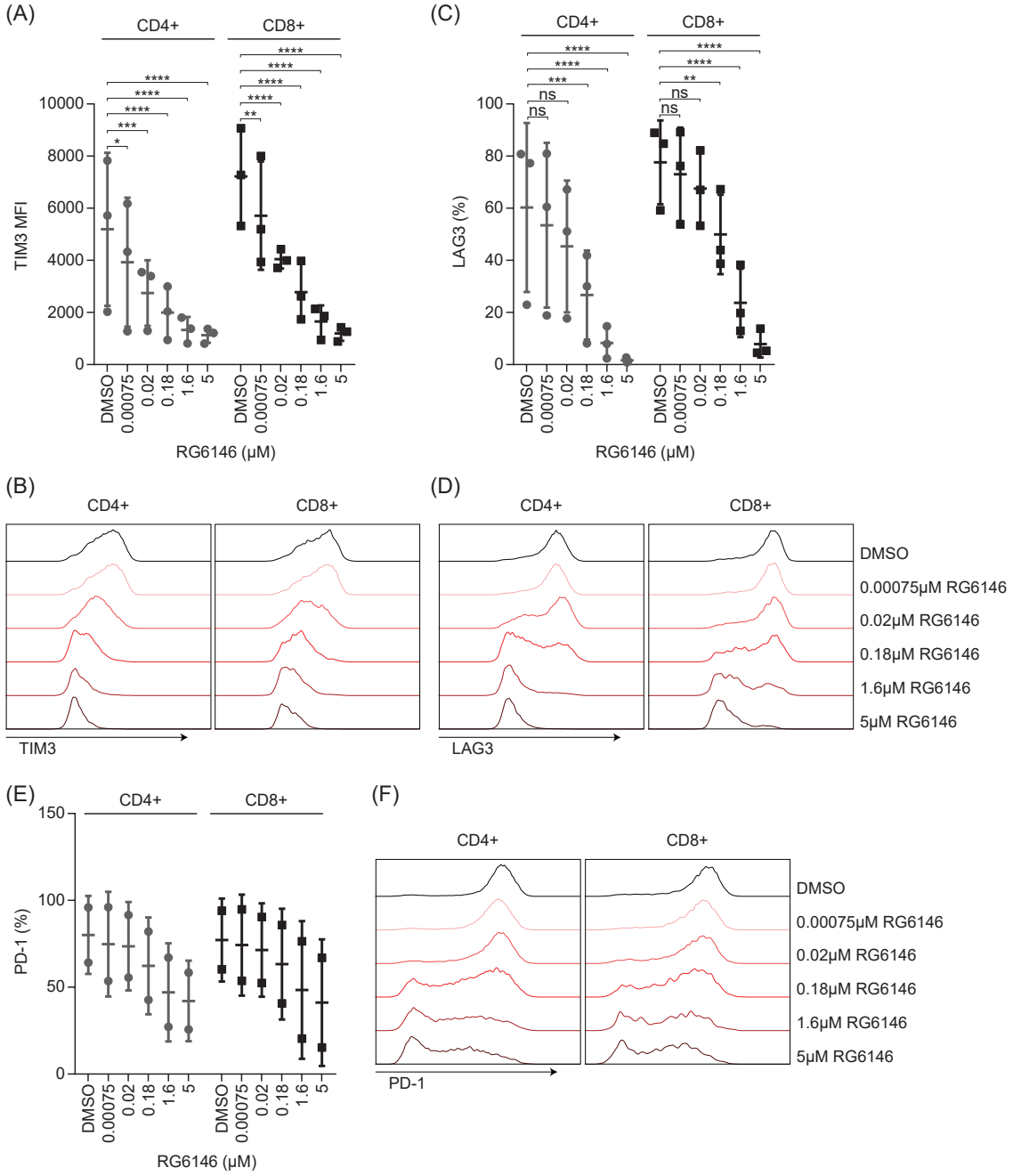

Figure 18: (A-F) Results of experiment described in *17 A* and 4 days of treatment. (A) Median fluorescence intensity (MFI) of TIM3 on $CD4^+$ and $CD8^+$ T cells. Data represents three biological independent PBMC Donors. Statistical significance indicates difference between DMSO and RG6146 (2-way ANOVA, *p<0.05, **p<0.01, ***p<0.001, ****p<0.0001). (B) Representative histograms of experiment described in *A*. (C) Percentage of $LAG3^+$ cells within $CD4^+$ and $CD8^+$ T cells. Data represents three biological independent PBMC Donors. Statistical significance indicates difference between DMSO and RG6146 (2-way ANOVA, **p<0.01, ***p<0.001, ****p<0.0001, ns: not significant). (D) Representative histograms of experiment described in *C*. (E) Percentage of $PD\text{-}1^+$ cells within $CD4^+$ and $CD8^+$ T cells. Data represents two biological independent PBMC Donors. (F) Representative histograms of experiment described in *E*.

Next, the effect of RG6146 on T cells was assessed in a time dependent manner during T cell activation (Figure 19-21). Since T cell proliferation was not visible after 2 days of RG6146 treatment (Data not shown), we focused on modulation of the activation markers CD69 and CD25 (Figure 19). While T cell viability was unchanged (Figure 19 A), a trend in upregulation of CD69 and downregulation of CD25 was visible after 2 days of treatment (Figure 19 B-E).

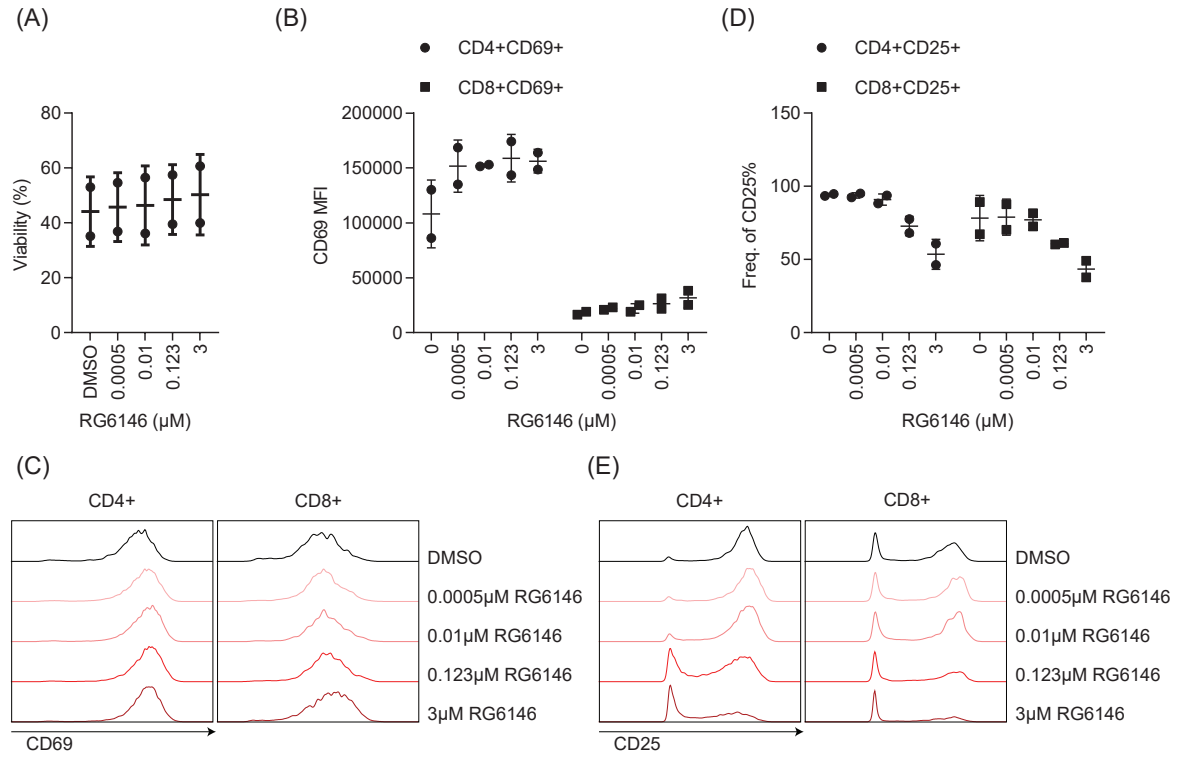

Figure 19: (A-E) Experimental set up as described in *17 A* using 2 days of treatment. (A) Percentage of viable Pan-T cells. Data represents two independent biological PBMC Donors. (B) Median fluorescence intensity (MFI) of CD69 on $CD4^+$ and $CD8^+$ T cells. Data represents two biological independent PBMC Donors. (C) Representative histograms of experiment described in *B*. (D) Percentage of $CD25^+$ cells within $CD4^+$ and $CD8^+$ T cell subsets. Data represents two biological independent PBMC Donors (E) Representative histograms of experiment described in *D*.

Treatment of T cells with RG6146 for 5 days did not affect viability and changed CD69 and CD25 level only at the highest concentration tested (Figure 20 A-E). Total proliferation was only marginally decreased by RG6146, however, $CD4^+$ and $CD8^+$ cells treated with high concentrations of RG6146 had undergone less cell divisions as compared to T cells treated with control (Figure 20 F-G).

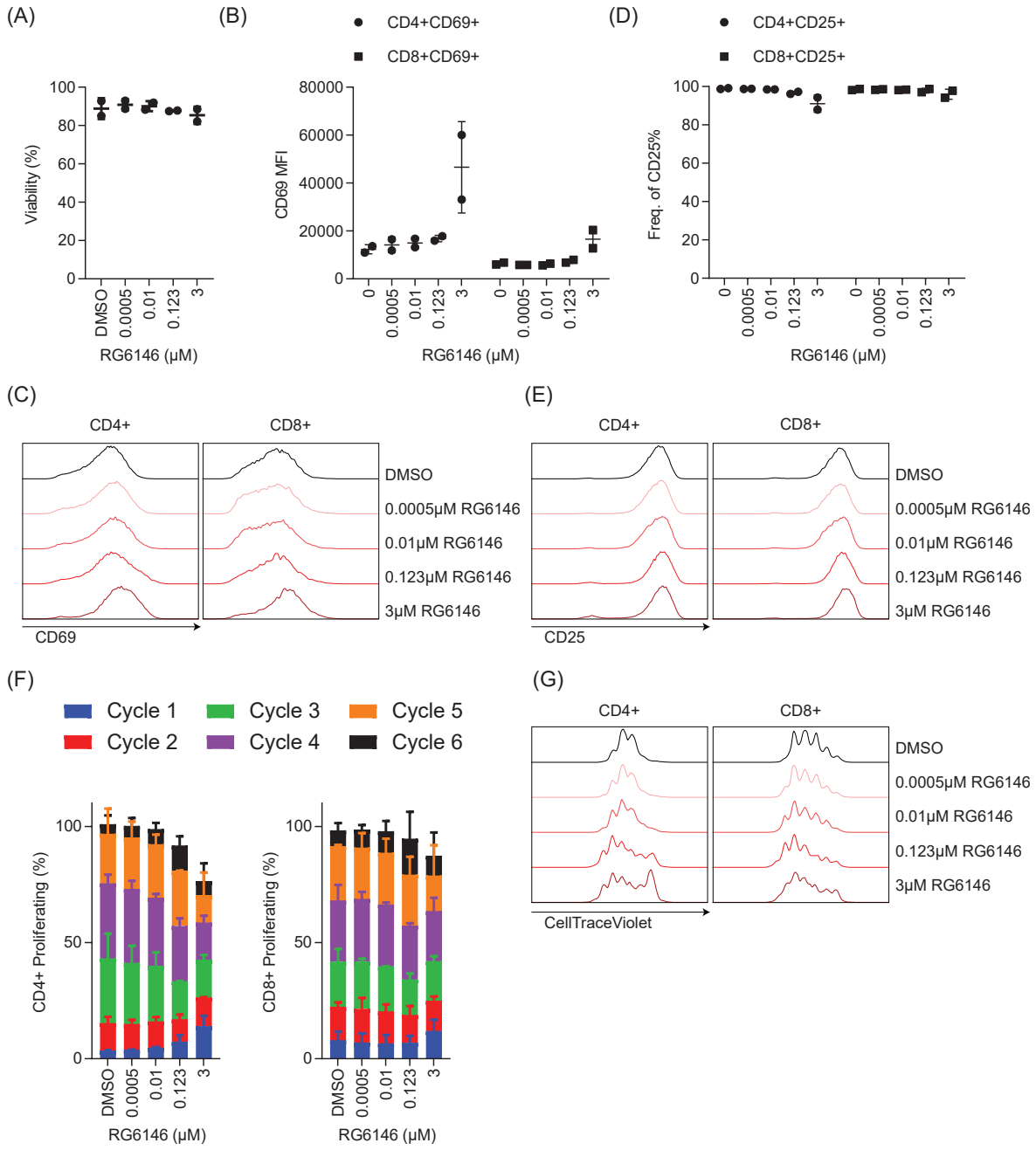

Figure 20: (A-G) Experimental set up as described in *17 A* using 5 days of treatment. (A) Percentage of viable Pan-T cells. Data represents two independent biological PBMC Donors. (B) Median fluorescence intensity (MFI) of CD69 on $CD4^+$ and $CD8^+$ T cells. Data represents two biological independent PBMC Donors. (C) Representative histograms of experiment described in *B*. (D) Percentage of $CD25^+$ cells within $CD4^+$ and $CD8^+$ T cell subsets. Data represents two biological independent PBMC Donors (E) Representative histograms of experiment described in *D*. (F) Percentage of proliferating $CD4^+$ and $CD8^+$ T cells. Proliferation cycle was determined through a dilution of Cell Trace Violet staining. Data represents mean of two biological independent PBMC Donors. (G) Representative histograms of experiment described in *F*.

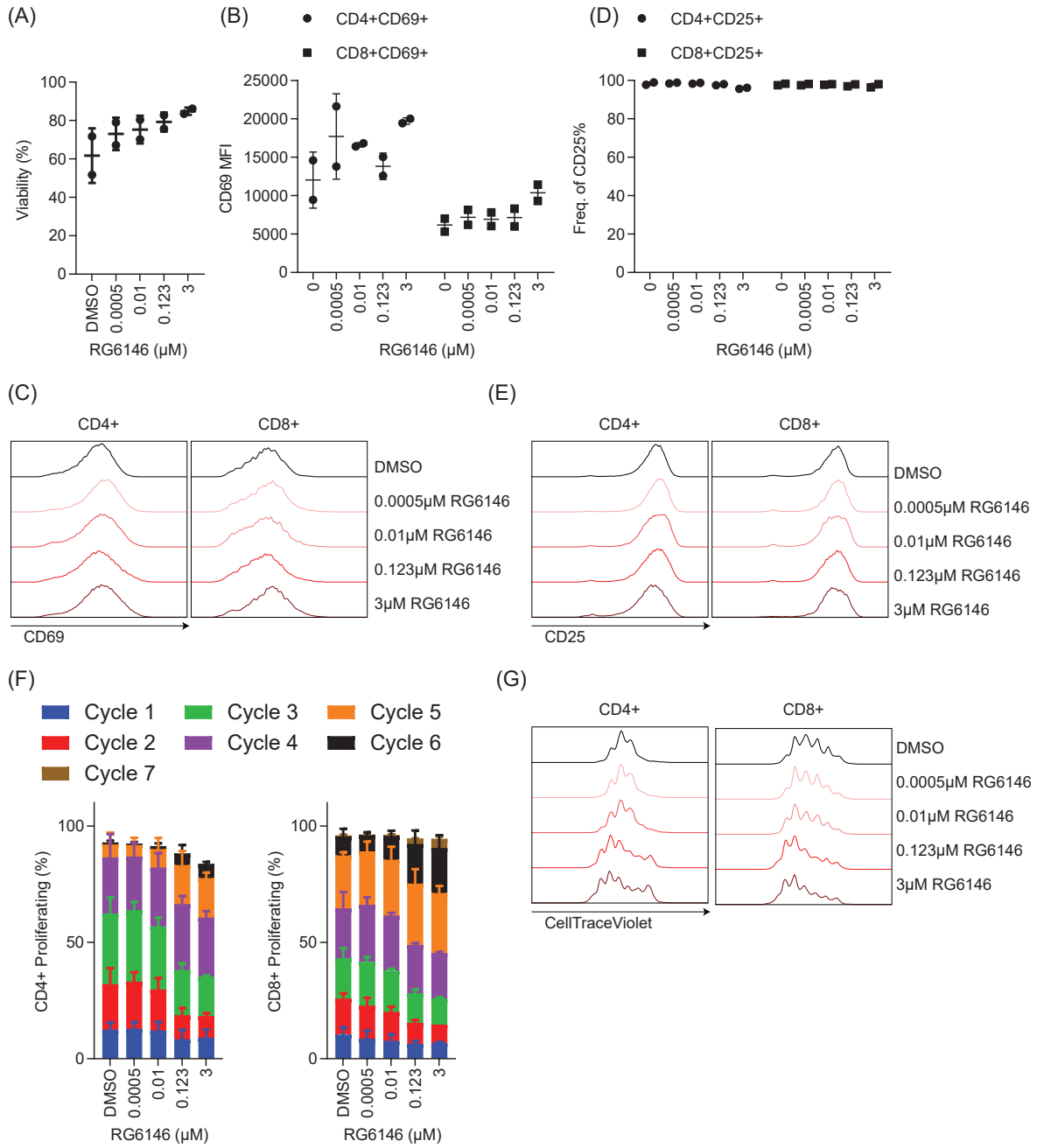

Figure 21: (A-G) Experimental set up as described in *17 A* and 7 days of treatment. (A) Percentage of viable Pan-T cells. Data represents two independent biological PBMC Donors. (B) Median fluorescence intensity (MFI) of CD69 on $CD4^+$ and $CD8^+$ T cells. Data represents two biological independent PBMC Donors. (C) Representative histograms of experiment described in *B*. (D) Percentage of $CD25^+$ cells within $CD4^+$ and $CD8^+$ T cell subsets. Data represents two biological independent PBMC Donors (E) Representative histograms of experiment described in *D*. (F) Percentage of proliferating $CD4^+$ and $CD8^+$ T cells. Proliferation cycles were determined through a dilution of Cell Trace Violet staining. Data represents mean of two biological independent PBMC Donors. (G) Representative histograms of experiment described in *F*.

A treatment period of 7 days enhanced viability and CD69 level, while CD25 level was unaffected (Figure 21 A-E). Interestingly, total number of proliferating $CD8^+$ cells was unchanged by RG6146, but T cells had undergone more division cycles than DMSO control treated cells (Figure 21 F-G).
These experiments suggest that RG6146 does not affect viability at the concentrations tested, but delays activation and proliferation of T cells especially at earlier time points. Longer treatment periods of RG6146, however, provoked an increase in proliferation when compared to treatment control.

4.2.2 The effect of RG6146 on T cell activation using a Mixed Lymphocyte Reaction

Activation of T cells using anti-CD3 and anti-CD28 is a potent way to analyze the effect of RG6146 on $CD4^+$ and $CD8^+$ T cells. Nevertheless, to verify these results it is important to assess the effect of RG6146 on T cell activation in an additional experimental setting such as the MLR.
The first step in the set up of the MLR, is the generation of DCs from $CD14^+$ monocytes isolated from PBMCs (Donor 1) (Figure 22 A). Addition of IL-4 and GM-CSF induces formation of immature DCs indicated by a decrease of CD14 and slight increase in CD40 and PD-L1 on the cell surface after four days (Figure 22 B). Longer treatment (5 days) with IL-4 and GM-CSF induced upregulation of MHC II, CD40 and CD86 (Figure 22 B). Mature DCs were generated upon addition of IL-4, GM-CSF, LPS and IFNγ for 16 h to immature DCs (4 days). Treatment with these cytokines enhanced the presentation of most tested surface markers except CD14 (Figure 22 B). Next, the effect of RG6146 on immature (day 5, control) and mature DCs (+LPS, IFNγ) was assessed. High concentrations of RG6146 decreased maturation by suppressing co-stimulatory markers CD80, CD86 and CD40 and the co-inhibitory marker PD-L1 (Figure 22 C). Since lower concentrations of RG6146 hardly affected DC maturation, a sub-micromolar concentration range of this BETi was used for the MLR.

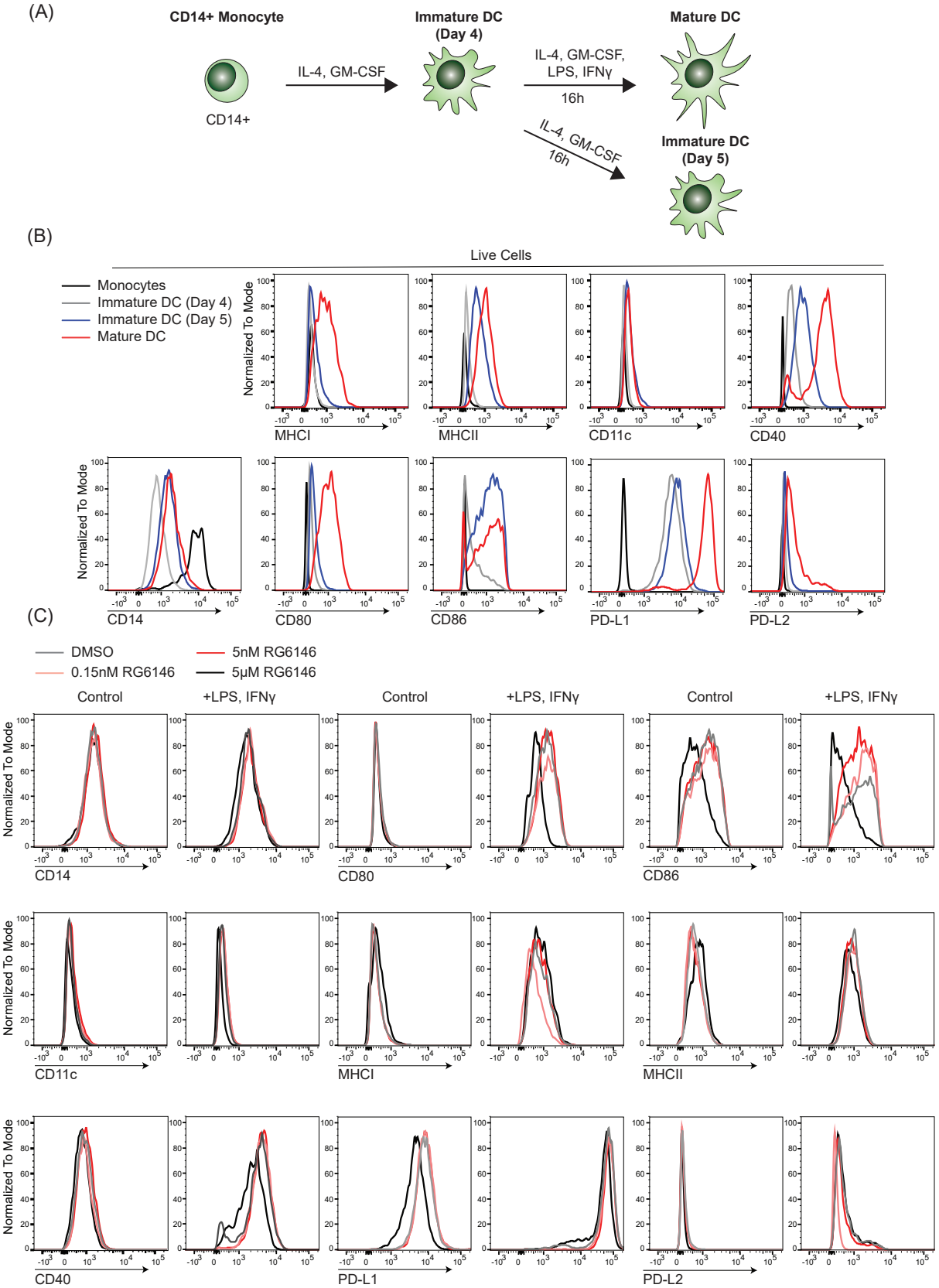
(A)
CD14+ Monocyte
CD14+
IL-4, GM-CSF
Immature DC (Day 4)
IL-4, GM-CSF, LPS, IFNγ
16h
Mature DC
IL-4, GM-CSF
16h
Immature DC (Day 5)
(B)
Live Cells
Monocytes
Immature DC (Day 4)
Immature DC (Day 5)
Mature DC
Normalized To Mode
MHCI
MHCII
CD11c
CD40
CD14
CD80
CD86
PD-L1
PD-L2
(C)
DMSO
0.15nM RG6146
5nM RG6146
5μM RG6146
Control
+LPS, IFNγ
Normalized To Mode
CD14
CD80
CD86
CD11c
MHCI
MHCII
CD40
PD-L1
PD-L2

Figure 22: (A) Shematic of the DC maturation process. Treatment of $CD14^+$ monocytes with IL-4 and GM-CSF induces formation of immature DCs. Further addition of IL-4, GM-CSF, LPS and IFNγ induces the formation of mature DCs. (B) Histograms of cell surface markers determined by flow cytometry of live single cells at different stages within the DC maturation process. Data represents one experiment. (C) The effect of RG6146 treatment on DC maturation and cell surface markers was assessed on immature DCs on Day 5 (Control) and mature DCs (+LPS, IFNγ) using flow cytometry of live single cells. Histograms of one biological experiment are shown.

In the MLR experiment, pan-T cells isolated from PBMCs (Donor 2) would not primarily recognize foreign antigens on MHC molecules, however, T cells recognize the DCs from a foreign Donor (Donor 1) and thereby get activated (Figure 23 A). Next, a suboptimal ratio of DCs:T cells was assessed by testing CD69 level and proliferation of T cells after 8 days. Identification of a suboptimal ratio is important to see potential effects of RG6146 on CD69 level and T cell proliferation in the following experiments. At a ratio of 1:40 (DCs:T cells), a trend in CD69 upregulation and T cell proliferation was visible (Figure 23 B-C). To further validate and verify these findings, a different PBMC Donor for T cell isolation was tested and T cell proliferation was assessed after 5 and 7 days (Figure 23 D-E). Repeatedly, the ratio of 1:40 DCs:T cells showed the most promising results as a suboptimal condition for T cell activation, but the selected time points were not ideal (Figure 23 D-E). After 5 days T cell proliferation was not yet detectable, while 7 days induced a strong T cell proliferation. Therefore, it was decided to use an assay length of 6.5 days to measure the effect of RG6146 on T cell activation in the MLR setting.
$CD4^+$ and $CD8^+$ T cell proliferation, CD69 and PD-1 level were analyzed by flow cytometry upon co-culture with DCs and treatment with sub-micromolar concentrations of RG6146 for 6.5 days. As a positive control, anti-PD-1, anti-LAG3 antibodies as well as untreated Pan-T cells stimulated with anti-CD3 and anti-CD28 were added to the co-culture (Figure 23 F-I). A small increase in $CD8^+$ T cell proliferation (Figure 23 F-G) and CD69 levels (Figure 23 H-I) was visible upon treatment with anti-PD-1 and anti-LAG3 molecules. RG6146 did not affect levels of any surface marker. In general, proliferation of both $CD4^+$ and $CD8^+$ T cells was low and therefore no clear statement can be made on how proliferation is changed by the different treatment regimens (Figure 23 F-G).
In summary, RG6146 treatment suppressed maturation of DCs, but no clear conclusion could be drawn on the BETi dependent effect on T cell proliferation in the MLR setting. So far it was shown that RG6146 has a rather negative effect on immune cell activation and maturation. Next, we wanted to know if RG6146 also modulates the immune suppressive function of T regs.

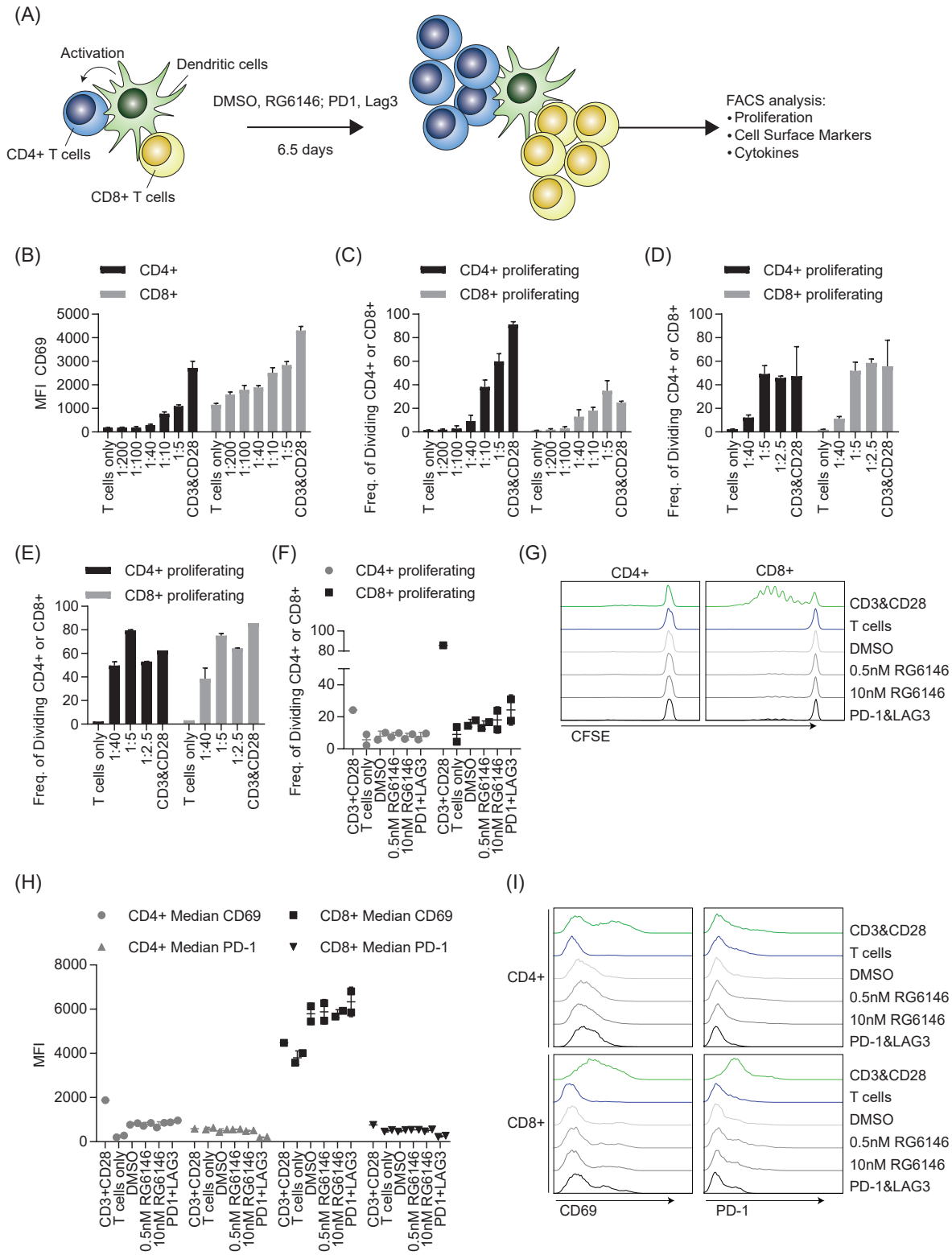
(A)
Activation
Dendritic cells
CD4+ T cells
CD8+ T cells
DMSO, RG6146; PD1, Lag3
6.5 days
FACS analysis:
• Proliferation
• Cell Surface Markers
• Cytokines
(B)
CD4+
CD8+
MFI CD69
(C)
CD4+ proliferating
CD8+ proliferating
Freq. of Dividing CD4+ or CD8+
(D)
CD4+ proliferating
CD8+ proliferating
Freq. of Dividing CD4+ or CD8+
(E)
CD4+ proliferating
CD8+ proliferating
Freq. of Dividing CD4+ or CD8+
(F)
CD4+ proliferating
CD8+ proliferating
Freq. of Dividing CD4+ or CD8+
(G)
CD4+
CD8+
CD3&CD28
T cells
DMSO
0.5nM RG6146
10nM RG6146
PD-1&LAG3
CFSE
(H)
CD4+ Median CD69
CD8+ Median CD69
CD4+ Median PD-1
CD8+ Median PD-1
MFI
(I)
CD4+
CD8+
CD3&CD28
T cells
DMSO
0.5nM RG6146
10nM RG6146
PD-1&LAG3
CD69
PD-1

Figure 23: (A) Shematic of mixed lymphocyte reaction assay. DCs were co-cultured with Pan-T cells thereby activating $CD4^+$ and $CD8^+$ T cell subsets. The effect of RG6146 and checkpoint inhibitors anti-PD-1, anti-LAG3 (PD-1, LAG3) treatment on T cell activation was monitored by flow cytometry of live single cells. (B) Different ratios of DCs:Pan-T cells were used to determine the median fluorescence intensity (MFI) of CD69 within $CD4^+$ and $CD8^+$ T cell subsets by flow cytometry after 8 days of set up. As a control a T cell monoculture was either untreated (T cells only) or incubated with anti-CD3 and anti-CD28 coated wells (CD3&CD28). Mean of technical triplicates of one experiment is shown. (C-E) Different ratios of DCs:Pan-T cells were used to determine the percentage of proliferating cells within $CD4^+$ and $CD8^+$ T cell subsets by flow cytometry after (C) 8 days, (D) 5 days and (E) 7 days of set up. As a control a T cell monoculture was either untreated (T cells only) or incubated with anti-CD3 and anti-CD28 coated wells (CD3&CD28). Data represents mean of three technical replicates of one experiment. (F) Percentage of proliferating cells within $CD4^+$ and $CD8^+$ T cell subsets upon treatment with RG6146, 10 µg/mL anti-PD-1 and anti-LAG3 (PD-1+LAG3) or anti-CD3, anti-CD28 (CD3+CD28) antibodies were determined by flow cytometry. A ratio of 1:40 (DCs:Pan-T cells) was used and data represents two biological independent experiments. (G) Representative histograms of data described in *F*. (H) MFI of CD69 and PD-1 within $CD4^+$ and $CD8^+$ T cell subsets upon treatment with RG6146, 10 µg/mL anti-PD-1 and anti-LAG3 or anti-CD3, anti-CD28 antibodies (CD3+CD28) were determined by flow cytometry. A ratio of 1:40 (DCs:Pan-T cells) was used and data represents two biological independent experiments. (I) Representative histograms of data described in *H*.

4.2.3 The effect of RG6146 on T cell suppressive functions

As described in literature, BETis are potential therapies for autoimmune diseases [52]. It was assessed, if RG6146 augments suppressive behavior of T regs or modulates activation of $CD4^+$ T convs (Figure 24 A-B). T convs (Donor 1) and irradiated $CD4^-$ cells (Donor 2) were co-cultured inducing proliferation of T convs by about 30 % (Figure 24 A & D). Addition of anti-PD-1&anti-LAG3 (PD-1LAG3) or anti-PD-1&anti-TIM3 (PD-1TIM3) antibodies, which were used as a positive control, did not change viability or proliferation of T convs (Figure 24 C-D). However, high concentrations of RG6146 alone and in combination with PD-1LAG3 or PD-1TIM3 reduced viability by about 10 % and proliferation by about 20 % after 5 days of treatment, which is in line with findings described in the previous section (Figure 24 C-D).
Since addition of T regs to the culture of T convs and $CD4^-$ cells suppresses activation of T convs, it is possible to assess how blocking antibodies and BETis modulate this effect (Figure 24 B). Viability of T convs and T regs was unchanged by PD-1LAG3, PD-1TIM3 and low concentrations of RG6146 treatment (Figure 25 A-B). However, high concentrations of RG6146 decreased viability and proliferation of T convs by about 10 % and 20 %, respectively (Figure 25 C). Since this effect was also visible for T convs without the addition of T regs, RG6146 induced suppression of T conv proliferation is most likely independent from T regs. Nonetheless, the suppression of $CD4^+$ cells by RG6146 is in line with our findings described in section 4.2.1.
In addition to proliferation, production and release of cytokines are further indicators of T cell activation. Intracellular and released granzyme B and IFNγ levels were strongly suppressed by addition of T regs (untreated control) (Figure 26 A-D). Granzyme B suppression was abrogated upon addition of blocking antibodies, however, RG6146 treatment alone and in combination with blocking antibodies dampened this effect indicating that RG6146 suppresses activation of T convs (Figure 26 A). A similar effect was measured for IFNγ at high RG6146 concentrations (Figure 26 B). Only a trend of increased MIP1α and TNF concentration in the supernatant of the co-culture was visible when treated with RG6146 (Figure 26 E-F). FasLigand was completely unaffected by T regs or compound treatment (Figure 26 G).
Taken together, RG6146 slightly decreased viability of T cells and strongly suppressed T cell proliferation especially at earlier time points. This phenotype was restored after longer incubation time. To assess if the negative effect of RG6146 on T cell activation also plays a role in the context of T cell mediated cancer cell killing will be analyzed in the following section.

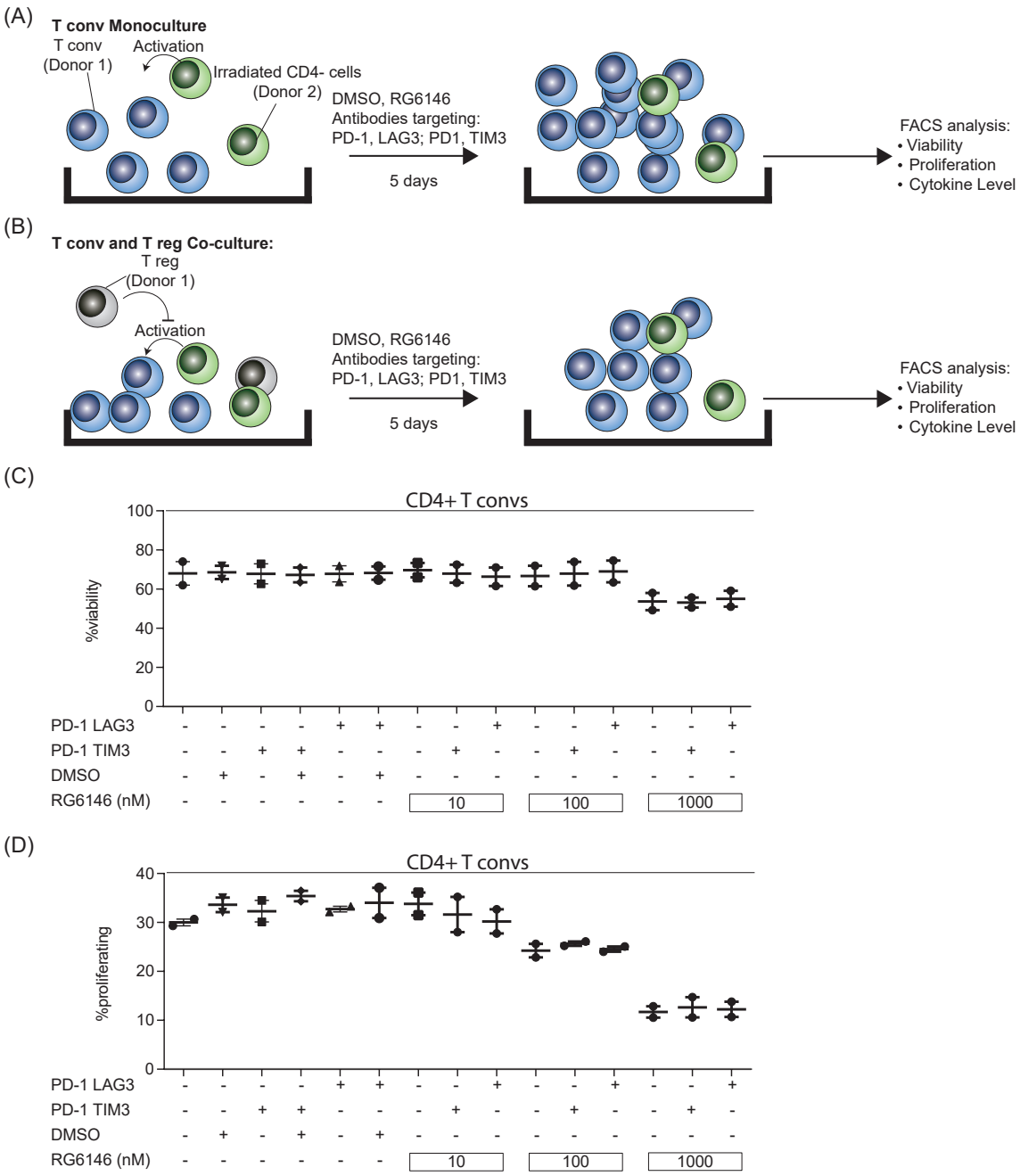

Figure 24: (A-B) Shematic of T reg suppression assay. (A) Conventional T cells (T convs) of PBMC Donor 1 were co-cultured with $CD4^{-}$- cells of PBMC Donor 2 leading to the activation of T convs. Viability, proliferation and cytokine level were assessed by flow cytometry of live single cells upon treatment with checkpoint inhibitors (10 µg/mL anti-PD-1 (PD-1), anti-TIM3 (TIM3), anti-LAG3 (LAG3)) or RG6146. (B) As described in *A* except that regulatory T cells (T regs) of PBMC Donor 1 were added to the co-culture thereby inhibiting the activation of T convs. (C-D) Assay set up as described in *A*. Percentage of (C) viable and (D) proliferating T convs was assessed by flow cytometry upon treatment with checkpoint inhibitors, RG6146 or control. Data of two biological independent Donors is shown.

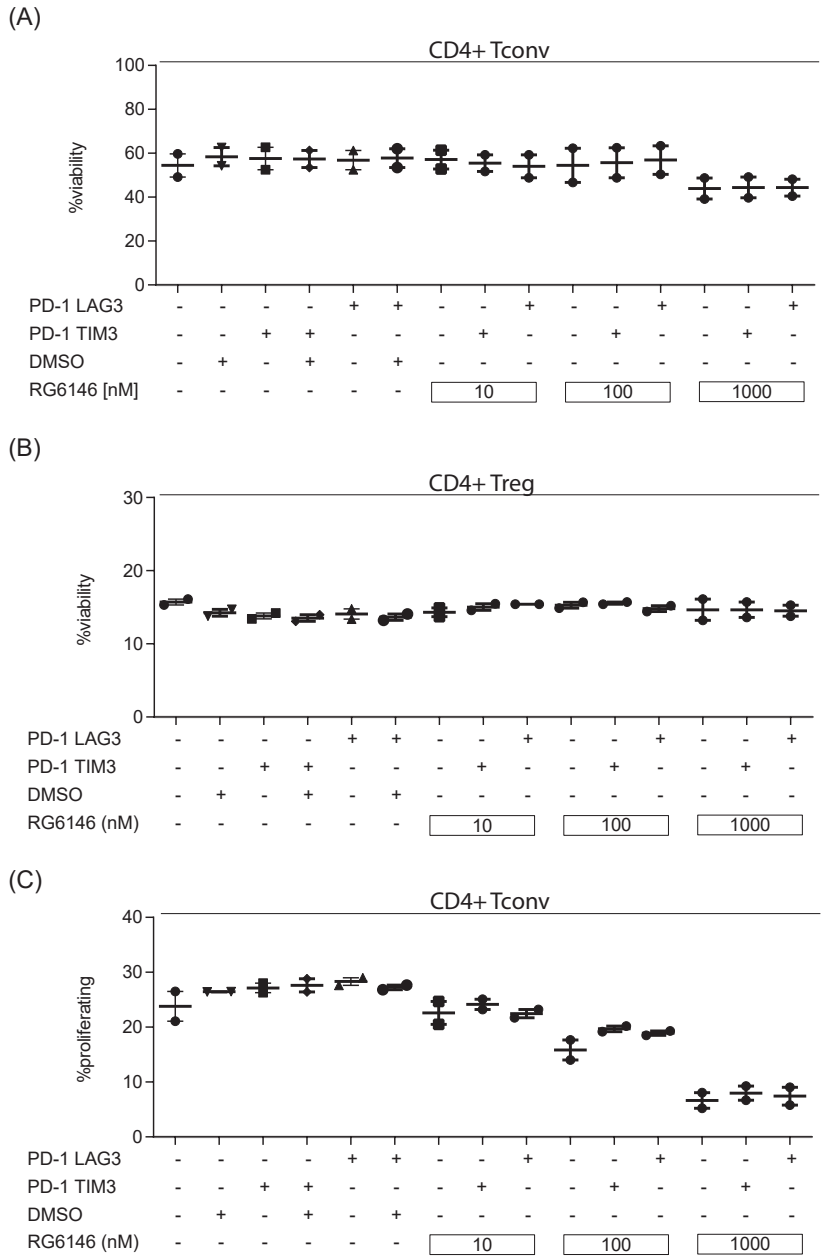

Figure 25: (A-C) Assay set up as described in *24 B*. Percentage of viable (A) T convs and (B) T regs was assessed by flow cytometry upon treatment with checkpoint inhibitors, RG6146 or control. Data of two biological independent Donors is shown. (C) Percentage of proliferating T convs was assessed by flow cytometry upon treatment with checkpoint inhibitors, RG6146 or control. Data of two biological independent Donors is shown.

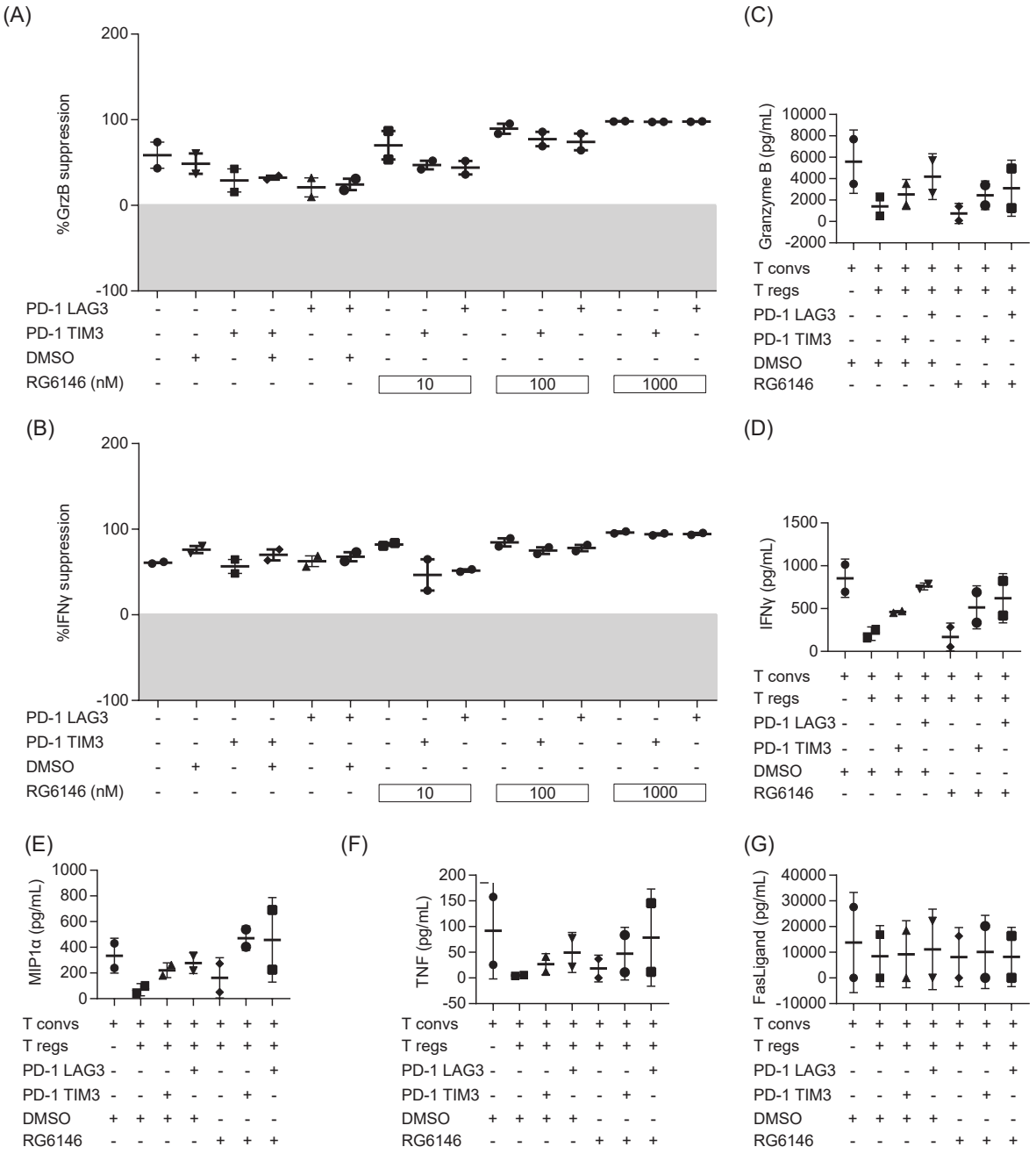

Figure 26: (A-G) Assay set up as described in *24 B.* (A-B) Percentage of (A) Granzyme B (GrzB) and (B) IFNγ suppression was determined by intracellular staining and flow cytometry of T convs. Data of two biological independent experiments is shown. (C-G) Concentration (pg/mL) of cytokines in the supernatant was analyzed by flow cytometry. Data of two biological independent experiments is shown. (C) Granzyme B, (D) IFNγ, (E) MIP1α, (F) TNF, (G) FasLigand.

4.3 Effect of BETis in the interface between immune and cancer cells

The individual observation of how BETis modulate cancer and immune cells gives a first impression of potential therapeutic strategies in the clinic. Based on the findings mentioned in the previous sections, RG6146 has a pronounced effect on viability of MM tumor models and has a slight suppressive effect on T cell activation. However, to unravel potential therapeutic strategies for future cancer treatment, it is critical to consider effects of epigenetic modifiers in influencing the T cell:target cell interface, which is only visible when both cell types are experimentally combined.

4.3.1 BETis enhance T cell mediated killing through the TNF signaling axis

A co-culture system was used to elucidate if small molecules, targeting writers, readers and erasers, enhance T cell mediated killing of cells. An immunogenic peptide (NLV) was loaded on the HLA-A*02:01 molecule of colorectal HCT-116 cancer cells and co-cultured with CMV specific T cells, which recognize the NLV:MHC complex. A library of small molecule epigenetic modifiers was added to the co-culture system and viability assessed 48 h post treatment. As a negative control, EBV peptide was loaded on the MHC I molecule, which is not recognized by the T cells. As a positive control SMAC mimetics (Birinapant and LCL161) were added, which have been shown to enhance T cell mediated killing previously [268] (Figure 27 A). Structurally distinct BETi, that all belong to the subclass of acetyl-lysine mimetics, significantly decreased viability of HCT-116 cells loaded with NLV peptide and induced a phenotype similar to SMAC mimetics (Figure 27 B). In contrast, selective targeting of bromodomains of the transcriptional coactivators CBP and p300 (ICBP112 and SGCCBP30) did not decrease viability to a similar extend. HDAC inhibitors (HDACi) (Panobinostat, Vorinostat, Entinostat) potently decreased viability of HCT-116-NLV and HCT-116-EBV in the co-culture as well as HCT-116 in the monoculture, indicating cytotoxicity (Figure 27 B-C). The effect of RG6146 in this co-culture setting was further assessed by a dose dependent treatment for 48 h (Figure 27 D). Similar to the results of the epigenetic small molecule screen, RG6146 specifically decreased viability of HCT-116-NLV cells co-cultured with CMV-specific T cells. These results indicate that RG6146 either directly activates T cells in this co-culture setting, or epigenetically rewires HCT-116 cells to be susceptible to T cell mediated killing.

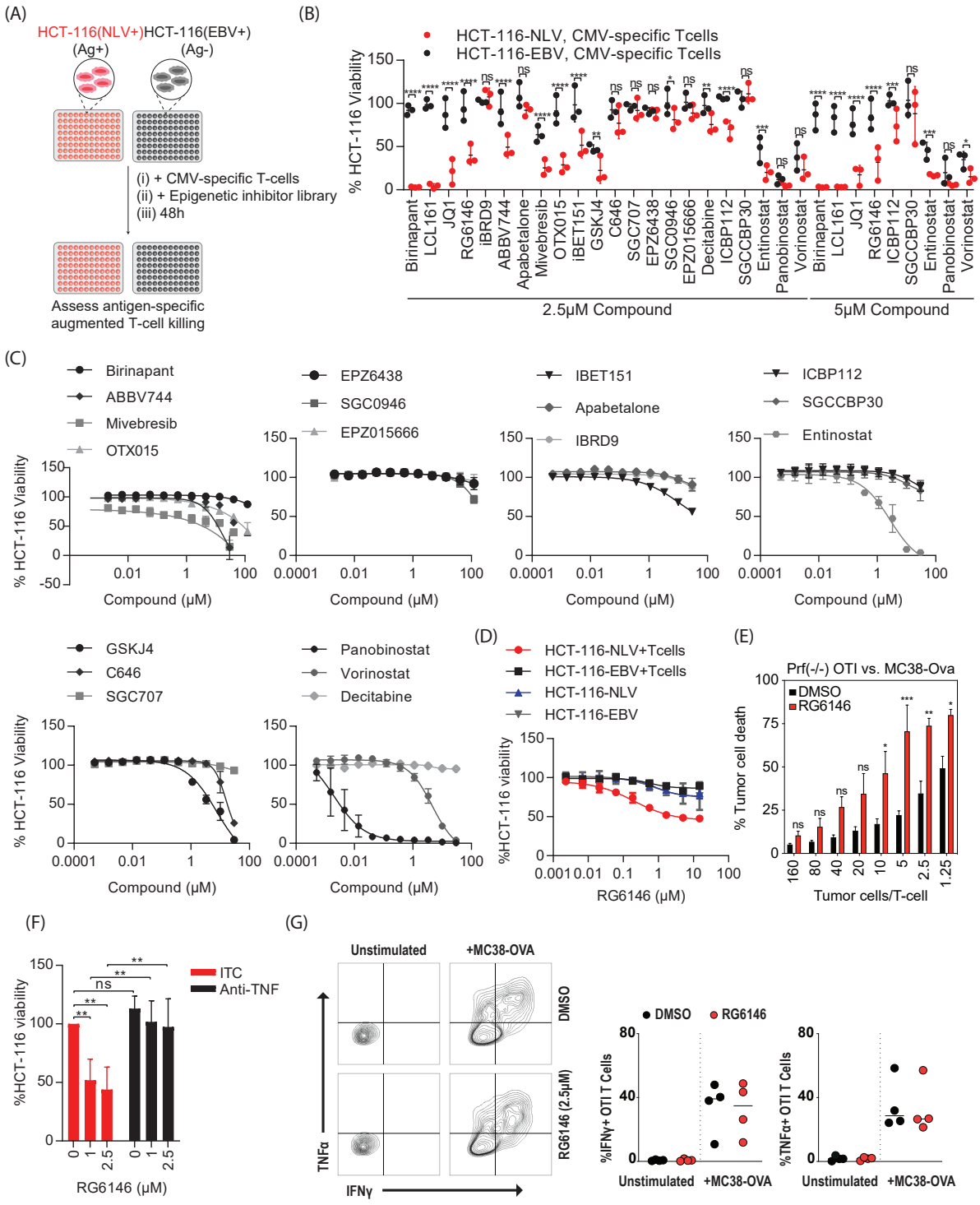

Figure 27: (A) Shematic of T cell:HCT-116 cell co-culture assay. 10 nM NLV or EBV (negative control) peptide was loaded on the MHC I molecule of HCT-116 cells and co-cultured with CMV-specific T cells and a library of small molecule epigenetic modifiers for 48 h. HCT-116 viability was assessed by CTG2.0. (B) Results of assay described in *A*. Data was normalized to DMSO and represents mean of three biological independent experiments. Statistical signif-

icance was calculated using GraphPad Prism 8 and indicates difference between cells loaded with NLV or EBV peptide (2-way ANOVA, *p<0.05, **p<0.01, ***p<0.001, ****p<0.0001, ns: not-significant). (C) Viability of HCT-116 cells treated with a dose response of various small molecule epigenetic modifiers or Birinapant was analyzed 72 h post treatment by CTG2.0. Data was normalized to DMSO control and represents mean of three biological independent experiments. (D) As described in *A* except that co-culture (T cells and HCT-116 cells) as well as mono-culture (HCT-116 cells only) was treated with a dose response of RG6146. Data was normalized to DMSO and represents one biological experiment containing technical triplicates. (E) Different ratios of MC38-Ova and perforin deficient ($Prf^{-}/^{-}$) OTI T cells were co-cultured for 18 h in the presence of 2.5 µM RG6146 or control and cell death analyzed by flow cytometry (propidium iodide positivity). The mean was calculated from three independent experiments. Statistical significance indicates difference between RG6146 and DMSO control (2-way ANOVA, *p<0.05, **p<0.01, ***p<0.001, ns: not-significant). (F) As described in *A* except that a TNF neutralizing antibody (Anti-TNF) or Isotype control (ITC) was added to the co-culture treated with RG6146. Mean of three biological independent experiments is shown. Statistical significance indicates difference between RG6146 and DMSO control (2-way ANOVA, **p<0.01, ns: not-significant). (G) OTI T cells alone (Unstimulated) or in combination with MC38-Ova cells were treated with RG6146 or control in the presence of GolgiStop for 5 h and intracellular cytokine staining of $CD5^{+}CD44^{+}$ T cells was measured by flow cytometry. Mean of four independent experiments is shown.

To test if RG6146 enhances T cell mediated killing, Simon Hogg conducted a co-culture system with murine colon adenocarcinoma MC38 cells presenting the ovalbumin peptide (MC38-Ova) on the MHC I molecule. The MHC I:Ova complex is recognized by Perforin knockout $CD8^{+}$ T cells derived from OTI transgenic mice (OTI T cells). Despite the inability to kill MC38-Ova cells through the granzyme B/ Perforin axis, RG6146 enhanced T cell mediated killing of cancer cells significantly (Figure 27 E). T cells are also able to kill cells by releasing IFNγ and TNF into the immunological synapse [85]. Addition of a TNF-blocking molecule to the co-culture system containing HCT-116-NLV cells and CMV-specific T cells, rescued the decrease in cell viability induced by RG6146 (Figure 27 F).
These results clearly show that BETis enhance T cell mediated killing of HCT-116 cells through a TNF dependent manner. If this effect is mediated by modulating target or immune cells intrinsically, will be evaluated in the following section.

4.3.2 Effect of BETi and TNF on T cells, cancer cells and other cell types

Intracellular cytokine staining of OTI T cells in co-culture with MC38-Ova cells, performed by Dane Newman, revealed that RG6146 does not enhance TNF or IFNγ production within T cells (Figure 27 G). Further, proliferation and activation of Pan-T cells stimulated with anti-CD3 and anti-CD28, treated with RG6146 and TNF showed exactly the same activation pattern as single agent RG6146 treatment (Figure 21 and 28).

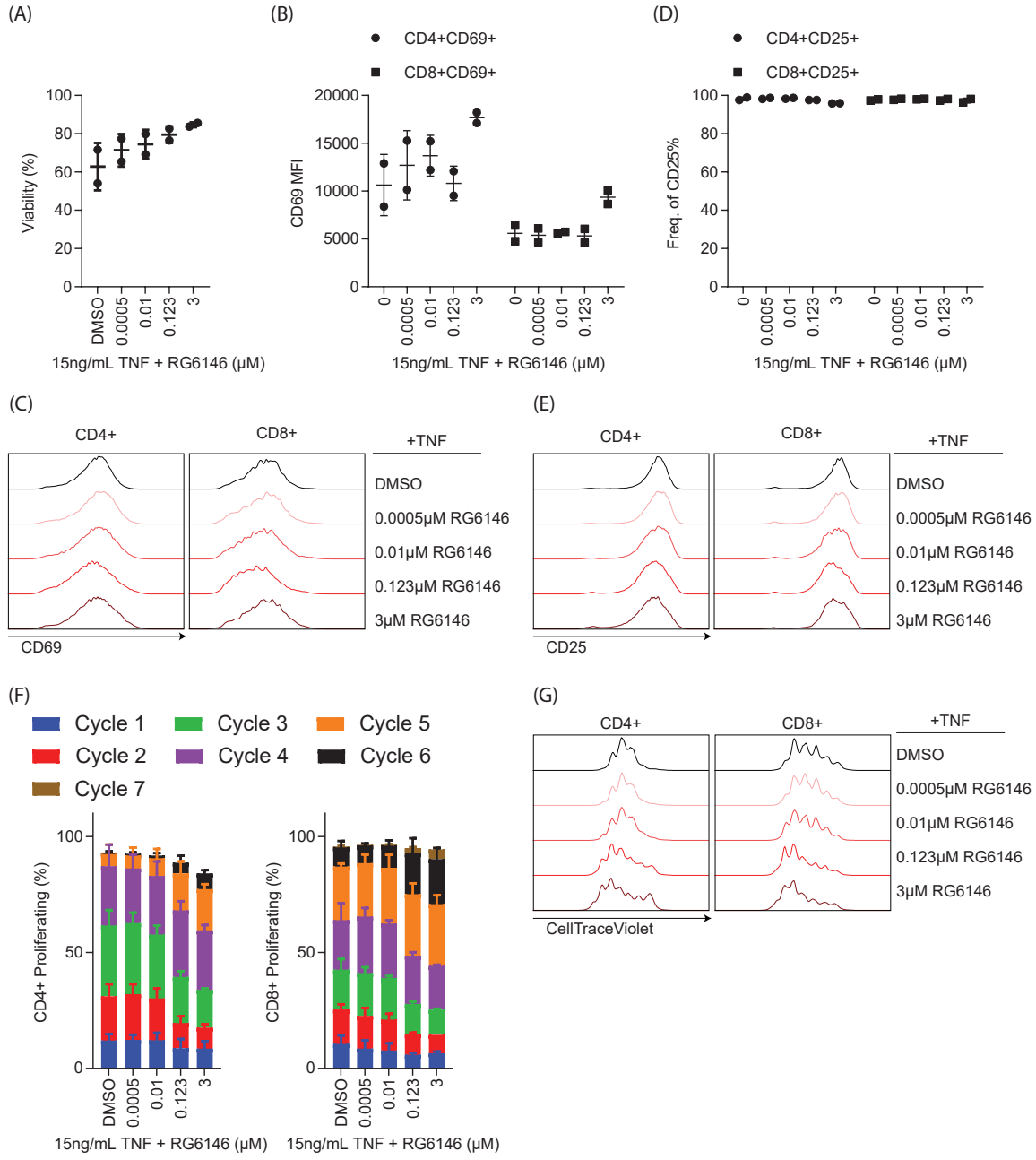

Figure 28: (A-G) Pan-T cells activated with anti-CD3 and anti-CD28 coated wells were treated with increasing concentration of RG6146 and 15 ng/mL TNF. Data of two individual PBMC Donors is shown. (A) Viabiliy in percent was assessed by flow cytometry on live single cells. (B) Median fluorescence intensity (MFI) of CD69 for $CD4^+$ and $CD8^+$ T cell subsets is shown. (C) Histogram of one representative Donor of data described in *B*. (D) Frequency of $CD25^+$ cells within $CD4^+$ or $CD8^+$ T cell subsets is shown. (E) Histogram of one representative Donor of data described in *D*. (F) Percentage of proliferating $CD4^+$ and $CD8^+$ T cells is shown. Cycles of cell proliferation were assessed by Cell Trace Violet dilution. (G) Histogram of one representative Donor of data described in *F*.

Overall, these results indicate that RG6146 does not enhance the production of TNF and the combination of TNF and RG6146 does not modulate T cell activation as compared to RG6146 single agent treatment. Therefore, enhanced T cell mediated killing induced by RG6146 and TNF is most likely through modulation of target cells.
In order to address the growth inhibition of BETi and TNF treatment on cancer cells, a screen of 89 cell lines was conducted by the company Oncolead testing the combination of RG6146 and TNF or RG6146 single agent treatment (Figure 29 A). The combination of RG6146 and TNF enhanced growth inhibition in 36 cell lines compared to single agent RG6146 treatment. In 35 cell lines combination treatment induced less than 10 % GI as compared to single agent treatment. 18 cell lines even lost sensitivity to the combination (Figure 29 A). Using a dose response of structurally distinct BETis, we investigated the effect of BETi single agent treatment, as well as combination with TNF in HCT-116 and MKN45 cancer cells (Figure 29 B-C). RG6146 single agent treatment induced a potent decrease in viability, which was further decreased upon addition of TNF. Other BETis tested showed a similar decrease in viability as RG6146 (Figure 29 B-C).
Although BETis primarily affect cancer cells by displacing BET proteins from super enhancers [26], BET proteins are also involved in the regulation of transcription in healthy cells. It was already shown that TNF and RG6146 do not modulate T cell activation as compared to single agent treatment (Figure 21 and 28). Next, the effect of RG6146 and TNF on non-malignant cells was assessed in a viability assay. The non-oncogenic cell lines HUVECC (Human Umbilical Vein Endothelial Cells), HEK293 (Human Embryonic Kidney) and PNT1A (Prostate Epithelial) were treated with a dose response of TNF or a combination of BETi and TNF and viability assessed after 72 h (Figure 30 A-B). Growth was only affected by TNF in HUVECC cells, while the other two cell lines were not sensitive to single agent TNF treatment (Figure 30 A). While BETi treatment decreased viability in all tested cell lines by about 50 %, no additional decrease was observed when combined with TNF in HUVECC and HEK293 cells (Figure 30 B). Combination treatment in PNT1A cells decreased viability slightly but significantly as compared to single agent treatment (Figure 30 B). These results indicate that at least some of the tested cell lines are not sensitive to the combination of BETi and TNF treatment.
In summary, results presented in this section show that RG6146 and TNF treatment do not change activation of T cells as compared to RG6146 single agent treatment. However, the combination significantly affected viability of some cancer cell lines tested. Not all cell lines responded to the same extent to this combination including non-oncogenic cells indicating that BETi and TNF specifically induce growth inhibition in cancer cells.

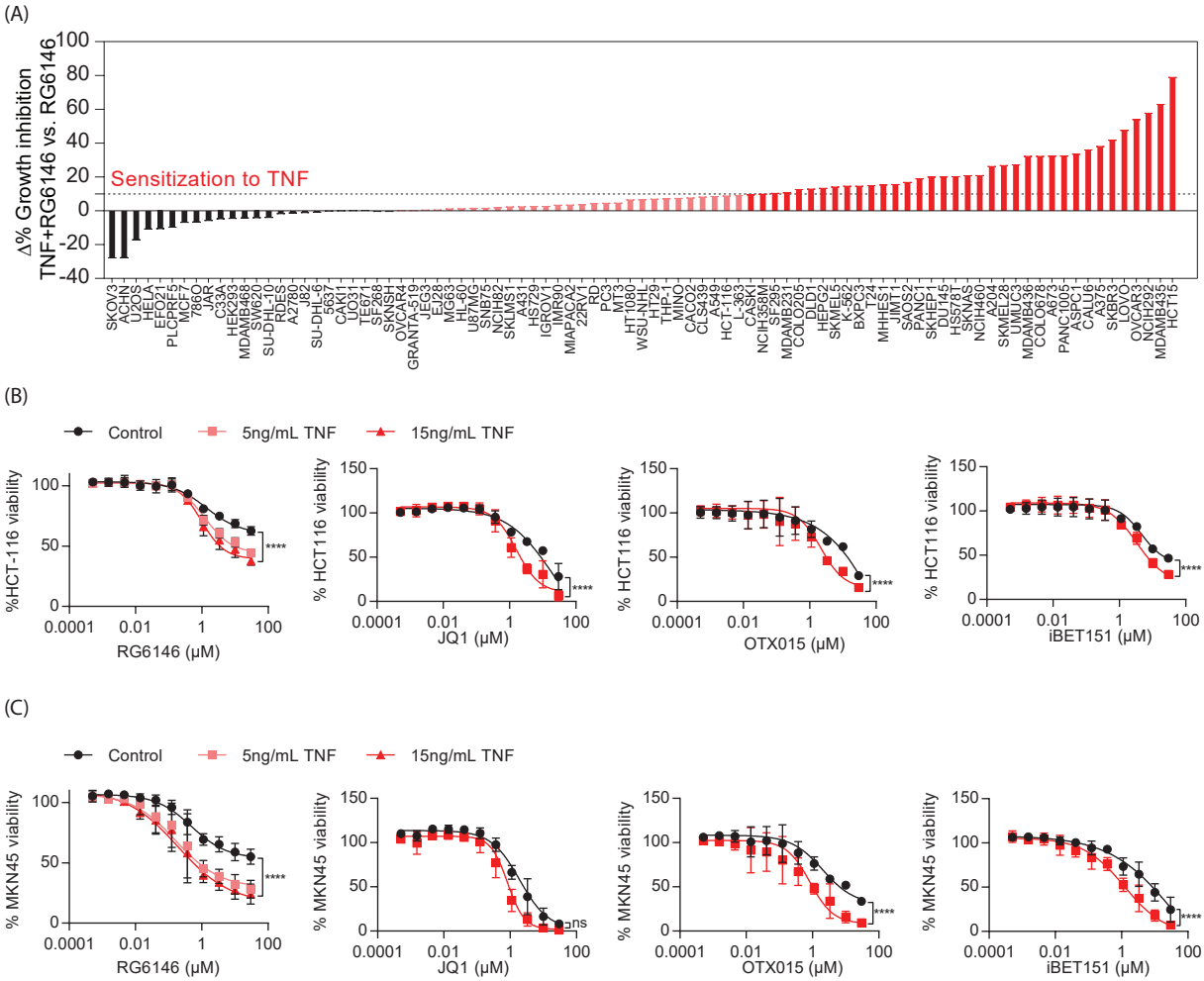

Figure 29: (A) Viability of 89 cancer cell lines of different tumor types treated with RG6146 alone or in combination with TNF. Cell lines exhibiting a growth inhibition (GI) >10 % with combination treatment versus single agent RG6146 were described as sensitized to TNF (red), 10 %>GI>0 % were hardly affected (light red) and cell lines with a GI<0 % were described as resistant (black). Data represents one biological experiment (B-C) Viability of (B) HCT-116 or (C) MKN45 cell lines was assessed by CTG2.0 72 h post treatment with a dose response of different BETis alone or in combination with TNF. Data was normalized to DMSO and shows mean of three biological independent experiments. Statistical significance indicates difference between highest concentration of BETi+TNF and BETi single agent treatment (2-way ANOVA, ****p<0.0001, ns: not-significant).

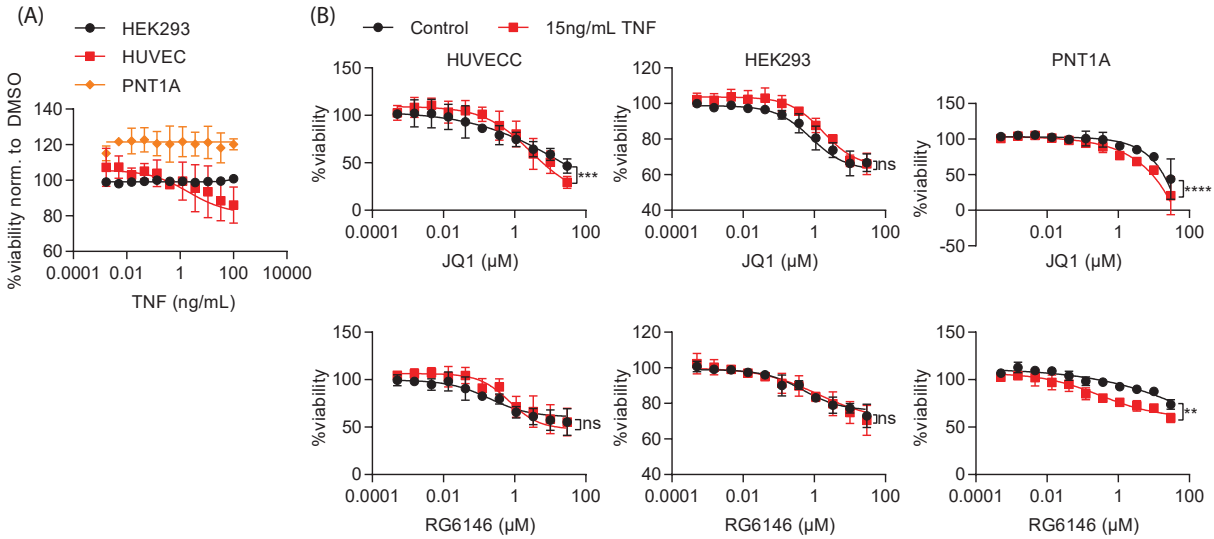

Figure 30: (A) Viability of non-oncogenic cell lines was assessed 72 h post treatment with a dose response of TNF by CTG2.0. Data was normalized to control and shows mean of three biological independent experiments. (B) Viability of HUVECC, HEK293 and PNT1A cell lines was assessed by CTG2.0 after 72 h of treatment with a dose response of BETi alone or in combination with TNF. Data was normalized to DMSO control and represents mean of three biological independent experiments. Statistical significance indicates difference between highest concentration of BETi+TNF and BETi single agent treatment (2-way ANOVA, **p<0.01, ***p<0.001, ****p<0.0001, ns: not significant)

4.3.3 TNF and RG6146 induce extrinsic apoptosis

TNF is a pleiotropic molecule that either induces NF-κB signaling promoting cell survival or cell death through activation of the extrinsic apoptosis pathway [101]. Extrinsic apoptosis is initiated through activation of caspase-8 and downstream effector caspases-3 and 7, which cleave various cellular substrates including PARP [140, 141, 142, 143]. Caspases-3/7 are also activated through the intrinsic apoptosis pathway [252, 253, 254]. RG6146 and TNF enhanced caspase-8, 3 and 7 activation in HCT-116 and MKN45 cells, while RG6146 single agent treatment did not show a change in caspase activity (Figure 31 A-D). Addition of the caspase-8 inhibitor ZIETD-FMK, which inhibits extrinsic apoptosis, rescued caspase activation induced by RG6146 and TNF for all caspases tested (Figure 31 A-D). These results suggest that intrinsic apoptosis is not activated by the combination treatment. PARP cleavage was only visible when treated with RG6146 and TNF and this could also be seen with other BETis in combination with TNF (Figure 31 E-L).

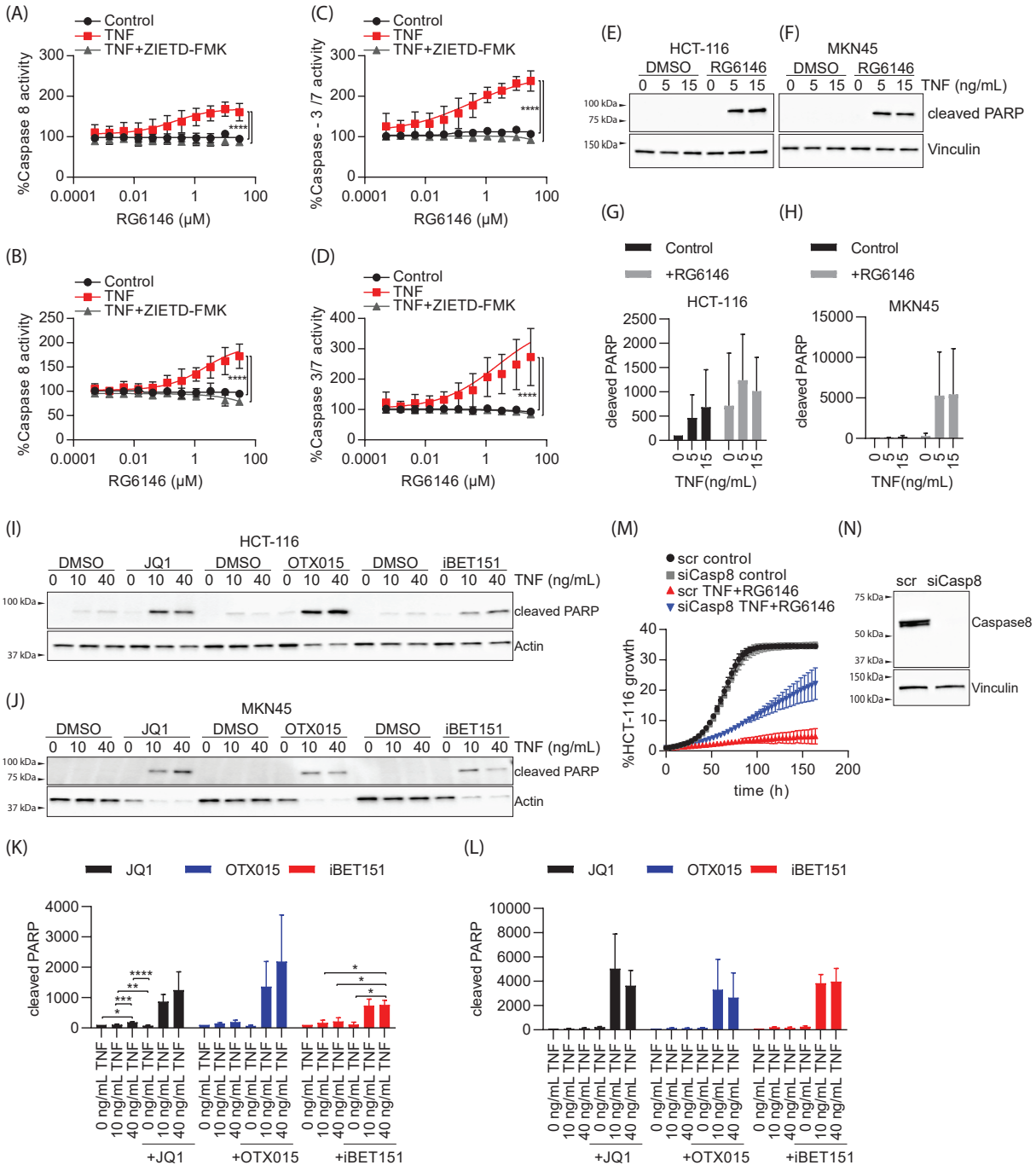

Figure 31: (A-B) Caspase-8 activity in percent of (A) HCT-116 and (B) MKN45 cells was assessed by Caspase-8 Glo 8 h post treatment with a dose response of RG6146 alone, in combination with 15 ng/mL TNF or with TNF and 1 µM of the Caspase-8 inhibitor ZIETD-FMK. Data was normalized to DMSO and mean of three biological independent experiments is shown. Statistical significance indicates difference between highest concentration of RG6146+TNF and RG6146 alone or RG6146+TNF+ZIETD-FMK (2-way ANOVA, ****p<0.0001). (C-D) As described for *A-B* except that Caspase-3/7 activity was measured in (C) HCT-116 and (D) MKN45 cells. (E-F) Cleaved PARP and Vinculin level assessed 24 h post treatment of (E) HCT-116 or

(F) MKN45 cells with TNF alone or in combination with 2.5 µM RG6146. One representative blot of three biological independent experiments is shown. (G-H) Quantification of western blots shown in *E-F*. Levels of cleaved PARP were normalized to untreatd control for (G) HCT-116 and (H) MKN45 cells. Mean of three biological independent experiments is shown. Statistical significance was calculated using a 2-way Anova (Data not significant). (I-J) Cleaved PARP and Actin level assessed 24 h post treatment of (I) HCT-116 or (J) MKN45 cells with TNF alone or in combination with 2.5 µM BETis. One representative blot of three biological independent experiments is shown. (K-L) Quantification of western blots shown in *I-J*. Levels of cleaved PARP were normalized to untreatd control for (K) HCT-116 and (L) MKN45 cells. Mean of three biological independent experiments is shown. Statistical significance was calculated using 2-way ANOVA where *p<0.05, **p<0.01, ***p<0.001, ****p<0.0001. If not shown:not significant. (M-N) HCT-116 cells were depleted of Caspase-8 (siCasp8) or scrambled control (scr) by reverse transfection using siPools. (M) HCT-116 cells were treated with control or the combination of 15 ng/mL TNF and 2.5 µM RG6146. Cell growth (%) was assessed over the course of treatment using live cell imaging. Data was normalized to time point 0. Mean of three technical replicates from one experiment is shown. Data represents one of three biological independent experiments. (N) HCT-116 knockdown efficiency visualized by western blot after 6 h treatment with 15 ng/mL TNF.

To verify that RG6146 and TNF induce the extrinsic apoptosis pathway, caspase-8 was silenced in HCT-116 cells (Figure 31 N) and cell growth monitored over time (Figure 31 M). The combination of RG6146 and TNF potently inhibits cell growth in HCT-116 cells transfected with control (scr). Knock down of caspase-8 partially rescued this phenotype (Figure 31 M). These results indicate that cell death induced through RG6146 and TNF is mediated mainly but not solely through the extrinsic apoptotic pathway.

4.3.4 TNF and RG6146 modulate pro-survival NF-κB signaling

BET proteins are involved in the recruitment of P-TEFb to the chromatin therby activating Pol II and inducing transcriptional elongation of target genes [23, 24]. Even though BETis are used to displace BET proteins from the chromatin, it is still not entirely understood which downstream target genes are affected by BETi treatment. Since TNF interacts with TNFR1, it was tested if RG6146 modulates levels of this surface receptor by flow cytometry (Figure 32 A). RG6146 single agent treatment decreased TNFR1 in HCT-116, but not in MKN45 cells. A similar effect was visible by TNF single agent treatment, while no additional downregulation was visible with the combination (Figure 32 A). To identify how TNF and RG6146 change expression of genes as single agent or in combination, RNA-sequencing was performed. HCT-116 and MKN45 cells were treated with RG6146 and TNF or control for 2 h. Subsequently, the cells were processed for RNA-sequencing and data was analyzed by Simon Hogg (Figure 32 B-E and Figure 33). In both cell lines, treatment of TNF potently induced expression of known NF-κB target genes such as *NFKBIA*, *BIRC3*, *TNFAIP3*, *NFKB2*, *NFKB1* [269, 270, 271, 272, 273] (Figure 32 B & 33 A). Further, a similar pattern of gene regulation upon single agent and combination treatment was detected in both cell lines and classified into five clusters (Figure 32 C-D & 33 B-C).

Cluster 1 describes genes that are increased upon RG6146 single agent treatment, decreased by TNF and slightly enhanced back to baseline level with the combination.

Cluster 2 describes genes decreased upon RG6146 single agent treatment and increased by addition of TNF. The combination decreases gene expression of genes in cluster 2, but less potent than genes in cluster 4.

Cluster 3 describes genes that are decreased with RG6146 and TNF single agent treatment and further decreased with the combination.

Cluster 4 describes genes that are decreased upon addition of RG6146 single agent treatment, enhanced with TNF and decreased with the combination of both molecules (Figure 32 D and 33 C).

Cluster 5 was only present upon RNAseq analysis of HCT-116 cells and includes genes increased by combination treatment (Figure 33 C).

Especially genes in cluster 2 (TNF induced, combination slightly suppressed) and Cluster 4 (TNF induced, combination strongly suppressed) were of interest for us. Overlay of genes in Cluster 2 and 4 from both cell lines resulted in 37 and 30 genes with the same modulation pattern, respectively (Figure 33 D). One example for cluster 2 is *NFκBIA* encoding IκBα, while *BIRC2* and *BIRC3* were detected in cluster 4 (Figure 32 E and 33 E).

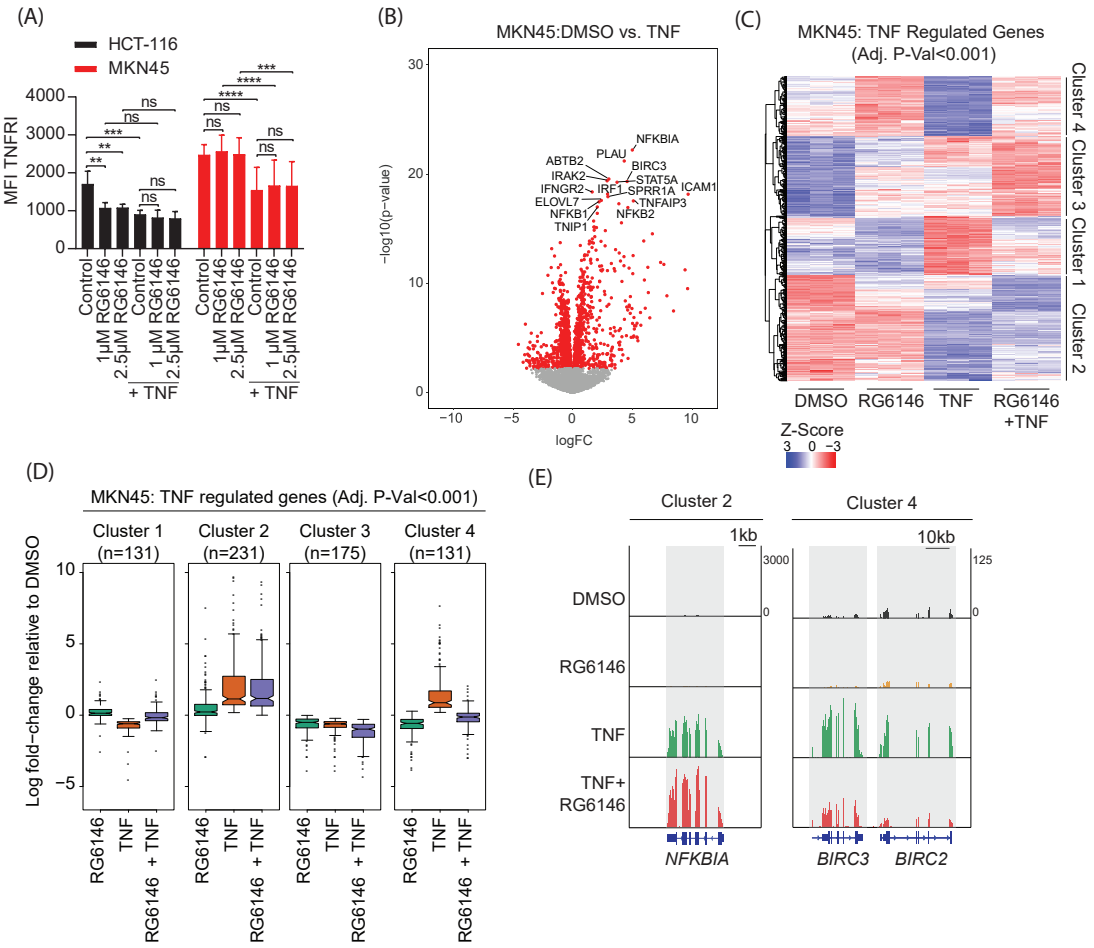

Figure 32: (A) Median fluorescence intensity of TNFR1 was analyzed by flow cytometry of live single cells in HCT-116 and MKN45 cells upon treatment with RG6146 and 15 ng/mL TNF for 24 h. (B-E) RNA-seq results of MKN45 cells treated with 2.5 µM RG6146 and 20 ng/mL TNF for 2 h. Data of three experiments is shown. (B) Genes differentially expressed (red) upon treatment with TNF versus DMSO (adjusted p-value<0.001) are summarized in the vulcano blot. (C) Heatmap of k-means clustered differentially expressed genes (normalized log counts per million (CPM)) by TNF treatment (adj. P-value<0.001). (D) Effects of treatment conditions on gene expression in cluster 1-4 is summarized in the boxplot (log fold-change values for genes). (E) RNA-seq signal at *NFKBIA* (representative Cluster 2 gene) and *BIRC2/3* loci (representative Cluster 4 loci) as shown in the IGV genome browser screenshot.

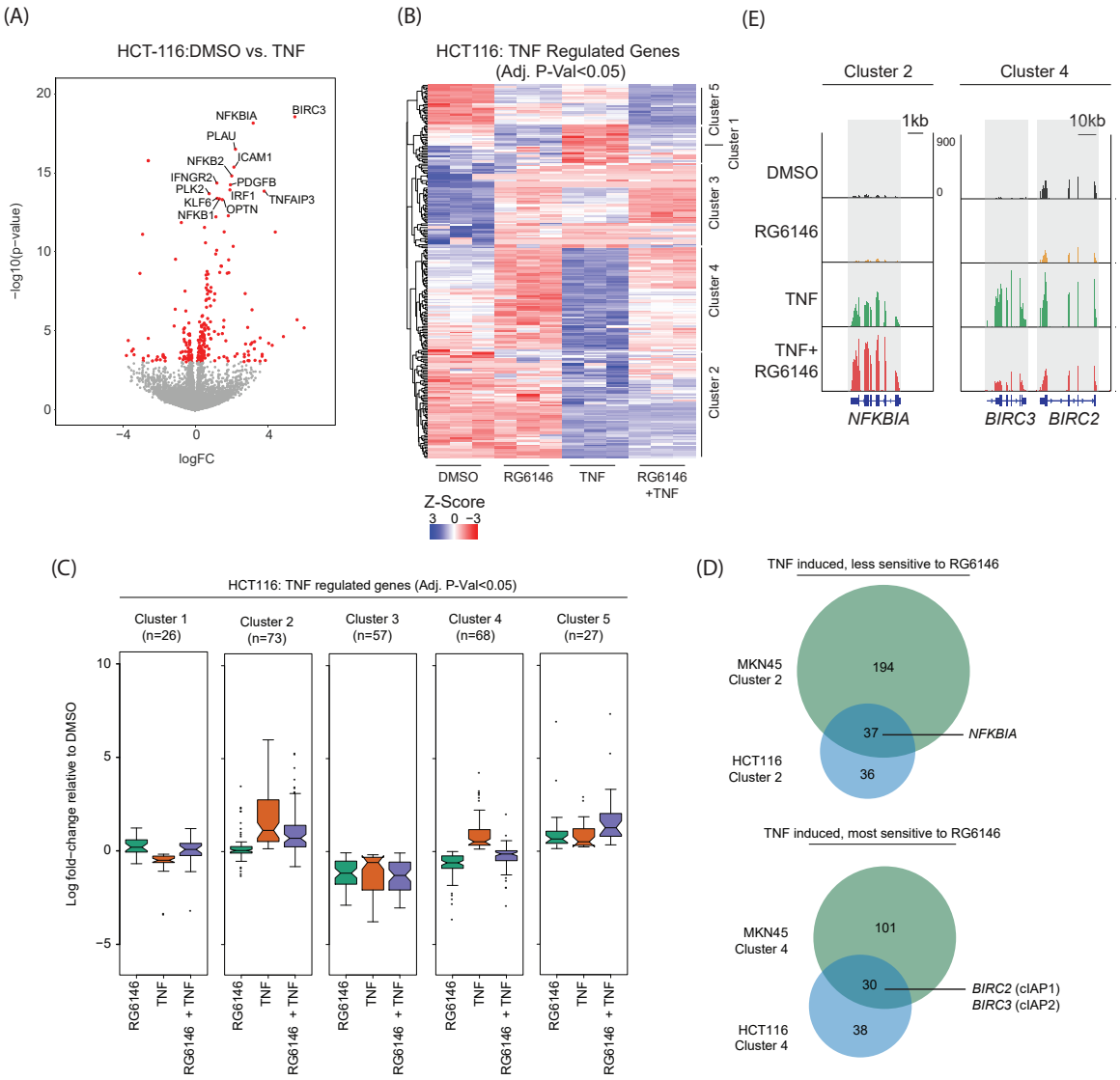

Figure 33: (A-E) RNA-seq results of HCT-116 cells treated with 2.5 µM RG6146 and 20 ng/mL TNF for 2 h. Data of three experiments is shown. (A) Genes differentially expressed (red) upon treatment with TNF versus DMSO (adjusted p-value<0.001) are shown in the vulcano blot. (B) Heatmap of k-means clustered differentially expressed genes (normalized log counts per million (CPM)) by TNF treatment (adj. P-value<0.05). (C) Effects of treatment conditions on gene expression in cluster 1-5 is summarized in the boxplot (log fold-change values for genes). (D) Overlap of RNA-seq data cluster 2 and cluster 4 of HCT-116 *(Figure 33 B-D)* and MKN45 cells *(Figure 32 B-D)*. (E)RNA-seq signal at *NFKBIA* (representative Cluster 2 gene) and *BIRC2/3* loci (representative Cluster 4 loci) as shown in the IGV genome browser screenshot.

BIRC2 (cIAP1) and *BIRC3* (cIAP2) transcription is controlled by NF-κB [274], however, both proteins are also crucial for potent NF-κB activation [116] and downregulation of these proteins by SMAC mimetics has been linked to complex IIb formation and induction of apoptosis [136, 137].
Next, we tested if cIAP1, cIAP2 and TRAF1, which are all involved in suppressing TNF-induced apoptosis [275], are decreased by RG6146 and TNF treatment. MKN45 cells were treated with different concentrations of TNF alone or in combination with RG6146. Subsequently, RNA and protein levels were analyzed by qRT-PCR and western blot, respectively (Figure 34 A-E). In TNF treated samples RNA levels of *BIRC3* and *TRAF1* were increased 2 h post treatment (Figure 34 A). The same increase was seen on the protein level starting at 6 h post treatment (Figure 34 B-E). Combination of RG6146 and TNF decreased *BIRC3* and *TRAF1* RNA, as well as, protein levels (Figure 34 A-E). While RNA level of cIAP1 was only slightly decreased by TNF and RG6146, a change on the protein level was visible after 24 h of treatment (Figure 34 A-E).
Since cIAP1 and cIAP2 are important regulators of NF-κB activation and expression of these genes was decreased by RG646 and TNF, it was tested if cIAP1 and cIAP2 overexpression is sufficient to rescue growth inhibition induced by combination treatment (Figure 34 F-G). Cell viability of MKN45 cells transfected with an empty vector control was reduced by RG6146 and TNF treatment as compared to RG6146 single agent (Figure 34 F). Simultaneous overexpression of cIAP1 and cIAP2 rescued this phenotype (Figure 34 F). Interestingly, overexpression of cIAP1 exhibited a similar phenotype as empty vector control transfected cells. On the other hand, cIAP2 overexpression partially rescued the effect induced by combination treatment (Figure 34 F). However, it is important to note, that the difference in cIAP2 level between transfected cell lines and EV control was higher than the difference in cIAP1 level (Figure 34 G).
The RG6146 and TNF dependent decrease of cIAP2 and TRAF1 protein levels was comparable (Figure 34 A-B) raising the question if TRAF1 overexpression can also rescue growth inhibition induced by RG6146 and TNF. High TRAF1 level was detected in transduced cell lines (Figure 34 H) and a dose response of TNF did not affect cell viability of wildtype or TRAF1 expressing cell lines (Figure 34 I). While the further reduction of viability by RG6146 and TNF as compared to RG6146 single agent treatment was significant in wild type cells, this was not the case for cells overexpressing TRAF1(Figure 34 J).

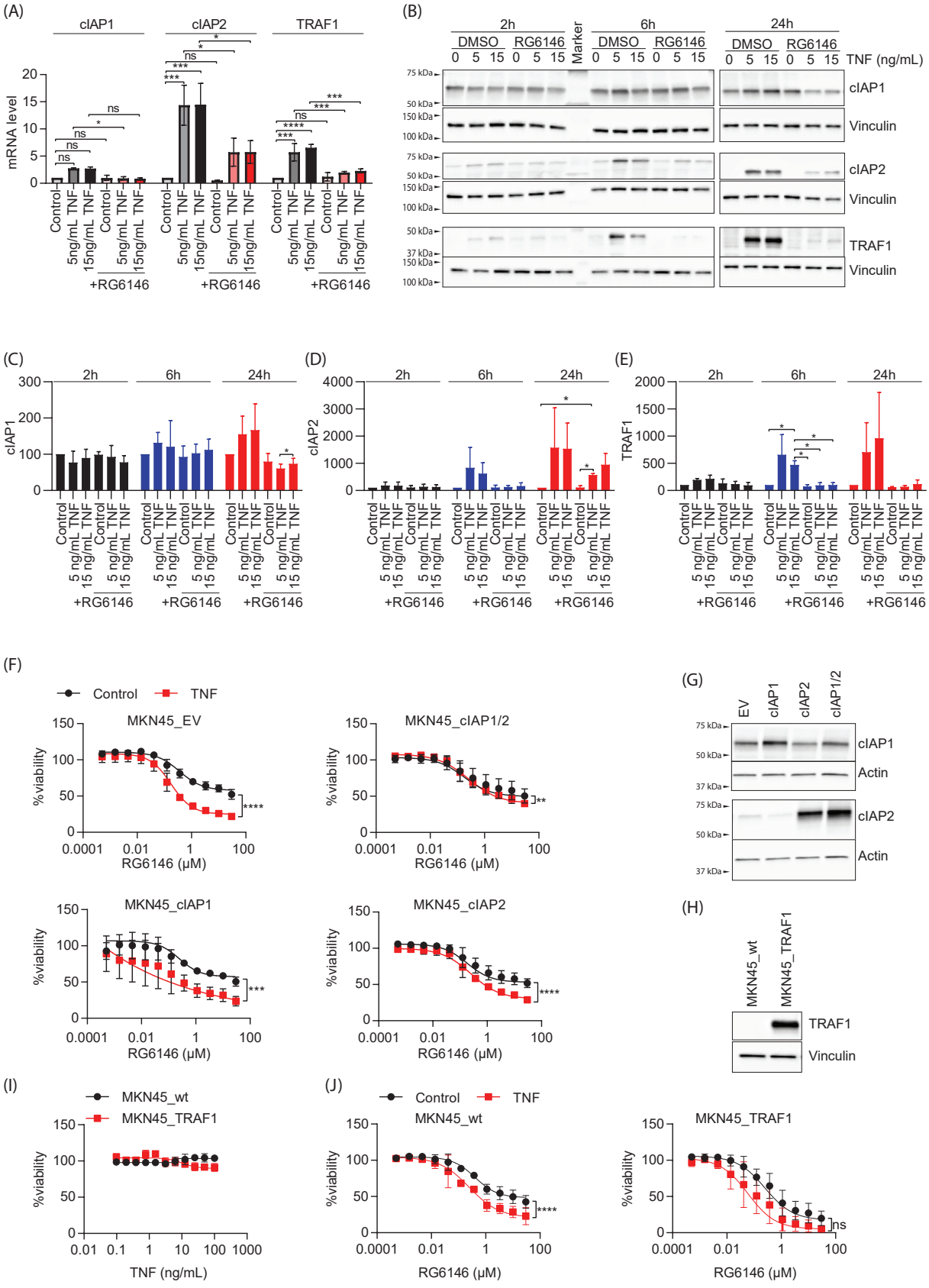
(A)
cIAP1
cIAP2
TRAF1
mRNA level
Control
5ng/mL TNF
15ng/mL TNF
+RG6146
(B)
2h
6h
24h
DMSO
RG6146
Marker
TNF (ng/mL)
cIAP1
Vinculin
cIAP2
TRAF1
(C)
(D)
(E)
(F)
Control
TNF
MKN45_EV
MKN45_cIAP1/2
MKN45_cIAP1
MKN45_cIAP2
%viability
RG6146 (μM)
(G)
EV
cIAP1
cIAP2
cIAP1/2
Actin
(H)
MKN45_wt
MKN45_TRAF1
(I)
TNF (ng/mL)
(J)
ns

Figure 34: (A) mRNA level of *BIRC2* (cIAP1), *BIRC3* (cIAP2) and *TRAF1* were assessed in MKN45 cells by qRT-PCR after 2 h of treatment with TNF +/− 2.5 µM RG6146. Data was normalized to *GAPDH* and shows mean of three biological independent experiments. Statistical significance indicates difference between control and TNF single agent as well as difference between TNF single agent and combination with RG6146 (1-way ANOVA for each RNA-group calculated separately, *p<0.05, ***p<0.001, ****p<0.0001, ns: not significant). (B) Protein level of cIAP1, cIAP2, TRAF1 or Vinculin were assessed at indicated time points upon treatment with TNF +/− 2.5 µM RG6146. Results of one representative western blot of three independent experiment is shown. (C-E) Quantification of western blots shown in *B*. Levels of (C) cIAP1, (D) cIAP2 and (E) TRAF1 were normalized to untreatd control. Mean of three biological independent experiments is shown. Statistical significance between treatments was calculated for each time point using 2-way ANOVA, *p<0.05, if not indicated: not significant. (F) Viability of MKN45 cells expressing an empty vector control (MKN45_EV), cIAP1 (MKN45_cIAP1), cIAP2 (MKN45_cIAP2) or cIAP1 and cIAP2 (MKN45_cIAP1/2) was assessed by CTG2.0 after 72 h of treatment with a dose response of RG6146 +/− 15 ng/mL TNF. Data was normalized to DMSO. Mean of three biological independent experiments is shown. Statistical significance indicates difference between highest concentration of RG6146+TNF and RG6146 single agent treatment (2-way ANOVA, **p<0.01, ***p<0.001, ****p<0.0001, ns: not significant). (G) Level of cIAP1, cIAP2 and Actin in cell lines described in *F* were visualized by western blot. (H) Wild-type MKN45 cells (MKN45_wt) or overexpressing TRAF1 (MKN45_TRAF1) were assessed for TRAF1 or Vinculin level by western blot (I) MKN45 cells described in *H* were treated with a dose response of TNF and viability assessed 72 h post treatment by CTG2.0. Data was normalized to control and shows mean of three biological independent experiments. (J) Cell lines described in *H* were treated with a dose response of RG6146 +/− 15 ng/mL TNF and viability assessed 72 h later by CTG2.0. Statistical significance indicates difference between highest concentration of RG6146+TNF and RG6146 single agent (2-way ANOVA, ****p<0.0001, ns: not significant).

BET proteins are known to bind to acetylated lysine residues on histone tails, interact with transcription factors and mediators and thereby modulate the transcription of target genes [23, 24]. Since RG6146 and TNF decreased transcription of NF-κB (p65/p50) target genes, a consequent next step was to investigate if BRD4 and p65 share the same binding sites at the chromatin. Simon Hogg performed a chromatin immunoprecipitation and sequencing (ChIP-seq) experiment in MC38 cells treated with RG6146, TNF or the combination (Figure 35-36). p65 binding to the chromatin was significantly enhanced upon TNF treatment and slightly but significantly decreased with the combination (Figure 35 A). Single agent RG6146 treatment did not affect p65 binding (Figure 35 A). Chromatin accessibility, tested by ATAC-seq, as well as Histone 3 Lysine 27 acetylation (H3K27ac) were enhanced with TNF treatment, but unchanged by RG6146 addition indicating that this BETi does not affect chromatin accessibility or acetylation (Figure 35 B-C). Additionally, TNF treatment enhanced the number of genes controlled by the presence of super-enhancers with most genes gaining super-enhancer activity involved in NF-κB signalling (Figure 35 D-E). RG6146 single agent treatment decreased BRD4 binding globally (Figure 36 A) affecting loss at super-enhancers as well as typical enhancers (Figure 36 B-E). Similarly, RG6146 single agent treatment decreased BRD4 binding at p65 bound *cis*-regulatory elements (CREs) significantly (Figure 35 F-G). Further, TNF treatment enhanced BRD4 recruitment to p65 bound CREs, which was significantly reduced with combination treatment. However, loss of BRD4 binding by RG6146 and TNF did not reach baseline level (Figure 35 F). RG6146 dependent loss of BRD4 binding was detected at promoter regions (peak 5kb from annotated TSS) as well as *cis*-regulatory enhancer elements driving the transcription of p65 target genes (Figure 35 G). One example for such a target gene is the super-enhancer driven chemokine *Ccl2* (Figure 35 H).
In summary, TNF treatment potently modulates the chromatin landscape and induces recruitment of p65 to the chromatin. TNF also induces BRD4 binding at p65 bound CRE and this effect is partially inhibited upon addition of RG6146.

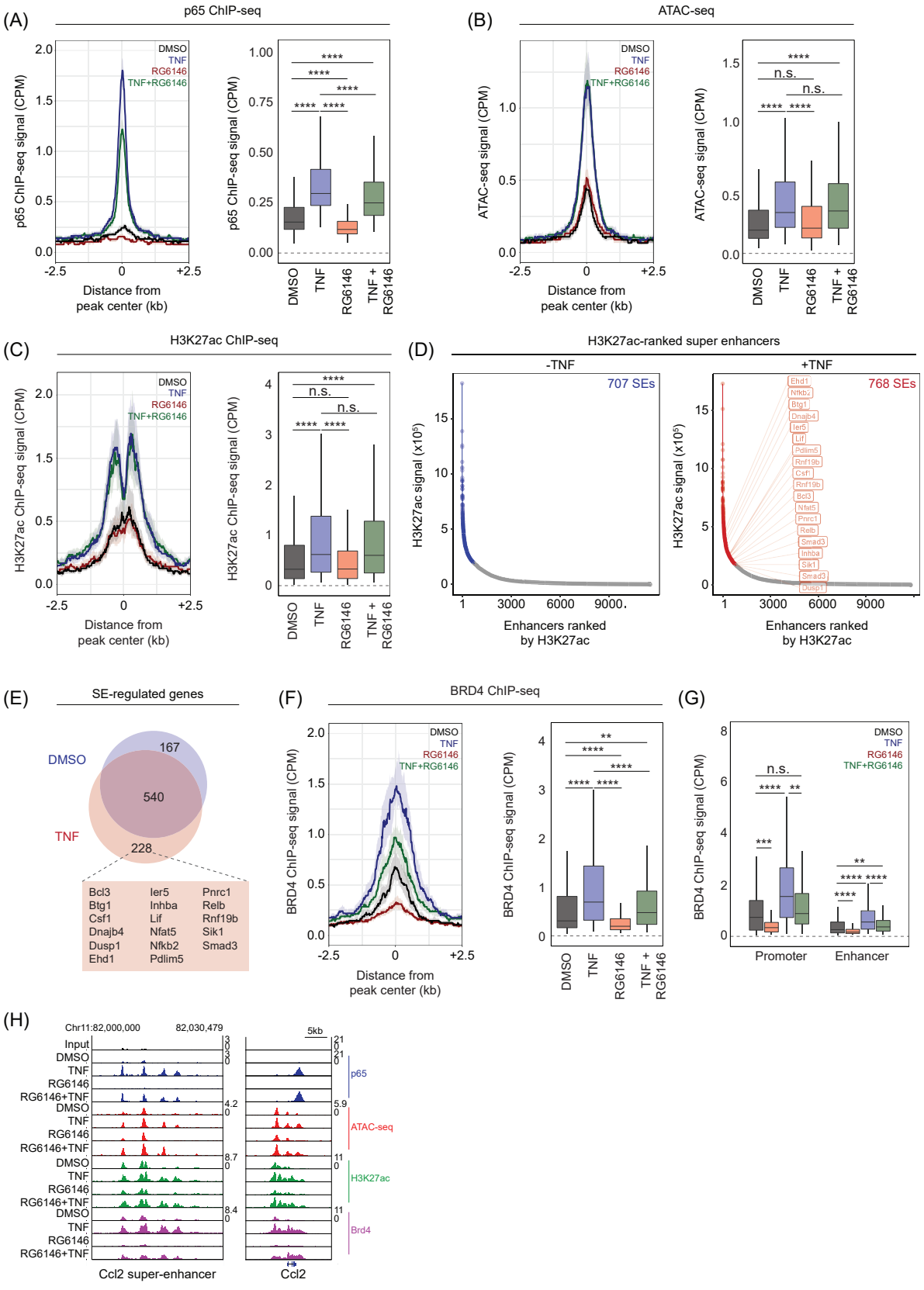
(A)
p65 ChIP-seq
p65 ChIP-seq signal (CPM)
DMSO
TNF
RG6146
TNF+RG6146
Distance from peak center (kb)
(B)
ATAC-seq
ATAC-seq signal (CPM)
n.s.
(C)
H3K27ac ChIP-seq
H3K27ac ChIP-seq signal (CPM)
(D)
H3K27ac-ranked super enhancers
-TNF
+TNF
707 SEs
768 SEs
H3K27ac signal (x10^5)
Enhancers ranked by H3K27ac
Ehd1
Nfkb2
Btg1
Dnajb4
Ier5
Lif
Pdlim5
Rnf19b
Csf1
Bcl3
Nfat5
Pnrc1
Relb
Smad3
Inhba
Sik1
Dusp1
(E)
SE-regulated genes
DMSO
TNF
167
540
228
Bcl3 Ier5 Pnrc1
Btg1 Inhba Relb
Csf1 Lif Rnf19b
Dnajb4 Nfat5 Sik1
Dusp1 Nfkb2 Smad3
Ehd1 Pdlim5
(F)
BRD4 ChIP-seq
BRD4 ChIP-seq signal (CPM)
(G)
Promoter
Enhancer
(H)
Chr11:82,000,000
82,030,479
5kb
Input
RG6146+TNF
p65
ATAC-seq
H3K27ac
Brd4
Ccl2 super-enhancer
Ccl2

Figure 35: (A-H) ChIP and ATAC-seq analysis of MC38 cells treated for 3 h with 2.5 µM RG6146, 10 ng/mL TNF or the combination. (A) Average profile of normalized p65 ChIP-seq signal in counts per million (CPM) at top 350 sites (± 2.5 kb) where p65 is recruited following TNF stimulation of MC38 cells. Quantification of p65 ChIP-seq signal across these regions is represented in the boxplot. Statistical significance indicates difference between treatments (Wilcoxon signed-rank test in Rstudio, ****p<0.0001). (B) Average profile of normalized ATAC-seq signal (CPM) at p65-bound sites ± 2.5 kb (from *A*). Quantification of ATAC-seq signal across these regions is shown in the boxplot. Statistical significance indicates difference between treatments (Wilcoxon signed-rank test in Rstudio, ****p<0.0001, ns: not significant). (C) Average profile of H3K27ac ChIP-seq signal (adjusted counts per million, CPM) at p65-bound sites ± 2.5 kb (from *A*). Quantification of H3K27ac ChIP-seq signal across these regions is summarized in the boxplot. Statistical significance indicates difference between treatments (Wilcoxon signed-rank test in Rstudio, ****p<0.0001, ns: not significant). (D) Signal of H3K27ac at super-enhancers (SEs) ranked by H3K27ac ChIP-seq of cells treated with TNF single agent (+TNF) or control (−TNF). Genes regulated by SEs (shown in red) are also summarized in *E*. (E) Overlap of genes regulated by SEs as described in *D* summarized in the Venn diagram highlighting those genes that overlap with MGSigDB's 'TNF via NF-κB' gene signature. (F) Average profile of BRD4 ChIP-seq signal (adjusted counts per million (CPM)) at p65-bound sites ± 2.5 kb (from *A*). Quantification of BRD4 ChIP-seq signal across these regions are shown in the boxplot. Statistical significance indicates difference between treatments (Wilcoxon signed-rank test in Rstudio, **p<0.01, ****p<0.0001, ns: not significant). (G) BRD4 ChIP-seq signal at p65-bound sites classified as either promoter (±5 k.b. from annotated TSS) or enhancer (>5 k.b. from annotated TSS). Statistical significance indicates difference between treatments (Wilcoxon signed-rank test in Rstudio, **p<0.01, ***p<0.001, and ****p<0.0001, ns: not significant). (H) Screenshot of IGV genome browser summarizing ChIP-seq signal at the *Ccl2* locus and upstream SE.

It was shown that RG6146 and TNF treatment decrease expression of pro-survival genes in the NF-κB pathway and that BRD4 co-occupies p65 bound CRE. Therefore, it was suspected that HCT-116 cells, expressing luciferase under the control of a NF-κB responsive element, would decrease luciferase activity when treated with TNF and RG6146. A dose response of TNF single agent treatment after 6 and 72 h increased luciferase signal indicating activation of the NF-κB pathway (Figure 37 A-B). However, while cells treated with the SMAC mimetic Birinapant and TNF for 6 h resulted in 60 % decrease of luciferase signal as compared to TNF single agent treatment, BETi in combination with TNF increased the luciferase signal significantly (Figure 37 C). A similar effect was seen also after 72 h (Figure 37 D).

In conclusion, these results show that RG6146 and TNF treatment reduce levels of proteins involved in the pro-survival NF-κB pathway including cIAP1 and cIAP2. Further, combination treatment reduced BRD4 binding at p65 bound CRE. However, NF-κB dependent luciferase activation was not decreased by RG6146 and TNF treatment indicating that RG6146 is not potent enough to reduce expression of all NF-κB target genes or that another mechanism is involved in this context.

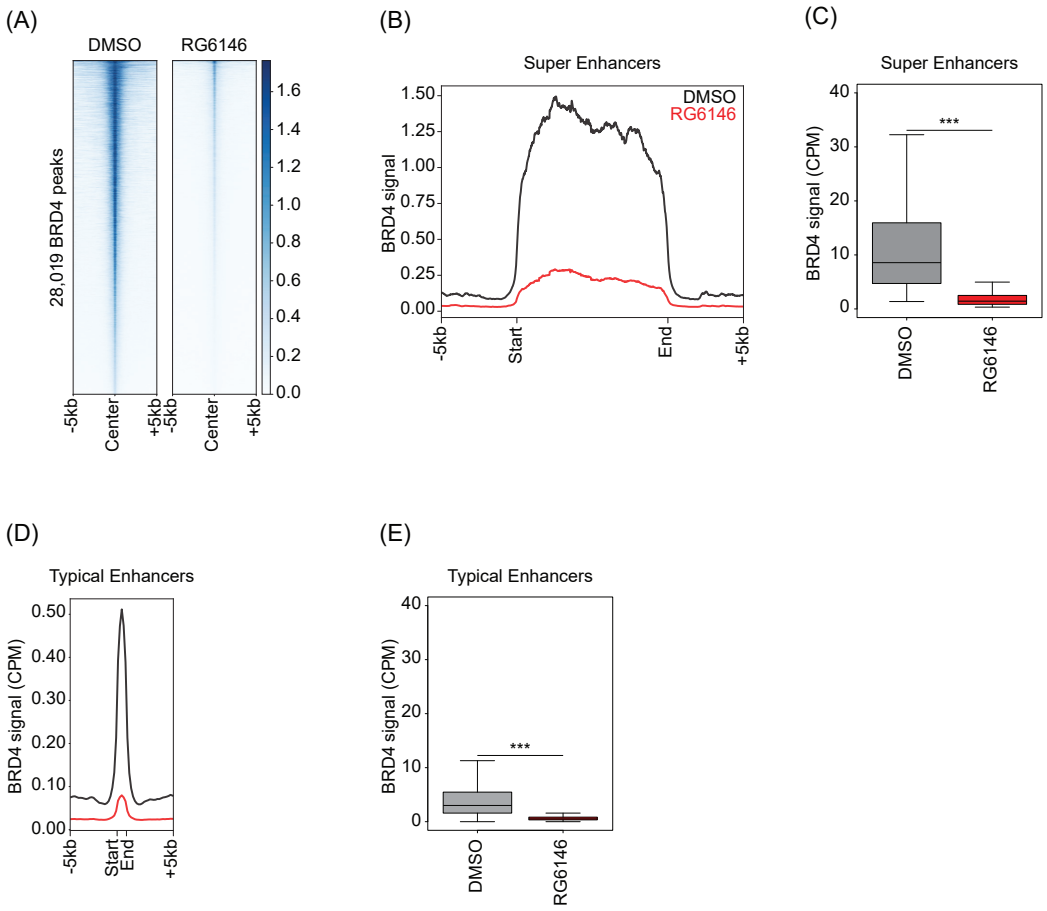

Figure 36: (A-E) ChIP-seq analysis of MC38 cells treated for 3 h with 2.5µM RG6146 or control. (A) Heatmap representing normalized BRD4-ChIP seq signal (centered on 28,019 BRD4 peaks identified in DMSO treated cells +/−5 kb) (B) Average profile of normalized BRD4 ChIP-seq signal across H3K27ac-ranked super enhancers. (C) Boxplot representing quantification of normalized BRD4 ChIP-seq signal at super-enhancers. (Students t-test, ***p<0.001). (D) Average profile of normalized BRD4 ChIP-seq signal across typical enhancers (all H3K27ac enhancers without super enhancers). (E) Boxplot representing quantification of normalized BRD4 ChIP-seq signal at typical enhancers (Students t-test, ***p<0.001).

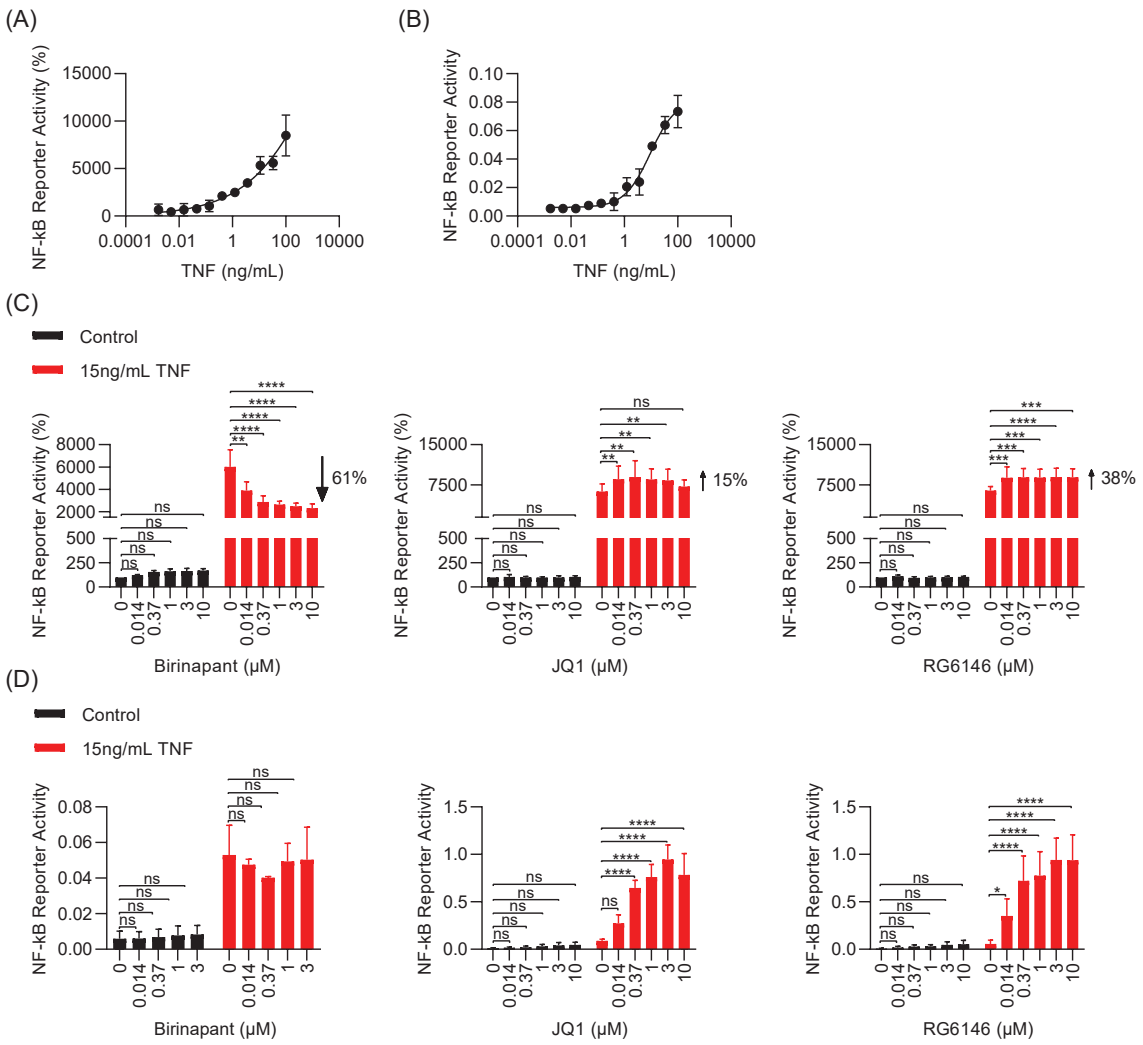

Figure 37: (A) NF-κB Activity was analyzed in HCT-116 cells by measuring Luciferase activity 6 h post treatment with a dose response of TNF. Data was normalized to DMSO and represents mean of three biological independent experiments. (B) As described in *A* except that Luciferase signal was analyzed 72 h post treatment and data was normalized to the viability after 72 h. (C) As described in *A* except that cells were treated with increasing concentrations of Birinapant or BETi single agent or in combination with 15 ng/mL TNF. Statistical significance indicates difference between RG6146 treatment and control (2-way ANOVA, **p<0.01, ***p<0.001, ****p<0.0001, ns: not significant). (D) As described in *C* except that Luciferase signal was assessed after 72 h and data was normalized to cell viability. Statistical significance indicates difference between RG6146 treatment and control (2-way ANOVA, *p<0.05, ****p<0.0001, ns: not significant).

4.3.5 RG6146 as a potential co-therapeutic intervention together with Immunotherapy *in vitro*

Although immunotherapies are potent treatment options for various cancer types, the potential of malignant cells to develop resistance during onset of treatment has been described [232]. Therefore, it is important to identify treatment combination strategies to prevent cancer cell adaption and induce uniform tumor regression of all heterogeneous tumor cell populations.

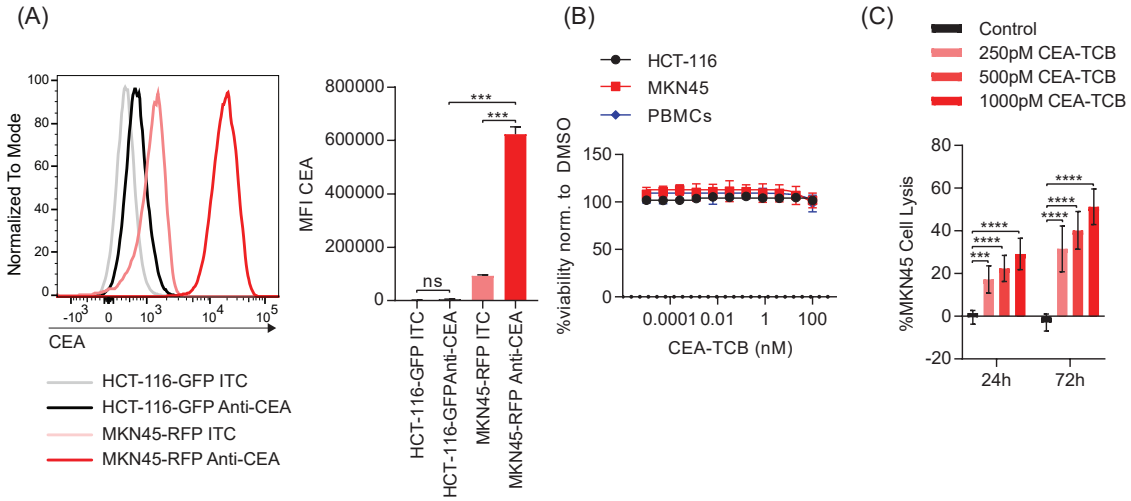

Figure 38: (A) CEA level of HCT-116-GFP and MKN45-RFP cells was assessed by flow cytometry on live single cells using a CEA specific antibody (anti-CEA) or Isotype Control (ITC). Data shows median fluorescence intensity (MFI) and includes mean of three biological independent experiments. Statistical significance indicates difference between ITC and anti-CEA as well as difference between CEA level of HCT-116-GFP and MKN45-RFP cells (2-way ANOVA, ***p<0.001, ns: not significant). (B) Viability of HCT-116 cells, MKN45 cells and PBMCs was assessed after 72 h of treatment with a dose response of CEA-TCB. Data of three biological independent experiments is shown and was normalized to control. (C) Lysis of MKN45 cells was assessed using the LDH assay system. MKN45 cells were co-cultured with PBMCs and increasing concentrations of CEA-TCB or control and cell lysis determined after 24 and 72 h. Mean of three biological independent experiments is shown. Statistical significance indicates difference between CEA-TCB and control (2-way ANOVA, ***p<0.001, ****p<0.0001, ns: not significant).

Since, RG6146 was shown to sensitize cancer cells to TNF induced cell death and it is known that activated T cells release TNF into the immunological synapse [85]; immunotherapy was employed to activate T cells and assess the effect in combination with RG6146. While HCT-116 cells lack CEA on the surface, MKN45 cells present CEA on the cell surface (Figure 38 A) and are therefore target cells of the CEA-TCB. CEA-TCB single

agent treatment did not affect viability of PBMCs, HCT-116 or MKN45 cells 72 h post treatment (Figure 38 B), however, CEA-TCB treatment in a co-culture with PBMCs and MKN45 cells induced significant MKN45 cell lysis after 24 and 72 h of treatment (Figure 38 C). Despite observing an effect on cell viability with treatment of RG6146 and TNF in previous experiments after 72 h, it was not possible to solely combine RG6146 with CEA-TCB at this time point. This is because CEA-TCB treatment is very potent in inducing target cell death as early as 24 h after assay set up (Figure 38 C).
Therefore, the assay set up was optimized in order to assess CEA-TCB effects in combination with RG6146. CEA-TCB was co-cultured with PBMCs and MKN45 cells for 24 h, which induced release of cytokines including TNF into the culture supernatant (Figure 39 A-B). Supernatant containing cytokines was then collected and added on freshly plated HCT-116 and MKN45 cells treated with a dose response of RG6146 for 72 h (Figure 39 A). As a control, supernatant of MKN45 or PBMC mono-cultured cells treated with CEA-TCB was added, which did not affect viability of MKN45 cells in combination with RG6146 (Figure 39 C-D). While supernatant of non-activated PBMCs co-cultured with MKN45 (no CEA-TCB) in combination with RG6146 had a similar effect on HCT-116 and MKN45 cell viability between different PBMC donors, supernatant of distinct activated PBMC donors (+ CEA-TCB) induced variable effects on cancer cell viability (Figure 39 E-J). Supernatant from one activated PBMC donor decreased viability only upon addition of RG6146 (Figure 39 E&H), while supernatant of the other two activated donors reduced viability by themself and viability was further decreased upon addition of RG6146 (Figure 39 F,G,I&J). Combination of RG6146 with supernatant of activated PBMCs decreased viability and induced apoptosis visualized by induction of PARP cleavage (Figure 39 E-L). Addition of a TNF blocking molecule significantly rescued growth inhibition induced by RG6146 and supernatant from activated PBMCs (Figure 39 M). These results clearly show that TNF, released by actived T cells, is able to induce cell death in combination with RG6146.

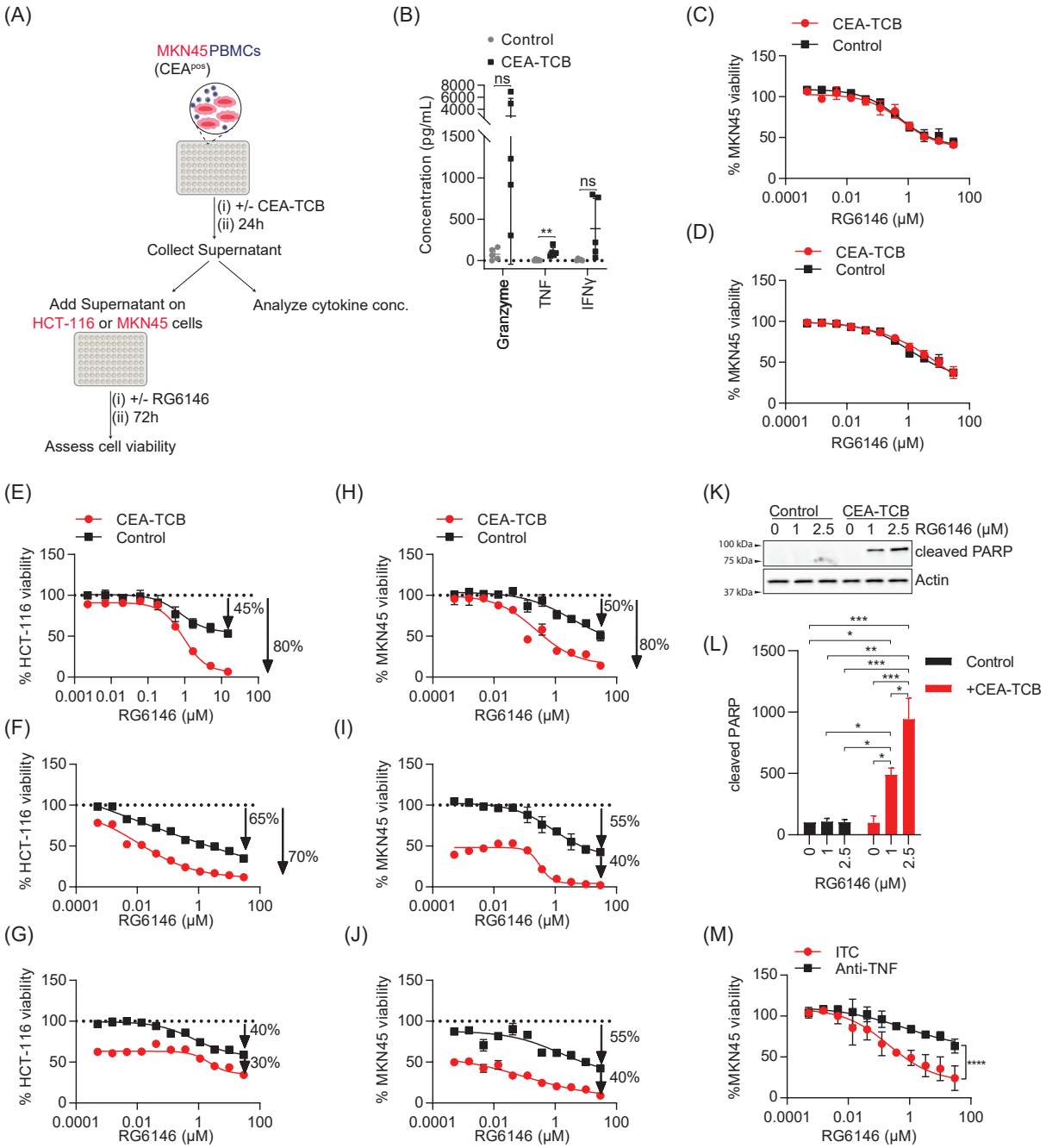

Figure 39: (A) Shematic of supernatant assay. MKN45 cells were co-cultured with PBMCs and 20 nM CEA-TCB or control for 24 h before supernatant collection, cytokine analysis and addition of supernatant on freshly plated HCT-116 and MKN45 cells. Cells were treated with a dose response of RG6146 or control and viability assessed by CTG2.0 after 72 h of treatment. Data was normalized to DMSO control of each treatment. (B) Cytokine concentration in the supernatant as described in *A* was analyzed using flow cytometry. Mean of five biological independent experiments is shown. Statistical significance shows difference between CEA-TCB and control treatment (Unpaired T-Test for each cytokine-group calculated separately, **p<0.01, ns: not significant). (C-D) Viability of MKN45 cells upon addition of supernatant from a (C) PBMC or (D) MKN45 cell monoculture (+/− CEA-TCB) and treatment with a dose response

of RG6146 for 72 h. Viability was assessed by CTG2.0 and results normalized to DMSO. Mean of three technical replicates of one experiment is shown. (E-J) Viability of (E-G) HCT-116 and (H-J) MKN45 cells as described in *A*. Data of three biological independent PBMC Donors is shown (K) Western blot to detect cleaved PARP and Actin in MKN45 cells treated with supernatant of a PBMC and MKN45 co-culture +/− CEA-TCB and increasing concentrations of RG6146. One representative experiment is shown. (L) Quantification of western blot described in *K*. Cleaved PARP levels were normalized to untreated control. Mean of three biological independent experiments is shown. Statistical significance of differences between treatments was calculated using a 2-way ANOVA (*p<0.05, **p<0.01. ***p<0.001, if not indicated: not significant). (M) As described in *A* except that the co-culture for supernatant production was treated with CEA-TCB and either a TNF-blocking molecule (anti-TNF) or isotype control (ITC). Mean of three biological independent experiments is shown. Statistical significance shows difference between highest concentration of RG6146 and anti-TNF or ITC (2-way ANOVA, ****p<0.0001).

Tumors are intrinsically heterogeneous and even though CEA-TCB treatment will recognize cells expressing high levels of CEA, tumor cells showing low CEA production potentially escape T cell attack and might develop resistance against therapy. Bystander killing is induced when activated T cells do not only kill target cells, but also cells in close proximity through the release of cytokines. These bystander cells would usually not be recognized by treatment with CEA-TCB (Figure 40 A). Hence, it was assessed if RG6146 boosts bystander killing of HCT-116 cells, which are CEA negative. RFP-positive MKN45 (CEA positive) cells were co-cultured with GFP-positive HCT-116 (CEA negative) cells and PBMCs. Afterwards, cells were treated with CEA-TCB or control and a dose response of RG6146, while cell growth was monitored over time (Figure 40 B). CEA-TCB in combination with RG6146 resulted in significant reduction of HCT-116 cell density compared to RG6146 single agent treatment (Figure 40 C-D).
In conclusion, RG6146 augments direct target cell killing induced by the CEA-TCB in a TNF dependent manner. In addition, RG6146 also boosts bystander killing of CEA negative cells indicating that this small molecule is a potential combination partner with immunotherapy.

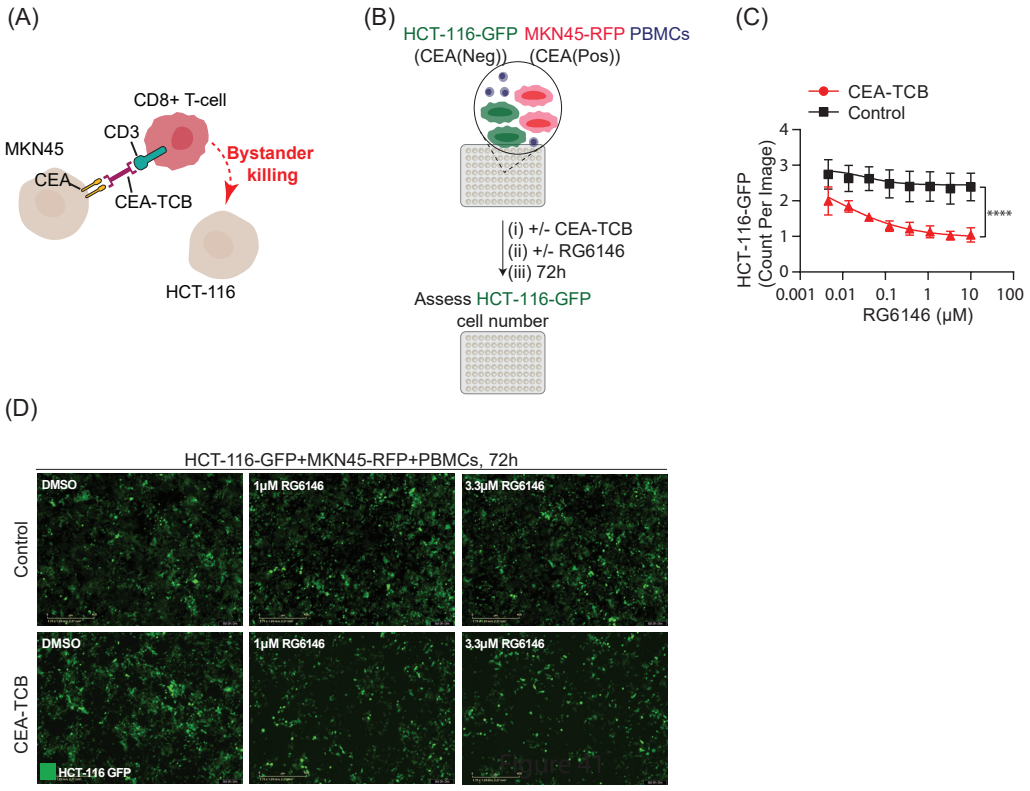

Figure 40: (A) Shematic of bystander killing. MKN45 cells expressing CEA are recognized by the CEA-TCB and induce T cell activation thereby promoting cell death of cells in close vicinity regardless of the presence of CEA (B) Shematic of bystander killing assay set up. HCT-116 cells expressing GFP (HCT-116-GFP) were co-cultured with MKN45 cells expressing RFP (MKN45-RFP) and PBMCs as well as a dose response of RG6146 +/− 40 nM CEA-TCB. Growth was monitored using a live cell imaging system and cell number of HCT-116 cells assessed after 72 h of treatment. (C) As described in *B*. Mean of three biological independent experiments is shown. Statistical significance shows difference between highest concentration of RG6146 and CEA-TCB and RG6146 single agent treatment (2-way ANOVA, ****p<0.0001). (D) Representative images of HCT-116-GFP cells of experiment described in *B*-*C*.

4.3.6 BETis as a potential co-therapeutic intervention together with Immunotherapy *in vivo*

To further validate *in vitro* findings, the next consequent step was to verify these results *in vivo*. Data acquired in previous *in vivo* studies by the oncology pharmacology department at Roche and our collaborators has shown that mouse model tumors are less sensitive to RG6146 treatment as compared to its precursor JQ1 (Data not shown). Therefore, a direct comparison of JQ1 and RG6146 on viability was conducted *in vitro* by analyzing

the human MKN45 and mouse MC38 colorectal cell lines (Figure 41 A). MC38 cells were more sensitive to JQ1 and RG6146 in combination with TNF as compared to MKN45 cells. Furthermore, in both cell lines treatment with JQ1 and TNF showed a lower IC_{90} value indicating higher sensitivity (Table 4). However, while low concentrations of JQ1 combined with TNF clearly induced a stronger decrease in viability in MC38 cells, RG6146 had a more potent effect on viability at low concentrations in MKN45 cells (Figure 41 A). Since MC38 was the selected tumor model for *in vivo* studies, it was assessed why this cell line is less sensitive to RG6146 *in vitro*. One explanation could be the presence of ABCB1, which is an export transporter responsible for the removal of RG6146 from the cytoplasm [238]. Therefore, it was tested if the ABCB1 inhibitor Zosuquidar sensitizes MC38 cells to RG6146 treatment. Since 0.5 µM Zosuquidar did not decrease MC38 cell viability in combination with TNF (Figure 41 B), this concentration was used for the combination with BETis. Zosuquidar induced a significant change in sensitivity to RG6146 and TNF treatment, while sensitivity was unchanged in cells treated with JQ1 and TNF (Figure 41 C). These results indicate that ABCB1 is responsible for the reduced sensitivity of MC38 cells to RG6146 and caused the use of JQ1 in MC38 tumor models *in vivo*.

Table 4: IC_{90} values (µM) of MC38 and MKN45 treated with TNF and BETi calculated by GraphPad Prism 8 from data shown in Figure 41 A

Cell line & Treatment	IC_{90} (µM)
MC38	
15 ng/mL TNF+ Dose response JQ1	0.7
15 ng/mL TNF+ Dose response RG6146	3
MKN45	
15 ng/mL TNF+ Dose response JQ1	2.5
15 ng/mL TNF+ Dose response RG6146	5

In vivo experiments were performed by Thomas Friess and Daniela Geiss. Syngeneic mice were inoculated with MC38 tumor cells expressing CEACAM5 and treated with the combination of CEA-TCB and JQ1, single agent or vehicle control while monitoring tumor volume (Figure 41 D) and verifying that body weight was stable over the course of treatment (Figure 41 E). JQ1 and CEA-TCB single agent decreased tumor volume by 50 and 60 %, respectively. The combination of both molecules, however, induced significant tumor regression (Figure 41 F-G).

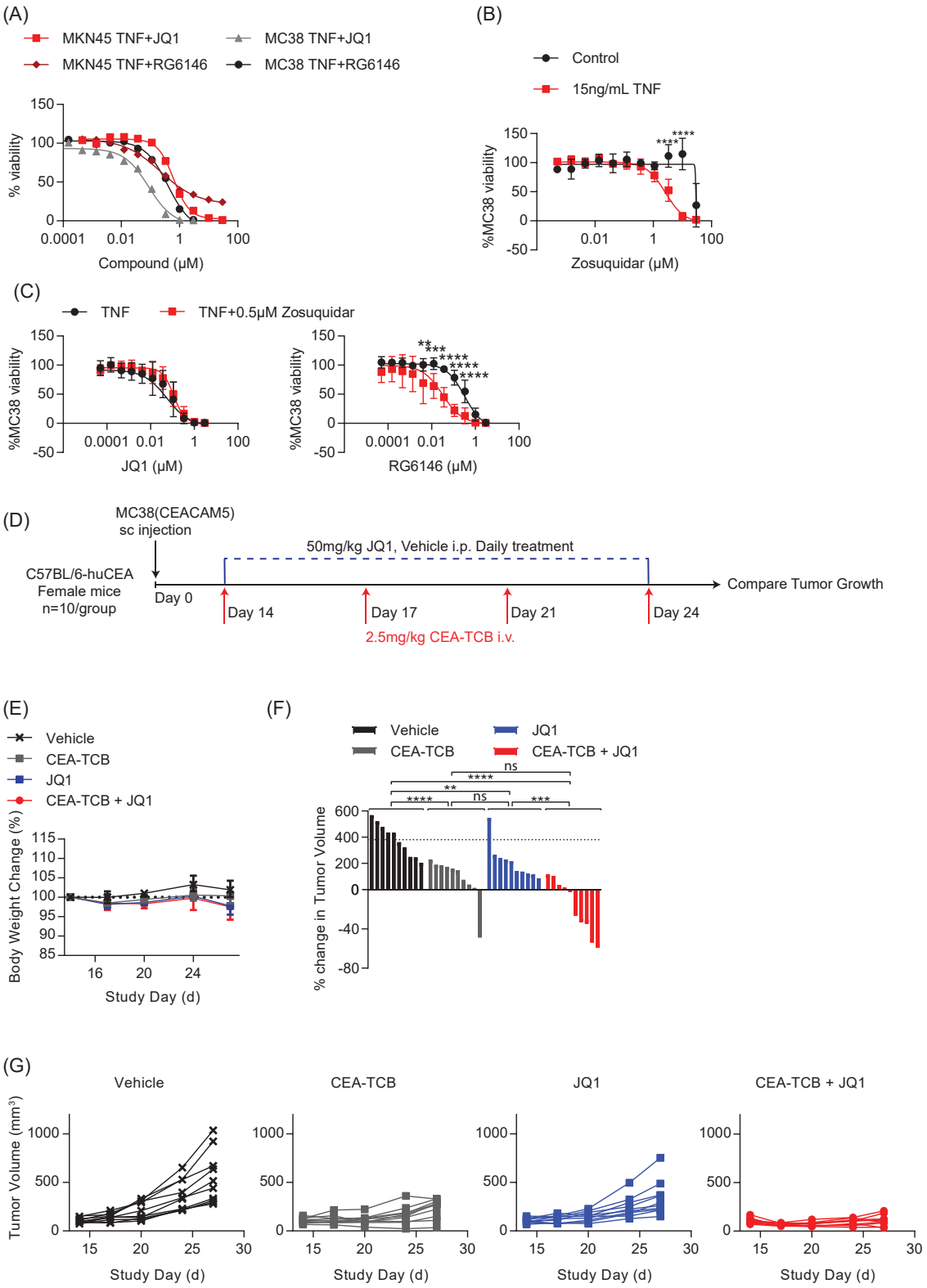

Figure 41: (A) Viability of MC38 or MKN45 cells treated with a combination of BETi and TNF for 72 h was assessed by CTG2.0. Data represents one biological experiment. (B) Viability of MC38 cells was assessed by CTG2.0 after 72 h of treatment with Zosuquidar alone

or in combination with 15 ng/mL TNF. Data was normalized to control and shows mean of three biological independent experiments. Statistical significance indicates difference between Zosuquidar+TNF and Zosuquidar single agent treatment, If not indicated, not significant (2-way ANOVA, ****p<0.0001). (C) Viability of MC38 cells was assessed 72 h post treatment with a dose response of BETi in combination with TNF +/− 0.5 µM Zosuquidar by CTG2.0. Data was normalized to DMSO and shows mean of three biological independent experiments. Statistical significance shows difference between BETi+TNF+Zosuquidar and BETi+TNF. If not indicated, not significant (2-way ANOVA, **p<0.01, ***p<0.001, ****p<0.0001). (D) Shematic of *in vivo* assay. Human CEA transgenic C57BL/6 mice bearing CEACAM5 expressing MC38 tumors (n=10 mice per treatment group) were treated with 2.5 mg/kg CEA-TCB antibody twice weekly, 50 mg/ kg JQ1 daily, or the combination and tumor growth was monitored throughout the study. (E) Percent change in body weight of mice described in *D.* (F) Bar graph showing the % change in tumor volume on day 13 compared to day 0 of study (relative to start of treatment) as described in *D.* Statistical significance shows difference between treatment groups (2-way ANOVA, **p<0.01, ***p<0.001, ****p<0.0001, ns: not significant). (G) Tumor growth curves showing tumor volume over the course of treatment as described in *D.*

To identify the role of TNF on tumor regression induced by CEA-TCB and JQ1, a TNF blocking molecule was added to the different treatment conditions. Under these conditions, the body weight of mice was unaffected during the course of treatment (Figure 42 A). In general, combination treatment of JQ1 and CEA-TCB induced a significant but less potent decrease in tumor volume as compared to the previous experiment (Figure 42 B-C). However, while anti-TNF treatment did not affect tumor growth in the vehicle control treated group, the effect of the JQ1 and CEA-TCB combination group was dampened by TNF blockade (Figure 42 B-C).

These results show that JQ1 and CEA-TCB induce potent tumor regression in MC38 syngeneic tumor models and this effect is most likely induced through BETi dependent sensitization of cells to TNF induced cell death.

To further validate the potential combination of BETi and immunotherapy, MC38 syngeneic mice were treated with anti-PD-1 therapy and JQ1 by Dane Newman (Figure 43 A). Data of two biological independent experiments showed a significant decrease of tumor volume upon JQ1 single agent treatment and a further significant decrease with combination treatment, while only a marginal change in tumor volume was observed with anti-PD-1 single agent treatment (Figure 43 B). Interestingly, even though JQ1 treatment reduced tumor growth, this did not lead to prolonged survival of most mice. Mice that did respond to anti-PD-1 treatment, however, showed a potent survival and this effect was amplified with combination treatment (Figure 43 C).

In conclusion, these *in vivo* experiments further strengthen our hypothesis that BETis are potent combination partners for immunotherapy including CEA-TCB and anti-PD-1 therapy by sensitizing cells to TNF induced cell death.

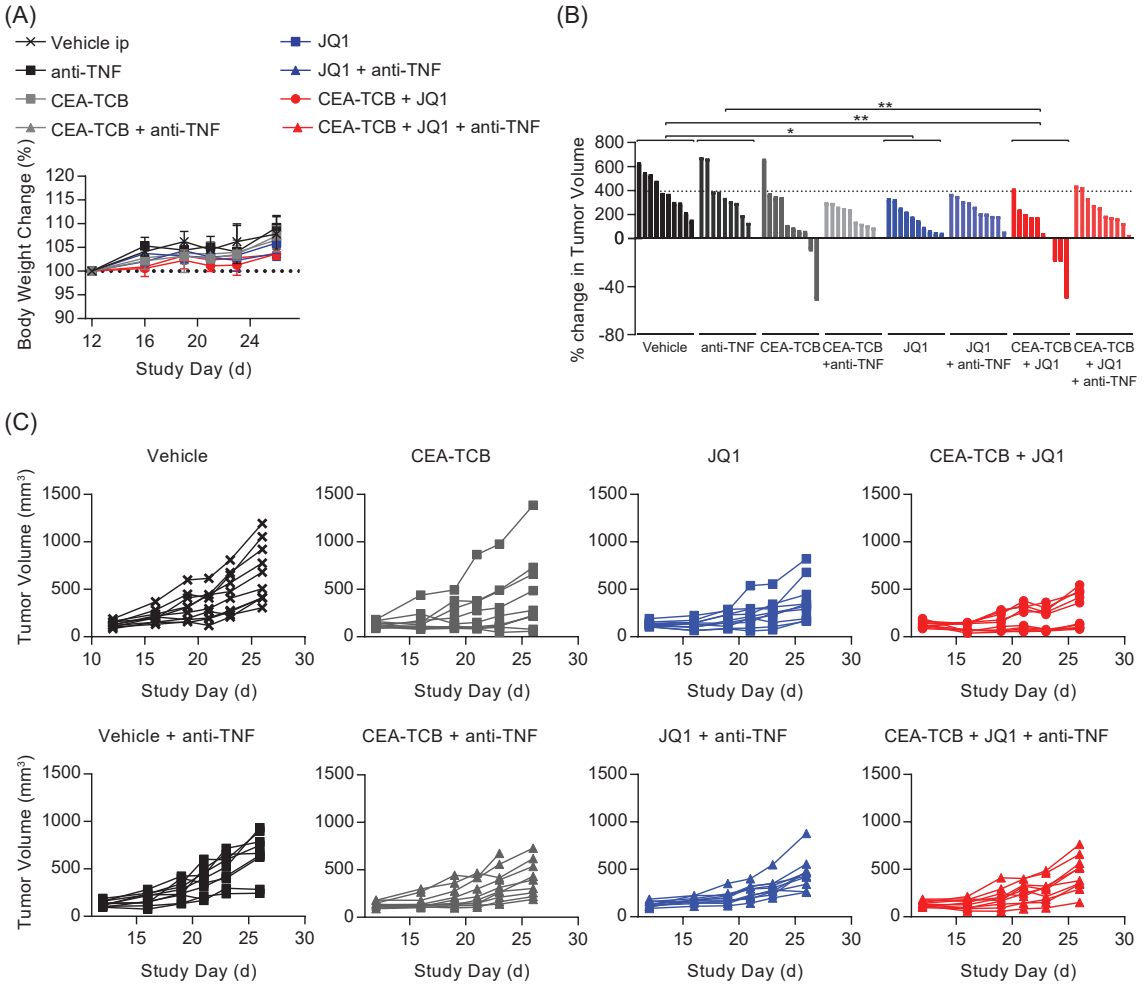

Figure 42: (A-C) As described in *Figure 41 A* except that mice were additionally treated with 2 mg/kg TNF neutralizing antibody twice-weekly. (A) Percent change in body weight of mice. (B) Bar graph showing the % change in tumor volume on day 14 compared to day 0 of study (relative to start of treatment). Statistical significance was calculated with GraphPad Prism 8. If not indicated, not-significant (2-way ANOVA, *p<0.05, **p<0.01). (C) Tumor growth curves showing tumor volume over the course of treatment.

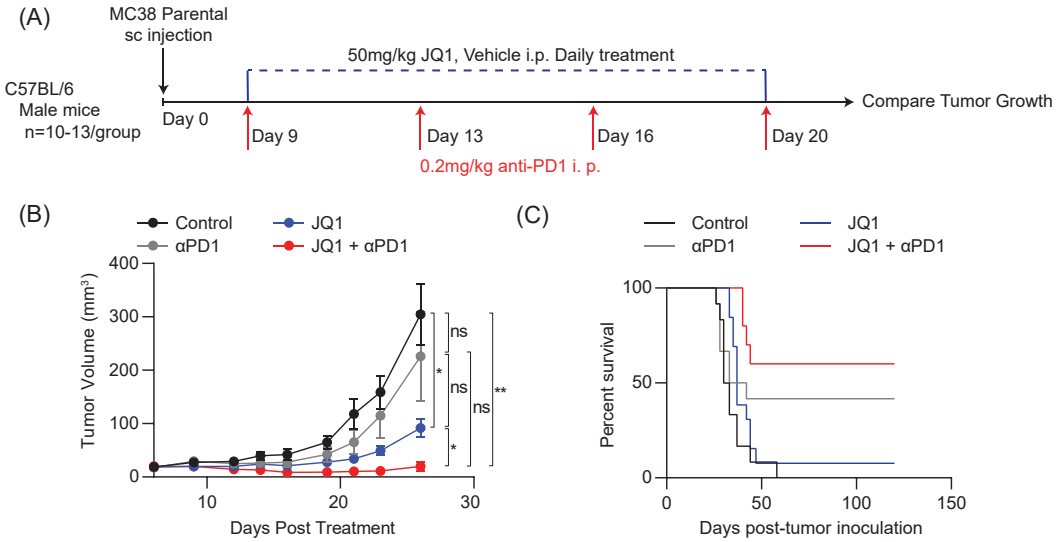

Figure 43: (A) Shematic of *in vivo* assay. Wild-type C57BL/6 mice bearing MC38 tumors (n=10-13 mice per treatment group) were treated with control or 50 mg/kg JQ1 daily (ip) and/or twice weekly with 0.2 mg/kg anti-PD-1 (αPD1) (ip). (B) Average tumor growth curves of experiment described in *A*. Mean of two independent experiments (+/− SEM) is shown. Statistical significance indicates difference between treatment groups of the last tumor measurement (2-way ANOVA, *p<0.05, **p<0.01). (C) Kaplan-meier survival curve of the experiment described in *A*. Overall survival of mice in percent is shown.

5 Discussion

5.1 Resistance of MM cell lines to RG6146 treatment

Acquired resistance to anti-cancer therapy is a challenge that can arise during the onset of treatment [276]. The understanding of how cancer cells avoid destruction by therapies is crucial to develop sucessful treatments such as combination therapies. In this thesis, mechanisms of primary resistance in MM cell lines to RG6146 were evaluated focusing on the expression of the transcription factor *MYC*, levels of pro- and anti-apoptotic proteins, in addition to the export transporter ABCB1.

Expression of *MYC* as well as RG6146 dependent decrease in c-Myc protein level were comparable between responders and non-responders indicating that sustained or elevated c-Myc level is not responsible for inducing resistance in the tested cell lines. Nonetheless, resistance to BETi treatment has been linked to *MYC* expression in acute myeloid leukemia (AML) [277]. In AML, BETi treatment initially decreased *MYC* expression, however, levels of this transcription factor were quickly restored [277]. This observed resistance mechanism was linked to the inactivation of PRC2 and subsequent remodeling of regulatory landscapes including the activation and recruitment of important players of the WNT signaling pathway to focal *MYC* enhancers [277]. Cancer cells thereby compensate for the loss of BRD4 at enhancer elements [277]. To further validate these findings, overexpression of *MYC* in responders should be assessed in the context of RG6146 treatment as well as proteins involved in the WNT signaling pathway.

Another hypothesis was built on the fact that BETis have been shown to modulate the balance between pro- and anti-apoptotic proteins and consequently induce cell death [265, 266]. Our results did not give a clear conclusion between the regulation of pro- and anti-apoptotic proteins by RG6146. Only a slight trend in upregulation of Mcl-1 was visible for the non-responder cell line KMS-11. Additional experiments are needed to further evaluate if Mcl-1 can induce resistance such as overexpression of Mcl-1 or other anti-apoptotic proteins in responders. Interestingly, breast and hepatocellular carcinoma cells have been shown to increase Mcl-1 levels upon BETi treatment thereby conferring resistance to therapy [278, 279]. In this context, a combination of BETi and Mcl-1-inhibitor was synergistic in cells with amplified *MCL1* expression [279]. Another protein that can be target to enhance sensitivity to BETi therapy is Bcl-2. In KMS-12-BM cells, co-treatment with the Bcl-2 inhibitor Venetoclax and RG6146 enhanced tumor regression when compared to single agent treatment. This is in line with findings by Spriano et al., where DLBCL cell lines, which are resistant to BET-inhibition, synergized with Venetoclax [280].

Lastly, it was investigated if the export transporter ABCB1 confers resistance to RG6146. ABCB1 is a well-known mechanism of cells to induce resistance to small molecules [242]

including RG6146 [238]. Indeed, the BETi-resistant cell line KMS-34 showed elevated levels of ABCB1, which were even further enhanced by addition of RG6146. Co-treatment with the ABCB1-inhibitor Zosuquidar restored sensitivity in this cell line. We therefore conclude that ABCB1 is at least in part responsible for inducing resistance in KMS-34 cells. A similar mechanism was seen for MC38 cells, which showed a higher sensitivity to JQ1 and TNF treatment as compared to RG6146 and TNF treatment. Also in MC38 cells, addition of Zosuquidar sensitized cells to RG6146 and TNF treatment, thereby further confirming that ABCB1 expression reduces sensitivity to RG6146.
Taken together, this thesis gave some insight in potential resistance mechanisms of MM cell lines to RG6146 treatment. During the course of this thesis, research groups have published various findings supporting our hypothesis of Mcl-1 mediated resistance in other tumor types [278, 279]. However, resistance to BETi might be mediated through additional mechanisms. In castration-resistant prostate cancer (CRPC), for example, resistance to BETi was induced through the loss of NCOR2, which is a potent inhibitor of DUB3 [281]. DUB3 deubiquitinates BRD4 and thereby stabilizes this BET protein. Catalytic activity of DUB3 is regulated by CDK4/6 phosphorylation, thereby showing a potential combination strategy of CDK4/6 and BET-inhibition in CRPC [281]. It would be interesting to test the protein levels of DUB3 and NCOR2 in resistant MM cells and validate if the described mechanisms also play a role in conferring resistance to RG6146 in this cancer type. Furthermore, in ovarian cancer resistance to BETi has been linked to kinome reprogramming [282]. This includes enhanced activity and dependence on PI3K/ERK signaling and stabilization of MYC/FOSL1 upon chronic BETi treatment [282]. This study opened a new therapeutic intervention using kinase inhibitors in combination with BETis in ovarian cancer [282].
My results together with the mentioned published findings highlight the heterogeneity of resistance-mechanisms developed by cancer cells. Further experiments are needed to validate which mechanisms induce primary resistance to RG6146 in KMS-11 cells. It remains elusive if several pathways are working in concert to confer resistance or if the modulation of one specific protein like Mcl-1 can induce treatment resilience. The comparison of RNA-seq analysis of sensitive versus resistant cell lines pre and post RG6146 treatment will give further insights.

5.2 RG6146 modulates immune cell function

The effect of BETis on T cells is under strong debate. In fact these molecules can have immunosuppressive and immune activating functions. The group of Mele et al. [52] showed that JQ1 suppresses the differentiation of naïve $CD4^+$ T cells into Th17 cells and inhibits the production of effector cytokines GM-CSF, IL-21 and IL-22. Further, direct binding of BRD4 to the *Il17* locus was inhibited by JQ1 thereby suppressing the production of

IL-17. Differentiation of naïve $CD4^+$ T cells into Th1, Th2 or T regs was not affected by JQ1 in their assays. Since BETi treatment also decreased the differentiation of Th17 cells *in vivo*, BETis are thought to be a promising treatment strategy for autoimmune diseases.[52] Wang et al. [283] recently proposed the underlying mechanisms of action that induces this phenotype. The group showed that JQ1 interacts with the bromodomain of p300 thereby inhibiting acetylation of RORγt, which is essential to induce transcription of effector cytokines.[283] Though, another group showed that despite decreasing IL-17 production in Th17 cells, inflammation was hardly affected by BETi treatment *in vivo* [284].

In contrast to the proposed immune suppressive functions of BETi, JQ1 has also been shown to enhance expansion of central memory T cells (TCM) and stem cell like memory T cells (TSCM) [53]. At the same time, the differentiation into effector memory T cells (TEM) was suppressed by BETi treatment. It is suspected that p300 recruits BRD4 to the BATF promoter thereby inducing differentiation into TEM and this mechanism is inhibited upon addition of BETi. Further, JQ1 enhanced persistence of adoptively transferred CAR T cells *in vivo* leading to enhanced antitumor effects. These experiments show promising combination treatment of BETi with CAR-T cell therapy.[53]

Due to the contradictory results regarding BETi effect on T cells described in literature, we focused on the effect of RG6146 on $CD4^+$ and $CD8^+$ T cell activation. At early time points, T cell activation was reduced by RG6146. A significant decrease in proliferation and co-inhibitory markers clearly indicate a T cell suppressive phenotype upon BETi treatment. A similar effect was also seen by Georgiev et al., who showed a decrease of *LAG3*, *GZMB* and *IFNG* transcription upon BETi treatment [285]. In contrast, Bandukwala et al. demonstrated that BETi augment RNA-levels of the co-inhibitory receptor *LAG3* in Th1 cells 4 h post treatment [284]. Georgiev et al. [285] also validated antiproliferative effects of BETi through downregulation of genes involved in G1/S-phase cell cycle transition and a significant decrease in T cell proliferation. Yet, no long term treatment was analyzed in their assays [285]. Interestingly, they also described a significant increase in BETi mediated death of T cells [285], which does not confirm our findings. However, this discrepancy might be explained through the different BETis used in the studies. We also observed a significant increase in CD69 level upon RG6146 treatment. This effect was unexpected considering that CD69 is an early marker for T cell activation. Despite suppression of T cell activation at early time points, the percentage of proliferating T cells was comparable to control treatment using a longer treatment time. Moreover, RG6146 treated T cells had undergone a higher number of division cycles than untreated T cells. These findings indicate that RG6146 does suppress T cell activation at early time points, but enhances proliferation and activation during onset of treatment. If RG6146 treatment induces just a delay or even boosts T cell activation during a longer treatment

period is unknown and needs further experimental validation. Whilst T cell activation was analyzed in three distinct assays *in vitro*, a clear answer about the role of BETis on T cell activation can only be achieved in *in vivo* models. This is especially valuable, because *in vitro* isolation of T cells usually yields only a low number of cells. These cells are potentially stressed by the isolation procedure and the following small molecule treatment might further enhance cellular stress responses. Therefore, *in vivo* and clinical data is the only reliable method to confirm *in vitro* findings.

While intracellular and released level of tested cytokines were mostly decreased by RG6146 treatment, a trend of increasing MIP1α level in the supernatant of the T reg suppression assay was detected. MIP1α is a chemoattractant inducing recruitment of B cells, $CD4^+$ and cytotoxic T cells [286] and has been shown to be produced by dendritic cells and $CD4^+$ T cells [287]. MIP1α recognition through the CCR5 receptor, is involved in the migration of naïve $CD8^+$ T cells towards antigen specific dendritic cell-$CD4^+$ T cell interaction [287]. This is an important mechanism since MIP1α and MIP1β blockade reduces number and effector activity of memory $CD8^+$ T cells [287]. RG6146 mediated increase in MIP1α levels is therefore a potential indication for enhanced recruitment of immune cells to a site of infection. It is to note that RG6146 does not specifically elicit its function in the tumor or at a site of infection and could therefore harbor the risk of inducing a systemic immune cell activation enhancing the threat of autoimmunity.

The discrepancy of results presented in different research studies might be explained by the use of different treatment time points, activation methods, T cell subsets used and small molecule dosage. Further, the underlying mechanism of action is still unknown. Therefore, it is of need to gain a deeper understanding of how and why BETi modulate T cell activation in the future.

While one main focus of this thesis was to elucidate the effect of RG6146 on T cell activation, one experiment also gave insights in potential effects of RG6146 on DCs. DC maturation was suppressed with increasing concentrations of RG6146, which is in line with findings by Schilderink et al. [288]. The authors demonstrated that iBET-151 was able to suppress maturation of DCs and reduces levels of pro-inflammatory cytokines including IL-6, IL-12p70 and IL-10 as well as costimulatory receptors CD80 and CD86. BETi treatment of DCs also enhanced the generation of $FoxP3^+$ T cells.[288] Toniolo et al. [289] investigated a similar mechanism by using JQ1 to suppress DC maturation in a STAT5 dependent manner. BETi treatment of DCs modulated levels of pro- and anti-inflammatory cytokines, decreased levels of the costimulatory markers CD80, CD86, CD83 and reduced proliferation of $CD4^+$ and $CD8^+$ T cells.[289] The suppressive effect of RG6146 on DC maturation was only visible at high RG6146 concentrations in our assays. Therefore, it will be of need to identify BETi concentrations that do not inhibit DC maturation to circumvent the generation of an immune suppressive environment.

5.3 RG6146 synergizes with TNF to induce cell death

While separate examination of cell types provided valuable insights on the molecular mechanism of BETis, evaluation of its influence on the interface between immune and cancer cells has further fostered the understanding of BETis and their potential combination strategies.

Our initial epigenetic small molecule screen identified BETis as the only class of epigenetic modifiers that consistently induced specific and profound T cell mediated HCT-116 cell killing. These results suggest that it requires the engagement of a specific set of transcriptional factors and not general defects in transcriptional activity to induce this phenotype. Still, other epigenetic therapies such as HAT-inhibitors, demethylating agents or HDACi might synergize with immunotherapy in a distinct mode. Indeed, previous studies have demonstrated that epigenetic modifiers are promising combination partners for immunotherapy. Demethylating agents and HDACi have been shown to enhance the expression of antigen presenting molecules and tumor antigens [290, 291]. Other epigenetic therapies induced viral mimicry and interferon production [292]. It would be interesting to test if epigenetic modifiers enhance TNF production in a similar manner.

In this thesis, it was shown that BETis sensitize cancer cells to TNF induced cell death by modulating NF-κB signaling, decreasing pro-survival target genes including *BIRC2* (cIAP1) and *BIRC3* (cIAP2) and induce cell death through extrinsic apoptosis (Figure 44). A similar mechanism was reported in a genetic screen in IFNγ-receptor-deficient melanoma cells challenged with MART-1 T cells [293]. The group found that cells deficient of *TRAF2* or *BIRC2* lowered the cytotoxic threshold towards TNF induced cell death. The authors discovered that combining *TRAF2* knockout with an IAP-inhibitor augments sensitivity to TNF and enhances therapeutic outcome in combination with immune checkpoint blockade.[293] In this context, SMAC mimetics which re-establish apoptotic pathways by inducing the degradation of IAPs [137], would be promising combination partners for immune oncology (IO) agents. Specifically, SMAC mimetics function by enhancing the NF-κB pathway, which eventually induces production of TNF thereby priming cells to induce apoptosis [136, 137, 294]. The similar function of BETis and SMAC mimetics prompts the question of why BETis would be the superior treatment option in this matter. Unlike SMAC mimetics, BETis are known to elicit additional effects on gene regulation in cells including the suppression of *PD-L1*, which can enhance immunomodulatory properties of IO agents [49]. To gain further understanding on the holistic mechanism of action, single cell RNA-seq of cells located in the TME will give a clear insight on the effect of BETis on immune cell subsets. Studying the mechanism of BETis in the TME in more detail will also help to choose patients that will respond best to combination therapy.

Our results show that TNF treatment enhances the recruitment of BRD4 to p65 bound *cis*-regulatory elements and a partial loss of BRD4 binding at these sites was visible upon addition of RG6146. The potential underlying mechanism of how BET proteins modulate NF-κB signaling has also been addressed by different research studies. One study suggests that BRD4 binds a p300 mediated acetylation of lysine-310 in the RelA(p65) protein thereby operating as a transcriptional coactivator of some NF-κB target genes [295, 296]. This is in line with our findings, where BETi suppressed expression of a specific set but not all genes activated upon TNF treatment. However, while cIAP2 level was not affected by BETi and TNF treatment in a study by Zou et al. [296], we show that TNF-induced cIAP2 production was strongly suppressed upon addition of RG6146. The hypothesis that BRD4 directly binds acetylated p65 was underpinned by studies focusing on the histone deacetylase SIRT1, which removes K310 acetylation of p65 resulting in inhibition of NF-κB target genes and sensitization of cells to TNF induced apoptosis [297]. Work in endothelial cells has shown that TNF induces p65 mediated recruitment of BRD4 to form *de novo* super-enhancer regions thereby inducing pro-inflammatory gene transcription [298]. Zou et al. presented results showing that BRD4 binding to acetylated p65 in A549 lung cancer cells stabilized and protected nuclear p65 from ubiquitination and degradation and treatment with JQ1 decreased TNF mediated induction of κB-driven reporter genes [298]. In contrast, we observed an increase in NF-κB luciferase reporter signal by RG6146 or JQ1 in combination with TNF. This would suggest a possible dual role of BETis in response to TNF. Thus, RG6146 could suppress some NF-κB target genes and simultaneously enhance some others following TNF treatment. In fact, RNA-seq analysis revealed genes that were even further enhanced upon addition of RG6146 indicating that not all NF-κB target genes are dependent on BET-binding. The fact that some NF-κB target genes are increased in the presence of BETis and TNF could also be explained by the concomitant suppression of the classical NF-κB pathway and activation of the alternative NF-κB-pathway (Figure 44). One prominent player of alternative NF-κB activation is the NF-κB inducing kinase (NIK), which is constitutively active but degraded in unstimulated conditions [299]. NIK degradation is mediated through binding of TRAF3 and complex formation with TRAF2, cIAP1 and cIAP2 [113, 135, 300, 301], which induce ubiquitination and proteasomal degradation of NIK [137]. TNF binding to TNFR2 suppresses degradation of NIK and initiates NF-κB translocation to the nucleus. How NIK is released from the complex is not entirely understood, but involves the recruitment of TRAF2,3 and cIAP1,2 to the receptor. Subsequently, TRAF3 is degraded, which is the direct binding partner of NIK.[301, 302, 303] In this scenario, unbound NIK is able to induce the alternative NF-κB activation and processing of p100 to p52 [302]. In short, cIAP1 and cIAP2 are essential for the activation and suppression of the classical and alternative NF–κB pathway, respectively. Therefore, it is possible that suppression

of cIAP1 and cIAP2 by RG6146 induces alternative NF–κB signaling. This hypothesis is supported by the finding that also SMAC mimetics show an induction of the classical and alternative NF-κB signaling pathway, processing of p100 to p52 and facilitating the transcription of NF-κB target genes [136, 137, 304, 305]. In particular, in glioblastoma cells, SMAC mimetics at non-toxic concentrations have been shown to induce cell elongation, migration and invasion through upregulation of alternative NF-κB signaling [305]. The similar mechanisms induced by SMAC mimetics and BETis raise the question if RG6146 in combination with TNF also induces cell migration. It is to note that the alternative NF-κB-pathway is mainly present in neuronal subtypes, endothelial cells and T lymphocytes [306] and the presence and function of this pathway has not been evaluated in the cancer cell lines used in the present study.

While cancer cell lines of diverse origin were sensitized to TNF-induced cell death upon BETi treatment in our study, some cell lines did not respond to the combination or showed enhanced survival. Identifying biomarkers to predict sensitivity would be beneficial to define patient populations responsive to the combination of BETi and immunotherapy. Various resistance mechanisms to TNF- mediated cell death have already been described. One was linked to mutations in the p53 tumor suppressor thereby inducing NF-κB activation and decreased apoptosis upon TNF treatment [307]. Knockdown of mutant p53 sensitized these cells to TNF-induced cell death [307]. In line with these findings, another group showed that TNF induces the interaction of mutant p53 with NF-κB to recruit RNA Pol II and induce transcription of tumor promoting genes [308]. Other potential resistance mechanisms include differential cleavage of secondary messenger molecules [309, 310] or constitutive activation of NF-κB [311]. The latter induces overexpression of anti-apoptotic downstream targets including FLIP, cIAPs and Bcl-xL [311]. Overexpression or mutation of *TRAF2* has been shown to induce resistance to T cell mediated TNF attack [293]. It is interesting to note that some mutations of TRAF2 enhance sensitivity to TNF induced cell death, thereby inducing an immune-editing pressure resulting in mutations in HLA I alleles and β_2 microglobulin (B2M) [293]. Overall, it is likely that TNF resistance in cell lines is mediated through different pathways. To get further insights, it is of need to identify alterations in gene signatures between responding and non-responding cell lines. Understanding which specific mechanism of action an epigenetic therapy can have on immune and cancer cells will be key to choose the right chemical agents to manipulate the immune system towards cancer cell killing. Combining an agent that potentiates T cell activation with a BETi-dependent TNF sensitization would be an attractive avenue for therapeutic intervention. Since it was seen that RG6146 delays T cell proliferation but enhances cell division at later time points, it is important to use immunotherapies that specifically induce cell death only at the cancer site, otherwise systemic activation of the immune system might induce undesirable side effects when combined with BETis.

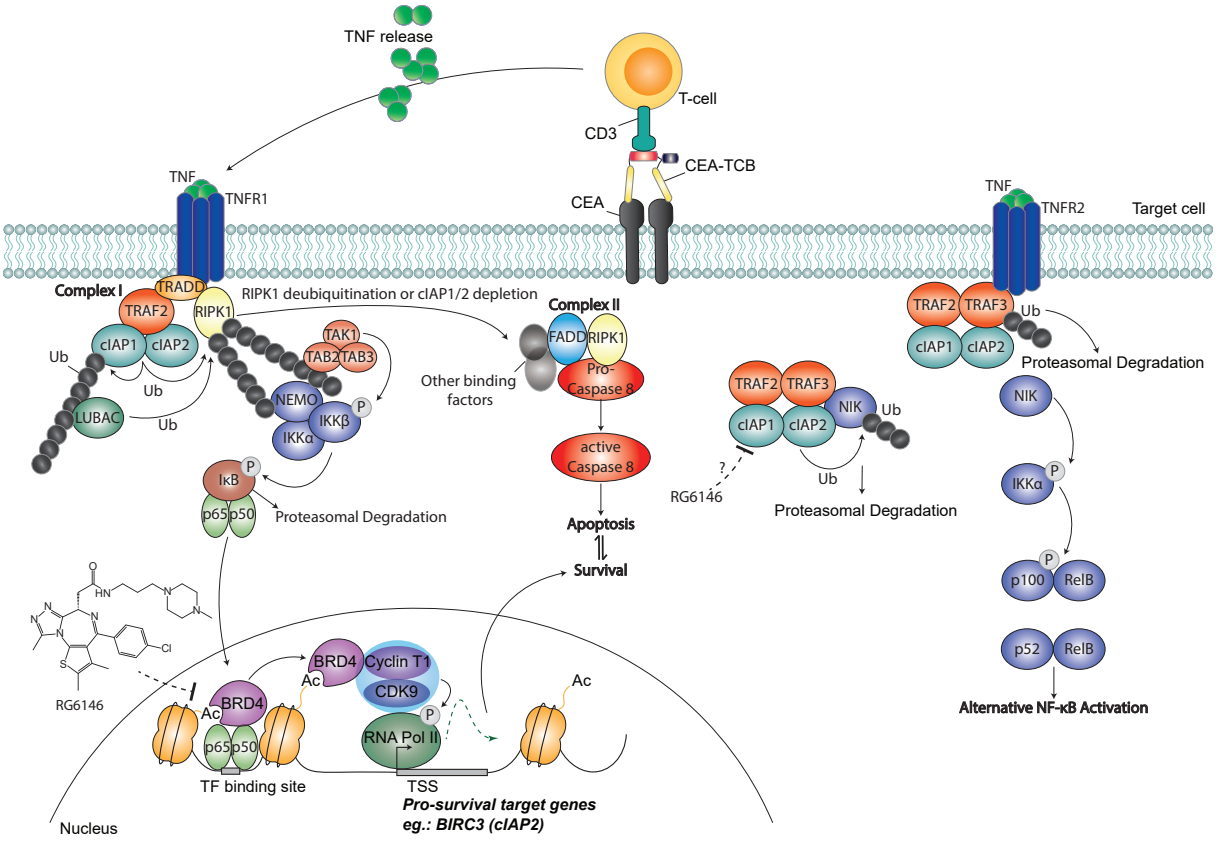

Figure 44: Potential mechanism of how BETis like RG6146 sensitize cells to TNF induced cell death:
Treatment with immunotherapy like the CEA-TCB induces T cell activation, release of TNF and subsequent binding of TNF to TNFR1 on cells. TNF preferentially induces formation of complex I, translocation of NF-κB (p65/p50) to the nucleus, where p65 interacts with BRD4 and induces transcription of pro-survival target genes like *BIRC3* (cIAP2). BET-inhibition using RG6146 leads to a partial loss of p65 binding and suppression of gene transcription. This induces formation of complex II and induction of apoptosis. If inhibition of BET proteins simultaneously activates the non-canonical NF-κB pathway needs to be further elucidated. P:Phosphorylation; Ub:Ubiquitination

6 Conclusion

Epigenetic processes are crucial in orchestrating gene expression. Therefore, it is not surprising that dysregulations of writer, reader and eraser proteins are causative protagonist in different types of diseases. Thus, epigenetic therapies have opened a novel opportunity to treat diseases including cancer. However, since manipulation of the epigenetic landscape influences a large variety of undiscovered transcriptional changes, the broad picture of how epigenetic modifiers like BETis shape the genetic landscape of a cell is not entirely understood. Work described in this thesis helps to understand the vast modulatory functions of BETis by elucidating the effect of the novel small molecule inhibitor RG6146 on different cell types. This work did not only give insights in potential intrinsic resistance mechanism of MM cells to BET-inhibition, but also elucidated the effect of BETis on healthy and immune cells. The main work of this thesis focused on the effect of BETis on the interface between cancer and immune cells. Taken together, by modulating the expression of NF-κB pro-survival target genes, sensitizing cells to TNF induced cell death and enhancing by-stander killing, we conclude that BETis in combination with immunotherapy is a promising therapeutic intervention strategy in many tumor types. In summary, this thesis helps to understand how RG6146 and other BETis modulate gene expression. Still, a lot of open questions remain to be answered in the future in order to entirely understand BET proteins and their inhibitors.

7 Material & Methods

7.1 Material

7.1.1 Chemicals

All chemicals used are listed in Table 5

Table 5: List of chemicals and their supplier

Chemical	Supplier
Animal-Free Blocking Solution (5X)	Cell Signaling
Bovin Serum Albumin	Roche
Cell Lysis Buffer (10X)	Cell Signaling Technology
Cell Extraction Buffer	Thermo Fisher Scientific
CellTiter-Glo® 2.0 Assay (CTG2.0)	Promega
Caspase-Glo® 8	Promega
Caspase-Glo® 3/7	Promega
CD14 MicroBeads, human	Miltenyi
CD4 Micro Beads	#130-045-101 Miltenyi
DC Protein Assay reagent A,B,S	Bio-Rad
DMSO	Sigma Aldrich
Ethylenediaminetetraacetic acid (EDTA)	AlfaAeser
Fixation/Permeabilization Solution Kit with BD GolgiPlug™	BD Pharmigen
Laemmli Buffer	AlfaAeser
LDH Assay	Roche
One-Glo™	Promega
Pan-T cell isolation Kit human	Miltenyi
Protease Inhibitor Cocktail Set III	Calbiochem
Phosphatase Inhibitor Cocktail Set II	Calbiochem
PMSF	Thermo Fisher Scientific
Ponceau S Solution	Sigma
Protease inhibitor	Sigma-Aldrich
qScript™ XLT One-Step RT-qPCR ToughMix®	Quanta Bioscience
Regulatory T cell Isolation Kit	#130-094-775 Miltenyi
$CD4^+CD25^+CD127^{dim/-}$ Regulatory T Cell Isolation Kit II	#130-094-775 Miltenyi
RNeasy Mini Kit	Qiagen
10x Tris/Glycine/SDS (TGS)	Bio-Rad

Chemical	Supplier
10x Tris Buffered Saline (TBS)	Bio-Rad
10 % Tween 20	Bio-Rad
0.25 % Trypsin	Thermo Fisher Scientific
TrypLE™ Express	Thermo Fisher Scientific
Pha-L	Sigma #L2769; 10 mg/mL
Western Bright Quantum	Advansta
Western Bright Sirius	Advansta
Versene	Thermo Fisher Scientific

Small and large molecule inhibitors as well as peptides and their respective targets are listed in Table 6.

Table 6: List of used inhibitors, the respective target and supplier

Name	Target/ Description	Supplier
RG6146	Bet proteins	Roche
JQ1	Bet proteins	Selleck Chemicals
OTX015	Bet proteins	Selleck Chemicals
Apabetalone	Bet proteins	Selleck Chemicals
Mivebresib	Bet proteins	Selleck Chemicals
i-BET151	Bet proteins	ChemScene
ABBV744	BRDII selective BET-inhibitor	Selleck Chemicals
i-BRD9	BRD9	Selleck Chemicals
GSKJ4 HCL	H3K27me3 Demethylase	Selleck Chemicals
EPZ6438	EZH2	Selleck Chemicals
SGC0946	DOT1L	Selleck Chemicals
SGC707	PRMT3	Selleck Chemicals
EPZ015666	PRMT5	Selleck Chemicals
Decitabine	DMT	TOCRIS
C646	p300/CBP	Selleck Chemicals
I-CBP112	p300/CBP	BPS Bioscience
SGCCBP30	p300/CBP	TargetMol
Entinostat	HDAC	TargetMol
Panobinostat	Pan-HDAC	TargetMol
Vorinostat	HDAC	TargetMol
Birinapant	SMAC-mimetic	Selleck Chemicals

Name	Description	Supplier
LCL-161	SMAC-mimetic	Selleck Chemicals
Zosuquidar	ABCB1	TargetMol
ZIETD-FMK	Caspase-8	R&D Systems
CEA-TCB	T cell bispecific antibody	Roche
anti-PD-1	PD-1	Roche
anti-LAG3	LAG3	Roche
anti-TIM3	TIM3	Roche
CEA-TCB	CEA and CD3	Roche
anti-PD-1 clone RMP1-14	(*in vivo* studies)	
Isotype control clone 2A3	(*in vivo* studies)	

TaqMan Gene Expression Assays used to determine RNA level are listed in Table 7 and were purchased from Thermo Fisher Scientific.

Table 7: List of Target RNA of TaqMan Gene Expression Assays and the corresponding reference

Target RNA	Reference
GAPDH	Hs02786624_g1
BIRC2	Hs01112284_m1
BIRC3	Hs00985031_g1
TRAF1	Hs01090170_m1

7.1.2 Gels, antibodies and markers

Precast SDS-gels, transfer packs as well as antibodies for western blot, flow cytometry and rescue experiments are listed in Table 8.

Table 8: List of gels, antibodies, markers and the respective supplier

Name	Supplier
Precast Gels and Transfer Packs:	
Trans-Blot® Turbo™ Midi Nitrocellulose Transfer Packs	Bio-Rad

Name	Supplier
4-15 % Criterion™ TGX™ Precast Midi Protein Gel: 26 well, 15 µL 18 well, 30 µL 12 + 2 well, 45 µL	Bio-Rad
Markers:	
Precision Plus Protein™ Kaleidoscope™ Prestained Protein Standards	Bio-Rad
Antibodies for western blot, all anti-human:	
Anti-Bcl-2 antibody [E17]	Abcam
Anti-Bcl-xL antibody [E18]	Abcam
Anti-c-Myc antibody [Y69]	abcam
Cleaved PARP (Asp214) (D64E10)	Cell Signaling
Anti-Mcl-1 antibody [Y37]	Abcam
MDR1/ABCB1 (E1Y7S) Rabbit mAb	Cell Signaling
Anti-Bim antibody [Y36]	Abcam
Anti-cIAP1	Abcam
Anti-cIAP2	Cell Signaling
Anti-TRAF1	Cell Signaling
Anti-Caspase 8	Cell Signaling
Vinculin (E1E9V) XP® Rabbit mAb	Cell Signaling
β-Actin (13E5)	Cell Signaling
Secondary Goat-anti-rabbit Antibody	Jackson Immuno Research
Antibodies for Flow Cytometry:	
CEACAM5/CD66e Antibody (CEA31)	Novus BioScience
Purified Mouse IgG1, κ Isotype Ctrl Antibody	BioLegend
Cell Trace™ CFSE	Thermo Fisher Scientific
Goat Anti-Mouse Ig, Human ads-Alexa Fluor® 647	Southern Biotech
Zombie NIR™ Fixable Viability Kit	BioLegend
Zombie Aqua™ Fixable Viability Kit	BioLegend
CellTrace™ Violet	Thermo Fisher Scientific
Alexa Fluor® 700 anti-human CD4 Antibody	BioLegend
APC anti-human CD8 Antibody	BioLegend
PE anti-human CD279 (PD-1) Antibody	BioLegend

Name	Supplier
FITC anti-human CD366 (Tim-3) Antibody	BioLegend
FITC anti-human CD223 (LAG3) Antibody	BioLegend
PE anti-human CD69 Antibody	BioLegend
CD11C V450	BioLegend
HLA-DR Monoclonal Antibody (TU36), Pacific Orange	Thermo Fisher Scientific
APC anti-human CD40 Antibody	Biolegend
Alexa Fluor® 488 anti-human CD80 Antibody	BioLegend
PE/Cyanine7 anti-human CD86 Antibody	BioLegend
PE anti-human CD274 (B7-H1, PD-L1) Antibody	BioLegend
PE/Cyanine7 anti-human CD11c Antibody	BioLegend
PE anti-human CD14 Antibody	BioLegend
Alexa Fluor® 647 anti-human CD273 (B7-DC, PD-L2) Antibody	BioLegend
Pacific Blue™ anti-human HLA-A2 Antibody	BioLegend
Alexa Fluor® 488 anti-human TCR α/β Antibody	BioLegend
PE/Cyanine7 anti-human CD8 Antibody	BioLegend
APC anti-human CD279 (PD-1) Antibody	BioLegend
anti-Granzyme B (PE)	#561142 BD Biosciences
anti-IFNγ (PE-Cy7)	#25-7319-82 Thermo Fisher Scientific
PE anti-human CD120a Antibody	BioLegend
PE Mouse IgG2a, κ Isotype Ctrl (FC) Antibody	BioLegend
Alexa Fluor® 647 anti-human CD243 (MDR-1)	BioLegend
Alexa Fluor® 647 anti-Mouse IgG2a, κ	
CD5 (clone 53-7.3)	BD Biosciences
CD44 (clone IM7)	Biolegend
TNFα (clones MP6-XT22)	eBioscience)
IFNγ (XMG1.2)	eBioscience
Beads for Cytokine Assay:	
General CBA Kit human	BD Biosciences
TNF	BD Biosciences
CD178	BD Biosciences
IFNγ	BD Biosciences
MIP1alpha	BD Biosciences
Granzyme	BD Biosciences

Name	Supplier
Antibodies for Rescue experiments and T cell activation:	
TNF alpha Monoclonal Antibody (28401)	Thermo Fisher Scientific
Mouse IgG1 Isotype Control (MOPC-21)	Thermo Fisher Scientific
CD3 Mouse anti-Human, Functional Grade, Clone: OKT3	Thermo Fisher Scientific
Purified NA/LE Mouse Anti-Human CD28 Clone CD28.2 (RUO)	BD Biosciences
For *in vivo*: anti-TNF-α Mab	BioLegend, #506347

7.1.3 Technical equipment

All technical equipment used is listed in Table 9.

Table 9: Technical equipment and respective manufacturer

Machine	Name	Manufacturer
Centrifuge	Centrifuge 5801R	Eppendorf
Cell Counter	Countess II	Invitrogen
Gel chamber	Criterion™ Vertical Electrophoresis Cell	Bio-Rad
Incucyte	IncuCyte S3	Essen BioScience
Microcentrifuge	Eppendorf™ 5424	Eppendorf
Microplate reader	Spectrostar-Nano	BMG Labtech
Microscope	Olympus CKX53	Olympus
NanoDrop	NanoDrop One	Thermo Scientific
Plate Reader	PHERAstar FSX	BMG LABTECH
Sonicator	Biorupter Pico	Diagenode
Transfer System	Trans-Blot® Turbo™	Bio-Rad
Western Blot Imager	Fusion FX7	Vilber
Flow Cytometry	Cytoflex S Benchtop FACS	Beckman Coulter
Flow Cytometry	BD LSR Fortessa	BD Biosciences
Flow Cytometry	Intellicyt iQue	Sartorius
qRT-PCR machine	LightCycler® 480 System	Roche

7.1.4 Cell lines

All cell lines used in this thesis were provided by the Roche non-clinical biorepository with the original source listed in Table 10.

Table 10: Cell lines, site of origin and source

Name	Description	Source
KMS-11	human, MM	CELLO
KMS-12-BM	human, MM	DSMZ
KMS-20	human, MM	JCRB
KMS-34	human, MM	CELLO
MM1S	human, MM	ATCC
OPM-2	human, MM	CELLO/DSMZ
NCI-H929	human, MM	CELLO/ATCC
MKN-45	human, gastric adenocarcinoma derived from liver metastasis	CELLO/DSMZ
HCT-116	human, colon	ATCC
HCT-116	NFκB Luciferase Reporter	BPS Bioscience
293FT	human, brain	Invitrogen
MC-38	mouse, colon	Roche Internal
HUVECC	human Umbilical Vein Endothelial	ATCC
HEK293	human embryonic kidney	ATCC
PNT1A	human post pubertal prostate normal immortalised with SV40	CELLO
B-LCL_Donor222	human immortalized B-Lymphoblastoid cell line (Donor 222)	-

7.1.5 Culture media

Cells were cultured according to ATCC culture methods. Cell lines, their corresponding medium and supplements are listed in table 11-12. Unless otherwise stated media was purchased from Thermo Fisher Scientific. After addition of all supplements media was filtered using a 0.22 µm filter.

Table 11: List of supplements used for cell culture medium and respective supplier

Supplements	Supplier
Endothelial Cell Growth Supplement (ECGS)	Sigma Aldrich
Fetal Bovine Serum	Thermo Fisher Scientific
Human Serum	Thermo Fisher Scientific
Geniticin	Thermo Fisher Scientific
Glutamine (100x)	Thermo Fisher Scientific
Heparin sodium salt from porcine intestinal mucosa Grade I-A, =180 USP units/mg	Sigma-Aldrich
Hepes	Thermo Fisher Scientific
Hygromycin	Invivogen
IL-2,Proleukin	Novartis
β-Mercaptoehtanol	Thermo Fisher Scientific
Non-essential amino acids (NEAA)	Thermo Fisher Scientific
Penicillin-Streptomycin (Pen-Strep)	Thermo Fisher Scientific
Puromycin	Thermo Fisher Scientific

Table 12: List of cell lines and corresponding culture-medium

Cell line	Medium
KMS-11	RPMI1640 (#A10491) + 10 % FBS
KMS-12-BM	RPMI1640 (#61870) + 20 % FBS
KMS-20	RPMI1640 (#A10491) + 10 % FBS
KMS-34	RPMI1640 (#61870) + 10 % FBS
MM1S	RPMI1640 (#61870) + 10% FBS + 10 mM HEPES
NCI-H929	RPMI1640 (#A10491) + 10 % FBS + 0.05 mM β-ME
OPM-2	RPMI1640 (#31870) + 10 % FBS + 2 mM Glutamine
HCT-116	RPMI1640 (#A10491) + 10 % FBS
HCT-116-NFκB-reporter	McCoys 5A (Gibco 26600) + 10 % FBS + 1 mg/mL Geniticin
MKN45	RPMI1640(#61870) + 20 % heat inactivated FBS
MC-38	DMEM (#41965)+ 10 % FBS + 25 mM Hepes
293FT	DMEM (#41966) + 10 % FBS + 2 mM Glutamine + NEAA
HUVECC	F-12K (#21127) + 10 % FBS + 100 µg/mL Heparin

Cell line	Medium
	+ 0.03-0.05 mg/mL ECGS
HEK-293	DMEM (#41965) + 10 % FBS + 1xNEAA
PNT1A	RPMI-1640 (#31870) + 10 % FBS + 2 mM Glutamine
CMV specific T cells	RPMI1640 (#61870) + 10 % FBS + 400 U/mL IL-2
B-LCL	RPMI-1640 (#A10491) + 10% FBS

7.2 Methods

7.2.1 Computer Software

ChimeraX [312] was used to generate the structure of the bromodomain of histone acetyltransferase Gcn5p in complex with a peptide from acetylated Histone H4 using the Protein Data Bank accession code:1E6I and Owen et al. [36].
The chemical structure of JQ1 and RG6146 was generated using ACD/ChemSketch (v2019.2.2, Advanced Chemistry Development, Inc., Toronto, ON, Canada).
For flow cytometry analysis FlowJo version 10.6.1 or 10.6.2 was used [313].
Where indicated and for determining statistical significance, GraphPad Prism version 7.00 or 8.00 for Windows was used, GraphPad Software, La Jolla California USA.
www.graphpad.com

7.2.2 Cell lines and culturing methods

Cell lines (Table 10) and derivatives thereof were cultured in their corresponding medium (Table 12) at 37 °C, 5 % CO_2 and 95 % humidity. Unless otherwise stated, all experiments were performed in the incbator at 37 °C, 5 % CO_2 and 95 % humidity. Cells were passaged when confluence reached 70-80 %. Adherent cell lines were trypsinized at 37 °C (0.25 % Trypsin), resuspended in medium, centrifuged at 150xg and split according to their cell density. Suspension cell lines were collected and passaged according to their cell density.
PBMC isolation: PBMCs were obtained from blood of healthy Donors. Buffy coats (Blutspendezentrum Beider Basel) were transferred into Erlenmeyer tubes and mixed 1:1 with Phosphate-buffered saline (PBS). Ficoll was adjusted to room temperature and 15 mL added in each Leucosep separation tube and centrifuged for 15 sec at 1000xg. 25 mL of blood/PBS mixture was added to each Leucosep separation tube and centrifuged at 1000xg for 10 min without break in a swinging rotor bucket. The enriched cell fraction containing PBMCs was collected in a 50 mL tube and washed three times with 50 mL PBS, 2 mM EDTA at 250xg for 10 min. Cells were resuspended in 50 mL RPMI (A10491)

+ 10 % Fetal bovine serum (FBS) and cell number adjusted. Cells were either directly used for experiments or frozen at 50 Mio cells/mL in 60 % RPMI (A10491) + 30 %FBS + 10 % Dimethyl sulfoxide (DMSO).

Feeder cell preparation for CMV-specific T cell maintenance: The first step of Feeder cell generation is the same as described for the PBMC isolation. After resuspending cells in 50mL RPMI + 10% FBS, cells were transferred into a 150 cm^2 Flask and kept in the incubator for 1 h. Monocytes will adhere to the Flask, while Feeder cells will stay in the supernatant. Supernatant was transferred to a 50 mL tube and centrifuged for 5 min at 800xrpm. Cell pellet was resuspended in 10 mL T cell medium, 30 µL PHA-L (30 µg/mL) added, transferred in a 15 mL tube and placed horizontally in the incubator for 1 h. PHA-L induces cytokine production during this time. LCL-cells were detached, centrifuged (150xg, 3 min), cell concentration adjusted to 1 Mio cells/ mL in RPMI + 10 % FBS and NLV peptide added to a final concentration of 10 nM for 20 min. LCL-cells were centrifuged, resuspended in T cell medium to a cell density of 1 Mio/mL and transferred to a 6-well plate (5 mL/well). Feeder cells were also transferred to a 6-well plate and irradiated at 2500 rad (25 Gy), while LCL-cells were irradiated at 5000 rad (50 Gy). Both cell types were counted and adjusted to reach a ratio of 1 LCL-cell:25-50 Feeder cells. Cells were centrifuged, washed with PBS, resuspended in fresh T cell medium and added to a 96 U-bottom plate (25x10^6 Feeder cells + 0.5-1x 10^6 LCL-NLV cells). CMV-specific T cells, which were originally obtained from Roche Innovation Center Zuerich [314], were seeded at a concentration of 10000 T cells/ well in T cell medium. Plates were placed into the incubator and medium regularly exchanged by replacing 80 µL of medium with 100 µL of fresh medium. After one week cells were transferred into a 48-well plate and one week later into a 6-well plate. T cell growth was monitored over time and cells passaged when density was over 1.5 Mio cells/mL.

7.2.3 Viability Assay

Cells were detached and seeded at 5000 cells/well in 100 µL for each well of a 96-well plate (#3917 CoStar) and let adhere overnight in the incubator. The next day small molecule dose response (1:3 dilution) or DMSO control were prepared at a final DMSO concentration of maximal 0.15 % DMSO. TNF was diluted in PBS+0.5 % BSA to reach the desired concentration. Cells were placed back into the incubator for 72 h. Before assessing viability, plates as well as CellTiterGlo2.0 reagent were adjusted to room temperature. 50 µL of CTG2.0 Assay reagent were added to 100 µL of cell solution and incubated for 10 min shaking. Luminescence was read on the PHERAStarFSX. Data was normalized to DMSO control without TNF.

7.2.4 Western Blot

Cells were detached and cell density adjusted to 0.15-0.25 Mio cells/ well in a 6-well plate depending on cell growth. Cells were placed in the incubator overnight, medium replaced the next day and cells treated with desired concentration of small molecule or 0.1 % DMSO control. Cells were placed back in the incubator for the required treatment time, washed with ice cold PBS and scraped off using a cell spatula and 75 µL of lysis buffer (Cell lysis buffer + Phosphate and Protease inhibitor). Cells in lysis buffer were stored at -20 °C until further use. Cells were sonicated five times for each cycle 30 sec on, 30 sec off afterwards centrifuged at 14050xrpm for 10 min at 4 °C. Supernatant was transferred into fresh Eppendorf tubes and samples normalized using the DC Protein Assay Kit. 1x Laemmli Buffer was added and solution heated at 95 °C for 10 min. Samples or loading control were loaded on 4-20 % or 4-15 % Criterion TGX precast gels and run at 180 V for about 45 min in 1x TGS. Proteins were transferred using nitrocellulose membrane with Bio-Rad trans blot turbo (25 V, 2.5 Ampere, 9 min). Blot was blocked with 1x Animal blocking solution (ABS (Cell Signalling)) for 1 h and incubated with the primary antibody in ABS+0.1 % Tween (Table 8) overnight at 4 °C. Blots were washed 3x with TBS + 0.1 % Tween for 20 min, before applying the secondary antibody (Table 8) for 1 h. Blots were washed 3x for 5 min with TBS + 0.1 % Tween and developed using 1:1 mixture of Western bright Sirius HRP substrates using the Fusion Fx7 and the Fusion Capt Advance Software. Protein Quantification was performed with the Fusion Capt Advance software and data normalized to untreated control.

7.2.5 *in vivo* study MM

This assay was performed by Thomas Friess, Stefanie Lechner and Daniela Geiss.
Preparation of cell lines: KMS-11, KMS-12-BM, KMS-20, KMS-34, MM1S, OPM-2 and NCI-H929 were purchased from ATCC and maintained by the internal cell bank of Roche Penzberg. NCI-H929 were cultured in RPMI 1640 ATCC formulation (Gibco A10491) containing 10 % FBS and 0.05 mM β-ME. All other cell lines were cultured in RPMI 1640 containing 10 % FBS and 2 mM L-glutamine. Cells were passaged twice a week and cell passage 2-3 used for transplantation.
KMS-11:
Female CIEA NOG mice (from Taconic European Office, 6-7 weeks of age upon arrival) were kept under specific-pathogen-free condition with daily cycles of 12 h light and 12 h darkness. KMS-11 cells were harvested, washed with PBS and 5 Mio cells inoculated subcutaneously in combination with martigel. After eight days, mice bearing solid tumor xenografts were randomized into two treatment groups (10 mice/group) and treated with vehicle control or 30 mg/kg RG6146 injected intraperitoneal (ip) daily. Treatment com-

menced from day 8-15. Body weight of animals was monitored twice weekly throughout the experiment and mice were checked daily for clinical symptoms or adverse events. Tumor volume was measured twice weekly and determined using the following equation: V = ab^2 / 2; a: length; b: width of tumor measured with a caliper.

KMS-12-BM:

The assay set up was similar as described for KMS-11 except that 10 Mio cells were injected into each animal and treatment with RG6146 commenced on day 12-16, day 19-22. For the combination of RG6146 and Venetoclax, mice were treated QD with 30 mg/kg RG6146 (ip) or 100 mg/kg Venetoclax (po) or the combination.

KMS-34:

The assay set up was similar as described for KMS-11 except that 10 Mio cells were injected into each animal (CIEA NOG mice, 4-5 weeks of age upon arrival) and treatment with RG6146 commenced on day 12-16, day 19-20.

MM1S:

The assay set up was similar as described for KMS-11 except that 10 Mio cells were injected into each animal (female CIEA NOG mice, 5-6 weeks of age upon arrival) and treatment with RG6146 commenced on day 16-29.

KMS-20:

The assay set up was similar as described for KMS-11 except that 10 Mio cells were injected into female SCID beige mice (from Charles River, Sulzfeld, Germany, 4-5 weeks of age upon arrival) and treatment with RG6146 commenced on day 13-17, day 20-24 and day 27-29.

OPM-2:

The assay set up was similar as described for KMS-11 except that 10 Mio cells were injected into female SCID beige mice (from Charles River, Sulzfeld, Germany, 6-8 weeks of age upon arrival) and treatment with 30 mg/kg RG6146 commenced on day 12-16, day 19-23 and day 26-30. Another group of mice was treated with 6 mg/kg RG6146 injected subcutaneously twice daily (BID) on study day 12-30.

NCI-H929:

The assay set up was similar as described for KMS-11 except that 5 Mio cells were injected into female SCID beige mice (from Charles River, Sulzfeld, Germany, 6-8 weeks of age upon arrival) and treatment with RG6146 commenced on day 13-17, day 20-24 and day 27-31.

7.2.6 Flow cytometry of cancer cells

7.2.6.1 Flow cytometry to detect ABCB1 MM cells were seeded at 0.4 Mio cells/well in a 12-well plate and the next day cells were treated with 0.03-10 µM RG6146 or DMSO control for 48 h. Cells were detached with TrypLE™, washed in PBS and stained with

ZombieNIR 1:500 and 1:50 diluted anti-ABCB1 Ab (Alexa Fluor® 647) or isotype control (Alexa Fluor® 647) at 4 °C for 30 min. Cells were washed twice with MACS buffer (PBS + 2mM EDTA + 0.5 % BSA), resuspended in 50 µL MACS buffer and read on cytoflex S benchtop FACS.

7.2.6.2 Flow cytometry to detect TNFR1 HCT-116 and MKN45 cells were seeded at 0.3 Mio cells/well in a 6-well plate and the next day cells were treated with 1-2.5 µM RG6146, DMSO control and/or 15 ng/mL TNF for 24 h. Cells were detached, washed and 0.1 Mio cells stained with ZombieNIR 1:500 and 1:200 diluted anti-TNFR1 (PE) or isotype control (PE) at 4 °C for 30 min. Cells were washed twice with MACS buffer, resuspended in 50 µL MACS buffer and read on cytoflex S benchtop FACS.

7.2.6.3 Flow cytometry to detect CEACAM5 HCT-116-GFP and MKN45-RFP cells were seeded at 0.3 Mio cells/well in a 6-well plate and the next day cells were detached, washed and 0.1 Mio cells stained with ZombieNIR 1:500 and a final concentration of 20 µg/mL CEACAM5/CD66e antibody or Mouse IgG1, κ Isotype Ctrl at 4 °C for 20 min. Cells were washed with MACS buffer, resuspended in 50 µL MACS buffer containing 20 µg/mL of Goat Anti-Mouse Ig, Human ads-Alexa Fluor® 647 for 40 min at 4 °C. Subsequently, cells were washed with MACS buffer, resuspended in 50 µL and read on cytoflex S benchtop FACS.

7.2.7 T cell Activation with anti-CD3, anti-CD28 and staining for flow cytometry

High binding plates were coated with 100 µL of anti-CD3 and anti-Human CD28 antibodies (Table 8) to reach a final concentration of 2 µg/mL and incubated at 4 °C overnight. Plates were washed 2x with sterile PBS. Pan-T cells were isolated from PBMCs following the manufacturer's protocol (Miltenyi, Table 8). Pan- T cells include activated, naive or memory T cells, TCRγ/δ+ T cells, and NKT cells (From Human Pan T cells; Miltenyi Biotec; accessed January 2021 <https://www.miltenyibiotec.com/CH-en/resources/macs-handbook/human-cells-and-organs/human-cell-types/pan-t-cells-human.html>). Subsequently, Pan-T cells were washed, stained with 1:1000 diluted CellTrace™ violet in PBS and incubated for 20 Min at 37 °C. The same amount of heat inactivated FBS (hiFBS) was added to the cell solution to bind unbound dye. Cells were washed with RPMI + 10 % FBS and 0.1 Mio cells were seeded in each well of the coated 96-well plates. Plates were centrifuged at 1500 rpm for 5 min. Cells were treated with a 1:3 dilution of RG6146 or DMSO control reaching a maximum concentration of 0.15 % DMSO. Depending on the set up of the experiment, also TNF was added to the cells. Cells were treated for the desired time in the incubator. Subsequently, cells were centrifuged, washed with PBS and stained with 50 µL antibody mix (Dilution 1:200) for 30 min.

Staining 1:
anti-CD4 (Alexa Fluor® 700), anti-CD8 (APC), anti-PD-1 (PE), anti-Tim-3 (FITC).
Staining 2:
anti-CD4 (Alexa Fluor® 700), anti-CD8 (APC), anti-LAG-3(FITC), anti-CD69 (PE).
Subsequently, cells were washed with 200 µL of MACS buffer and resuspended in 50 µL MACS buffer to acquire signal with the Cytoflex S benchtop.

7.2.8 Mixed Lymphocyte Reaction

Monocytes were isolated from PBMCs. PBMCs were thawed and resuspended in RPMI (A10491) + 1 % human serum + pen-strep, filtered through a 70 µM sieve (Merck), centrifuged and monocyte isolation performed by using CD14 Micro beads (Miltenyi Biotec) following the manufacturer's guidelines. 3 Mio monocytes were seeded in 3 mL RPMI (A10491) + 1 % human serum + penstrep for each well of a 6-well plate and treated with 20ng/mL GM-CSF and IL-4 (both Peprotech). Cells were placed in the incubator and after 48 h additional 1.5 mL of medium containing IL-4 and GM-CSF to reach the same final concentration of 20 ng/mL were added to the cells for another 24 h. Subsequently, cells were detached from the plates through resuspension and washing plate with cold PBS and MACS buffer to help cell detachment. Cells were centrifuged at 1500xrpm for 5 min and 2 Mio cells were plated in 2 mL of medium in each well of a 6-well plate. 20 ng/mL IL-4, GM-CSF and 10 ng/mL IFNγ (Peprotech), LPS (Sigma) were added and incubated overnight. In one experiment, the DCs were treated with different concentrations of RG6146 overnight to compare the effect of BETis on DCs matured with all cytokines versus only IL-4 and GM-CSF. For the positive control, plates were coated with anti-CD3 and anti-CD28 as described in 7.2.7. The next day mature DCs were detached by addition of ice cold MACS buffer and virgously resuspended by pipetting. DCs were counted and resuspended in RPMI (A10491) + 10 % FBS + penstrep and desired number of DCs depending on the DC:T cell ratio added to the plate. To analyze DC maturation some cells were kept after each activation step and stained as described in Flow cytometry of DCs. Pan-T cells were isolated from PBMCs (different Donor as DCs) according to the Miltenyi isolation protocol and cell trace violet staining as described in 7.2.7. Pan-T cells were seeded at a cell density of 0.1 Mio cells/ well to the DCs. Co-culture was pre-treated with 10 µg/mL anti-PD-1 and anti-LAG3 antibodies for 1 h before adding different concentrations of RG6146. Cells were placed in the incubator for the desired time.
Flow cytometry of DCs:
Monocytes, immature and mature DCs were collected and transferred to a 96-well U-bottom plate (#3799). Cells were washed with PBS and separated to prepare two different staining's containing antibodies described in Table 13 prepared (all diluted 1:200, ZombieNIR 1:500). 50 µL of staining was added to the cells and incubated for 20-30 min

at 4 °C. Cells were washed with 200 µL MACS buffer, resuspended in 100 µL MACS buffer and data acquired with the Fortessa.

Table 13: FACS Staining panel for dendritic cells

Staining 1:	
	CD11C V450
	HLA-DR Monoclonal Antibody (TU36), Pacific Orange
	APC anti-human CD40 Antibody
	Alexa Fluor® 488 anti-human CD80 Antibody
	PE/Cyanine7 anti-human CD86 Antibody
	PE anti-human CD274 (B7-H1, PD-L1) Antibody
	ZombieNIR
Staining 2:	
	PE/Cyanine7 anti-human CD11c Antibody
	HLA-DR Monoclonal Antibody (TU36), Pacific Orange
	PE anti-human CD14 Antibody
	Alexa Fluor® 647 anti-human CD273 (B7-DC, PD-L2) Antibody
	Pacific Blue® anti-human HLA-A2 Antibody
	ZombieNIR

Flow cytometry of T cells:
T cells were resuspended and transferred to a 96-well U-bottom plate (#3799), washed with PBS and stained with antibodies as described in Table 14 (all diluted 1:200, ZombieNIR 1:500) for 30 min at 4 °C. Cells were washed twice with 200 µL MACS buffer, cells resuspended in 100 µL MACS buffer and data acquired at the cytoflex S benchtop FACS machine.

Table 14: FACS Staining panel for T cells

anti-TCR α/β (Alexa Fluor® 488)
anti-CD4 (Alexa Fluor® 700)
anti-CD8 (PE/Cyanine7)
anti-CD69 (PE)
anti-PD-1 (APC)
ZombieNIR
CellTrace™ Violet

7.2.9 T reg suppression Assay

For the following assay R10 medium (supplemented with penstrep and GlutaMax) was used.

Isolation of T convs and CD4$^-$ cells

100 Mio PBMCs were treated according to the Miltenyi CD4$^+$CD25$^+$ Regulatory T Cell Isolation Kit (Miltenyi) and loaded on an LD column (Miltenyi). Flow through and wash (CD25$^-$ cells) were collected and centrifuged at 440 xg for 6 min. Cells were resuspended and treated according to the Miltenyi protocol using CD4 MicroBeads to separate CD4$^-$ cells (flowthrough) and CD4$^+$ cells (bound to column). 10 Mio CD4$^+$CD25$^-$ cells (T conv) were stained with 1 mL PBS + 1 % BSA in a final concentration of 5 µM Cell Trace CFSE for 5 Min in the dark (room temperature). Cells were washed twice with medium and adjusted to 2 Mio cells/mL. The CD4$^-$CD25$^-$ cells were irradiated at 5000 rad and cell number adjusted to 1.25 Mio cells/mL.

Isolation of T regs

100 Mio PBMCs were treated according to the Miltenyi CD4$^+$CD25$^+$CD127$^{dim/-}$ Regulatory T Cell Isolation Kit II and loaded on a LD column to collect flowthrough and wash containing CD127^{dim} cells. Cells were further processed to collect CD25$^+$ cells bound to the MS column (Miltenyi). 10 Mio CD4$^+$ CD25$^+$ CD127^{dim} (T regs) were stained in 1 mL PBS + 1 % BSA 5 µM Cell Trace Violet solution for 5 Min in the dark. Cells were washed in medium and resuspended at 1.6 Mio cells/mL.

Co-culture set up

Per well 0.05x10^6 T regs and 10 µg/mL anti-PD-1, anti-LAG3 or anti-PD-1, anti-TIM3 were added to the wells. The plate was incubated for 30 Min at room temperature, before addition of 0.1x10^6 T convs to each well. After another 30 min of incubation the CD4$^-$ CD25$^-$ cells (from a different PBMC Donor) were added at a concentration of 0.1x10^6 cells/well. The next day different concentrations of RG6146 or DMSO control were added to the co-culture and incubated for another 4 days in the incubator. Cells were processed by adding 2 µL Golgi Plug and Golgi Stop (BD Pharmingen) per 1 mL medium and incubated for 5 hours in the incubator. Cells were washed and stained with Zombie Aqua (1:1000) and anti-CD4 (Alexa Fluor 700, 1:100) for 30 min at 4 °C. Fix/Perm solution was added to the cells (2 in 1 solution) overnight at 4 °C and cells washed twice with BD Perm/Wash. Subsequently, cells were stained for anti-Granzyme B (PE, 1:100) and anti-IFNγ (PE-Cy7, 1:200) for 1 h at 4 °C. Cells were washed, resuspended in Permwash and analyzed using the Cytoflex. The suppression of T convs activation was assessed by calculating the suppression of Granzyme B and IFNγ:

100-((C/C$_0$)*100); with C:Level of Cytokine in the co-culture upon treatment or untreated; C$_0$: Level of Cytokine in the untreated T convs mono-culture

7.2.10 HCT-116 NLV co-culture assay and compound screening

HCT-116 cells were detached with Versene, transferred to a 15 mL tube and incubated with NLV (NLVPMVATV; thinkpeptides) or EBV (GLCTLVAML; thinkpeptides) peptide at a final concentration of 10 nM for 1 h rotating in the incubator. Cells were washed once with PBS and cell density adjusted to 0.01 Mio cells/ well in 100 µL of RPMI A10491 + 10 % hiFBS in a 96-well plate (#3917). Cells were kept in the incubator for a minimum of 1.5 h to let cell adhere to the bottom of the plate. CMV specific T cells were generated as described in 7.2.2, collected, washed with PBS and resuspended in medium to reach a final cell density of 0.01 Mio cells/well in 100 µL and added to the HCT-116 cells (1:1 Effector:Target ratio). The co-culture was placed in the incubator for 30 min before addition of 2.5-5 µM of small molecule (Table 6) or DMSO control reaching a maximal DMSO concentration of 0.25 %. After 48 h supernatant containing the T cells was removed, plates washed with PBS and 100 µL of fresh PBS added to the cells. 100 µL of CTG2.0 assay reagent was added to the cells and luminescence read using the PHERAStarFSX. Data was normalized to the DMSO control.
For the anti-TNF rescue experiment, the HCT-116 cells were plated in 50 µL of medium per well. The T cells were resuspended in a mixture of medium and anti-TNF or ITC (Table 8) to reach a final concentration of 20 µg/mL of the antibodies in the co-culture.

7.2.11 MC38-Ova and OTI T cell co-culture

The study described in 7.2.11.1 and 7.2.11.2 was performed by Simon Hogg and Dane Newman.

7.2.11.1 OTI T cell activation 6-10 week old perforin-wild-type (C57Bl/6.OTI) or perforin-deficient (C57Bl/6.OTI.Prf^{-}/$^{-}$) mice were used to harvest whole spleens. Spleens were then dissociated through a 70 µM cell strainer. Subsequently, 20 ng/mL of SIINFEKL peptide (Sigma-Aldrich) and 100 IU/mL recombinant human IL-2 (Biolegend) were added in RPMI media supplemented with 10 % FBS, GlutaMax (2 mM), penicillin/streptomycin, non-essential amino acids, sodium pyruvate (1 mM), HEPES (10 mM) and β-mercaptoethanol (50 µM) to activate and expand OTI T cells. After 3 days of incubation, OTI T cells were passaged into fresh media (IL-2 only, without SIINFEKL), and cultured for additional 1-4 days prior to use in co-culture killing assays.

7.2.11.2 MC38-Ova and OTI co-culture screen MC38 cells stably expressing MSCV-OVA-GFP (MC38-OVA) were plated at 0.15 Mio cells per well in a 48-well plate. MC38-OVA cells were incubated for 6-8 h to give time to adhere. Activated OTI cells were washed with PBS, re-suspended in supplemented DMEM and serial diluted before ad-

dition to MC38-OVA target cells. Co-culture was treated with RG6146 or DMSO control and incubated for 18-20 h at 37°C with 10 % CO_2. Subsequently, the supernatant, which contained OTI T cells and dead cells was collected, and adherent MC38 cells were trypsinized. Cells contained in the supernatand and detached cells were combined, washed in flow cytometry buffer (PBS + 2 % FBS + 5 mM EDTA) and OTI cells stained with anti-mouse CD5 APC-conjugated antibody (clone 53-7.3; eBioscience). Cells were washed twice with flow cytometry buffer and 2 µg/mL propidium iodide added directly prior to analysis. Flow cytometry was performed on an LSR II flow cytometer (BD Biosciences). Data was analyzed with FlowJo (Tree Star). The $CD5^+$ OTI cells were gated out of analysis. Dead MC38-OVA cells were recognized as GFP-PI^+.

7.2.11.3 Intracellular staining of OTI T cells This assay was performed by Dane Newman. A co-culture of MC38-OVA cells and activated OTI T cells (1:4 Effector:Target ratio) was cultured in 0.6 µL/mL GolgiStop (BD Biosciences) as well as RG6146 or DMSO control for 5 h. After harvest, cells were stained with Zombie Aqua and fluorochrome-labelled T cell-specific antibodies targeting CD5 (clone 53-7.3) and CD44 (clone IM7). After cell fixation using 4 % paraformaldehyde for 10 min, cells were washed with staining buffer and resuspended in Perm/Wash buffer for 15 min. Subsequently, cells were stained with fluorochrome-labelled antibodies targeting TNFα and IFNγ (clones MP6-XT22 and XMG1.2). Cells were examined by flow cytometry (BD LSR Fortessa X-20, BD Biosciences).

7.2.12 Cell line screen

This Screen was performed by Oncolead. Cell lines (obtained from ATCC, NCI, CLS and DSMZ) were cultured according to recommendation. A dose response of RG6146, DMSO control or 15 ng/mL TNF was added to cells and treatment proceeded for 120 h before cell number was assessed using total protein concentration. Adherent and suspension cells were fixed for 1 hour at 4°C with 10 % or 50 % tricholoracetic acid, respectively. Cells were washed with deionized water and dried. Cells were stained using 0.04 % (wt/v) Sulforhodamine B (SRB) for 30 minutes at room temperature. Cells were washed six times with 1 % (v/v) acetic acid and plates were dried. SRB was solubilized in 10 mM Tris base prior to measurement of fluorescence with a Seelux-LED96 plate reader (492, 520 and 560 nm). The background density (medium only) was subtracted from each experimental well. TNF synergy was determined by subtracting maximal growth inhibition of RG6146 alone from maximal growth inhibition of RG6146+TNF.

7.2.13 Caspase Assay

Cells were detached and seeded at 0.04 Mio cells/ well in 100 µL medium for each well of a 96-well plate (#3917 CoStar) and let adhere overnight in the incubator. The next day small molecule dose response (1:3 dilution) or DMSO control were prepared, as well as 1 µM of Caspase-8 inhibitor (ZIETD-FMK) at a final DMSO concentration of maximal 0.15 %. TNF was diluted in PBS + 0.5 % BSA to reach the desired concentration. Cells were placed back into the incubator for 8 h. Before assessing Caspase activity, plates as well as Caspase-Glo3/7, 8 reagent were adjusted to room temperature. 100 µL of assay reagent were added to 100 µL of cell solution and incubated for 60 min shaking. Luminescence was read on the PHERAStarFSX. Data was normalized to DMSO control of each condition.

7.2.14 Knockdown of Caspase 8

siPools targeting Caspase-8 or control (siTOOLs Biotech) were prediluted to reach 1 µM and 30 µL of this solution added to 1 mL Opti-MEM to reach a final siPool concentration of 3 nM. Solution was vortexed and centrifuged. 20 µL of RNAiMAX was mixed with 1 mL Opti-MEM (Lipofectamine RNAiMAX Transfection Reagent #13778150; Opti-MEM #51985026 both ThermoFisher) and this mixture was added to the Opti-MEM + siPools solution, mixed well and incubate for 5 min at room temperature. This mixture was added on the bottom of a petri dish and 2 Mio of HCT-116 cells in 8 mL added dropwise to the transfection mix. The next day cells were collected and seeded at 1500 cells/well in a clear flat bottom 96-well plate. 2.5 uM RG6146, 15 ng/mL TNF or control were added to the plate and plates placed in the IncuCyte S3 Live-cell Analysis System (Essen BioScience) to monitor cell growth over time. Data was normalized to time point of treatment (T0). Cells not used for the growth assay were replated and treated with 15 ng/mL TNF for 8 h before collecting cells and assessing knockdown efficacy by western blot.

7.2.15 Sample preparation for RNA-seq

Cells were washed, detached and cell density adjusted to 0.25 Mio cells/ well in a 6-well plate. The next day, cells were treated with 2.5 µM RG6146 or DMSO control for 1 h. Subsequently, 20 ng/mL TNF or PBS 0.5 % BSA were added for additional 2 h. Before harvest, cells were washed with PBS and incubated with 500 µL TrypLE™ Express for cells to detach. Cells were collected in 1.5 mL Eppendorf Tubes, centrifuged and washed with PBS. Cell pellet was frozen in liquid nitrogen and stored at -80 °C for further use. RNA-sequencing was performed at Roche internally and analysis was performed by Simon Hogg.

7.2.16 3′-mRNA sequencing

Analysis of this assay was performed by Simon Hogg.
RNA extraction was performed with the Qiagen RNeasy Mini Kit (#74104), following the manufacturer's instructions with the exception that lysate was loaded on a QIAshredder column before loading on a spin column. 100 ng RNA was used as an input to generate sequencing libraries with the Illumina TruSeq Stranded mRNA LT Sample Preparation Kit (Set B, #RS-122-2102) following the manufacturer's instruction. Sequencing of libraries was performed on an Illumina HiSeq4000 using paired-end sequencing 2x50 bp reads to an average depth of 18 to 37 million sequences per sample. Base calling was conducted using BCL to FASTQ file converter bcl2fastq (v2.17.1.14) from Illumina. To estimate gene expression levels, STAR aligner (v2.5.2a) with default mapping parameters was used to map paired-end RNASeq reads to the human genome (hg38) [315]. SAMTOOLS software [316] was used to combine numbers of mapped reads for all RefSeq transcript variants of a gene (counts) into a single value. Differential gene expression analysis was conducted by the VoomLimma workflow to compute statistical significance. All further RNA-seq data analysis and generation of figures was done in Rstudio (v3.6.1). GO Term analysis was conducted using the software ToppGene. Gene Set Enrichment Analysis (GSEA) software (v3.0) was used for identification of enriched gene sets, obtained from the MSigDB KEGG and Hallmarks datasets.

7.2.17 quantitative real time-PCR (qRT-PCR)

Cells were detached with 0.25 % Trypsin and cell density adjusted to 0.25 Mio cells/ well in a 6-well plate depending on cell growth. Cells were placed in the incubator overnight, medium replaced the next day and cells treated with desired concentration of small molecule or 0.1 % DMSO control. Cells were placed back in the incubator for the required treatment time, washed with ice cold PBS and scraped off using 350 µL of cell extraction buffer (RNeasy Mini Kit) and stored at -80 °C until further use. RNA extraction and purification procedure was handled as described by the manufacture's protocol (RNeasy Mini Kit) including DNA digest (RNase-Free DNase Set). PCR-mix contained 300 ng RNA, 10 µL qScript™ XLT One-Step RT-qPCR ToughMix® (Quanta Bio), 1 µL TaqMan Gene expression assay (Table 7) and filled with water to 20 µL. 10 µL of this mix were loaded into each well of LightCycler® 480 Multiwell Plate 96 (Roche). Plates were sealed with LightCycler® 480 Sealing Foil (Roche) and placed into the LightCycler® 480 System (Roche). The qRT-PCR program is summarized in table 15. The 2ΔΔCt-Method was used to calculate the relative RNA expression and normalized to *GAPDH* housekeeping genes.

Table 15: qRT-PCR program

Number of cycles	Temperature	Time
1 cycle	50 °	20 min
1 cycle	95 °	1 min
45 cycles	95 °	15 sec
	60 °	1 min

7.2.18 Overexpression

BIRC2 (GeneID: 321827), *BIRC3* (GeneID: 321828; BIRC3_Restriction_Resistant (GeneID: 327673) (for double overexpression)), *TRAF1* (GeneID: 327672) or control overexpressing cassettes (GeneID: 321830) in lentiviral plasmids (pD2107-CMV: CMV-ORF, Lenti-ElecD) were purchased from Atum and lentivirus was generated in house. 15 µg of plasmid were mixed with 1.5 mL Opti-MEM and Mission Lentiviral packaging (1:100, Sigma #SHP-001-1.7mL). To this mix, 45 µL of XtremeGENE HP DNA transfection reagent (Roche #6366236001) was added drop by drop, mixed and incubated at room temperature for 15 min. 293FT cells were plated the previous day at 10 Mio cells/100 mm Petri dish, medium exchanged and transfection mix added dropwise to cells. 24 h later, the culture medium was changed to IMDM (ThermoFisher #21980032) + 10 % FBS and incubated for another 24 h. Subsequently, supernatant was collected and filtered through a 0.45 µM filter, 4 mL PEG-IT (Systembio #LV810A-1) added and stored in the fridge. Fresh IMDM + 10 % FBS was added and collected 24 h later as described before. Subsequently, supernatant was pooled and centrifuged at 1500xg for 30 min. Virus pellet was resuspended in IMDM and frozen at -80 °C. MKN45 cells were plated at a cell density of 0.25 Mio and 24 h later medium exchanged containing 10-100 µL virus and polybrene diluted 1:1000 (Merck #TR-1003-G). The following day, medium was exchanged containing 2 µg/mL Puromycine or 600 µg/mL Hygromycin. Status of overexpression was detected by western blot.

7.2.19 Chromatin immunoprecipitation and sequencing ChIP-seq and ATAC-seq assay set up and analysis

Experimental set up and data analysis for this assay was performed by Simon Hogg and all buffers used are listed in table 16. MC38-Ova cells were treated with RG6146 (2.5 µM), TNF (10 ng/mL) or the combination for 3 hours, cells were washed with ice cold PBS and crosslinked within tissue culture plates with 1 % formaldehyde for 20 minutes at room

temperature. 1.25 M glycine was used for quenching prior to manually scraping cells off plates. Cells were washed three times with ice-cold nuclear extraction buffer, and cell lysis was performed in ChIP lysis buffer. Cells were sonicated with a Covaris ultrasonicator at maximum power for 16 minutes to generate an average DNA fragment size of 300-500 bp. A 1:1 dilution of sonicated chromatin in ChIP dilution buffer was used in combination with a 1:1 ratio of protein A and G magnetic beads (Life Technologies) and immunoprecipitation reactions were performed overnight at 4°C. Antibodies used for ChIP-seq include: NF-κB p65 polyclonal antibody (Diagenode, C15310256), H3K27Ac (Abcam, ab4729), and BRD4 (Bethyl, A301-985A100). Next, samples were washed once in ChIP dilution buffer, wash buffer 1, wash buffer 2, and TE buffer prior to incubation for 4 h shaking in reverse crosslinking buffer at 55°C. Supernatant was reverse-crosslinked overnight (12-16 hours) at 65°C prior to ChIP DNA isolation using Zymogen ChIP DNA Clean and Concentrator Kit (Zymo Research, D5205). Libraries for ChIP-seq were prepared using the NEBNext Ultra II DNA Library Prep Kit (NEB, E7645) and sequenced on an Illumina NextSeq 550 with 75 bp single-end reads. D1000 high-sensitivity screen tape with a 4200 TapeStation Instrument (Agilent Technologies) was used to conduct Library QC and quantification. Size was selected between 200 bp and 500 bp with the use of a Pippin Prep system (Sage Science).

Raw sequencing reads, contained in the ChIP-seq and ATAC-seq datasets, were demultiplexed using bcl2fastq (v2.17.1.14) and quality control assessed with FASTQC (v0.11.5). Adaptor sequences were removed using CutAdapt (v1.14) and reads aligned to the reference genome (mm10) using Bowtie2 (v2.3.5). SAM and BAM files were processed with Samtools (v1.4.1), after which Model-based Analysis of ChIP-Seq (MACS2, v2.2.5) was conducted for peak calling. The bamCoverage function (Deeptools, v3.0.0) with the settings (–normalizeUsing CPM –smoothLength 150 –binSize 50 -e 200 scaleFactor 1) converted BAM files into BigWig files. Subsequently, these files were imported into Integrative Genomics Viewer (IGV, v2.7.0) for visualization of specific loci. Average profile plots and heatmaps were generated by computing read average read density across defined genomic intervals using computeMatrix (Deeptools (v3.0.0)). Data was plotted by plotProfile and plotHeatmap. Genomic regions spanning mm10 blacklist intervals (ENCODE) were excluded in Deeptools.

Putative super enhancer regions from H3K27ac ChIP-seq data were annotated by Ranking Ordering of Super Enhancer (ROSE, v1.0.5). To reduce promoter bias, a 12.5 k.b. stitching distance and a 2.5 k.b. TSS exclusion was used. MACS2 (default parameters) was used to conduct peak calling . Subsequent annotation of ATAC-Seq/ChIP-Seq peaks to proximal genes and motif analyses was done with annotatePeaks.pl and findPeaks (Homer, v4.8).

Table 16: List of buffers used for ChIP-seq

ChIP lysis buffer	20 mM Tris-HCl 150 mM $NaCl_2$ 2 mM EDTA 1 % IGEPAL CA-630 (Sigma-Aldrich) 0.3 % SDS in water
ChIP dilution buffer	20 mM Tris-HCl 150 mM $NaCl_2$ 2 mM EDTA 1 % Triton-X phosphatase/protease inhibitors in water
wash buffer 1	0.1 % SDS 1 % Triton X-100 2 mM EDTA 500 mM NaCl 20 mM Tris-HCl pH 8
wash buffer 2	0.5 % deoxycholate 0.5 % NP-40 2 mM EDTA 250 mM LiCl 20 mM Tris-HCl pH 8
TE buffer	1 mM EDTA 10 mM Tris-HCl pH 7.5
reverse crosslinking buffer	200 mM NaCl 100 mM NaHCO3 1 % SDS 300 µg/mL Proteinase-K

7.2.20 NF-κB based Luciferase Assay

For this assay HCT-116 cells were used, which stabelly express a NF-κB luciferase reporter construct. This construct contains a firefly luciferase gene under the control of an NF-κB response element located upstream of the TATA promoter (From NF-κB Reporter (Luc) - HCT116 Recombinant Cell Line; BPS BioScience; accessed October 2020 <https://bpsbioscience.com/nf-kappa-b-reporter-luc-hct116-recombinant-cell-line>).

0.005 Mio cells were seeded per well in a 96-well flat bottom plate and cells treated the next day with a dose response of RG6146 or TNF as well as RG6146 in combination with 15 ng/mL TNF. Cells were kept in the incubator for 8 or 72 h. Temperature of plates was equilibrated to room temperature for 30 min before addition of 100 µL OneGlo (Promega). Cells were placed on a shaker for 1 min and Luciferase signal assessed at the PHERAStarFSX. For the 72 h time point plates were seeded in duplicate and one plate assessed for Luciferase-Reporter signal, while the other plate was assessed for viability using CTG2.0. Data was normalized to each control or to the viability for the 72 h time point.

7.2.21 CEA-TCB Co-culture assay

MKN45 cells were detached and 0.025 Mio cells/ well were seeded in a 96-well flat bottom plate in 100 µL/well in assay medium (RPMI1640 (31870) + Glutamine + 1 % FBS). Cells were kept in the incubator to give time to adhere overnight. PBMCs were isolated from buffy coats and if thawed the day before, PBMCs were kept in the incubator in RPMI + GlutaMAX + 10 % FBS. PBMCs were added to the MKN45 cells at 0.25 Mio cells/ mL in 50 µL assay medium. CEA-TCB were diluted in assay medium to final concentrations of 1, 0.5, 0.25 nM or control in 50 µL assay medium. As a negative control, PBMCs and MKN45 cells were left untreated (Spontaneous Release) and MKN45 cells were seeded in 150 µL without PBMCs (Maximal Release). After 24 and 48 h, 50 µL of assay medium containing 4 % of Triton were added to the MKN45 cells (Maximal Release) to reach a final concentration of 1 % Triton inducing cell lysis 2 h prior to assay read out. For read out of cell lysis, plates were centrifuged for 2 min at 350 g and 50 µL of supernatant was transferred to a new 96-well flat bottom plate. Dye and catalyst solution (Cytotoxicity Detection kit, (LDH), Roche) was mixed as described in the manufacturer's protocol and 50 µL/well added to the supernatant and incubated for 30 min protected from light. The plate was read using the SpectroStar Nano and %-tumor lysis calculated as described in the manufacturer's protocol.

7.2.22 CEA-TCB Supernatant Assay

Set up of the co-culture including MKN45 cells and PBMCs as described in 7.2.21 and treated +/−20 nM CEA-TCB. As a control supernatant was also generated from a Monoculture containing either PBMCs or MKN45 cells +/− CEA-TCB. After 24 h of coculture, supernatant was collected and 100 µL of supernatant was frozen at -20 °C for cytokine analysis. The rest of the supernatant was filtered (0.22 µM SterfiFlip, Millipore) and added on HCT-116 or MKN45 cells plated the previous day at 5000 cells/ well in a 96-well plate (#3917 CoStar) and treated with a dose response of RG6146 or DMSO control (0.15 %). 72 h post treatment, viability was assessed by CTG2.0 treatment as de-

scribed in 7.2.3. Data was normalized to DMSO control +/− CEA-TCB. For the rescue experiment with TNF blockade, Anti-TNF or Isotype Control (Table 8) were added to the co-culture of MKN45 and PBMCs to reach a final concentration of 10 µg/mL.
For the western blot assay, co-culture was set up as described above and supernatant collected 24 h later. MKN45 cells were seeded at 0.25 Mio cells/ well in a 6-well plate and let adhere overnight. The next day, medium was exchanged with freshly generated supernatant from the co-culture assay and treated with 1-2.5 µM RG6146 or DMSO control for 24 h. Samples were harvested and protein level assessed as described in 7.2.4.

7.2.23 Flow cytometry cytokine Analysis

Samples collected in the CEA-TCB assay were diluted 1:1 and 1:10 in assay diluent (BD BioScience #558264) and 10 µL placed in a V-bottom plate (Falcon # 353263). Standard of the corresponding beads (Table 8) was diluted 1:2.5 and also added to the V-bottom plate. Beads described in table 8 were vortexed and diluted 1:50 in bead diluent and 10 µL added to the samples. Cells were shaked at 500xrpm for 5 min and incubated on a plate shaker for 1 h at 300-600rpm at room temperature. PE Detection reagent from the same Kit was diluted 1:50 in detection reaction diluent, 10 µL added to the sample and after an initial 5 min shake at 500xrpm, plates were incubated on a plate shaker for 2 h in the dark at 300xrpm. 100 µL/well wash buffer was added on a 1.2 µM filter plate (Millipore #MSBVN1210) and vacuum applied to drain wells. 150 µL of wash buffer were added to the sample, transferred to the filter plate and vacuum applied. 40 µL of wash buffer were added to the filter plate, shaked on a plate shaker to resuspend sample and data acquired on the iQue FACS machine. Cytokine concentration was calculated using the iQue Forecyt® software.

7.2.24 Bystander Killing Assay

A co-culture of HCT-116-GFP and MKN45-RFP cells were seeded at 0.02 Mio cells/ well in a 96-well (#3903 CoStar) and let adhere in the incubator overnight. PBMCs, if not freshly isolated on the day of the assay, were thawed, resuspended in RPMI + 10 % FBS and kept in the incubator overnight. The next day, PBMCs were added at a cell density of 0.4 Mio cells/ well to the co-culture as well as 40 nM CEA-TCB or control. The co-culture was treated with a dose response of RG6146 or DMSO control reaching a maximal concentration of 0.15 % DMSO. The assay plates were placed in the incubator for six days and cell confluence as well as GFP and RFP staining monitored by the Incucyte S3 Cell imaging system. Data was analyzed with the software of the instrument by looking at GFP (mm^3) corresponding to HCT-116 cell confluence. Data was normalized to HCT-116 cell confluence at time point of treatment (T0).

7.2.25 *in vivo* study MC38 CEA-TCB

This *in vivo* study was performed by the Oncology Pharmacology department at Roche innovation center Munich from Thomas Friess and Daniela Geiss.
MC38 cells were transfected with CEACAM5 (MC38_HOMSA_CEACAM5) internally and cultured in DMEM high-glucose medium supplemented with NEAA, 4 mM glutamine, 2 mM sodium pyruvate, 10 % FBS, 500 µg/mL G-418 in the incubator. Cells were passaged twice a week and the third passage was used for transplantation. Cells were injected subcutaneously with martigel at a concentration of 0.5 Mio cells into mice.
Female C57/Bl6 human CEA transgenic (huCEA tg) mice (from Charles River, France; 5-8 weeks of age at arrival) were checked daily for clinical symptoms, adverse events and the body weight was monitored throughout the experiment. Animals were randomized when tumor size reached 100 or 130 mm^3. Each treatment group contained 10 animals. 2.5 mg/kg CEA-TCB antibody was administered intravenously (iv) as single agent or in combination twice weekly (4x). 50 mg/kg JQ1 (HY-13030, MedChemExpress) was administered ip as single agent or in combination once daily for 14 days. For the rescue experiment, 2 mg/kg anti TNF-α Mab (cat 506347, BioLegend) was given as single agent or in combination twice weekly and was injected iv (4x).
Twice a week the tumor volume was measured and determined using the equation:
$V = ab^2 / 2$ with a: length; b: width of tumor measured with a caliper. The tumor growth inhibition (TGI) for mice in the same treatment group was calculated using the following formula: $(1 - [T - T_0] / [C_{22} - C_0]) \times 100$. T: Mean tumor volume of mice in the same treatment group (last measurement), T_0: Mean tumor volume of mice in the same treatment group (first measurement), C: Mean tumor volume of mice in the control group (last measurement), C_0: Mean tumor volume of mice in the control group (first measurement).
The %-change in tumor volume was calculated with the following equation: $([M - M_0] / [M_0]) \times 100$. M: Tumor volume last measurement, M_0: Tumor volume first measurement.

7.2.26 *in vivo* study MC38 anti-PD-1

This *in vivo* study was performed by Dane Newman.
MC38 cells (wild type) were injected subcutaneously into male C57BL/6 mice (6-8 weeks old). Mice were randomized into four groups after 6 days of tumor inoculation (10-13 mice/group). Treatment with DMSO or JQ1 was performed daily at a concentration of 50 mg/kg ip (days 6-22 post tumor inoculation). Anti-PD-1 treatment was performed at 0.2 mg/kg (clone RMP1-14) or isotype control (ITC; clone 2A3) ip (Days 9, 13, 26 and 20 post tumor inoculation). Tumor volume was measured as described in 7.2.25. Results contain data from two biological independent experiments.

Contributions

Thomas Friess' group performed the *in vivo* assays described in Figure 12, 16, 41 E-G and 42. **Thomas Friess**, **Stefanie Lechner** and **Daniela Geiss** performed the *in vivo* studies described in Figure 12. **Thomas Friess** and **Stefanie Lechner** performed the *in vivo* studies described in Figure 16. **Thomas Friess** and **Daniela Geiss** performed the *in vivo* assays with JQ1 and CEA-TCB summarized in Figure 41 E-G and 42.
Simon Hogg performed the *in vitro* assay described in Figure 27 E, RNA-seq Analysis shown in Figure 32 B-E and 33 as well as the ChIP-seq experiment described in Figure 35 and 36.
Dane Newman performed the *in vitro* assay described in Figure 27 G and the *in vivo* study described in Figure 43.
The cell screen described in Figure 29 A was conducted by the company **Oncolead**, Karlsfeld Germany.
The figures 11, 12, 13, 14, 15, 16 are partially or completely included in the following manuscript, which is currently prepared for submission:

- **Lisa C. Wellinger***, Simon J. Hogg*, Dane M. Newman, Thomas Friess, Daniela Geiss, Stefanie Lechner, Andrea Newbold, Peter Fraser, Jake Shortt, Daniel Rohle, Astrid Ruefli-Brasse, Ricky W. Johnstone. Targeting Hematologic Malignancies With Second-Generation BET Bromodomain Inhibitor RG6146
  *these authors contributed equally

The figures 27, 29, 31, 32, 33, 34, 35, 36, 38, 39, 40, 41, 42 and 43 are partially or completely included in the following manuscript, which is currently under review at Cancer Discovery and available as a preprint on bioRxiv:
bioRxiv 2021.02.15.429851; doi: https://doi.org/10.1101/2021.02.15.429851 :

- **Lisa C. Wellinger***, Simon J. Hogg*, Dane M. Newman, Thomas Friess, Daniela Geiss, Jessica Michie, Kelly M. Ramsbottom, Marina Bacac, Tanja Fauti, Daniel Marbach, Laura Jarassier, Phillip Thienger, Axel Paehler, Leonie A. Cluse, Conor J. Kearney, Stephin J. Vervoort, Jane Oliaro, Jake Shortt, Astrid Ruefli-Brasse, Daniel Rohle#, Ricky W. Johnstone#. BET Inhibition Enhances TNF Mediated Anti-Tumor Immunity
  *these authors contributed equally; #these authors contributed equally

The figures 27, 29, 31, 38, 39, 40, 41, 42 and 43 are partially or completely included in the following patent:

- Marina, Bacac, Tanja A. Fauti, Simon J. Hogg, Ricky W. Johnstone, Astrid Ruefli-Brasse, Daniel Rohle, **Lisa C. Wellinger**. Sensitization of cancer cells to TNF by BET inhibition *WO 2020/169698*, August 2020

Bibliography

[1] Anthony T. Annunziato. DNA Packaging: Nucleosomes and Chromatin. *Nature Education*, 1(1):26, 2008.

[2] Cheryl H. Arrowsmith, Chas Bountra, Paul V. Fish, Kevin Lee, and Matthieu Schapira. Epigenetic protein families: a new frontier for drug discovery. *Nat Rev Drug Discov*, 11(5):384–400, May 2012.

[3] Raphael Margueron, Patrick Trojer, and Danny Reinberg. The key to development: interpreting the histone code? *Current Opinion in Genetics & Development*, 15(2):163–176, April 2005.

[4] T. Jenuwein. Translating the Histone Code. *Science*, 293(5532):1074–1080, August 2001.

[5] V Bollati and A Baccarelli. Environmental epigenetics. *Heredity*, 105(1):105–112, July 2010.

[6] Elizabeth M. Martin and Rebecca C. Fry. Environmental Influences on the Epigenome: Exposure- Associated DNA Methylation in Human Populations. *Annu. Rev. Public Health*, 39(1):309–333, April 2018.

[7] X-J Yang and E Seto. HATs and HDACs: from structure, function and regulation to novel strategies for therapy and prevention. *Oncogene*, 26(37):5310–5318, August 2007.

[8] M. Shogren-Knaak. Histone H4-K16 Acetylation Controls Chromatin Structure and Protein Interactions. *Science*, 311(5762):844–847, February 2006.

[9] Noriyuki Suka, Kunheng Luo, and Michael Grunstein. Sir2p and Sas2p opposingly regulate acetylation of yeast histone H4 lysine16 and spreading of heterochromatin. *Nat Genet*, 32(3):378–383, November 2002.

[10] Mona D. Shahbazian and Michael Grunstein. Functions of Site-Specific Histone Acetylation and Deacetylation. *Annu. Rev. Biochem.*, 76(1):75–100, June 2007.

[11] S. Rahman, M. E. Sowa, M. Ottinger, J. A. Smith, Y. Shi, J. W. Harper, and P. M. Howley. The Brd4 Extraterminal Domain Confers Transcription Activation Independent of pTEFb by Recruiting Multiple Proteins, Including NSD3. *Molecular and Cellular Biology*, 31(13):2641–2652, July 2011.

[12] Ji-Eun Lee, Young-Kwon Park, Sarah Park, Younghoon Jang, Nicholas Waring, Anup Dey, Keiko Ozato, Binbin Lai, Weiqun Peng, and Kai Ge. Brd4 binds to active

enhancers to control cell identity gene induction in adipogenesis and myogenesis. *Nat Commun*, 8(1):2217, December 2017.

[13] Catherine A Musselman, Marie-Eve Lalonde, Jacques Côté, and Tatiana G Kutateladze. Perceiving the epigenetic landscape through histone readers. *Nat Struct Mol Biol*, 19(12):1218–1227, December 2012.

[14] Douglas Hanahan and Robert A Weinberg. The Hallmarks of Cancer. *Cell*, 100(1):57–70, January 2000.

[15] Andrew P. Feinberg and Bert Vogelstein. Hypomethylation distinguishes genes of some human cancers from their normal counterparts. *Nature*, 301(5895):89–92, January 1983.

[16] Peter A. Jones and Stephen B. Baylin. The Epigenomics of Cancer. *Cell*, 128(4):683–692, February 2007.

[17] Minoru Toyota, Nita Ahuja, Mutsumi Ohe-Toyota, James G Herman, Stephen B Baylin, and Jean-Pierre J Issa. CpG island methylator phenotype in colorectal cancer. *Proc. Natl. Acad. Sci. USA*, page 6, 1999.

[18] Daniel J Weisenberger, Kimberly D Siegmund, Mihaela Campan, Joanne Young, Tiffany I Long, Mark A Faasse, Gyeong Hoon Kang, Martin Widschwendter, Deborah Weener, Daniel Buchanan, Hoey Koh, Lisa Simms, Melissa Barker, Barbara Leggett, Joan Levine, Myungjin Kim, Amy J French, Stephen N Thibodeau, Jeremy Jass, Robert Haile, and Peter W Laird. CpG island methylator phenotype underlies sporadic microsatellite instability and is tightly associated with BRAF mutation in colorectal cancer. *Nat Genet*, 38(7):787–793, July 2006.

[19] Nilesh Zaware and Ming-Ming Zhou. Bromodomain biology and drug discovery. *Nat Struct Mol Biol*, 26(10):870–879, October 2019.

[20] Chen-Yi Wang and Panagis Filippakopoulos. Beating the odds: BETs in disease. *Trends in Biochemical Sciences*, 40(8):468–479, August 2015.

[21] F Jeanmougin. The bromodomain revisited. *Trends in Biochemical Sciences*, 22(5):151–153, May 1997.

[22] Panagis Filippakopoulos, Sarah Picaud, Maria Mangos, Tracy Keates, Jean-Philippe Lambert, Dalia Barsyte-Lovejoy, Ildiko Felletar, Rudolf Volkmer, Susanne Müller, Tony Pawson, Anne-Claude Gingras, Cheryl H. Arrowsmith, and Stefan Knapp. Histone Recognition and Large-Scale Structural Analysis of the Human Bromodomain Family. *Cell*, 149(1):214–231, March 2012.

[23] Moon Kyoo Jang, Kazuki Mochizuki, Meisheng Zhou, Ho-Sang Jeong, John N. Brady, and Keiko Ozato. The Bromodomain Protein Brd4 Is a Positive Regulatory Component of P-TEFb and Stimulates RNA Polymerase II-Dependent Transcription. *Molecular Cell*, 19(4):523–534, August 2005.

[24] Zhiyuan Yang, Jasper H.N. Yik, Ruichuan Chen, Nanhai He, Moon Kyoo Jang, Keiko Ozato, and Qiang Zhou. Recruitment of P-TEFb for Stimulation of Transcriptional Elongation by the Bromodomain Protein Brd4. *Molecular Cell*, 19(4):535–545, August 2005.

[25] Anna C. Belkina and Gerald V. Denis. BET domain co-regulators in obesity, inflammation and cancer. *Nat Rev Cancer*, 12(7):465–477, July 2012.

[26] Jakob Lovén, Heather A. Hoke, Charles Y. Lin, Ashley Lau, David A. Orlando, Christopher R. Vakoc, James E. Bradner, Tong Ihn Lee, and Richard A. Young. Selective Inhibition of Tumor Oncogenes by Disruption of Super-Enhancers. *Cell*, 153(2):320–334, April 2013.

[27] Panagis Filippakopoulos and Stefan Knapp. Targeting bromodomains: epigenetic readers of lysine acetylation. *Nat Rev Drug Discov*, 13(5):337–356, May 2014.

[28] Sebastian Pott and Jason D Lieb. What are super-enhancers? *Nat Genet*, 47(1):8–12, January 2015.

[29] Bas Tolhuis, Robert-Jan Palstra, Erik Splinter, Frank Grosveld, and Wouter de Laat. Looping and Interaction between Hypersensitive Sites in the Active β-globin Locus. *Molecular Cell*, 10(6):1453–1465, December 2002.

[30] Michael H. Kagey, Jamie J. Newman, Steve Bilodeau, Ye Zhan, David A. Orlando, Nynke L. van Berkum, Christopher C. Ebmeier, Jesse Goossens, Peter B. Rahl, Stuart S. Levine, Dylan J. Taatjes, Job Dekker, and Richard A. Young. Mediator and cohesin connect gene expression and chromatin architecture. *Nature*, 467(7314):430–435, September 2010.

[31] Wulan Deng, Jongjoo Lee, Hongxin Wang, Jeff Miller, Andreas Reik, Philip D. Gregory, Ann Dean, and Gerd A. Blobel. Controlling Long-Range Genomic Interactions at a Native Locus by Targeted Tethering of a Looping Factor. *Cell*, 149(6):1233–1244, June 2012.

[32] Warren A. Whyte, David A. Orlando, Denes Hnisz, Brian J. Abraham, Charles Y. Lin, Michael H. Kagey, Peter B. Rahl, Tong Ihn Lee, and Richard A. Young. Master Transcription Factors and Mediator Establish Super-Enhancers at Key Cell Identity Genes. *Cell*, 153(2):307–319, April 2013.

[33] Denes Hnisz, Brian J. Abraham, Tong Ihn Lee, Ashley Lau, Violaine Saint-André, Alla A. Sigova, Heather A. Hoke, and Richard A. Young. Super-Enhancers in the Control of Cell Identity and Disease. *Cell*, 155(4):934–947, November 2013.

[34] Andrea G. Cochran, Andrew R. Conery, and Robert J. Sims. Bromodomains: a new target class for drug development. *Nat Rev Drug Discov*, 18(8):609–628, August 2019.

[35] Panagis Filippakopoulos, Jun Qi, Sarah Picaud, Yao Shen, William B. Smith, Oleg Fedorov, Elizabeth M. Morse, Tracey Keates, Tyler T. Hickman, Ildiko Felletar, Martin Philpott, Shonagh Munro, Michael R. McKeown, Yuchuan Wang, Amanda L. Christie, Nathan West, Michael J. Cameron, Brian Schwartz, Tom D. Heightman, Nicholas La Thangue, Christopher A. French, Olaf Wiest, Andrew L. Kung, Stefan Knapp, and James E. Bradner. Selective inhibition of BET bromodomains. *Nature*, 468(7327):1067–1073, December 2010.

[36] D. J. Owen. The structural basis for the recognition of acetylated histone H4 by the bromodomain of histone acetyltransferase Gcn5p. *The EMBO Journal*, 19(22):6141–6149, November 2000.

[37] Christophe Dhalluin, Justin E Carlson, Lei Zeng, Cheng He, Aneel K Aggarwal, and Ming-Ming Zhou. Structure and ligand of a histone acetyltransferase bromodomain. *Nature*, 399:6, 1999.

[38] R. H. Jacobson. Structure and Function of a Human TAFII250 Double Bromodomain Module. *Science*, 288(5470):1422–1425, May 2000.

[39] Jeanne Morinière, Sophie Rousseaux, Ulrich Steuerwald, Montserrat Soler-López, Sandrine Curtet, Anne-Laure Vitte, Jérôme Govin, Jonathan Gaucher, Karin Sadoul, Darren J. Hart, Jeroen Krijgsveld, Saadi Khochbin, Christoph W. Müller, and Carlo Petosa. Cooperative binding of two acetylation marks on a histone tail by a single bromodomain. *Nature*, 461(7264):664–668, October 2009.

[40] Laura Soucek and Gerard I Evan. The ups and downs of Myc biology. *Current Opinion in Genetics & Development*, 20(1):91–95, February 2010.

[41] Jake E. Delmore, Ghayas C. Issa, Madeleine E. Lemieux, Peter B. Rahl, Junwei Shi, Hannah M. Jacobs, Efstathios Kastritis, Timothy Gilpatrick, Ronald M. Paranal, Jun Qi, Marta Chesi, Anna C. Schinzel, Michael R. McKeown, Timothy P. Heffernan, Christopher R. Vakoc, P. Leif Bergsagel, Irene M. Ghobrial, Paul G. Richardson, Richard A. Young, William C. Hahn, Kenneth C. Anderson, Andrew L. Kung,

James E. Bradner, and Constantine S. Mitsiades. BET Bromodomain Inhibition as a Therapeutic Strategy to Target c-Myc. *Cell*, 146(6):904–917, September 2011.

[42] L. L. da Motta, I. Ledaki, K. Purshouse, S. Haider, M. A. De Bastiani, D. Baban, M. Morotti, G. Steers, S. Wigfield, E. Bridges, J-L. Li, S. Knapp, D. Ebner, F. Klamt, A. L. Harris, and A. McIntyre. The BET inhibitor JQ1 selectively impairs tumour response to hypoxia and downregulates CA9 and angiogenesis in triple negative breast cancer. *Oncogene*, 36(1):122–132, January 2017.

[43] Christopher A. French, Isao Miyoshi, Jon C. Aster, Ichiro Kubonishi, Todd G. Kroll, Paola Dal Cin, Sara O. Vargas, Antonio R. Perez-Atayde, and Jonathan A. Fletcher. BRD4 Bromodomain Gene Rearrangement in Aggressive Carcinoma with Translocation t(15;19). *The American Journal of Pathology*, 159(6):1987–1992, December 2001.

[44] Christopher A French, Isao Miyoshi, Ichiro Kubonishi, Holcombe E Grier, Antonio R Perez-Atayde, and Jonathan A Fletcher. BRD4-NUT Fusion Oncogene: A Novel Mechanism in Aggressive Carcinoma. *Cancer Research*, 63:304–307, January 2003.

[45] C. A. French, C. L. Ramirez, J. Kolmakova, T. T. Hickman, M. J. Cameron, M. E. Thyne, J. L. Kutok, J. A. Toretsky, A. K. Tadavarthy, U. R. Kees, J. A. Fletcher, and J. C. Aster. BRD-NUT oncoproteins: a family of closely related nuclear proteins that block epithelial differentiation and maintain the growth of carcinoma cells. *Oncogene*, 27(15):2237–2242, April 2008.

[46] Hannah Farmer, Nuala McCabe, Christopher J. Lord, Andrew N. J. Tutt, Damian A. Johnson, Tobias B. Richardson, Manuela Santarosa, Krystyna J. Dillon, Ian Hickson, Charlotte Knights, Niall M. B. Martin, Stephen P. Jackson, Graeme C. M. Smith, and Alan Ashworth. Targeting the DNA repair defect in BRCA mutant cells as a therapeutic strategy. *Nature*, 434(7035):917–921, April 2005.

[47] Chaoyang Sun, Jun Yin, Yong Fang, Jian Chen, Kang Jin Jeong, Xiaohua Chen, Christopher P. Vellano, Zhenlin Ju, Wei Zhao, Dong Zhang, Yiling Lu, Funda Meric-Bernstam, Timothy A. Yap, Maureen Hattersley, Mark J. O'Connor, Huawei Chen, Stephen Fawell, Shiaw-Yih Lin, Guang Peng, and Gordon B. Mills. BRD4 Inhibition Is Synthetic Lethal with PARP Inhibitors through the Induction of Homologous Recombination Deficiency. *Cancer Cell*, 33(3):401–416.e8, March 2018.

[48] Hengrui Zhu, Fee Bengsch, Nikolaos Svoronos, Melanie R. Rutkowski, Benjamin G. Bitler, Michael J. Allegrezza, Yuhki Yokoyama, Andrew V. Kossenkov, James E. Bradner, Jose R. Conejo-Garcia, and Rugang Zhang. BET Bromodomain Inhibition

Promotes Anti-tumor Immunity by Suppressing PD-L1 Expression. *Cell Reports*, 16(11):2829–2837, September 2016.

[49] Simon J. Hogg, Stephin J. Vervoort, Sumit Deswal, Christopher J. Ott, Jason Li, Leonie A. Cluse, Paul A. Beavis, Phillip K. Darcy, Benjamin P. Martin, Andrew Spencer, Anna K. Traunbauer, Irina Sadovnik, Karin Bauer, Peter Valent, James E. Bradner, Johannes Zuber, Jake Shortt, and Ricky W. Johnstone. BET-Bromodomain Inhibitors Engage the Host Immune System and Regulate Expression of the Immune Checkpoint Ligand PD-L1. *Cell Reports*, 18(9):2162–2174, February 2017.

[50] Gordon J. Freeman, Andrew J. Long, Yoshiko Iwai, Karen Bourque, Tatyana Chernova, Hiroyuki Nishimura, Lori J. Fitz, Nelly Malenkovich, Taku Okazaki, Michael C. Byrne, Heidi F. Horton, Lynette Fouser, Laura Carter, Vincent Ling, Michael R. Bowman, Beatriz M. Carreno, Mary Collins, Clive R. Wood, and Tasuku Honjo. Engagement of the Pd-1 Immunoinhibitory Receptor by a Novel B7 Family Member Leads to Negative Regulation of Lymphocyte Activation. *Journal of Experimental Medicine*, 192(7):1027–1034, October 2000.

[51] Y. Iwai, M. Ishida, Y. Tanaka, T. Okazaki, T. Honjo, and N. Minato. Involvement of PD-L1 on tumor cells in the escape from host immune system and tumor immunotherapy by PD-L1 blockade. *Proceedings of the National Academy of Sciences*, 99(19):12293–12297, September 2002.

[52] Deanna A. Mele, Andres Salmeron, Srimoyee Ghosh, Hon-Ren Huang, Barbara M. Bryant, and Jose M. Lora. BET bromodomain inhibition suppresses TH17-mediated pathology. *The Journal of Experimental Medicine*, 210(11):2181–2190, October 2013.

[53] Yuki Kagoya, Munehide Nakatsugawa, Yuki Yamashita, Toshiki Ochi, Tingxi Guo, Mark Anczurowski, Kayoko Saso, Marcus O. Butler, Cheryl H. Arrowsmith, and Naoto Hirano. BET bromodomain inhibition enhances T cell persistence and function in adoptive immunotherapy models. *Journal of Clinical Investigation*, 126(9):3479–3494, August 2016.

[54] Charles A Janeway, Paul Travers, Marc Walport, and Mark J Shlomchik. Immunobiology: The Immune System in Health and Disease. In *Immunobiology: The Immune System in Health and Disease.*, page The components of the immune system. Garland Science, New York, 5th edition. edition, 2001.

[55] Charles A Janeway, Paul Travers, Marc Walport, and Mark J Shlomchik. Immunobiology: The Immune System in Health and Disease. In *Immunobiology: The Im-*

mune System in Health and Disease., page Antigen recognition by T cells. Garland Science, New York, 5th edition. edition, 2001.

[56] Charles A Janeway, Paul Travers, Marc Walport, and Mark J Shlomchik. Immunobiology: The Immune System in Health and Disease. In *Immunobiology: The Immune System in Health and Disease.*, page The production of armed effector T cells. Garland Science, New York, 5th edition. edition, 2001.

[57] C. M. Bacon, E. F. Petricoin, J. R. Ortaldo, R. C. Rees, A. C. Larner, J. A. Johnston, and J. J. O'Shea. Interleukin 12 induces tyrosine phosphorylation and activation of STAT4 in human lymphocytes. *Proceedings of the National Academy of Sciences*, 92(16):7307–7311, August 1995.

[58] N. G. Jacobson, S. J. Szabo, R. M. Weber-Nordt, Z. Zhong, R. D. Schreiber, J. E. Darnell, and K. M. Murphy. Interleukin 12 signaling in T helper type 1 (Th1) cells involves tyrosine phosphorylation of signal transducer and activator of transcription (Stat)3 and Stat4. *The Journal of Experimental Medicine*, 181(5):1755–1762, May 1995.

[59] Susanne J. Szabo, Sean T. Kim, Gina L. Costa, Xiankui Zhang, C. Garrison Fathman, and Laurie H. Glimcher. A Novel Transcription Factor, T-bet, Directs Th1 Lineage Commitment. *Cell*, 100(6):655–669, March 2000.

[60] Abul K. Abbas, Kenneth M. Murphy, and Alan Sher. Functional diversity of helper T lymphocytes. *Nature*, 383(6603):787–793, October 1996.

[61] Jordy Saravia, Nicole M. Chapman, and Hongbo Chi. Helper T cell differentiation. *Cell Mol Immunol*, 16(7):634–643, July 2019.

[62] Charles A Janeway, Paul Travers, Marc Walport, and Mark J Shlomchik. Immunobiology: The Immune System in Health and Disease. In *Immunobiology: The Immune System in Health and Disease.*, page The course of the adaptive response to infection. Garland Science, New York, 5th edition. edition, 2001.

[63] J Hou, U Schindler, W. Henzel, T. Ho, M Brasseur, and S. McKnight. An interleukin-4-induced transcription factor: IL-4 Stat. *Science*, 265(5179):1701–1706, September 1994.

[64] Wei-ping Zheng and Richard A Flavell. The Transcription Factor GATA-3 Is Necessary and Sufficient for Th2 Cytokine Gene Expression in CD4 T Cells. *Cell*, 89(4):587–596, May 1997.

[65] Antonio Lanzavecchia. Licence to kill. *Nature*, 393(6684):413–414, June 1998.

[66] Danita H. Schuurhuis, Sandra Laban, René E.M. Toes, Paola Ricciardi-Castagnoli, Monique J. Kleijmeer, Ellen I.H. van der Voort, Delphine Rea, Rienk Offringa, Hans J. Geuze, Cornelis J.M. Melief, and Ferry Ossendorp. Immature Dendritic Cells Acquire CD8+Cytotoxic T Lymphocyte Priming Capacity upon Activation by T Helper Cell-Independent or -Dependent Stimuli. *Journal of Experimental Medicine*, 192(1):145–150, July 2000.

[67] Christopher M Smith, Nicholas S Wilson, Jason Waithman, Jose A Villadangos, Francis R Carbone, William R Heath, and Gabrielle T Belz. Cognate CD4+ T cell licensing of dendritic cells in CD8+ T cell immunity. *Nat Immunol*, 5(11):1143–1148, November 2004.

[68] Shimon Sakaguchi, Noriko Sakaguchi, Masanao Asano, Misako Itoh, and Masaaki Toda. Immunologic Self-Tolerance Maintained by Activated T Cells Expressing IL-2 Receptor α-Chains (CD25). *The Journal of Immunology*, 155:1151–1164, 1995.

[69] Simon Read, Vivianne Malmström, and Fiona Powrie. Cytotoxic T Lymphocyte-Associated Antigen 4 Plays an Essential Role in the Function of CD25+CD4+ Regulatory Cells That Control Intestinal Inflammation. *The Journal of Experimental Medicine*, 192(2):295–302, July 2000.

[70] Takeshi Takahashi, Tomoyuki Tagami, Sayuri Yamazaki, Toshimitsu Uede, Jun Shimizu, Noriko Sakaguchi, Tak W. Mak, and Shimon Sakaguchi. Immunologic Self-Tolerance Maintained by CD25+CD4+Regulatory T Cells Constitutively Expressing Cytotoxic T Lymphocyte-Associated Antigen 4. *The Journal of Experimental Medicine*, 192(2):303–310, July 2000.

[71] Jason D. Fontenot, Marc A. Gavin, and Alexander Y. Rudensky. Foxp3 programs the development and function of CD4+CD25+ regulatory T cells. *Nat Immunol*, 4(4):330–336, April 2003.

[72] S. Hori. Control of Regulatory T Cell Development by the Transcription Factor Foxp3. *Science*, 299(5609):1057–1061, February 2003.

[73] Shimon Sakaguchi, Norihisa Mikami, James B. Wing, Atsushi Tanaka, Kenji Ichiyama, and Naganari Ohkura. Regulatory T Cells and Human Disease. *Annu. Rev. Immunol.*, 38(1):541–566, April 2020.

[74] Peter S. Linsley, JoAnne L. Greene, William Brady, Jürgen Bajorath, Jeffrey A. Ledbetter, and Robert Peach. Human B7-1 (CD80) and B7-2 (CD86) bind with similar avidities but distinct kinetics to CD28 and CTLA-4 receptors. *Immunity*, 1(9):793–801, December 1994.

[75] Alison V. Collins, Douglas W. Brodie, Robert J.C. Gilbert, Andrea Iaboni, Raquel Manso-Sancho, Björn Walse, David I. Stuart, P.Anton van der Merwe, and Simon J. Davis. The Interaction Properties of Costimulatory Molecules Revisited. *Immunity*, 17(2):201–210, August 2002.

[76] O. S. Qureshi, Y. Zheng, K. Nakamura, K. Attridge, C. Manzotti, E. M. Schmidt, J. Baker, L. E. Jeffery, S. Kaur, Z. Briggs, T. Z. Hou, C. E. Futter, G. Anderson, L. S. K. Walker, and D. M. Sansom. Trans-Endocytosis of CD80 and CD86: A Molecular Basis for the Cell-Extrinsic Function of CTLA-4. *Science*, 332(6029):600–603, April 2011.

[77] Lukas Cederbom, Hakan Hall, and Fredrik Ivars. CD4+CD25+ regulatory T cells down-regulate co-stimulatory molecules on antigen-presenting cells. *European Journal of Immunology*, 30:1538–1543, August 2000.

[78] Maurus de la Rosa, Sascha Rutz, Heike Dorninger, and Alexander Scheffold. Interleukin-2 is essential for CD4+CD25+ regulatory T cell function. *Eur. J. Immunol.*, 34(9):2480–2488, September 2004.

[79] Pushpa Pandiyan, Lixin Zheng, Satoru Ishihara, Jennifer Reed, and Michael J Lenardo. CD4+CD25+Foxp3+ regulatory T cells induce cytokine deprivation-mediated apoptosis of effector CD4+ T cells. *Nat Immunol*, 8(12):1353–1362, December 2007.

[80] Hai Zhao, Xuelian Liao, and Yan Kang. Tregs: Where We Are and What Comes Next? *Front. Immunol.*, 8:1578, November 2017.

[81] Xin Xie, Michael J. T. Stubbington, Jesper K. Nissen, Kristian G. Andersen, Daniel Hebenstreit, Sarah A. Teichmann, and Alexander G. Betz. The Regulatory T Cell Lineage Factor Foxp3 Regulates Gene Expression through Several Distinct Mechanisms Mostly Independent of Direct DNA Binding. *PLoS Genet*, 11(6):e1005251, June 2015.

[82] Dat Q. Tran, Deborah D. Glass, Gulbu Uzel, Dirk A. Darnell, Christine Spalding, Steven M. Holland, and Ethan M. Shevach. Analysis of Adhesion Molecules, Target Cells, and Role of IL-2 in Human FOXP3 $^{+}$ Regulatory T Cell Suppressor Function. *J Immunol*, 182(5):2929–2938, March 2009.

[83] Takatoshi Chinen, Arun K. Kannan, Andrew G. Levine, Xiying Fan, Ulf Klein, Ye Zheng, Georg Gasteiger, Yongqiang Feng, Jason D. Fontenot, and Alexander Y. Rudensky. An essential role for the IL-2 receptor in Treg cell function. *Nat Immunol*, 17(11):1322–1333, November 2016.

[84] Atsushi Tanaka and Shimon Sakaguchi. Regulatory T cells in cancer immunotherapy. *Cell Res*, 27(1):109–118, January 2017.

[85] Charles A. Janeway, Paul Travers, Marc Walport, and Mark J. Shlomchik. Immunobiology: The Immune System in Health and Disease. In *Immunobiology: The Immune System in Health and Disease.*, pages T cell–mediated cytotoxicity. Garland Science, New York, 5th edition. edition, 2001.

[86] Bruce Motyka, Gregory Korbutt, Michael J Pinkoski, Jeffrey A Heibein, Antonio Caputo, Marita Hobman, Michele Barry, Irene Shostak, Tracy Sawchuk, Charles F.B Holmes, Jack Gauldie, and R.Chris Bleackley. Mannose 6-Phosphate/Insulin-like Growth Factor II Receptor Is a Death Receptor for Granzyme B during Cytotoxic T Cell-Induced Apoptosis. *Cell*, 103(3):491–500, October 2000.

[87] Michele Barry and R. Chris Bleackley. Cytotoxic T lymphocytes: all roads lead to death. *Nat Rev Immunol*, 2(6):401–409, June 2002.

[88] D. Masson, M. Nabholz, C. Estrade, and J. Tschopp. Granules of cytolytic T-lymphocytes contain two serine esterases. *The EMBO Journal*, 5(7):1595–1600, July 1986.

[89] R. R. Dourmashkin, Patrice Deteix, C. B. Simone, and P. Henkart. Electron microscopic demonstration of lesions in target cell membranes associated with antibody-dependent cellular cytotoxicity. *Clin. exp. Immunol.*, 42:554–560, 1980.

[90] Eckhard R. Podack and Gunther Dennert. Assembly of two types of tubules with putative cytolytic function by cloned natural killer cells. *Nature*, 302(5907):442–445, March 1983.

[91] G. Dennert and E. R. Podack. Cytolysis by H-2-specific T killer cells. Assembly of tubular complexes on target membranes. *The Journal of Experimental Medicine*, 157(5):1483–1495, May 1983.

[92] Jamie A. Lopez, Olivia Susanto, Misty R. Jenkins, Natalya Lukoyanova, Vivien R. Sutton, Ruby H. P. Law, Angus Johnston, Catherina H. Bird, Phillip I. Bird, James C. Whisstock, Joseph A. Trapani, Helen R. Saibil, and Ilia Voskoboinik. Perforin forms transient pores on the target cell plasma membrane to facilitate rapid access of granzymes during killer cell attack. *Blood*, 121(14):2659–2668, April 2013.

[93] Michael J. Pinkoski, Marita Hobman, Jeffrey A. Heibein, Kevin Tomaselli, Feng Li, Prem Seth, Christopher J. Froelich, and R. Chris Bleackley. Entry and Trafficking

of Granzyme B in Target Cells During Granzyme B-Perforin-Mediated Apoptosis. *Blood*, 92(3):1044–1054, August 1998.

[94] Alison J. Darmon, Donald W. Nicholson, and R. Chris Bleackley. Activation of the apoptotic protease CPP32 by cytotoxic T-cell-derived granzyme B. *Nature*, 377(6548):446–448, October 1995.

[95] S. J. Martin, G. P. Amarante-Mendes, L. Shi, T. H. Chuang, C. A. Casiano, G. A. O'Brien, P. Fitzgerald, E. M. Tan, G. M. Bokoch, A. H. Greenberg, and D. R. Green. The cytotoxic cell protease granzyme B initiates apoptosis in a cell-free system by proteolytic processing and activation of the ICE/CED-3 family protease, CPP32, via a novel two-step mechanism. *The EMBO Journal*, 15(10):2407–2416, May 1996.

[96] Jan Paul Medema, René E. M. Toes, Carsten Scaffidi, Timothy S. Zheng, Richard A. Flavell, Cornelius J. M. Melief, Marcus E. Peter, Rienk Offringa, and Peter H. Krammer. Cleavage of FLICE (caspase-8) by granzyme B during cytotoxic T lymphocyte-induced apoptosis. *Eur. J. Immunol.*, 27(12):3492–3498, December 1997.

[97] Michele Barry, Jeffrey A. Heibein, Michael J. Pinkoski, Siow-Fong Lee, Richard W. Moyer, Douglas R. Green, and R. Chris Bleackley. Granzyme B Short-Circuits the Need for Caspase 8 Activity during Granule-Mediated Cytotoxic T-Lymphocyte Killing by Directly Cleaving Bid. *Mol. Cell. Biol.*, 20(11):3781–3794, June 2000.

[98] Jeffrey A. Heibein, Ing Swie Goping, Michele Barry, Michael J. Pinkoski, Gordon C. Shore, Douglas R. Green, and R. Chris Bleackley. Granzyme B-Mediated Cytochrome C Release Is Regulated by the Bcl-2 Family Members Bid and Bax. *Journal of Experimental Medicine*, 192(10):1391–1402, November 2000.

[99] Susan Elmore. Apoptosis: A Review of Programmed Cell Death. *Toxicol Pathol*, 35(4):495–516, June 2007.

[100] Harald Wajant and Daniela Siegmund. TNFR1 and TNFR2 in the Control of the Life and Death Balance of Macrophages. *Front. Cell Dev. Biol.*, 7:91, May 2019.

[101] Dirk Brenner, Heiko Blaser, and Tak W. Mak. Regulation of tumour necrosis factor signalling: live or let die. *Nat Rev Immunol*, 15(6):362–374, June 2015.

[102] E. Y. Jones, D. I. Stuart, and N. P. C. Walker. Structure of tumour necrosis factor. *Nature*, 338(6212):225–228, March 1989.

[103] Roy A. Black, Charles T. Rauch, Carl J. Kozlosky, Jacques J. Peschon, Jennifer L. Slack, Martin F. Wolfson, Beverly J. Castner, Kim L. Stocking, Pranitha Reddy,

Subhashini Srinivasan, Nicole Nelson, Norman Boiani, Kenneth A. Schooley, Mary Gerhart, Raymond Davis, Jeffrey N. Fitzner, Richard S. Johnson, Raymon J. Paxton, Carl J. March, and Douglas Pat Cerretti. A metalloproteinase disintegrin that releases tumour-necrosis factor-α from cells. *Letters to Nature*, 385, February 1997.

[104] Sujuan Yang, Julie Wang, David Douglass Brand, and Song Guo Zheng. Role of TNF-TNF Receptor 2 Signal in Regulatory T Cells and Its Therapeutic Implications. *Front. Immunol.*, 9:784, April 2018.

[105] H Wajant, K Pfizenmaier, and P Scheurich. Tumor necrosis factor signaling. *Cell Death Differ*, 10(1):45–65, January 2003.

[106] Y. Jiang. Prevention of Constitutive TNF Receptor Signaling by Silencer of Death Domains. *Science*, 283(5401):543–546, January 1999.

[107] Christos Karathanasis, Juliane Medler, Franziska Fricke, Sonja Smith, Sebastian Malkusch, Darius Widera, Simone Fulda, Harald Wajant, Sjoerd J. L. van Wijk, Ivan Dikic, and Mike Heilemann. Single-molecule imaging reveals the oligomeric state of functional TNFα-induced plasma membrane TNFR1 clusters in cells. *Sci. Signal.*, 13(614):eaax5647, January 2020.

[108] Daniel F Legler, Olivier Micheau, Marie-Agnès Doucey, Jürg Tschopp, and Claude Bron. Recruitment of TNF Receptor 1 to Lipid Rafts Is Essential for TNFα-Mediated NF-κB Activation. *Immunity*, 18(5):655–664, May 2003.

[109] Hailing Hsu, Jessie Xiong, and David V. Goeddel. The TNF receptor 1-associated protein TRADD signals cell death and NF-κB activation. *Cell*, 81(4):495–504, May 1995.

[110] Hailing Hsu, Hong-Bing Shu, Ming-Gui Pan, and David V Goeddel. TRADD-TRAF2 and TRADD-FADD Interactions Define Two Distinct TNF Receptor 1 Signal Transduction Pathways. *Cell*, 84(2):299–308, January 1996.

[111] Hailing Hsu, Jianing Huang, Hong-Bing Shu, Vijay Baichwal, and David V Goeddel. TNF-Dependent Recruitment of the Protein Kinase RIP to the TNF Receptor-1 Signaling Complex. *Immunity*, 4(4):387–396, April 1996.

[112] Olivier Micheau and Jürg Tschopp. Induction of TNF Receptor I-Mediated Apoptosis via Two Sequential Signaling Complexes. *Cell*, 114(2):181–190, July 2003.

[113] Mike Rothe, Ming-Gui Pan, William J. Henzel, T.Merrill Ayres, and David V. Goeddel. The TNFR2-TRAF signaling complex contains two novel proteins related to baculoviral inhibitor of apoptosis proteins. *Cell*, 83(7):1243–1252, December 1995.

[114] H.-B. Shu, M. Takeuchi, and D. V. Goeddel. The tumor necrosis factor receptor 2 signal transducers TRAF2 and c-IAP1 are components of the tumor necrosis factor receptor 1 signaling complex. *Proceedings of the National Academy of Sciences*, 93(24):13973–13978, November 1996.

[115] Mathieu J.M. Bertrand, Snezana Milutinovic, Kathleen M. Dickson, Wai Chi Ho, Alain Boudreault, Jon Durkin, John W. Gillard, James B. Jaquith, Stephen J. Morris, and Philip A. Barker. cIAP1 and cIAP2 Facilitate Cancer Cell Survival by Functioning as E3 Ligases that Promote RIP1 Ubiquitination. *Molecular Cell*, 30(6):689–700, June 2008.

[116] Eugene Varfolomeev, Tatiana Goncharov, Anna V. Fedorova, Jasmin N. Dynek, Kerry Zobel, Kurt Deshayes, Wayne J. Fairbrother, and Domagoj Vucic. c-IAP1 and c-IAP2 Are Critical Mediators of Tumor Necrosis Factor α (TNFα)-induced NF-κB Activation. *J. Biol. Chem.*, 283(36):24295–24299, September 2008.

[117] Hongxiu Li, Masayuki Kobayashi, Marzenna Blonska, Yun You, and Xin Lin. Ubiquitination of RIP Is Required for Tumor Necrosis Factor α-induced NF-κB Activation. *J. Biol. Chem.*, 281(19):13636–13643, May 2006.

[118] Y. Yang. Ubiquitin Protein Ligase Activity of IAPs and Their Degradation in Proteasomes in Response to Apoptotic Stimuli. *Science*, 288(5467):874–877, May 2000.

[119] Jasmin N Dynek, Tatiana Goncharov, Erin C Dueber, Anna V Fedorova, Anita Izrael-Tomasevic, Lilian Phu, Elizabeth Helgason, Wayne J Fairbrother, Kurt Deshayes, Donald S Kirkpatrick, and Domagoj Vucic. c-IAP1 and UbcH5 promote K11-linked polyubiquitination of RIP1 in TNF signalling. *EMBO J*, 29(24):4198–4209, December 2010.

[120] Chee-Kwee Ea, Li Deng, Zong-Ping Xia, Gabriel Pineda, and Zhijian J. Chen. Activation of IKK by TNFα Requires Site-Specific Ubiquitination of RIP1 and Polyubiquitin Binding by NEMO. *Molecular Cell*, 22(2):245–257, April 2006.

[121] Chuan-Jin Wu, Dietrich B. Conze, Tao Li, Srinivasa M. Srinivasula, and Jonathan D. Ashwell. Sensing of Lys 63-linked polyubiquitination by NEMO is a key event in NF-κB activation. *Nat Cell Biol*, 8(4):398–406, April 2006.

[122] Atsuhiro Kanayama, Rashu B. Seth, Lijun Sun, Chee-Kwee Ea, Mei Hong, Abdullah Shaito, Yu-Hsin Chiu, Li Deng, and Zhijian J. Chen. TAB2 and TAB3 Activate the NF-κB Pathway through Binding to Polyubiquitin Chains. *Molecular Cell*, 15(4):535–548, August 2004.

[123] Tobias L. Haas, Christoph H. Emmerich, Björn Gerlach, Anna C. Schmukle, Stefanie M. Cordier, Eva Rieser, Rebecca Feltham, James Vince, Uwe Warnken, Till Wenger, Ronald Koschny, David Komander, John Silke, and Henning Walczak. Recruitment of the Linear Ubiquitin Chain Assembly Complex Stabilizes the TNF-R1 Signaling Complex and Is Required for TNF-Mediated Gene Induction. *Molecular Cell*, 36(5):831–844, December 2009.

[124] Takayoshi Kirisako, Kiyoko Kamei, Shigeo Murata, Michiko Kato, Hiromi Fukumoto, Masato Kanie, Soichi Sano, Fuminori Tokunaga, Keiji Tanaka, and Kazuhiro Iwai. A ubiquitin ligase complex assembles linear polyubiquitin chains. *EMBO J*, 25(20):4877–4887, October 2006.

[125] Fuminori Tokunaga, Shin-ichi Sakata, Yasushi Saeki, Yoshinori Satomi, Takayoshi Kirisako, Kiyoko Kamei, Tomoko Nakagawa, Michiko Kato, Shigeo Murata, Shoji Yamaoka, Masahiro Yamamoto, Shizuo Akira, Toshifumi Takao, Keiji Tanaka, and Kazuhiro Iwai. Involvement of linear polyubiquitylation of NEMO in NF-κB activation. *Nat Cell Biol*, 11(2):123–132, February 2009.

[126] Björn Gerlach, Stefanie M. Cordier, Anna C. Schmukle, Christoph H. Emmerich, Eva Rieser, Tobias L. Haas, Andrew I. Webb, James A. Rickard, Holly Anderton, Wendy W.-L. Wong, Ueli Nachbur, Lahiru Gangoda, Uwe Warnken, Anthony W. Purcell, John Silke, and Henning Walczak. Linear ubiquitination prevents inflammation and regulates immune signalling. *Nature*, 471(7340):591–596, March 2011.

[127] Chen Wang, Li Deng, Mei Hong, Giridhar R. Akkaraju, Jun-ichiro Inoue, and Zhijian J. Chen. TAK1 is a ubiquitin-dependent kinase of MKK and IKK. *Nature*, 412(6844):346–351, July 2001.

[128] A. Israël. The IKK Complex, a Central Regulator of NF- κB Activation. *Cold Spring Harbor Perspectives in Biology*, 2(3):a000158–a000158, March 2010.

[129] Z. Chen, J. Hagler, V. J. Palombella, F. Melandri, D. Scherer, D. Ballard, and T. Maniatis. Signal-induced site-specific phosphorylation targets I kappa B alpha to the ubiquitin-proteasome pathway. *Genes & Development*, 9(13):1586–1597, July 1995.

[130] I. Alkalay, A. Yaron, A. Hatzubai, A. Orian, A. Ciechanover, and Y. Ben-Neriah. Stimulation-dependent I kappa B alpha phosphorylation marks the NF-kappa B inhibitor for degradation via the ubiquitin-proteasome pathway. *Proceedings of the National Academy of Sciences*, 92(23):10599–10603, November 1995.

[131] J. T. Winston, P. Strack, P. Beer-Romero, C. Y. Chu, S. J. Elledge, and J. W. Harper. The SCFβ -TRCP-ubiquitin ligase complex associates specifically with phosphorylated destruction motifs in IκBα and β-catenin and stimulatesIκBα ubiquitination in vitro. *Genes & Development*, 13(3):270–283, February 1999.

[132] Karine Enesa, Mustafa Zakkar, Hera Chaudhury, Le A. Luong, Lesley Rawlinson, Justin C. Mason, Dorian O. Haskard, Jonathan L. E. Dean, and Paul C. Evans. NF-κB Suppression by the Deubiquitinating Enzyme Cezanne: A Novel Negative Feedback Loop In Pro-Inflammatory Signaling. *J. Biol. Chem.*, 283(11):7036–7045, March 2008.

[133] Ato Wright, William W. Reiley, Mikyoung Chang, Wei Jin, Andrew Joon Lee, Minying Zhang, and Shao-Cong Sun. Regulation of Early Wave of Germ Cell Apoptosis and Spermatogenesis by Deubiquitinating Enzyme CYLD. *Developmental Cell*, 13(5):705–716, November 2007.

[134] Ingrid E. Wertz, Karen M. O'Rourke, Honglin Zhou, Michael Eby, L. Aravind, Somasekar Seshagiri, Ping Wu, Christian Wiesmann, Rohan Baker, David L. Boone, Averil Ma, Eugene V. Koonin, and Vishva M. Dixit. De-ubiquitination and ubiquitin ligase domains of A20 downregulate NF-κB signalling. *Nature*, 430(7000):694–699, August 2004.

[135] Gongxian Liao, Minying Zhang, Edward W. Harhaj, and Shao-Cong Sun. Regulation of the NF-κB-inducing Kinase by Tumor Necrosis Factor Receptor-associated Factor 3-induced Degradation. *J. Biol. Chem.*, 279(25):26243–26250, June 2004.

[136] James E. Vince, W. Wei-Lynn Wong, Nufail Khan, Rebecca Feltham, Diep Chau, Afsar U. Ahmed, Christopher A. Benetatos, Srinivas K. Chunduru, Stephen M. Condon, Mark McKinlay, Robert Brink, Martin Leverkus, Vinay Tergaonkar, Pascal Schneider, Bernard A. Callus, Frank Koentgen, David L. Vaux, and John Silke. IAP Antagonists Target cIAP1 to Induce TNFα-Dependent Apoptosis. *Cell*, 131(4):682–693, November 2007.

[137] Eugene Varfolomeev, John W. Blankenship, Sarah M. Wayson, Anna V. Fedorova, Nobuhiko Kayagaki, Parie Garg, Kerry Zobel, Jasmin N. Dynek, Linda O. Elliott, Heidi J.A. Wallweber, John A. Flygare, Wayne J. Fairbrother, Kurt Deshayes, Vishva M. Dixit, and Domagoj Vucic. IAP Antagonists Induce Autoubiquitination of c-IAPs, NF-κB Activation, and TNFα-Dependent Apoptosis. *Cell*, 131(4):669–681, November 2007.

[138] Lai Wang, Fenghe Du, and Xiaodong Wang. TNF-α Induces Two Distinct Caspase-8 Activation Pathways. *Cell*, 133(4):693–703, May 2008.

[139] Tencho Tenev, Katiuscia Bianchi, Maurice Darding, Meike Broemer, Claudia Langlais, Fredrik Wallberg, Anna Zachariou, Juanita Lopez, Marion MacFarlane, Kelvin Cain, and Pascal Meier. The Ripoptosome, a Signaling Platform that Assembles in Response to Genotoxic Stress and Loss of IAPs. *Molecular Cell*, 43(3):432–448, August 2011.

[140] M. Chen and J. Wang. Initiator caspases in apoptosis signaling pathways *APOPTOSIS*, 7(4):313–319, 2002.

[141] Muneesh Tewari, Long T Quan, Karen O'Rourke, Serge Desnoyers, Zhi Zeng, David R Beidler, Guy G Poirier, Guy S Salvesen, and Vishva M Dixit. Yama/CPP32β, a mammalian homolog of CED-3, is a CrmA-inhibitable protease that cleaves the death substrate poly(ADP-ribose) polymerase. *Cell*, 81(5):801–809, June 1995.

[142] Dean S. Rosenthal, Ruchuang Ding, Cynthia M.G. Simbulan-Rosenthal, John P. Vaillancourt, Donald W. Nicholson, and Mark Smulson. Intact Cell Evidence for the Early Synthesis, and Subsequent Late Apopain-Mediated Suppression, of Poly(ADP-ribose) during Apoptosis. *Experimental Cell Research*, 232(2):313–321, May 1997.

[143] D. Boucher, V. Blais, and J.-B. Denault. Caspase-7 uses an exosite to promote poly(ADP ribose) polymerase 1 proteolysis. *Proceedings of the National Academy of Sciences*, 109(15):5669–5674, April 2012.

[144] Frederik H. Igney and Peter H. Krammer. Death and anti-death: tumour resistance to apoptosis. *Nat Rev Cancer*, 2(4):277–288, April 2002.

[145] Honglin Li, Hong Zhu, Chi-jie Xu, and Junying Yuan. Cleavage of BID by Caspase 8 Mediates the Mitochondrial Damage in the Fas Pathway of Apoptosis. *Cell*, 94(4):491–501, August 1998.

[146] N. Roy. The c-IAP-1 and c-IAP-2 proteins are direct inhibitors of specific caspases. *The EMBO Journal*, 16(23):6914–6925, December 1997.

[147] Andrew Oberst, Christopher P. Dillon, Ricardo Weinlich, Laura L. McCormick, Patrick Fitzgerald, Cristina Pop, Razq Hakem, Guy S. Salvesen, and Douglas R. Green. Catalytic activity of the caspase-8-FLIPL complex inhibits RIPK3-dependent necrosis. *Nature*, 471(7338):363–367, March 2011.

[148] Olivier Micheau, Margot Thome, Pascal Schneider, Nils Holler, Jürg Tschopp, Donald W. Nicholson, Christophe Briand, and Markus G. Grütter. The Long Form of

FLIP Is an Activator of Caspase-8 at the Fas Death-inducing Signaling Complex. *J. Biol. Chem.*, 277(47):45162–45171, November 2002.

[149] Kenneth Murphy and Casey Weaver. Janeway's Immunobiology. In *Janeway's Immunobiology*, page The development of B and T lymphocytes. Positive and Negative selection of T cells. Garland Science, New York, 9th edition. edition, 2017.

[150] H. Ikeda, N. Ohta, K. Furukawa, H. Miyazaki, L. Wang, K. Furukawa, K. Kuribayashi, L. J. Old, and H. Shiku. Mutated mitogen-activated protein kinase: A tumor rejection antigen of mouse sarcoma. *Proceedings of the National Academy of Sciences*, 94(12):6375–6379, June 1997.

[151] Hirokazu Matsushita, Matthew D. Vesely, Daniel C. Koboldt, Charles G. Rickert, Ravindra Uppaluri, Vincent J. Magrini, Cora D. Arthur, J. Michael White, Yee-Shiuan Chen, Lauren K. Shea, Jasreet Hundal, Michael C. Wendl, Ryan Demeter, Todd Wylie, James P. Allison, Mark J. Smyth, Lloyd J. Old, Elaine R. Mardis, and Robert D. Schreiber. Cancer exome analysis reveals a T-cell-dependent mechanism of cancer immunoediting. *Nature*, 482(7385):400–404, February 2012.

[152] Mahesh Yadav, Suchit Jhunjhunwala, Qui T. Phung, Patrick Lupardus, Joshua Tanguay, Stephanie Bumbaca, Christian Franci, Tommy K. Cheung, Jens Fritsche, Toni Weinschenk, Zora Modrusan, Ira Mellman, Jennie R. Lill, and Lélia Delamarre. Predicting immunogenic tumour mutations by combining mass spectrometry and exome sequencing. *Nature*, 515(7528):572–576, November 2014.

[153] M. Cobbold, H. De La Pena, A. Norris, J. M. Polefrone, J. Qian, A. M. English, K. L. Cummings, S. Penny, J. E. Turner, J. Cottine, J. G. Abelin, S. A. Malaker, A. L. Zarling, H.-W. Huang, O. Goodyear, S. D. Freeman, J. Shabanowitz, G. Pratt, C. Craddock, M. E. Williams, D. F. Hunt, and V. H. Engelhard. MHC Class I-Associated Phosphopeptides Are the Targets of Memory-like Immunity in Leukemia. *Science Translational Medicine*, 5(203):203ra125–203ra125, September 2013.

[154] Hester A. Doyle, Jing Zhou, Martin J. Wolff, Bohdan P. Harvey, Robert M. Roman, Renelle J. Gee, Raymond A. Koski, and Mark J. Mamula. Isoaspartyl Post-translational Modification Triggers Anti-tumor T and B Lymphocyte Immunity. *J. Biol. Chem.*, 281(43):32676–32683, October 2006.

[155] André Kahles, Kjong-Van Lehmann, Nora C. Toussaint, Matthias Hüser, Stefan G. Stark, Timo Sachsenberg, Oliver Stegle, Oliver Kohlbacher, Chris Sander, Gunnar Rätsch, Samantha J. Caesar-Johnson, John A. Demchok, Ina Felau, Melpomeni Kasapi, Martin L. Ferguson, Carolyn M. Hutter, Heidi J. Sofia, Roy Tarnuzzer, Zhining Wang, Liming Yang, Jean C. Zenklusen, Jiashan (Julia) Zhang, Sudha Chudamani,

Jia Liu, Laxmi Lolla, Rashi Naresh, Todd Pihl, Qiang Sun, Yunhu Wan, Ye Wu, Juok Cho, Timothy DeFreitas, Scott Frazer, Nils Gehlenborg, Gad Getz, David I. Heiman, Jaegil Kim, Michael S. Lawrence, Pei Lin, Sam Meier, Michael S. Noble, Gordon Saksena, Doug Voet, Hailei Zhang, Brady Bernard, Nyasha Chambwe, Varsha Dhankani, Theo Knijnenburg, Roger Kramer, Kalle Leinonen, Yuexin Liu, Michael Miller, Sheila Reynolds, Ilya Shmulevich, Vesteinn Thorsson, Wei Zhang, Rehan Akbani, Bradley M. Broom, Apurva M. Hegde, Zhenlin Ju, Rupa S. Kanchi, Anil Korkut, Jun Li, Han Liang, Shiyun Ling, Wenbin Liu, Yiling Lu, Gordon B. Mills, Kwok-Shing Ng, Arvind Rao, Michael Ryan, Jing Wang, John N. Weinstein, Jiexin Zhang, Adam Abeshouse, Joshua Armenia, Debyani Chakravarty, Walid K. Chatila, Ino de Bruijn, Jianjiong Gao, Benjamin E. Gross, Zachary J. Heins, Ritika Kundra, Konnor La, Marc Ladanyi, Augustin Luna, Moriah G. Nissan, Angelica Ochoa, Sarah M. Phillips, Ed Reznik, Francisco Sanchez-Vega, Chris Sander, Nikolaus Schultz, Robert Sheridan, S. Onur Sumer, Yichao Sun, Barry S. Taylor, Jioajiao Wang, Hongxin Zhang, Pavana Anur, Myron Peto, Paul Spellman, Christopher Benz, Joshua M. Stuart, Christopher K. Wong, Christina Yau, D. Neil Hayes, Joel S. Parker, Matthew D. Wilkerson, Adrian Ally, Miruna Balasundaram, Reanne Bowlby, Denise Brooks, Rebecca Carlsen, Eric Chuah, Noreen Dhalla, Robert Holt, Steven J.M. Jones, Katayoon Kasaian, Darlene Lee, Yussanne Ma, Marco A. Marra, Michael Mayo, Richard A. Moore, Andrew J. Mungall, Karen Mungall, A. Gordon Robertson, Sara Sadeghi, Jacqueline E. Schein, Payal Sipahimalani, Angela Tam, Nina Thiessen, Kane Tse, Tina Wong, Ashton C. Berger, Rameen Beroukhim, Andrew D. Cherniack, Carrie Cibulskis, Stacey B. Gabriel, Galen F. Gao, Gavin Ha, Matthew Meyerson, Steven E. Schumacher, Juliann Shih, Melanie H. Kucherlapati, Raju S. Kucherlapati, Stephen Baylin, Leslie Cope, Ludmila Danilova, Moiz S. Bootwalla, Phillip H. Lai, Dennis T. Maglinte, David J. Van Den Berg, Daniel J. Weisenberger, J. Todd Auman, Saianand Balu, Tom Bodenheimer, Cheng Fan, Katherine A. Hoadley, Alan P. Hoyle, Stuart R. Jefferys, Corbin D. Jones, Shaowu Meng, Piotr A. Mieczkowski, Lisle E. Mose, Amy H. Perou, Charles M. Perou, Jeffrey Roach, Yan Shi, Janae V. Simons, Tara Skelly, Matthew G. Soloway, Donghui Tan, Umadevi Veluvolu, Huihui Fan, Toshinori Hinoue, Peter W. Laird, Hui Shen, Wanding Zhou, Michelle Bellair, Kyle Chang, Kyle Covington, Chad J. Creighton, Huyen Dinh, HarshaVardhan Doddapaneni, Lawrence A. Donehower, Jennifer Drummond, Richard A. Gibbs, Robert Glenn, Walker Hale, Yi Han, Jianhong Hu, Viktoriya Korchina, Sandra Lee, Lora Lewis, Wei Li, Xiuping Liu, Margaret Morgan, Donna Morton, Donna Muzny, Jireh Santibanez, Margi Sheth, Eve Shinbrot, Linghua Wang, Min Wang, David A. Wheeler, Liu Xi, Fengmei Zhao, Julian Hess, Elizabeth L. Appelbaum, Matthew Bailey, Matthew G. Cordes, Li Ding, Catrina C.

Fronick, Lucinda A. Fulton, Robert S. Fulton, Cyriac Kandoth, Elaine R. Mardis, Michael D. McLellan, Christopher A. Miller, Heather K. Schmidt, Richard K. Wilson, Daniel Crain, Erin Curley, Johanna Gardner, Kevin Lau, David Mallery, Scott Morris, Joseph Paulauskis, Robert Penny, Candace Shelton, Troy Shelton, Mark Sherman, Eric Thompson, Peggy Yena, Jay Bowen, Julie M. Gastier-Foster, Mark Gerken, Kristen M. Leraas, Tara M. Lichtenberg, Nilsa C. Ramirez, Lisa Wise, Erik Zmuda, Niall Corcoran, Tony Costello, Christopher Hovens, Andre L. Carvalho, Ana C. de Carvalho, José H. Fregnani, Adhemar Longatto-Filho, Rui M. Reis, Cristovam Scapulatempo-Neto, Henrique C.S. Silveira, Daniel O. Vidal, Andrew Burnette, Jennifer Eschbacher, Beth Hermes, Ardene Noss, Rosy Singh, Matthew L. Anderson, Patricia D. Castro, Michael Ittmann, David Huntsman, Bernard Kohl, Xuan Le, Richard Thorp, Chris Andry, Elizabeth R. Duffy, Vladimir Lyadov, Oxana Paklina, Galiya Setdikova, Alexey Shabunin, Mikhail Tavobilov, Christopher McPherson, Ronald Warnick, Ross Berkowitz, Daniel Cramer, Colleen Feltmate, Neil Horowitz, Adam Kibel, Michael Muto, Chandrajit P. Raut, Andrei Malykh, Jill S. Barnholtz-Sloan, Wendi Barrett, Karen Devine, Jordonna Fulop, Quinn T. Ostrom, Kristen Shimmel, Yingli Wolinsky, Andrew E. Sloan, Agostino De Rose, Felice Giuliante, Marc Goodman, Beth Y. Karlan, Curt H. Hagedorn, John Eckman, Jodi Harr, Jerome Myers, Kelinda Tucker, Leigh Anne Zach, Brenda Deyarmin, Hai Hu, Leonid Kvecher, Caroline Larson, Richard J. Mural, Stella Somiari, Ales Vicha, Tomas Zelinka, Joseph Bennett, Mary Iacocca, Brenda Rabeno, Patricia Swanson, Mathieu Latour, Louis Lacombe, Bernard Têtu, Alain Bergeron, Mary McGraw, Susan M. Staugaitis, John Chabot, Hanina Hibshoosh, Antonia Sepulveda, Tao Su, Timothy Wang, Olga Potapova, Olga Voronina, Laurence Desjardins, Odette Mariani, Sergio Roman-Roman, Xavier Sastre, Marc-Henri Stern, Feixiong Cheng, Sabina Signoretti, Andrew Berchuck, Darell Bigner, Eric Lipp, Jeffrey Marks, Shannon McCall, Roger McLendon, Angeles Secord, Alexis Sharp, Madhusmita Behera, Daniel J. Brat, Amy Chen, Keith Delman, Seth Force, Fadlo Khuri, Kelly Magliocca, Shishir Maithel, Jeffrey J. Olson, Taofeek Owonikoko, Alan Pickens, Suresh Ramalingam, Dong M. Shin, Gabriel Sica, Erwin G. Van Meir, Hongzheng Zhang, Wil Eijckenboom, Ad Gillis, Esther Korpershoek, Leendert Looijenga, Wolter Oosterhuis, Hans Stoop, Kim E. van Kessel, Ellen C. Zwarthoff, Chiara Calatozzolo, Lucia Cuppini, Stefania Cuzzubbo, Francesco DiMeco, Gaetano Finocchiaro, Luca Mattei, Alessandro Perin, Bianca Pollo, Chu Chen, John Houck, Pawadee Lohavanichbutr, Arndt Hartmann, Christine Stoehr, Robert Stoehr, Helge Taubert, Sven Wach, Bernd Wullich, Witold Kycler, Dawid Murawa, Maciej Wiznerowicz, Ki Chung, W. Jeffrey Edenfield, Julie Martin, Eric Baudin, Glenn Bubley, Raphael Bueno, Assunta De Rienzo, William G. Richards, Steven Kalkanis, Tom Mikkelsen, Houtan

Noushmehr, Lisa Scarpace, Nicolas Girard, Marta Aymerich, Elias Campo, Eva Giné, Armando López Guillermo, Nguyen Van Bang, Phan Thi Hanh, Bui Duc Phu, Yufang Tang, Howard Colman, Kimberley Evason, Peter R. Dottino, John A. Martignetti, Hani Gabra, Hartmut Juhl, Teniola Akeredolu, Serghei Stepa, Dave Hoon, Keunsoo Ahn, Koo Jeong Kang, Felix Beuschlein, Anne Breggia, Michael Birrer, Debra Bell, Mitesh Borad, Alan H. Bryce, Erik Castle, Vishal Chandan, John Cheville, John A. Copland, Michael Farnell, Thomas Flotte, Nasra Giama, Thai Ho, Michael Kendrick, Jean-Pierre Kocher, Karla Kopp, Catherine Moser, David Nagorney, Daniel O'Brien, Brian Patrick O'Neill, Tushar Patel, Gloria Petersen, Florencia Que, Michael Rivera, Lewis Roberts, Robert Smallridge, Thomas Smyrk, Melissa Stanton, R. Houston Thompson, Michael Torbenson, Ju Dong Yang, Lizhi Zhang, Fadi Brimo, Jaffer A. Ajani, Ana Maria Angulo Gonzalez, Carmen Behrens, Jolanta Bondaruk, Russell Broaddus, Bogdan Czerniak, Bita Esmaeli, Junya Fujimoto, Jeffrey Gershenwald, Charles Guo, Alexander J. Lazar, Christopher Logothetis, Funda Meric-Bernstam, Cesar Moran, Lois Ramondetta, David Rice, Anil Sood, Pheroze Tamboli, Timothy Thompson, Patricia Troncoso, Anne Tsao, Ignacio Wistuba, Candace Carter, Lauren Haydu, Peter Hersey, Valerie Jakrot, Hojabr Kakavand, Richard Kefford, Kenneth Lee, Georgina Long, Graham Mann, Michael Quinn, Robyn Saw, Richard Scolyer, Kerwin Shannon, Andrew Spillane, Jonathan Stretch, Maria Synott, John Thompson, James Wilmott, Hikmat Al-Ahmadie, Timothy A. Chan, Ronald Ghossein, Anuradha Gopalan, Douglas A. Levine, Victor Reuter, Samuel Singer, Bhuvanesh Singh, Nguyen Viet Tien, Thomas Broudy, Cyrus Mirsaidi, Praveen Nair, Paul Drwiega, Judy Miller, Jennifer Smith, Howard Zaren, Joong-Won Park, Nguyen Phi Hung, Electron Kebebew, W. Marston Linehan, Adam R. Metwalli, Karel Pacak, Peter A. Pinto, Mark Schiffman, Laura S. Schmidt, Cathy D. Vocke, Nicolas Wentzensen, Robert Worrell, Hannah Yang, Marc Moncrieff, Chandra Goparaju, Jonathan Melamed, Harvey Pass, Natalia Botnariuc, Irina Caraman, Mircea Cernat, Inga Chemencedji, Adrian Clipca, Serghei Doruc, Ghenadie Gorincioi, Sergiu Mura, Maria Pirtac, Irina Stancul, Diana Tcaciuc, Monique Albert, Iakovina Alexopoulou, Angel Arnaout, John Bartlett, Jay Engel, Sebastien Gilbert, Jeremy Parfitt, Harman Sekhon, George Thomas, Doris M. Rassl, Robert C. Rintoul, Carlo Bifulco, Raina Tamakawa, Walter Urba, Nicholas Hayward, Henri Timmers, Anna Antenucci, Francesco Facciolo, Gianluca Grazi, Mirella Marino, Roberta Merola, Ronald de Krijger, Anne-Paule Gimenez-Roqueplo, Alain Piché, Simone Chevalier, Ginette McKercher, Kivanc Birsoy, Gene Barnett, Cathy Brewer, Carol Farver, Theresa Naska, Nathan A. Pennell, Daniel Raymond, Cathy Schilero, Kathy Smolenski, Felicia Williams, Carl Morrison, Jeffrey A. Borgia, Michael J. Liptay, Mark Pool, Christopher W. Seder,

Kerstin Junker, Larsson Omberg, Mikhail Dinkin, George Manikhas, Domenico Alvaro, Maria Consiglia Bragazzi, Vincenzo Cardinale, Guido Carpino, Eugenio Gaudio, David Chesla, Sandra Cottingham, Michael Dubina, Fedor Moiseenko, Renumathy Dhanasekaran, Karl-Friedrich Becker, Klaus-Peter Janssen, Julia Slotta-Huspenina, Mohamed H. Abdel-Rahman, Dina Aziz, Sue Bell, Colleen M. Cebulla, Amy Davis, Rebecca Duell, J. Bradley Elder, Joe Hilty, Bahavna Kumar, James Lang, Norman L. Lehman, Randy Mandt, Phuong Nguyen, Robert Pilarski, Karan Rai, Lynn Schoenfield, Kelly Senecal, Paul Wakely, Paul Hansen, Ronald Lechan, James Powers, Arthur Tischler, William E. Grizzle, Katherine C. Sexton, Alison Kastl, Joel Henderson, Sima Porten, Jens Waldmann, Martin Fassnacht, Sylvia L. Asa, Dirk Schadendorf, Marta Couce, Markus Graefen, Hartwig Huland, Guido Sauter, Thorsten Schlomm, Ronald Simon, Pierre Tennstedt, Oluwole Olabode, Mark Nelson, Oliver Bathe, Peter R. Carroll, June M. Chan, Philip Disaia, Pat Glenn, Robin K. Kelley, Charles N. Landen, Joanna Phillips, Michael Prados, Jeffry Simko, Karen Smith-McCune, Scott VandenBerg, Kevin Roggin, Ashley Fehrenbach, Ady Kendler, Suzanne Sifri, Ruth Steele, Antonio Jimeno, Francis Carey, Ian Forgie, Massimo Mannelli, Michael Carney, Brenda Hernandez, Benito Campos, Christel Herold-Mende, Christin Jungk, Andreas Unterberg, Andreas von Deimling, Aaron Bossler, Joseph Galbraith, Laura Jacobus, Michael Knudson, Tina Knutson, Deqin Ma, Mohammed Milhem, Rita Sigmund, Andrew K. Godwin, Rashna Madan, Howard G. Rosenthal, Clement Adebamowo, Sally N. Adebamowo, Alex Boussioutas, David Beer, Thomas Giordano, Anne-Marie Mes-Masson, Fred Saad, Therese Bocklage, Lisa Landrum, Robert Mannel, Kathleen Moore, Katherine Moxley, Russel Postier, Joan Walker, Rosemary Zuna, Michael Feldman, Federico Valdivieso, Rajiv Dhir, James Luketich, Edna M. Mora Pinero, Mario Quintero-Aguilo, Carlos Gilberto Carlotti, Jose SebastiÃ£o Dos Santos, Rafael Kemp, Ajith Sankarankuty, Daniela Tirapelli, James Catto, Kathy Agnew, Elizabeth Swisher, Jenette Creaney, Bruce Robinson, Carl Simon Shelley, Eryn M. Godwin, Sara Kendall, Cassaasyundra Shipman, Carol Bradford, Thomas Carey, Andrea Haddad, Jeffey Moyer, Lisa Peterson, Mark Prince, Laura Rozek, Gregory Wolf, Rayleen Bowman, Kwun M. Fong, Ian Yang, Robert Korst, W. Kimryn Rathmell, J. Leigh Fantacone-Campbell, Jeffrey A. Hooke, Albert J. Kovatich, Craig D. Shriver, John DiPersio, Bettina Drake, Ramaswamy Govindan, Sharon Heath, Timothy Ley, Brian Van Tine, Peter Westervelt, Mark A. Rubin, Jung Il Lee, Natália D. Aredes, and Armaz Mariamidze. Comprehensive Analysis of Alternative Splicing Across Tumors from 8,705 Patients. *Cancer Cell*, 34(2):211–224.e6, August 2018.

[156] D. L. Barnd, M. S. Lan, R. S. Metzgar, and O. J. Finn. Specific, major histocom-

patibility complex-unrestricted recognition of tumor-associated mucins by human cytotoxic T cells. *Proceedings of the National Academy of Sciences*, 86(18):7159–7163, September 1989.

[157] P. van der Bruggen, C. Traversari, P. Chomez, C. Lurquin, E. De Plaen, B. Van den Eynde, A. Knuth, and T. Boon. A gene encoding an antigen recognized by cytolytic T lymphocytes on a human melanoma. *Science*, 254(5038):1643–1647, December 1991.

[158] Francis Brasseur, Marie Marchand, Remain Vanwuck, Michel Hérin, Bernard Lethé, Patrick Chomez, and Thierry Boon. Letter to the editor. *Int. J. Cancer*, 52(5):839–841, November 1992.

[159] C. Traversari, P. van der Bruggen, I. F. Luescher, C. Lurquin, P. Chomez, A. Van Pel, E. De Plaen, A. Amar-Costesec, and T. Boon. A nonapeptide encoded by human gene MAGE-1 is recognized on HLA-A1 by cytolytic T lymphocytes directed against tumor antigen MZ2-E. *The Journal of Experimental Medicine*, 176(5):1453–1457, November 1992.

[160] Rina Zakut, Suzanne L. Topalian, Yutaka Kawakami, Marie Mancini, Siona Eliyahu, and Steven A. Rosenberg. Differential Expression of MAGE-1, -2, and -3 Messenger RNA in Transformed and Normal Human Cell Lines. *Cancer Research*, 53:5–8, January 1993.

[161] J. Weber, M. Salgaller, D. Samid, B. Johnson, M. Herlyn, N. Lassam, J. Treisman, and S. A. Rosenberg. Expression of the MAGE-1 tumor antigen is up-regulated by the demethylating agent 5-aza-2'-deoxycytidine. *Cancer Research*, 54(7):1766–1771, April 1994.

[162] Keith R. Jerome, Donna L. Barnd, Katharine M. Bendt, Cinda M. Boyer, Joyce Taylor-Papadimitriou, Ian F. C. McKenzie, Robert C. Bast, and Olivera J. Finn. Cytotoxic T-Lymphocytes Derived from Patients with Breast Adenocarcinoma. *Cancer Research*, 51:2908–2916, January 1991.

[163] Shailendra K. Gautam, Sushil Kumar, Vi Dam, Dario Ghersi, Maneesh Jain, and Surinder K. Batra. MUCIN-4 (MUC4) is a novel tumor antigen in pancreatic cancer immunotherapy. *Seminars in Immunology*, 47:101391, February 2020.

[164] Daniel S. Chen and Ira Mellman. Elements of cancer immunity and the cancer-immune set point. *Nature*, 541(7637):321–330, January 2017.

[165] Gavin P. Dunn, Allen T. Bruce, Hiroaki Ikeda, Lloyd J. Old, and Robert D. Schreiber. Cancer immunoediting: from immunosurveillance to tumor escape. *Nat Immunol*, 3(11):991–998, November 2002.

[166] Vijay Shankaran, Hiroaki Ikeda, Allen T. Bruce, J. Michael White, Paul E. Swanson, Lloyd J. Old, and Robert D. Schreiber. IFNγ and lymphocytes prevent primary tumour development and shape tumour immunogenicity. *Nature*, 410(6832):1107–1111, April 2001.

[167] Gavin P. Dunn, Lloyd J. Old, and Robert D. Schreiber. The Three Es of Cancer Immunoediting. *Annu. Rev. Immunol.*, 22(1):329–360, April 2004.

[168] Michel DuPage, Claire Mazumdar, Leah M. Schmidt, Ann F. Cheung, and Tyler Jacks. Expression of tumour-specific antigens underlies cancer immunoediting. *Nature*, 482(7385):405–409, February 2012.

[169] Charles De Smet, Christophe Lurquin, Bernard Lethé, Valérie Martelange, and Thierry Boon. DNA Methylation Is the Primary Silencing Mechanism for a Set of Germ Line- and Tumor-Specific Genes with a CpG-Rich Promoter. *Mol. Cell. Biol.*, 19(11):7327–7335, November 1999.

[170] Z. Sheng Guo, Julie A. Hong, Kari R. Irvine, G. Aaron Chen, Paul J. Spiess, Yang Liu, Gang Zeng, John R. Wunderlich, Dao M. Nguyen, Nicholas P. Restifo, and David S. Schrump. *De novo* Induction of a Cancer/Testis Antigen by 5-Aza-2′-Deoxycytidine Augments Adoptive Immunotherapy in a Murine Tumor Model. *Cancer Res*, 66(2):1105–1113, January 2006.

[171] C. Uyttenhove, J. Maryanski, and T. Boon. Escape of mouse mastocytoma P815 after nearly complete rejection is due to antigen-loss variants rather than immunosuppression. *The Journal of Experimental Medicine*, 157(3):1040–1052, March 1983.

[172] Barbara Seliger, Christina Harders, Sabine Lohmann, Frank Momburg, Stefanie Urlinger, Robert Tampé, and Christoph Huber. Down-regulation of the MHC class I antigenprocessing machinery after oncogenic transformation of murine fibroblasts. *European Journal of Immunology*, 28:122–133, 1998.

[173] Federico Garrido and Natalia Aptsiauri. Cancer immune escape: MHC expression in primary tumours versus metastases. *Immunology*, 158(4):255–266, December 2019.

[174] S. D. Bradley, Z. Chen, B. Melendez, A. Talukder, J. S. Khalili, T. Rodriguez-Cruz, S. Liu, M. Whittington, W. Deng, F. Li, C. Bernatchez, L. G. Radvanyi, M. A. Davies, P. Hwu, and G. Lizee. BRAFV600E Co-opts a Conserved MHC

Class I Internalization Pathway to Diminish Antigen Presentation and CD8+ T-cell Recognition of Melanoma. *Cancer Immunology Research*, 3(6):602–609, June 2015.

[175] Demetrius Moskophidis, Franziska Lechner, Hanspeter Pircher, and Rolf M. Zinkernagel. Virus persistence in acutely infected immunocompetent mice by exhaustion of antiviral cytotoxic effector T cells. *Nature*, 362(6422):758–761, April 1993.

[176] Allan J. Zajac, Joseph N. Blattman, Kaja Murali-Krishna, David J.D. Sourdive, M. Suresh, John D. Altman, and Rafi Ahmed. Viral Immune Evasion Due to Persistence of Activated T Cells Without Effector Function. *Journal of Experimental Medicine*, 188(12):2205–2213, December 1998.

[177] Alexandra Schnell, Lloyd Bod, Asaf Madi, and Vijay K. Kuchroo. The yin and yang of co-inhibitory receptors: toward anti-tumor immunity without autoimmunity. *Cell Res*, 30(4):285–299, April 2020.

[178] E. John Wherry, Sang-Jun Ha, Susan M. Kaech, W. Nicholas Haining, Surojit Sarkar, Vandana Kalia, Shruti Subramaniam, Joseph N. Blattman, Daniel L. Barber, and Rafi Ahmed. Molecular Signature of CD8+ T Cell Exhaustion during Chronic Viral Infection. *Immunity*, 27(4):670–684, October 2007.

[179] E John Wherry. T cell exhaustion. *Nat Immunol*, 12(6):492–499, June 2011.

[180] Meromit Singer, Chao Wang, Le Cong, Nemanja D. Marjanovic, Monika S. Kowalczyk, Huiyuan Zhang, Jackson Nyman, Kaori Sakuishi, Sema Kurtulus, David Gennert, Junrong Xia, John Y.H. Kwon, James Nevin, Rebecca H. Herbst, Itai Yanai, Orit Rozenblatt-Rosen, Vijay K. Kuchroo, Aviv Regev, and Ana C. Anderson. A Distinct Gene Module for Dysfunction Uncoupled from Activation in Tumor-Infiltrating T Cells. *Cell*, 166(6):1500–1511.e9, September 2016.

[181] Yvette Latchman, Clive R. Wood, Tatyana Chernova, Divya Chaudhary, Madhuri Borde, Irene Chernova, Yoshiko Iwai, Andrew J. Long, Julia A. Brown, Raquel Nunes, Edward A. Greenfield, Karen Bourque, Vassiliki A. Boussiotis, Laura L. Carter, Beatriz M. Carreno, Nelly Malenkovich, Hiroyuki Nishimura, Taku Okazaki, Tasuku Honjo, Arlene H. Sharpe, and Gordon J. Freeman. PD-L2 is a second ligand for PD-1 and inhibits T cell activation. *Nat Immunol*, 2(3):261–268, March 2001.

[182] Vikram R. Juneja, Kathleen A. McGuire, Robert T. Manguso, Martin W. LaFleur, Natalie Collins, W. Nicholas Haining, Gordon J. Freeman, and Arlene H. Sharpe. PD-L1 on tumor cells is sufficient for immune evasion in immunogenic tumors and inhibits CD8 T cell cytotoxicity. *Journal of Experimental Medicine*, 214(4):895–904, April 2017.

[183] Jennifer H. Yearley, Christopher Gibson, Ni Yu, Christina Moon, Erin Murphy, Jonathan Juco, Jared Lunceford, Jonathan Cheng, Laura Q.M. Chow, Tanguy Y. Seiwert, Masahisa Handa, Joanne E. Tomassini, and Terrill McClanahan. PD-L2 Expression in Human Tumors: Relevance to Anti-PD-1 Therapy in Cancer. *Clin Cancer Res*, 23(12):3158–3167, June 2017.

[184] Jian Gao, Qianqian Zheng, Na Xin, Wei Wang, and Chenghai Zhao. CD155, an onco-immunologic molecule in human tumors. *Cancer Sci*, 108(10):1934–1938, October 2017.

[185] Satoshi Nishiwada, Masayuki Sho, Satoshi Yasuda, Keiji Shimada, Ichiro Yamato, Takahiro Akahori, Shoichi Kinoshita, Minako Nagai, Noboru Konishi, and Yoshiyuki Nakajima. Clinical Significance of CD155 Expression in Human Pancreatic Cancer. *ANTICANCER RESEARCH*, page 11, 2015.

[186] Takashi Inozume, Tomonori Yaguchi, Junpei Furuta, Kazutoshi Harada, Yutaka Kawakami, and Shinji Shimada. Melanoma Cells Control Antimelanoma CTL Responses via Interaction between TIGIT and CD155 in the Effector Phase. *Journal of Investigative Dermatology*, 136(1):255–263, January 2016.

[187] Karsten Mahnke and Alexander H. Enk. TIGIT-CD155 Interactions in Melanoma: A Novel Co-Inhibitory Pathway with Potential for Clinical Intervention. *Journal of Investigative Dermatology*, 136(1):9–11, January 2016.

[188] Xian-Yang Li, Indrajit Das, Ailin Lepletier, Venkateswar Addala, Tobias Bald, Kimberley Stannard, Deborah Barkauskas, Jing Liu, Amelia Roman Aguilera, Kazuyoshi Takeda, Matthias Braun, Kyohei Nakamura, Sebastien Jacquelin, Steven W. Lane, Michele W.L. Teng, William C. Dougall, and Mark J. Smyth. CD155 loss enhances tumor suppression via combined host and tumor-intrinsic mechanisms. *Journal of Clinical Investigation*, 128(6):2613–2625, June 2018.

[189] Edward Y. Woo, Christina S. Chu, Theresa J. Goletz, Katia Schlienger, Heidi Yeh, George Coukos, Stephen C. Rubin, Larry R. Kaiser, and Carl H. June. Regulatory CD4+CD25+ T Cells in Tumors from Patients with Early-Stage Non-Small Cell Lung Cancer and Late-Stage Ovarian Cancer. *Cancer Research*, 61:4766–4772, June 2001.

[190] Tyler J. Curiel, George Coukos, Linhua Zou, Xavier Alvarez, Pui Cheng, Peter Mottram, Melina Evdemon-Hogan, Jose R. Conejo-Garcia, Lin Zhang, Matthew Burow, Yun Zhu, Shuang Wei, Ilona Kryczek, Ben Daniel, Alan Gordon, Leann Myers, Andrew Lackner, Mary L. Disis, Keith L. Knutson, Lieping Chen, and Weiping Zou.

Specific recruitment of regulatory T cells in ovarian carcinoma fosters immune privilege and predicts reduced survival. *Nat Med*, 10(9):942–949, September 2004.

[191] Tetsuro Sasada, Motohide Kimura, Yuka Yoshida, Michiyuki Kanai, and Arimichi Takabayashi. CD4+CD25+ regulatory T cells in patients with gastrointestinal malignancies: Possible involvement of regulatory T cells in disease progression. *Cancer*, 98(5):1089–1099, September 2003.

[192] Gaynor J. Bates, Stephen B. Fox, Cheng Han, Russell D. Leek, José F. Garcia, Adrian L. Harris, and Alison H. Banham. Quantification of Regulatory T Cells Enables the Identification of High-Risk Breast Cancer Patients and Those at Risk of Late Relapse. *JCO*, 24(34):5373–5380, December 2006.

[193] Hyo Jin Park, Anthony Kusnadi, Eun-Jung Lee, Won Woo Kim, Byoung Chul Cho, Ik Jae Lee, Jinsil Seong, and Sang-Jun Ha. Tumor-infiltrating regulatory T cells delineated by upregulation of PD-1 and inhibitory receptors. *Cellular Immunology*, 278(1-2):76–83, July 2012.

[194] Marco De Simone, Alberto Arrigoni, Grazisa Rossetti, Paola Gruarin, Valeria Ranzani, Claudia Politano, Raoul J.P. Bonnal, Elena Provasi, Maria Lucia Sarnicola, Ilaria Panzeri, Monica Moro, Mariacristina Crosti, Saveria Mazzara, Valentina Vaira, Silvano Bosari, Alessandro Palleschi, Luigi Santambrogio, Giorgio Bovo, Nicola Zucchini, Mauro Totis, Luca Gianotti, Giancarlo Cesana, Roberto A. Perego, Nirvana Maroni, Andrea Pisani Ceretti, Enrico Opocher, Raffaele De Francesco, Jens Geginat, Hendrik G. Stunnenberg, Sergio Abrignani, and Massimiliano Pagani. Transcriptional Landscape of Human Tissue Lymphocytes Unveils Uniqueness of Tumor-Infiltrating T Regulatory Cells. *Immunity*, 45(5):1135–1147, November 2016.

[195] Elham Azizi, Ambrose J. Carr, George Plitas, Andrew E. Cornish, Catherine Konopacki, Sandhya Prabhakaran, Juozas Nainys, Kenmin Wu, Vaidotas Kiseliovas, Manu Setty, Kristy Choi, Rachel M. Fromme, Phuong Dao, Peter T. McKenney, Ruby C. Wasti, Krishna Kadaveru, Linas Mazutis, Alexander Y. Rudensky, and Dana Pe′er. Single-Cell Map of Diverse Immune Phenotypes in the Breast Tumor Microenvironment. *Cell*, 174(5):1293–1308.e36, August 2018.

[196] Christopher Groth, Xiaoying Hu, Rebekka Weber, Viktor Fleming, Peter Altevogt, Jochen Utikal, and Viktor Umansky. Immunosuppression mediated by myeloid-derived suppressor cells (MDSCs) during tumour progression. *Br J Cancer*, 120(1):16–25, January 2019.

[197] Kenneth Murphy and Casey Weaver. Janeway's Immunobiology. In *Janeway's Immunobiology*, pages Basic Concepts in Immunology, Principles of innate immunity. Garland Science, New York, 9th edition. edition, 2017.

[198] Dmitry I. Gabrilovich, Vincenzo Bronte, Shu-Hsia Chen, Mario P. Colombo, Augusto Ochoa, Suzanne Ostrand-Rosenberg, and Hans Schreiber. The Terminology Issue for Myeloid-Derived Suppressor Cells. *Cancer Res*, 67(1):425–425, January 2007.

[199] Claire E. Lewis and Jeffrey W. Pollard. Distinct Role of Macrophages in Different Tumor Microenvironments. *Cancer Res*, 66(2):605–612, January 2006.

[200] Paola Italiani and Diana Boraschi. From Monocytes to M1/M2 Macrophages: Phenotypical vs. Functional Differentiation. *Front. Immunol.*, 5, October 2014.

[201] Zvi Granot and Zvi G. Fridlender. Plasticity beyond Cancer Cells and the "Immunosuppressive Switch". *Cancer Res*, 75(21):4441–4445, November 2015.

[202] Christophe Caux, Rodrigo Nalio Ramos, George C. Prendergast, Nathalie Bendriss-Vermare, and Christine Ménétrier-Caux. A Milestone Review on How Macrophages Affect Tumor Growth. *Cancer Res*, 76(22):6439–6442, November 2016.

[203] Peihua Jiang, Carl F. Lagenaur, and Vinodh Narayanan. Integrin-associated Protein Is a Ligand for the P84 Neural Adhesion Molecule. *J. Biol. Chem.*, 274(2):559–562, January 1999.

[204] P.-A. Oldenborg. Role of CD47 as a Marker of Self on Red Blood Cells. *Science*, 288(5473):2051–2054, June 2000.

[205] E Brown. Integrin-associated protein (CD47) and its ligands. *Trends in Cell Biology*, 11(3):130–135, March 2001.

[206] S. B. Willingham, J.-P. Volkmer, A. J. Gentles, D. Sahoo, P. Dalerba, S. S. Mitra, J. Wang, H. Contreras-Trujillo, R. Martin, J. D. Cohen, P. Lovelace, F. A. Scheeren, M. P. Chao, K. Weiskopf, C. Tang, A. K. Volkmer, T. J. Naik, T. A. Storm, A. R. Mosley, B. Edris, S. M. Schmid, C. K. Sun, M.-S. Chua, O. Murillo, P. Rajendran, A. C. Cha, R. K. Chin, D. Kim, M. Adorno, T. Raveh, D. Tseng, S. Jaiswal, P. O. Enger, G. K. Steinberg, G. Li, S. K. So, R. Majeti, G. R. Harsh, M. van de Rijn, N. N. H. Teng, J. B. Sunwoo, A. A. Alizadeh, M. F. Clarke, and I. L. Weissman. The CD47-signal regulatory protein alpha (SIRPa) interaction is a therapeutic target for human solid tumors. *Proceedings of the National Academy of Sciences*, 109(17):6662–6667, April 2012.

[207] Siddhartha Jaiswal, Mark P. Chao, Ravindra Majeti, and Irving L. Weissman. Macrophages as mediators of tumor immunosurveillance. *Trends in Immunology*, 31(6):212–219, June 2010.

[208] A Mantovani, S Sozzani, M Locati, P Allavena, and A Sica. Macrophage polarization: tumor-associated macrophages as a paradigm for polarized M2 mononuclear phagocytes. *Trends in Immunology*, 23(11):549–555, November 2002.

[209] Oscar R. Colegio, Ngoc-Quynh Chu, Alison L. Szabo, Thach Chu, Anne Marie Rhebergen, Vikram Jairam, Nika Cyrus, Carolyn E. Brokowski, Stephanie C. Eisenbarth, Gillian M. Phillips, Gary W. Cline, Andrew J. Phillips, and Ruslan Medzhitov. Functional polarization of tumour-associated macrophages by tumour-derived lactic acid. *Nature*, 513(7519):559–563, September 2014.

[210] Qiyi Zhao, Dong-Ming Kuang, Yan Wu, Xiao Xiao, Xue-Feng Li, Tuan-Jie Li, and Limin Zheng. Activated $CD69^{+}$ T Cells Foster Immune Privilege by Regulating IDO Expression in Tumor-Associated Macrophages. *J.I.*, 188(3):1117–1124, February 2012.

[211] Alex D. Waldman, Jill M. Fritz, and Michael J. Lenardo. A guide to cancer immunotherapy: from T cell basic science to clinical practice. *Nat Rev Immunol*, May 2020.

[212] Matthew M. Gubin, Xiuli Zhang, Heiko Schuster, Etienne Caron, Jeffrey P. Ward, Takuro Noguchi, Yulia Ivanova, Jasreet Hundal, Cora D. Arthur, Willem-Jan Krebber, Gwenn E. Mulder, Mireille Toebes, Matthew D. Vesely, Samuel S. K. Lam, Alan J. Korman, James P. Allison, Gordon J. Freeman, Arlene H. Sharpe, Erika L. Pearce, Ton N. Schumacher, Ruedi Aebersold, Hans-Georg Rammensee, Cornelis J. M. Melief, Elaine R. Mardis, William E. Gillanders, Maxim N. Artyomov, and Robert D. Schreiber. Checkpoint blockade cancer immunotherapy targets tumour-specific mutant antigens. *Nature*, 515(7528):577–581, November 2014.

[213] Julie R. Brahmer, Scott S. Tykodi, Laura Q.M. Chow, Wen-Jen Hwu, Suzanne L. Topalian, Patrick Hwu, Charles G. Drake, Luis H. Camacho, John Kauh, Kunle Odunsi, Henry C. Pitot, Omid Hamid, Shailender Bhatia, Renato Martins, Keith Eaton, Shuming Chen, Theresa M. Salay, Suresh Alaparthy, Joseph F. Grosso, Alan J. Korman, Susan M. Parker, Shruti Agrawal, Stacie M. Goldberg, Drew M. Pardoll, Ashok Gupta, and Jon M. Wigginton. Safety and Activity of Anti-PD-L1 Antibody in Patients with Advanced Cancer. *N Engl J Med*, 366(26):2455–2465, June 2012.

[214] Roy S. Herbst, Jean-Charles Soria, Marcin Kowanetz, Gregg D. Fine, Omid Hamid, Michael S. Gordon, Jeffery A. Sosman, David F. McDermott, John D. Powderly, Scott N. Gettinger, Holbrook E. K. Kohrt, Leora Horn, Donald P. Lawrence, Sandra Rost, Maya Leabman, Yuanyuan Xiao, Ahmad Mokatrin, Hartmut Koeppen, Priti S. Hegde, Ira Mellman, Daniel S. Chen, and F. Stephen Hodi. Predictive correlates of response to the anti-PD-L1 antibody MPDL3280A in cancer patients. *Nature*, 515(7528):563–567, November 2014.

[215] Manish J. Butte, Mary E. Keir, Theresa B. Phamduy, Arlene H. Sharpe, and Gordon J. Freeman. Programmed Death-1 Ligand 1 Interacts Specifically with the B7-1 Costimulatory Molecule to Inhibit T Cell Responses. *Immunity*, 27(1):111–122, July 2007.

[216] F. Stephen Hodi, Steven J. O'Day, David F. McDermott, Robert W. Weber, Jeffrey A. Sosman, John B. Haanen, Rene Gonzalez, Caroline Robert, Dirk Schadendorf, Jessica C. Hassel, Wallace Akerley, Alfons J.M. van den Eertwegh, Jose Lutzky, Paul Lorigan, Julia M. Vaubel, Gerald P. Linette, David Hogg, Christian H. Ottensmeier, Celeste Lebbé, Christian Peschel, Ian Quirt, Joseph I. Clark, Jedd D. Wolchok, Jeffrey S. Weber, Jason Tian, Michael J. Yellin, Geoffrey M. Nichol, Axel Hoos, and Walter J. Urba. Improved Survival with Ipilimumab in Patients with Metastatic Melanoma. *N Engl J Med*, 363(8):711–723, August 2010.

[217] Edo Kon and Itai Benhar. Immune checkpoint inhibitor combinations: Current efforts and important aspects for success. *Drug Resistance Updates*, 45:13–29, July 2019.

[218] Grazia R. Tundo, Diego Sbardella, Pedro M. Lacal, Grazia Graziani, and Stefano Marini. On the Horizon: Targeting Next-Generation Immune Checkpoints for Cancer Treatment. *Chemotherapy*, 64(2):62–80, 2019.

[219] Yan Zhang, Xuexiang Du, Mingyue Liu, Fei Tang, Peng Zhang, Chunxia Ai, James K. Fields, Eric J. Sundberg, Olga S. Latinovic, Martin Devenport, Pan Zheng, and Yang Liu. Hijacking antibody-induced CTLA-4 lysosomal degradation for safer and more effective cancer immunotherapy. *Cell Res*, 29(8):609–627, August 2019.

[220] Kazuhide Sato, Noriko Sato, Biying Xu, Yuko Nakamura, Tadanobu Nagaya, Peter L. Choyke, Yoshinori Hasegawa, and Hisataka Kobayashi. Spatially selective depletion of tumor-associated regulatory T cells with near-infrared photoimmunotherapy. *Sci. Transl. Med.*, 8(352):352ra110–352ra110, August 2016.

[221] Saman Maleki Vareki. High and low mutational burden tumors versus immuno-

logically hot and cold tumors and response to immune checkpoint inhibitors. *j. immunotherapy cancer*, 6(1):157, s40425–018–0479–7, December 2018.

[222] Antoni Ribas, Reinhard Dummer, Igor Puzanov, Ari VanderWalde, Robert H.I. Andtbacka, Olivier Michielin, Anthony J. Olszanski, Josep Malvehy, Jonathan Cebon, Eugenio Fernandez, John M. Kirkwood, Thomas F. Gajewski, Lisa Chen, Kevin S. Gorski, Abraham A. Anderson, Scott J. Diede, Michael E. Lassman, Jennifer Gansert, F. Stephen Hodi, and Georgina V. Long. Oncolytic Virotherapy Promotes Intratumoral T Cell Infiltration and Improves Anti-PD-1 Immunotherapy. *Cell*, 170(6):1109–1119.e10, September 2017.

[223] John B.A.G. Haanen. Converting Cold into Hot Tumors by Combining Immunotherapies. *Cell*, 170(6):1055–1056, September 2017.

[224] Maria-Elisabeth Goebeler and Ralf C. Bargou. T cell-engaging therapies -BiTEs and beyond. *Nat Rev Clin Oncol*, April 2020.

[225] W. Schaefer, J. T. Regula, M. Bahner, J. Schanzer, R. Croasdale, H. Durr, C. Gassner, G. Georges, H. Kettenberger, S. Imhof-Jung, M. Schwaiger, K. G. Stubenrauch, C. Sustmann, M. Thomas, W. Scheuer, and C. Klein. Immunoglobulin domain crossover as a generic approach for the production of bispecific IgG antibodies. *Proceedings of the National Academy of Sciences*, 108(27):11187–11192, July 2011.

[226] Christian Klein, Wolfgang Schaefer, Joerg T. Regula, Charles Dumontet, Ulrich Brinkmann, Marina Bacac, and Pablo Umaña. Engineering therapeutic bispecific antibodies using CrossMab technology. *Methods*, 154:21–31, February 2019.

[227] Marina Bacac, Christian Klein, and Pablo Umana. CEA TCB: A novel head-to-tail 2:1 T cell bispecific antibody for treatment of CEA-positive solid tumors. *OncoImmunology*, 5(8):e1203498, August 2016.

[228] M. Bacac, T. Fauti, J. Sam, S. Colombetti, T. Weinzierl, D. Ouaret, W. Bodmer, S. Lehmann, T. Hofer, R. J. Hosse, E. Moessner, O. Ast, P. Bruenker, S. Grau-Richards, T. Schaller, A. Seidl, C. Gerdes, M. Perro, V. Nicolini, N. Steinhoff, S. Dudal, S. Neumann, T. von Hirschheydt, C. Jaeger, J. Saro, V. Karanikas, C. Klein, and P. Umana. A Novel Carcinoembryonic Antigen T-Cell Bispecific Antibody (CEA TCB) for the Treatment of Solid Tumors. *Clinical Cancer Research*, 22(13):3286–3297, July 2016.

[229] S. Lehmann, R. Perera, H.-P. Grimm, J. Sam, S. Colombetti, T. Fauti, L. Fahrni, T. Schaller, A. Freimoser-Grundschober, J. Zielonka, S. Stoma, M. Rudin, C. Klein,

P. Umana, C. Gerdes, and M. Bacac. In Vivo Fluorescence Imaging of the Activity of CEA TCB, a Novel T-Cell Bispecific Antibody, Reveals Highly Specific Tumor Targeting and Fast Induction of T-Cell-Mediated Tumor Killing. *Clinical Cancer Research*, 22(17):4417–4427, September 2016.

[230] Sten Hammarström. The carcinoembryonic antigen (CEA) family: structures, suggested functions and expression in normal and malignant tissues. *Seminars in Cancer Biology*, 9(2):67–81, April 1999.

[231] Yonina R. Murciano-Goroff, Allison Betof Warner, and Jedd D. Wolchok. The future of cancer immunotherapy: microenvironment-targeting combinations. *Cell Res*, 30(6):507–519, June 2020.

[232] Nicholas P. Restifo, Mark J. Smyth, and Alexandra Snyder. Acquired resistance to immunotherapy and future challenges. *Nat Rev Cancer*, 16(2):121–126, February 2016.

[233] Huili Li, Katherine B. Chiappinelli, Angela A. Guzzetta, Hariharan Easwaran, Ray-Whay Chiu Yen, Rajita Vatapalli, Michael J. Topper, Jianjun Luo, Roisin M. Connolly, Nilofer S. Azad, Vered Stearns, Drew M. Pardoll, Nancy Davidson, Peter A. Jones, Dennis J. Slamon, Stephen B. Baylin, Cynthia A. Zahnow, and Nita Ahuja. Immune regulation by low doses of the DNA methyltransferase inhibitor 5-azacitidine in common human epithelial cancers. *Oncotarget*, 5(3):587–598, February 2014.

[234] Katherine B. Chiappinelli, Pamela L. Strissel, Alexis Desrichard, Huili Li, Christine Henke, Benjamin Akman, Alexander Hein, Neal S. Rote, Leslie M. Cope, Alexandra Snyder, Vladimir Makarov, Sadna Buhu, Dennis J. Slamon, Jedd D. Wolchok, Drew M. Pardoll, Matthias W. Beckmann, Cynthia A. Zahnow, Taha Merghoub, Timothy A. Chan, Stephen B. Baylin, and Reiner Strick. Inhibiting DNA Methylation Causes an Interferon Response in Cancer via dsRNA Including Endogenous Retroviruses. *Cell*, 162(5):974–986, August 2015.

[235] Anthony E. Dear. Epigenetic Modulators and the New Immunotherapies. *N Engl J Med*, 374(7):684–686, February 2016.

[236] Hazem E. Ghoneim, Yiping Fan, Ardiana Moustaki, Hossam A. Abdelsamed, Pradyot Dash, Pranay Dogra, Robert Carter, Walid Awad, Geoff Neale, Paul G. Thomas, and Ben Youngblood. De Novo Epigenetic Programs Inhibit PD-1 Blockade-Mediated T Cell Rejuvenation. *Cell*, 170(1):142–157.e19, June 2017.

[237] Simon J. Hogg, Paul A. Beavis, Mark A. Dawson, and Ricky W. Johnstone. Targeting the epigenetic regulation of antitumour immunity. *Nat Rev Drug Discov*, September 2020.

[238] Matthew L. Hemming, Matthew A. Lawlor, Jessica L. Andersen, Timothy Hagan, Otari Chipashvili, Thomas G. Scott, Chandrajit P. Raut, Ewa Sicinska, Scott A. Armstrong, George D. Demetri, and James E. Bradner. Enhancer Domains in Gastrointestinal Stromal Tumor Regulate KIT Expression and Are Targetable by BET Bromodomain Inhibition. *Cancer Res*, 79(5):994–1009, March 2019.

[239] Hui Chen, Hudan Liu, and Guoliang Qing. Targeting oncogenic Myc as a strategy for cancer treatment. *Sig Transduct Target Ther*, 3(1):5, December 2018.

[240] A. Dib, A. Gabrea, O. K. Glebov, P. L. Bergsagel, and W. M. Kuehl. Characterization of MYC Translocations in Multiple Myeloma Cell Lines. *JNCI Monographs*, 2008(39):25–31, July 2008.

[241] Hervé Avet-Loiseau, Fabienne Gerson, Florence Magrangeas, Stéphane Minvielle, Jean-Luc Harousseau, and Régis Bataille. Rearrangements of the c-myc oncogene are present in 15% of primary human multiple myeloma tumors. *Blood*, 98(10):3082–3086, November 2001.

[242] Ilaria Genovese, Andrea Ilari, Yehuda G. Assaraf, Francesco Fazi, and Gianni Colotti. Not only P-glycoprotein: Amplification of the ABCB1- containing chromosome region 7q21 confers multidrug resistance upon cancer cells by coordinated overexpression of an assortment of resistance-related proteins. *Drug Resistance Updates*, 32:23–46, May 2017.

[243] Robert Eskes, Solange Desagher, Bruno Antonsson, and Jean-Claude Martinou. Bid Induces the Oligomerization and Insertion of Bax into the Outer Mitochondrial Membrane. *Mol. Cell. Biol.*, 20(3):929–935, February 2000.

[244] Grant Dewson, Tobias Kratina, Huiyan W. Sim, Hamsa Puthalakath, Jerry M. Adams, Peter M. Colman, and Ruth M. Kluck. To Trigger Apoptosis, Bak Exposes Its BH3 Domain and Homodimerizes via BH3:Groove Interactions. *Molecular Cell*, 30(3):369–380, May 2008.

[245] Grant Dewson, Tobias Kratina, Peter Czabotar, Catherine L. Day, Jerry M. Adams, and Ruth M. Kluck. Bak Activation for Apoptosis Involves Oligomerization of Dimers via Their α6 Helices. *Molecular Cell*, 36(4):696–703, November 2009.

[246] Michael C. Wei, Tullia Lindsten, Vamsi K. Mootha, Solly Weiler, Atan Gross, Mona Ashiya, Craig B. Thompson, and Stanley J. Korsmeyer. tBID, a membrane-targeted

death ligand, oligomerizes BAK to release cytochrome c. *Genes & Development*, 14:2060–2071, 2000.

[247] Hyungjin Kim, Ho-Chou Tu, Decheng Ren, Osamu Takeuchi, John R. Jeffers, Gerard P. Zambetti, James J.-D. Hsieh, and Emily H.-Y. Cheng. Stepwise Activation of BAX and BAK by tBID, BIM, and PUMA Initiates Mitochondrial Apoptosis. *Molecular Cell*, 36(3):487–499, November 2009.

[248] Ana J. Garcia-Saez, Manuela Coraiola, Mauro Dalla Serra, Ismael Mingarro, Peter Muller, and Jesus Salgado. Peptides corresponding to helices 5 and 6 of Bax can independently form large lipid pores. *FEBS Journal*, 273(5):971–981, March 2006.

[249] Stephanie Bleicken, Gunnar Jeschke, Carolin Stegmueller, Raquel Salvador-Gallego, Ana J. García-Sáez, and Enrica Bordignon. Structural Model of Active Bax at the Membrane. *Molecular Cell*, 56(4):496–505, November 2014.

[250] D. Westphal, R. M. Kluck, and G. Dewson. Building blocks of the apoptotic pore: how Bax and Bak are activated and oligomerize during apoptosis. *Cell Death Differ*, 21(2):196–205, February 2014.

[251] M. Narita, S. Shimizu, T. Ito, T. Chittenden, R. J. Lutz, H. Matsuda, and Y. Tsujimoto. Bax interacts with the permeability transition pore to induce permeability transition and cytochrome c release in isolated mitochondria. *Proceedings of the National Academy of Sciences*, 95(25):14681–14686, December 1998.

[252] Peng Li, Deepak Nijhawan, Imawati Budihardjo, Srinivasa M Srinivasula, Manzoor Ahmad, Emad S Alnemri, and Xiaodong Wang. Cytochrome c and dATP-Dependent Formation of Apaf-1/Caspase-9 Complex Initiates an Apoptotic Protease Cascade. *Cell*, 91(4):479–489, November 1997.

[253] Hua Zou, William J Henzel, Xuesong Liu, Alexis Lutschg, and Xiaodong Wang. Apaf-1, a Human Protein Homologous to C. elegans CED-4, Participates in Cytochrome c-Dependent Activation of Caspase-3. *Cell*, 90(3):405–413, August 1997.

[254] Stefan J. Riedl and Guy S. Salvesen. The apoptosome: signalling platform of cell death. *Nat Rev Mol Cell Biol*, 8(5):405–413, May 2007.

[255] Anthony Letai, Michael C. Bassik, Loren D. Walensky, Mia D. Sorcinelli, Solly Weiler, and Stanley J. Korsmeyer. Distinct BH3 domains either sensitize or activate mitochondrial apoptosis, serving as prototype cancer therapeutics. *Cancer Cell*, 2(3):183–192, September 2002.

[256] K. Wang, X. M. Yin, D. T. Chao, C. L. Milliman, and S. J. Korsmeyer. BID: a novel BH3 domain-only death agonist. *Genes & Development*, 10(22):2859–2869, November 1996.

[257] L. O'Connor. Bim: a novel member of the Bcl-2 family that promotes apoptosis. *The EMBO Journal*, 17(2):384–395, January 1998.

[258] Elizabeth Yang, Jiping Zha, Jennifer Jockel, Lawrence H. Boise, Craig B. Thompson, and Stanley J. Korsmeyer. Bad, a heterodimeric partner for Bcl-xL and Bcl-2, displaces bax and promotes cell death. *Cell*, 80(2):285–291, January 1995.

[259] Benedito A. Carneiro and Wafik S. El-Deiry. Targeting apoptosis in cancer therapy. *Nat Rev Clin Oncol*, March 2020.

[260] J. Yang. Prevention of Apoptosis by Bcl-2: Release of Cytochrome c from Mitochondria Blocked. *Science*, 275(5303):1129–1132, February 1997.

[261] S. Kharbanda, P. Pandey, L. Schofield, S. Israels, R. Roncinske, K. Yoshida, A. Bharti, Z.-M. Yuan, S. Saxena, R. Weichselbaum, C. Nalin, and D. Kufe. Role for Bcl-xL as an inhibitor of cytosolic cytochrome C accumulation in DNA damage-induced apoptosis. *Proceedings of the National Academy of Sciences*, 94(13):6939–6942, June 1997.

[262] D. Nijhawan. Elimination of Mcl-1 is required for the initiation of apoptosis following ultraviolet irradiation. *Genes & Development*, 17(12):1475–1486, June 2003.

[263] Emily H.-Y.A. Cheng, Michael C. Wei, Solly Weiler, Richard A. Flavell, Tak W. Mak, Tullia Lindsten, and Stanley J. Korsmeyer. BCL-2, BCL-XL Sequester BH3 Domain-Only Molecules Preventing BAX- and BAK-Mediated Mitochondrial Apoptosis. *Molecular Cell*, 8(3):705–711, September 2001.

[264] Kaleigh Fernald and Manabu Kurokawa. Evading apoptosis in cancer. *Trends in Cell Biology*, 23(12):620–633, December 2013.

[265] S. J. Hogg, A. Newbold, S. J. Vervoort, L. A. Cluse, B. P. Martin, G. P. Gregory, M. Lefebure, E. Vidacs, R. W. Tothill, J. E. Bradner, J. Shortt, and R. W. Johnstone. BET Inhibition Induces Apoptosis in Aggressive B-Cell Lymphoma via Epigenetic Regulation of BCL-2 Family Members. *Molecular Cancer Therapeutics*, 15(9):2030–2041, September 2016.

[266] Mai H. Bui, Xiaoyu Lin, Daniel H. Albert, Leiming Li, Lloyd T. Lam, Emily J. Faivre, Scott E. Warder, Xiaoli Huang, Denise Wilcox, Cherrie K. Donawho, George S. Sheppard, Le Wang, Steve Fidanze, John K. Pratt, Dachun Liu, Lisa

Hasvold, Tamar Uziel, Xin Lu, Fred Kohlhapp, Guowei Fang, Steven W. Elmore, Saul H. Rosenberg, Keith F. McDaniel, Warren M. Kati, and Yu Shen. Preclinical Characterization of BET Family Bromodomain Inhibitor ABBV-075 Suggests Combination Therapeutic Strategies. *Cancer Res*, 77(11):2976–2989, June 2017.

[267] Alexander W. Hird and Adriana E. Tron. Recent advances in the development of Mcl-1 inhibitors for cancer therapy. *Pharmacology & Therapeutics*, 198:59–67, June 2019.

[268] Conor J. Kearney, Najoua Lalaoui, Andrew J. Freeman, Kelly M. Ramsbottom, John Silke, and Jane Oliaro. PD-L1 and IAPs co-operate to protect tumors from cytotoxic lymphocyte-derived TNF. *Cell Death Differ*, 24(10):1705–1716, October 2017.

[269] S. Sun, P. Ganchi, D. Ballard, and W. Greene. NF-kappa B controls expression of inhibitor I kappa B alpha: evidence for an inducible autoregulatory pathway. *Science*, 259(5103):1912–1915, March 1993.

[270] Z.-L. Chu, T. A. McKinsey, L. Liu, J. J. Gentry, M. H. Malim, and D. W. Ballard. Suppression of tumor necrosis factor-induced cell death by inhibitor of apoptosis c-IAP2 is under NF- kappaB control. *Proceedings of the National Academy of Sciences*, 94(19):10057–10062, September 1997.

[271] A. Krikos, C. D. Lahrety, and V M Dixit. Transcriptional activation of the tumor necrosis factor alpha-inducible zinc finger protein, A20, is mediated by kappa B elements. *The Journal of Biological Chemistry*, 267:17971–17976, September 1992.

[272] Luigia Lombardi, Paolo Ciana, Catarlna Cappellini, Dino Trecca, Luisa Guerrini, Anna Migliazza, Anna Teresa Maiolo, and Antonino Neri. Structural and functional characterization of the promoter regions of the NFKB2 gene. *Nucl Acids Res*, 23(12):2328–2336, 1995.

[273] R. M. Ten, C.V. Paya, N. Israël, O. Le Bail, M. G. Mattei, J. L. Virelizier, P. Kourilsky, and A. Israël. The characterization of the promoter of the gene encoding the p50 subunit of NF-kB indicates that it participates in its own regulation. *EMBO J.*, 11(1):195–203, 1992.

[274] Christian Stehlik, Rainer de Martin, Ichiro Kumabashiri, Johannes A. Schmid, Bernd R. Binder, and Joachim Lipp. Nuclear Factor (NF)-κB-regulated X-chromosome-linked iap Gene Expression Protects Endothelial Cells from Tumor Necrosis Factor α-induced Apoptosis. *Journal of Experimental Medicine*, 188(1):211–216, July 1998.

[275] C. Wang. NF-kappaB Antiapoptosis: Induction of TRAF1 and TRAF2 and c-IAP1 and c-IAP2 to Suppress Caspase-8 Activation. *Science*, 281(5383):1680–1683, September 1998.

[276] Neil Vasan, José Baselga, and David M. Hyman. A view on drug resistance in cancer. *Nature*, 575(7782):299–309, November 2019.

[277] Philipp Rathert, Mareike Roth, Tobias Neumann, Felix Muerdter, Jae-Seok Roe, Matthias Muhar, Sumit Deswal, Sabine Cerny-Reiterer, Barbara Peter, Julian Jude, Thomas Hoffmann, Łukasz M. Boryń, Elin Axelsson, Norbert Schweifer, Ulrike Tontsch-Grunt, Lukas E. Dow, Davide Gianni, Mark Pearson, Peter Valent, Alexander Stark, Norbert Kraut, Christopher R. Vakoc, and Johannes Zuber. Transcriptional plasticity promotes primary and acquired resistance to BET inhibition. *Nature*, 525(7570):543–547, September 2015.

[278] Hua-Peng Zhang, Gong-Quan Li, Yi Zhang, Wen-Zhi Guo, Jia-Kai Zhang, Jie Li, Jian-Feng Lv, and Shui-Jun Zhang. Upregulation of Mcl-1 inhibits JQ1-triggered anticancer activity in hepatocellular carcinoma cells. *Biochemical and Biophysical Research Communications*, 495(4):2456–2461, January 2018.

[279] Gonghong Yan, Heping Wang, Augustin Luna, Behnaz Bozorgui, Xubin Li, Maga Sanchez, Zeynep Dereli, Nermin Kahraman, Goknur Kara, Xiaohua Chen, Yiling Lu, Ozgun Babur, Murat Cokol, Bulent Ozpolat, Chris Sander, Gordon B. Mills, and Anil Korkut. Adaptive response to BET inhibition induces therapeutic vulnerability to MCL1 inhibitors in breast cancer. preprint, Cancer Biology, July 2019.

[280] Filippo Spriano, Eugenio Gaudio, Luciano Cascione, Chiara Tarantelli, Federica Melle, Giovanna Motta, Valdemar Priebe, Andrea Rinaldi, Gaetanina Golino, Afua Adjeiwaa Mensah, Luca Aresu, Emanuele Zucca, Stefano Pileri, Michael Witcher, Bill Brown, Claes Wahlestedt, Francis Giles, Anastasios Stathis, and Francesco Bertoni. Antitumor activity of the dual BET and CBP/EP300 inhibitor NEO2734. *Blood Advances*, 4(17):4124–4135, September 2020.

[281] Xin Jin, Yuqian Yan, Dejie Wang, Donglin Ding, Tao Ma, Zhenqing Ye, Rafael Jimenez, Liguo Wang, Heshui Wu, and Haojie Huang. DUB3 Promotes BET Inhibitor Resistance and Cancer Progression by Deubiquitinating BRD4. *Molecular Cell*, 71(4):592–605.e4, August 2018.

[282] Alison M. Kurimchak, Claude Shelton, Kelly E. Duncan, Katherine J. Johnson, Jennifer Brown, Shane O'Brien, Rashid Gabbasov, Lauren S. Fink, Yuesheng Li, Nicole Lounsbury, Magid Abou-Gharbia, Wayne E. Childers, Denise C. Connolly, Jonathan Chernoff, Jeffrey R. Peterson, and James S. Duncan. Resistance to BET

Bromodomain Inhibitors Is Mediated by Kinome Reprogramming in Ovarian Cancer. *Cell Reports*, 16(5):1273–1286, August 2016.

[283] Xiunan Wang, Yan Yang, Dandan Ren, Yuanyuan Xia, Wenguang He, Qingsi Wu, Junling Zhang, Miao Liu, Yinan Du, Cuiping Ren, Bin Li, Jijia Shen, and Yuxia Zhang. JQ1, a bromodomain inhibitor, suppresses Th17 effectors by blocking p300-mediated acetylation of RORγt. *Br J Pharmacol*, 177(13):2959–2973, July 2020.

[284] H. S. Bandukwala, J. Gagnon, S. Togher, J. A. Greenbaum, E. D. Lamperti, N. J. Parr, A. M. H. Molesworth, N. Smithers, K. Lee, J. Witherington, D. F. Tough, R. K. Prinjha, B. Peters, and A. Rao. Selective inhibition of CD4+ T-cell cytokine production and autoimmunity by BET protein and c-Myc inhibitors. *Proceedings of the National Academy of Sciences*, 109(36):14532–14537, September 2012.

[285] Peter Georgiev, Yun Wang, Eric S. Muise, Madhavi L. Bandi, Wendy Blumenschein, Manjiri Sathe, Elaine M. Pinheiro, and Stuart D. Shumway. BET Bromodomain Inhibition Suppresses Human T Cell Function. *IH*, 3(7):294–305, July 2019.

[286] T. J. Schall, K. Bacon, R. D. Camp, J. W. Kaspari, and D. V. Goeddel. Human macrophage inflammatory protein alpha (MIP-1 alpha) and MIP-1 beta chemokines attract distinct populations of lymphocytes. *The Journal of Experimental Medicine*, 177(6):1821–1826, June 1993.

[287] Flora Castellino, Alex Y. Huang, Grégoire Altan-Bonnet, Sabine Stoll, Clemens Scheinecker, and Ronald N. Germain. Chemokines enhance immunity by guiding naive CD8+ T cells to sites of CD4+ T cell-dendritic cell interaction. *Nature*, 440(7086):890–895, April 2006.

[288] Ronald Schilderink, Matthew Bell, Eleonora Reginato, Chris Patten, Inmaculada Rioja, Francisca W. Hilbers, Pawel A. Kabala, Kris A. Reedquist, David F. Tough, Paul Peter Tak, Rab K. Prinjha, and Wouter J. de Jonge. BET bromodomain inhibition reduces maturation and enhances tolerogenic properties of human and mouse dendritic cells. *Molecular Immunology*, 79:66–76, November 2016.

[289] Patricia A. Toniolo, Suhu Liu, Jennifer E. Yeh, Pedro M. Moraes-Vieira, Sarah R. Walker, Vida Vafaizadeh, José Alexandre M. Barbuto, and David A. Frank. Inhibiting STAT5 by the BET Bromodomain Inhibitor JQ1 Disrupts Human Dendritic Cell Maturation. *J.I.*, 194(7):3180–3190, April 2015.

[290] Adam R Karpf and David A Jones. Reactivating the expression of methylation silenced genes in human cancer. *Oncogene*, 21(35):5496–5503, August 2002.

[291] Adam R. Karpf, Amy W. Lasek, Ted O. Ririe, Adrianne N. Hanks, Douglas Grossman, and David A. Jones. Limited Gene Activation in Tumor and Normal Epithelial Cells Treated with the DNA Methyltransferase Inhibitor 5-Aza-2'-deoxycytidine. *Mol Pharmacol*, 65(1):18–27, January 2004.

[292] Peter A. Jones, Hitoshi Ohtani, Ankur Chakravarthy, and Daniel D. De Carvalho. Epigenetic therapy in immune-oncology. *Nat Rev Cancer*, 19(3):151–161, March 2019.

[293] David W. Vredevoogd, Thomas Kuilman, Maarten A. Ligtenberg, Julia Boshuizen, Kelly E. Stecker, Beaunelle de Bruijn, Oscar Krijgsman, Xinyao Huang, Juliana C.N. Kenski, Ruben Lacroix, Riccardo Mezzadra, Raquel Gomez-Eerland, Mete Yildiz, Ilknur Dagidir, Georgi Apriamashvili, Nordin Zandhuis, Vincent van der Noort, Nils L. Visser, Christian U. Blank, Maarten Altelaar, Ton N. Schumacher, and Daniel S. Peeper. Augmenting Immunotherapy Impact by Lowering Tumor TNF Cytotoxicity Threshold. *Cell*, 178(3):585–599.e15, July 2019.

[294] Sean L. Petersen, Lai Wang, Asligul Yalcin-Chin, Lin Li, Michael Peyton, John Minna, Patrick Harran, and Xiaodong Wang. Autocrine TNFα Signaling Renders Human Cancer Cells Susceptible to Smac-Mimetic-Induced Apoptosis. *Cancer Cell*, 12(5):445–456, November 2007.

[295] Bo Huang, Xiao-Dong Yang, Ming-Ming Zhou, Keiko Ozato, and Lin-Feng Chen. Brd4 Coactivates Transcriptional Activation of NF-κB via Specific Binding to Acetylated RelA. *MCB*, 29(5):1375–1387, March 2009.

[296] Z. Zou, B. Huang, X. Wu, H. Zhang, J. Qi, J. Bradner, S. Nair, and L.-F. Chen. Brd4 maintains constitutively active NF-κB in cancer cells by binding to acetylated RelA. *Oncogene*, 33(18):2395–2404, May 2014.

[297] Fan Yeung, Jamie E. Hoberg, Catherine S. Ramsey, Michael D. Keller, David R. Jones, Roy A. Frye, and Marty W. Mayo. Modulation of NF-κB-dependent transcription and cell survival by the SIRT1 deacetylase. *EMBO J*, 23(12):2369–2380, June 2004.

[298] Jonathan D. Brown, Charles Y. Lin, Qiong Duan, Gabriel Griffin, Alexander J. Federation, Ronald M. Paranal, Steven Bair, Gail Newton, Andrew H. Lichtman, Andrew L. Kung, Tianlun Yang, Hong Wang, Francis W. Luscinskas, Kevin J. Croce, James E. Bradner, and Jorge Plutzky. NF-κB Directs Dynamic Super Enhancer Formation in Inflammation and Atherogenesis. *Molecular Cell*, 56(2):219–231, October 2014.

[299] Matthew S. Hayden and Sankar Ghosh. Regulation of NF-κB by TNF family cytokines. *Seminars in Immunology*, 26(3):253–266, June 2014.

[300] Brian J. Zarnegar, Yaya Wang, Douglas J. Mahoney, Paul W. Dempsey, Herman H. Cheung, Jeannie He, Travis Shiba, Xiaolu Yang, Wen-chen Yeh, Tak W. Mak, Robert G. Korneluk, and Genhong Cheng. Noncanonical NF-κB activation requires coordinated assembly of a regulatory complex of the adaptors cIAP1, cIAP2, TRAF2 and TRAF3 and the kinase NIK. *Nat Immunol*, 9(12):1371–1378, December 2008.

[301] Sivakumar Vallabhapurapu, Atsushi Matsuzawa, Weizhou Zhang, Ping-Hui Tseng, Jonathan J. Keats, Haopeng Wang, Dario A. A. Vignali, P. Leif Bergsagel, and Michael Karin. Nonredundant and complementary functions of TRAF2 and TRAF3 in a ubiquitination cascade that activates NIK-dependent alternative NF-κB signaling. *Nat Immunol*, 9(12):1364–1370, December 2008.

[302] Hideki Sanjo, Dirk M. Zajonc, Rebecca Braden, Paula S. Norris, and Carl F. Ware. Allosteric Regulation of the Ubiquitin:NIK and Ubiquitin:TRAF3 E3 Ligases by the Lymphotoxin-β Receptor. *J. Biol. Chem.*, 285(22):17148–17155, May 2010.

[303] Xiaoming Li, Yili Yang, and Jonathan D. Ashwell. TNF-RII and c-IAP1 mediate ubiquitination and degradation of TRAF2. *Nature*, 416(6878):345–347, March 2002.

[304] Rebecca A. Csomos, Casey W. Wright, Stefanie Galbán, Karolyn A. Oetjen, and Colin S. Duckett. Two distinct signalling cascades target the NF-κB regulatory factor c-IAP1 for degradation. *Biochemical Journal*, 420(1):83–91, May 2009.

[305] A. Tchoghandjian, C. Jennewein, I. Eckhardt, K. Rajalingam, and S. Fulda. Identification of non-canonical NF-κB signaling as a critical mediator of Smac mimetic-stimulated migration and invasion of glioblastoma cells. *Cell Death Dis*, 4(3):e564–e564, March 2013.

[306] Petrus J. W. Naudé, Johan A. den Boer, Paul G. M. Luiten, and Ulrich L. M. Eisel. Tumor necrosis factor receptor cross-talk: TNF receptor cross-talk. *FEBS Journal*, 278(6):888–898, April 2011.

[307] L. Weisz, A. Damalas, M. Liontos, P. Karakaidos, G. Fontemaggi, R. Maor-Aloni, M. Kalis, M. Levrero, S. Strano, V. G. Gorgoulis, V. Rotter, G. Blandino, and M. Oren. Mutant p53 Enhances Nuclear Factor kappaB Activation by Tumor Necrosis Factor in Cancer Cells. *Cancer Research*, 67(6):2396–2401, March 2007.

[308] Homa Rahnamoun, Hanbin Lu, Sascha H. Duttke, Christopher Benner, Christopher K. Glass, and Shannon M. Lauberth. Mutant p53 shapes the enhancer

landscape of cancer cells in response to chronic immune signaling. *Nat Commun*, 8(1):754, December 2017.

[309] M. Hayakawa, N. Ishida, K. Takeuchi, S. Shibamoto, T. Hori, N. Okull, F. Ito, and M. Tsujimotoll. Arachidonic Acid-selective Cytosolic Phospholipase A2 Is Crucial in the Cytotoxic Action of Tumor Necrosis Factor. *The Journal of Biological Chemistry*, 268(15):11290–11295, 1993.

[310] Nour-Eddine El Mahdani, Maya Ameyar, Zhenzi Cai, Odile Colard, Joëlle Masliah, and Salem Chouaib. Resistance to TNF-Induced Cytotoxicity Correlates with an Abnormal Cleavage of Cytosolic Phospholipase A2. *J Immunol*, 165(12):6756–6761, December 2000.

[311] L. Bernal-Mizrachi, C. M. Lovly, and L. Ratner. The role of NF- kB-1 and NF-kB-2-mediated resistance to apoptosis in lymphomas. *Proceedings of the National Academy of Sciences*, 103(24):9220–9225, June 2006.

[312] Thomas D. Goddard, Conrad C. Huang, Elaine C. Meng, Eric F. Pettersen, Gregory S. Couch, John H. Morris, and Thomas E. Ferrin. UCSF ChimeraX: Meeting modern challenges in visualization and analysis. *Protein Science*, 27(1):14–25, January 2018.

[313] FlowJo™ Software for Windows Version 10.6.2, 2019.

[314] Christina Claus, Claudia Ferrara, Wei Xu, Johannes Sam, Sabine Lang, Franziska Uhlenbrock, Rosmarie Albrecht, Sylvia Herter, Ramona Schlenker, Tamara Hüsser, Sarah Diggelmann, John Challier, Ekkehard Mössner, Ralf J. Hosse, Thomas Hofer, Peter Brünker, Catherine Joseph, Jörg Benz, Philippe Ringler, Henning Stahlberg, Matthias Lauer, Mario Perro, Stanford Chen, Christine Küttel, Preethi L. Bhavani Mohan, Valeria Nicolini, Martina Carola Birk, Amandine Ongaro, Christophe Prince, Reto Gianotti, Gregory Dugan, Christopher T. Whitlow, Kiran Kumar Solingapuram Sai, David L. Caudell, Armando G. Burgos-Rodriguez, J. Mark Cline, Michael Hettich, Maurizio Ceppi, Anna Maria Giusti, Flavio Crameri, Wouter Driessen, Peter N. Morcos, Anne Freimoser-Grundschober, Victor Levitsky, Maria Amann, Sandra Grau-Richards, Thomas von Hirschheydt, Stella Tournaviti, Michael Molhoj, Tanja Fauti, Viola Heinzelmann-Schwarz, Volker Teichgräber, Sara Colombetti, Marina Bacac, Alfred Zippelius, Christian Klein, and Pablo Umaña. Tumor-targeted 4-1BB agonists for combination with T cell bispecific antibodies as off-the-shelf therapy. *Sci. Transl. Med.*, 11(496):5989, June 2019.

[315] Alexander Dobin, Carrie A. Davis, Felix Schlesinger, Jorg Drenkow, Chris Zaleski,

Sonali Jha, Philippe Batut, Mark Chaisson, and Thomas R. Gingeras. STAR: ultrafast universal RNA-seq aligner. *Bioinformatics*, 29(1):15–21, January 2013.

[316] H. Li, B. Handsaker, A. Wysoker, T. Fennell, J. Ruan, N. Homer, G. Marth, G. Abecasis, R. Durbin, and 1000 Genome Project Data Processing Subgroup. The Sequence Alignment/Map format and SAMtools. *Bioinformatics*, 25(16):2078–2079, August 2009.